

COMSAT

Technical Review

Volume 10 Number 1, Spring 1980

COMSAT TECHNICAL REVIEW

Volume 10 Number 1, Spring 1980

- Advisory Board* Joseph V. Charyk
William W. Hagerty
John V. Harrington
B. I. Edelson
Sidney Metzger
- Editorial Board* Pier L. Bargellini, Chairman
S. J. Campanella
William L. Cook
C. Dorian
H. W. Fliieger
Jorge C. Fuenzalida
William J. Getsinger
R. W. Kreutel
Robert K. Kwan
Akos G. Revesz
George R. Welti
- Editorial Staff* Daniel N. Crampton
MANAGING EDITOR
Margaret B. Jacocks
Elizabeth Christie
Pearl Coleman
TECHNICAL EDITORS
Edgar Bolen
PRODUCTION

COMSAT TECHNICAL REVIEW is published twice a year by Communications Satellite Corporation (COMSAT). Subscriptions, which include the two issues published within a calendar year, are: one year, \$7 U.S.; two years, \$12; three years, \$15; single copies, \$5; article reprints, \$1. Make checks payable to COMSAT and address to Treasurer's Office, Communications Satellite Corporation, 950 L'Enfant Plaza, S.W., Washington, D.C. 20024, U.S.A.

- 1 THE 1979 WORLD ADMINISTRATIVE RADIO CONFERENCE AND SATELLITE COMMUNICATIONS C. Dorian, J.B. Potts, E. Reinhart, AND H. Weiss
- 27 AN INTERNATIONAL EXPERIMENT IN HIGH-SPEED COMPUTER NETWORKING VIA SATELLITE W. Cook, A. Kaul, G. Hodge, AND J. Marchese
- 91 FAST ALGORITHMS FOR THE COMPUTATION OF BINARY LOGARITHMS O.A. Horna
- 103 NEW TV ENERGY DISPERSAL TECHNIQUES FOR INTERFERENCE REDUCTION S.E. Yam
- 151 VOICE-ACTIVATED-SWITCH PERFORMANCE CRITERIA G.G. Szarvas AND H. G. Suyderhoud
- 179 AUTOMATIC SEISMIC OBSERVATORY COMMUNICATIONS SYSTEM K. Greene, W. Sones, M. Grossman, M. Jones, AND N. Jacobus
- 223 CTR NOTES
A MODEL FOR CALCULATION OF RAIN-INDUCED CROSS-POLARIZATION DISCRIMINATION AT 6/4 GHz D.J. Kennedy 223
GEOSYNCHRONOUS SATELLITE LOG FOR 1980
W.L. Morgan 233
- 263 TRANSLATIONS OF ABSTRACTS
FRENCH 263 SPANISH 267
- 271 1979 CTR AUTHOR INDEX
- 273 1979 INDEX OF PRESENTATIONS AND PUBLICATIONS BY COMSAT AUTHORS

The 1979 World Administrative Radio Conference and Satellite Communications

C. DORIAN, J. B. POTTS, E. REINHART, AND H. WEISS

(Manuscript received February 11, 1980)

Abstract

With the conclusion of the 1979 World Administrative Radio Conference (WARC-79), the most important results as they affect the various space services are reviewed to provide timely distribution to the space community. This paper includes the more important aspects of the frequency allocations, the output of technical and regulatory committees, and some of the more general results. The overall assessment is that the results appear generally favorable to the continued growth of space communications services.

Introduction

It has been 20 years since the last general World Administrative Radio Conference was held.* The 1979 WARC was convened in Geneva for 10 weeks with the expectation that its results would influence the utilization of the radio frequency spectrum until the end of this century.

*Specialized World Administrative Radio Conferences dealing with a particular radiocommunication service or group of services have been held at intervals of two to five years.

The tremendous growth in voice, data, and video communications in the fixed-satellite service (FSS) was beginning to crowd certain parts of the available orbit and spectrum space; without additional frequency allocations, the growth of the FSS could have been inhibited within two decades. New services, such as broadcasting from satellites, also needed adequate allocations for up-link connections.

While frequency allocations were the most important concern at the conference, other technical and regulatory matters were also treated. This paper summarizes the most important results of WARC-79 relating to various satellite communications services. Although in-depth evaluation or assessment for the long term is not possible, those results felt to have direct bearing on near-term applications and the most pertinent technical rules will be emphasized. A qualitative evaluation will be used in an attempt to indicate the importance of the material not specifically provided.

The Final Acts of WARC-79 will enter into force as of January 1, 1982, after ratification by member Administrations of the International Telecommunications Union; however, different effective dates will apply to the many specific provisions of the Final Acts, such as new tolerances on carrier frequency stability and on spurious emission levels, as well as to some footnote provisions of the Table of Frequency Allocations.

The Final Acts of WARC-79 also incorporate or abrogate the various effective dates of the results of previous conferences, as needed, to make the Final Acts a cohesive, noncontradictory set of International Radio Regulations.

Allocations

The pre-WARC allocations to the fixed-satellite service (FSS), inter-satellite service (ISS), broadcasting-satellite service (BSS), mobile-satellite service (MSS) and to the maritime mobile- and aeronautical mobile-satellite services* are listed in Tables 1a, 2a, 3a, 4a, and 5a.

*These are not the only space services; space research, space operation, and the radio determination-, radionavigation-, maritime radionavigation-, aeronautical radionavigation-, earth exploration-, amateur-, standard frequency and time signal-, and meteorological-satellite services all appear in the Table of Allocations, but are not included here.

respectively. These tables indicate for each band the regional extent* of the allocation (if less than worldwide) and the amount of spectrum involved. Where appropriate, Earth-to-space (up-link) bands and space-to-Earth (down-link) bands are listed separately, with commonly paired bands on the same line. Note that allocations to the BSS are by definition in the space-to-Earth direction, while feeder links for broadcasting satellites use bands allocated to the FSS (Earth-to-space).

TABLE 1. FIXED-SATELLITE SERVICE ALLOCATIONS

a. Pre-WARC Below 35 GHz					
Band	Earth-to-Space (GHz)	Band- width (MHz)	Band	Space-to-Earth (GHz)	Band- width (MHz)
S	2.655-2.690 R2,3	35	S	2.5-2.535 R2,3	35
	4.4-4.7	300		3.4-3.7	300
	5.725-5.850 R1	125			
	5.850-5.925 R1,3	75			
6	5.925-6.425	500	4	3.7-4.2	500
	8	7.9-8.4		500	7
10.95-11.2 R1		250			
12.5-12.75 R1,2		250			
14	14.0-14.5	500	11	10.95-11.2	250
				11.45-11.7	250
				11.7-12.2 R2	500
30	27.5-31.0	3500	20	12.5-12.75 R1,3	250
				17.7-21.2	3500

Above 35 GHz					
	Earth-to-Space (GHz)	Band- width (GHz)		Space-to-Earth (GHz)	Band- width (GHz)
	50-51	1		40-41	1
	92-95	3		102-105	3
	140-142	2		150-152	2
			220-230†	10	
			265-275†	10	

*For allocation purposes, the world is divided into three geographical regions: Region 1 contains Europe, Africa, the USSR, and the Peoples Republic of Mongolia; Region 2 consists of the Americas and Greenland; and Region 3 includes Asia (except the USSR and Mongolia), Australia, New Zealand, etc.

†No direction specified.

TABLE 1. FIXED SATELLITE SERVICE ALLOCATIONS (continued)

b. Post-WARC Below 35 GHz					
Band	Earth-to-Space ^a (GHz)	Band- width (MHz)	Band	Space-to-Earth (GHz)	Band- width (MHz)
S	2.655-2.690 R2 ^b ,3 ^b	35	S	{ 2.5-2.535 R2 ^b ,3 ^b 2.535-2.690 R2 ^b	{ 35 155
6	{ 5.725-5.85 R1 5.85-7.075	{ 125 1225	4	{ 3.4-4.2 4.5-4.8	{ 800 300
8	7.9-8.4	500	7	7.25-7.75	500
14	12.5-12.7 R1	200	11	10.7-11.7	1000
	12.7-12.75 R1,2	50			
	{ 12.75-13.25 14.0-14.5	{ 500 500			
30	27.0-27.5 R2,3 ^c	500	12	{ 11.7-12.3 R2 ^{b,c} 12.2-12.5 R3 ^{b,d} 12.5-12.75 R1,3	{ 600 300 250
	27.5-31.0	3500	20	17.7-21.2	3500
	Above 35 GHz				
	Earth-to-Space (GHz)	Band- width (GHz)		Space-to-Earth (GHz)	Band- width (GHz)
	42.5-43.5	1		37.5-40.5	3
	47.2-49.2 ^e	2			
	49.2-50.2	1			
	50.4-51.4	1			
	71-74	3	81-84	3	
	74-75.5	1.5			
	92-95	3	102-105	3	
	202-217	15	149-164	15	
	265-275	10	231-241	10	
	Total Bandwidth:	37.5	Total Bandwidth:	34	

^a Does not include bands that are limited to BSS feeder links (see Table 3b).

^b Limited to national and sub-Regional Systems.

^c Upper band limit (12.3 GHz) may be replaced by a new value in the range 12.1-12.3 GHz at the 1983 RARC for Region 2.

^d Footnote allocation.

^e Intended for use by, but not restricted to, BSS feeder links.

TABLE 2. INTERSATELLITE SERVICE ALLOCATIONS

a. Pre-WARC	
Band (GHz)	Bandwidth (GHz)
54.25-58.2	3.95
59-64	5
105-130	25
170-182	12
185-190	5
Total Bandwidth	50.95
b. Post-WARC	
Band (GHz)	Bandwidth (GHz)
22.55-23.55	1
32-33	1
54.25-58.2	3.95
59-64	5
116-134	18
170-182	12
185-190	5
Total Bandwidth	45.95

TABLE 3. BROADCASTING-SATELLITE SERVICE ALLOCATIONS

a. Pre-WARC				
Earth-to-Space (GHz)	Band	Space-to-Earth (GHz)	Band- width (MHz)	
Feeder links to broadcasting satellites may, with appropriate coordination, use any of the FSS (Earth-to-space) allocations shown in Table 1a.	UHF	0.62-0.79 ^a	170	
	S	2.50-2.69 ^b	190	
	12	{ 11.7-12.2 12.2-12.5 R1	500	
			300	
	23	22.5-23 R3	500	
	42	41-43	2000	
	85	84-86	2000	

TABLE 3. BROADCASTING-SATELLITE SERVICE ALLOCATIONS (continued)

b. Post-WARC				
Earth-to-Space (GHz)	Band- width (MHz)	Band	Space-to-Earth (GHz)	Band- width (MHz)
Feeder links for the BSS may, in principle, use any of the FSS (Earth-to-space) bands listed in Table 1b with appropriate coordination. However, the following bands were set aside for exclusive or preferential use by such feeder links:				
10.7-11.7 R1	1000 } 300 } 800 }	12	UHF 0.62-0.79 ^a	170
14.5-14.8 exc. Europe			S 2.50-2.69 ^b	190
17.3-18.1			{ 11.7-12.1 R1,3 12.1-12.2 12.2-12.5 R1,2 12.5-12.7 R2,3 ^b 12.7-12.75 R3 ^b	400 100 300 200 50
27-27.5 R2,3	500	23	22.5-23 R2,3	500
47.2-49.2	2000	42	40.5-42.5	2000
		85	84-86	2000

^a Limited to TV by Footnotes 332A (pre-WARC) and 3661 (post-WARC).

^b Limited to community reception.

TABLE 4. MOBILE SATELLITE SERVICE ALLOCATIONS

a. Pre-WARC		
Earth-to-Space	Space-to-Earth	Footnote
	240-328.6 MHz ^a	308A
	335.4-399.9 MHz ^a	308A
406-406.1 ^b		317A
b. Post-WARC		
Earth-to-Space	Space-to-Earth	Footnote
121.45-121.55 MHz ^{a,b}	—	3572A
242.95-243.05 ^{a,b}	—	3572A
	235-322 ^a	3618
	335.4-399.9 ^a	3618
405.5-406 ^c Canada		3533A
406-406.1 ^b		3634
406.1-410 ^c Canada		3633A
(608-614) ^{d,e} R2		
	806-890 [†] R2,R3, Norway, Sweden	3662C,3662CA,3670B
	942-960 [†] R3, Norway Sweden	3662C,3662CA

TABLE 4. MOBILE SATELLITE SERVICE ALLOCATIONS (continued)

b. Post-WARC (continued)		
Earth-to-Space	Space-to-Earth	Footnote
1645.5-1646.5 ^f	1544-1545 ^f	3695A
7900-8025 ^a	7250-7375 ^a	3764B
(14-14.5 GHz) ^{a,g}		
(29.5-30) ^a	(19.7-20.2 GHz) ^a	
30-31	20.2-21.2	
	39.5-40.5	
	43.5-47 [†]	3814C
(50.4-51.4) ^a		—
	66-71 [†]	3814C
71-74	81-84	—
	95-100 [†]	3814C
	134-142 [†]	3814C
	190-200 [†]	3814C
	252-265 [†]	3814C

^a Footnote allocation.

^b Emergency position indicating radio-beacons only.

^c Footnote allocation excludes aeronautical mobile-satellite service.

^d Excludes aeronautical mobile-satellite service.

^e Secondary allocation.

^f Distress and safety operations only.

^g Footnote allocation to land mobile-satellite service only.

[†] No direction specified

TABLE 5. MARITIME AND AERONAUTICAL MOBILE-SATELLITE SERVICE ALLOCATIONS

a. Pre-WARC			
Maritime Mobile Satellite		Aeronautical Mobile Satellite	
Earth-to-Space	Space-to-Earth	Earth-to-Space	Space-to-Earth
1636.5-1645 MHz	1535-1543.5 MHz	1644-1660 MHz	1542.5-1558.5 MHz
			1558.5-1636.5*
			5000-5250*
			15.4-15.7 GHz*
		Both Services (both directions)	
		43-48 GHz	
		66-71	
		95-101	
		142-150	
		190-200	
		250-265	

TABLE 5. MARITIME AND AERONAUTICAL MOBILE-SATELLITE SERVICE ALLOCATIONS (continued)

b. Post-WARC			
Maritime Mobile Satellite		Aeronautical Mobile Satellite	
Earth-to-Space	Space-to-Earth	Earth-to-Space	Space-to-Earth
1626.5-1645.5 MHz	1530-1544 MHz	1646.5-1660.5 MHz	1545-1559 MHz
		1610-1625.5**†	
		5000-5250**†	
		15.4-15.7 GHz**†	

* Footnote allocation.

† No direction specified.

The allocation proposals submitted to WARC-79 showed that most nations, developing and developed alike, recognized the need for substantial increases for commercial FSS systems in the vicinity of the 6/4- and 14/11-GHz band pairs, for maritime mobile- and aeronautical mobile-satellite systems in the neighborhood of 1.6 GHz, and for domestic broadcasting- and fixed-satellite systems in the 11.7- to 12.7-GHz band in Region 2. In addition, there was a widely recognized need to provide dedicated FSS up-link allocations for use with the 12-GHz BSS allotments contained in the WARC-77 Plan for Regions 1 and 3 and for the corresponding Region 2 Plan that is to be developed at the 1983 Regional Administrative Radio Conference (RARC-83).

The allocation proposals submitted to WARC-79 showed that most nations, developing and developed alike, recognized the need for substantial increases for commercial FSS systems in the vicinity of the 6/4- and 14/11-GHz band pairs, for maritime mobile- and aeronautical mobile-satellite systems in the neighborhood of 1.6 GHz, and for domestic broadcasting- and fixed-satellite systems in the 11.7- to 12.7-GHz band in Region 2. In addition, there was a widely recognized need to provide dedicated FSS up-link allocations for use with the 12-GHz BSS allotments contained in the WARC-77 Plan for Regions 1 and 3 and for the corresponding Region 2 Plan that is to be developed at the 1983 Regional Administrative Radio Conference (RARC-83).

The ultimate decisions of WARC-79 regarding new allocations for the space services in question are summarized below for each service.

Fixed-Satellite Service (FSS)

The WARC-79 allocations to the FSS, except those up-link bands

dedicated to use for BSS feeder links, are listed in Table 1b using the same conventions as in Table 1a. The following actions are worthy of note. The band 2.535-2.690 GHz was newly allocated to the FSS in Region 2 in the space-to-Earth direction to allow optional use of the existing BSS allocation 2.5-2.69 GHz (see Table 3a) in the FSS. The power flux density (PFD) limit on the FSS that previously applied in the 2.5- to 2.535-GHz band was changed to agree with the existing BSS PFD limit to facilitate the use of small earth stations in FSS applications. It should be noted that, above 2.655 GHz, the FSS allocation is bidirectional. Additional up-link frequencies for use with both FSS and BSS down-links are available in the 6.425- to 7.075-GHz extension to the pre-WARC 6-GHz FSS up-link band.

The unused pre-WARC 4.4- to 4.7-GHz up-link allocation was eliminated, but the loss of bandwidth was more than offset by augmenting the 6-GHz band with an upward extension of 650 MHz to include the band 6.425-7.075 GHz. In addition, the 5.85- to 5.925-GHz pre-WARC Region 1 and 3 allocation was made worldwide, with a reduction of the radiolocation service to secondary status in this band.

While the 3.4- to 3.7-GHz allocation to FSS (space-to-Earth) was not changed, the radiolocation service in the 3.4- to 3.6-GHz portion was changed to a secondary service in the Allocation Table, with footnotes retaining its primary status in Regions 2 and 3 and in certain European countries. These footnotes urge that radiolocation operations cease by 1985; thereafter, every practicable effort must be made to protect the FSS which, in addition, would not be required to coordinate.

The 4.5- to 4.8-GHz band was also allocated to the FSS (space-to-Earth), although footnotes exclude several European countries. A declaration signed by these countries, the USA, Canada, and Australia as key members of INTELSAT pledged that the signatories would not withhold support for INTELSAT's use of either band extension by reason of the footnote restrictions. The net result was a two-part worldwide down-link allocation of 1100-MHz bandwidth. The sub-band 3.4-3.6 GHz may not be fully available for many years in the USA and certain other developed countries, and domestic coordination restrictions are likely to limit the use of both this sub-band and the 4.5- to 4.8-GHz part of the allocation to international applications in these countries. Nonetheless, the available bandwidth of the 6/4-GHz band pair was more than doubled in most countries of the world.

The 8/7-GHz band pair, used for government FSS systems, was retained without change in band limits, but the formerly exclusive

sub-bands at 7.25–7.3 and 7.975–8.025 GHz are now shared with the terrestrial fixed and mobile services and, by footnote, with the MSS.

The bandwidth of the 14/11-GHz band pair was exactly doubled by adding new down-link allocations at 10.7–10.95 and 11.2–11.45 GHz and a new up-link allocation at 12.75–13.25 GHz. This created a contiguous down-link band (10.7–11.7 GHz) and a split up-link band (12.75–13.25 and 14.0–14.5 GHz) whose two 500-MHz parts are separated by 750 MHz. In the USA, it is expected that domestic coordination restrictions on the down-link band will limit applications to international systems.

In the 12-GHz band, both the upper limit of the pre-WARC 11.7- to 12.2-GHz FSS down-link allocation in Region 2 and the requirement that this allocation be shared with the BSS were changed. The upper limit was raised to 12.3 GHz, and the BSS allocation was expanded and shifted to the band 12.1–12.7 GHz. The resultant 200-MHz overlap between the FSS and the BSS allocations will remain only until 1983. Then RARC-83 will choose a frequency in the range 12.1–12.3 GHz that will become both the new upper limit of the FSS down-link allocation and the new lower limit for the BSS allocation, thus totally eliminating any requirement for the arc segmentation between the two space services that was imposed at the 1977 WARC. If the dividing line is set at 12.2 GHz, then, with the entire orbital arc available to both the FSS and the BSS, the total number of satellites that can be accommodated will be at least doubled in each service from that available using the pre-WARC allocations with arc segmentation.

Another significant change in the 12-GHz FSS down-link allocation was a footnote permitting transponders on FSS satellites to be used for BSS TV transmissions up to a maximum e.i.r.p. of 53 dBW per channel, provided that these transmissions neither cause greater interference nor require more interference protection than the coordinated FSS frequency assignment. This change was incorporated to permit operational implementation of the service now being tested experimentally on ANIK B.

In addition to the changes just enumerated in the 12-GHz FSS down-link allocation for Region 2, the WARC-79 adopted a footnote which allocated the band 12.2–12.5 GHz for FSS down-links in Region 3. As with the Region 2 allocation, the band is restricted to national and sub-Regional systems.

Finally, the WARC-79 retained the Region 1 and 3 FSS allocations in the 12.5- to 12.75-GHz band (down-link in Region 3, bidirectional

in Region 1) and also the 12.7- to 12.75-GHz portion of the pre-WARC Region 2 up-link allocation in this band.

In considering the implementation of the foregoing Regional FSS down-link allocations in the range 11.7–12.75 GHz, it should be noted that none of them have a clearly identified matching up-link band. Presumably, the worldwide FSS up-link allocation in the 14- to 14.5-GHz band and possibly the 12.75- to 13.25-GHz band will be used for this purpose. However, since these bands are already matched to the worldwide FSS down-link allocation at 10.7–11.7 GHz, such use will require inter-system coordination in certain segments of the geostationary orbit.

The limits of the 30/20-GHz FSS band pair were not changed, but the exclusive FSS allocation in the sub-bands 19.7–21.2 and 29.5–31 GHz was ended by a primary footnote allocation of the lower band to the terrestrial fixed and mobile services in some 46 developing countries and by allocation of the upper 1 GHz of each sub-band to the MSS.

At frequencies above 35 GHz, there was a significant increase in the total spectrum allocated to the FSS, as may be seen by comparing Tables 1b and 1a. The spectrum was increased from 32 GHz to 71.5 GHz, but because each band is now restricted to a single direction of transmission, the amount available for a given direction is increased by only 11.5 GHz in the up-link direction and by 8 GHz in the down-link direction. The Earth-to-space band at 47.2–49.2 GHz is intended primarily for feeder links to broadcasting satellites in the band 40.5–42.5 GHz, which accounts in part for the larger up-link allocation. All allocations are worldwide and are shared with terrestrial services.

Intersatellite Service (ISS)

The WARC-79 allocations to the FSS are displayed in Table 2b. The principal change is the addition of 1-GHz-wide bands for each direction of transmission at 23 and 33 GHz to permit the introduction of the service earlier and at lower cost than would be possible with the pre-WARC allocations above 50 GHz. Another change was a reduction of the allocation around 120 GHz from 25 to 18 GHz, leading to a net reduction of 5 GHz in the total spectrum allocated to the ISS. As with the above-35-GHz allocations to the FSS, all ISS allocations must now be shared with terrestrial services. This is not expected to be a problem with the pre-WARC ISS bands, which are coincident with atmospheric absorption bands, but sharing criteria may have to be imposed to avoid mutual interference with the fixed and mobile services, and the

broadcasting-satellite services at 23 GHz and with the radionavigation service at 33 GHz.

Broadcasting-Satellite Service (BSS)

The pre- and post-WARC allocations to the BSS are shown in Tables 3a and 3b, respectively. It is apparent that the number of bands and the total spectrum allocated to the BSS remained essentially unchanged. The principal changes were to extend the 22.5- to 23-GHz allocation to include Region 2 as well as Region 3, and to shift two other allocations by 500 MHz. Thus, the worldwide allocation at 42 GHz was shifted downward and the Region 2 allocation at 12 GHz was shifted upward by this amount.

The change at 12 GHz is by far the more important. As described in connection with the Region 2 FSS allocation at 12 GHz, the BSS band was changed from 11.7–12.2 GHz to 12.1–12.7 GHz, with a new lower band limit in the range 12.1–12.3 GHz to be decided at RARC-83. After 1983, the bandwidth of the 12-GHz BSS band will be between 400 MHz and 600 MHz (probably 500 MHz).

Whatever the decision regarding the ultimate bandwidth of the 12-GHz BSS band, the 1983 RARC for Region 2 is almost certain to develop a plan of frequency and orbital position allotments to individual countries for the BSS. However, there will be no further requirement to restrict broadcasting satellites to specified orbital arc segments. The total orbital arc available for planning in Region 2 will be limited only by inter-Regional sharing considerations, that is, the necessity of avoiding interference to the services of Regions 1 and 3 that have primary allocations in the band used for the Region 2 Plan. In Region 1, these include the terrestrial fixed and broadcasting services and the BSS up to 12.5 GHz, both directions of transmission in the FSS, and the terrestrial fixed and mobile (except aeronautical mobile) services of some 43 Region 1 countries in the band 12.5–12.7 GHz. In Region 3, the services to be protected are the terrestrial fixed, mobile (except aeronautical mobile), and broadcasting services up to 12.7 GHz, and the FSS (space-to-Earth) and BSS in the band 12.2–12.7 GHz.

Within Region 2, the 12-GHz BSS allocation is to be shared with the fixed, mobile (except aeronautical mobile), and broadcasting services on a primary basis, but footnotes to the allocations require that these services not impose restrictions on the BSS Plan to be prepared at RARC-83, nor cause interference to broadcasting satellites operating in accordance with that Plan. It is of interest to note that the allotments

in the Region 2 BSS Plan may also be used for transmissions in the FSS (space-to-Earth) provided that these transmissions do not cause more interference or require more interference protection than BSS transmissions operating in accordance with the Plan.

The problem of which FSS up-link bands should be used for feeder links to 12-GHz broadcasting satellites in the existing plan for Regions 1 and 3 and in the 1983 Plan for Region 2 received a great deal of attention at WARC-79. As shown in Table 3b, three FSS (Earth-to-space) allocations were designated specifically for and limited to this purpose: 10.7–11.7 GHz in Region 1 only, 14.5–14.8 GHz worldwide except for the countries of Europe, and 17.3–18.1 GHz worldwide. All three of these bands will probably be used at the Region 1 and 3 up-link planning conference called for in a WARC-79 Resolution, but only the 17.3- to 18.1-GHz band is expected to be used in planning the BSS up-links for Region 2 at RARC-83. For the BSS allocations at 23 and 42 GHz, WARC-79 indicated that the FSS up-link allocations at 27–27.5 and 47.2–49.2 GHz were preferable for feeder link use.

Mobile-Satellite Service (MSS)

The mobile-satellite service (MSS) includes the land, maritime, and aeronautical mobile-satellite services. The bands listed in Tables 4a and 4b are allocated to the MSS in general and may, with certain exceptions, be used for all three of these services. These allocations appear mostly in footnotes, with the major change from the pre-WARC situation being additions at 7/8 GHz and 30/20 GHz. Of particular interest are the bands 806–890 MHz and 942–960 MHz, where a number of countries obtained an additional footnote allocation to permit use of these bands by the mobile-satellite services, except the aeronautical mobile-satellite service. The primary user is expected to be the land mobile-satellite service.

The bands listed in Table 5a and 5b are restricted to the maritime mobile-satellite and aeronautical mobile-satellite services for the pre- and post-WARC situations, respectively. Table 5a contains the pre-WARC allocations at 1535–1660 MHz. The specific maritime mobile-satellite allocations are 1636.5–1644 MHz (Earth-to-space) and 1535–1542.5 MHz (space-to-Earth).*

*The 4- and 6-GHz fixed-satellite bands are used for links between the satellite and fixed earth stations in accordance with the International Radio Regulations.

The WARC-79 resulted in the readjustment of the radio frequencies as shown in Table 5b to accommodate the growth and increased need for frequencies to serve maritime requirements. The existing 7.5-MHz allocation was increased to 19 MHz in the Earth-to-space direction and to 14 MHz in the space-to-Earth direction. The additional 5 MHz of up-link spectrum is expected to accommodate a unidirectional, high-speed, wideband data service. To satisfy the requirements of the many services, it was necessary to reduce the bandwidth of the up- and down-link allocations for the aeronautical mobile-satellite service from 15 to 14 MHz.

Technical Matters

General

In the technical area, the Radio Regulations deal with the interaction between systems and, in particular, with the characteristics of systems and transmissions and the containment of intersystem interference.

Table 6 lists the Articles and Appendices pertaining to space services which have predominant or partial technical substance, as they appear in the Final Acts of WARC-79. Table 7 lists Recommendations and Resolutions of primarily technical content, relating to future CCIR (International Radio Consultative Committee of the International Telecommunications Union) studies or actions by WARC-79.

Specific discussion

Detailed discussion of text changes and special provisions relating to these Articles is limited to the most significant changes affecting satellite systems.

ARTICLE 25 (FORMERLY ARTICLE 7, SECTION VII)

This Article, relating to e.i.r.p. and pointing constraints for terrestrial radio relay systems in bands shared with space services, has had two footnotes of significance added. The first provides for possible e.i.r.p./pointing constraints in frequency bands above 15 GHz as the result of future CCIR action. The second, which provides for inter-Regional adherence to e.i.r.p./pointing constraints for the case in which different Regions have different allocations, is also subject to future CCIR action.

As a result of allocation actions at WARC-79, the paragraphs listing the frequency bands to which the provisions of Article 25 apply have

TABLE 6. TECHNICAL ARTICLES AND APPENDICES

GWARC-79	Text Designation Previous	Title of Text
Article 1	Article 1	Terms and Definitions.
Article 2	Article 2/III	Nomenclature of the Frequency and Wavelength used in Radiocommunications.
Article 3	Article 2/I, II	Designation of Emissions.
Article 4	Article 12	Technical Characteristics.
Article 16	Article 14/Exc. IV	Interference.
Article 17	Article 14/IV	Tests.
Article 25	Article 7/VII	Terrestrial Radiocommunication Services sharing Frequency Bands with Radiocommunication Services above 1 GHz.
Article 26	Article 7/VIII	Space Radiocommunication Services sharing Frequency Bands with Terrestrial Radiocommunication Services above 1 GHz.
Article 27	Article 7/IX	Special Rules Relating to Space Radiocommunication Services.
Appendix 3	Appendix 3	Table of Transmitter Frequency Tolerances.
Appendix 4	Appendix 4	Table of Maximum Permitted Spurious Emission Power Levels.
Appendix 5	Appendix 5	Additional Characteristics for the Classification of Emissions; Determination of Necessary Bandwidths including Examples for their Calculation and Associated Examples for the Designation of Emissions.
Appendix 28	Appendix 28	Method for the Determination of the Coordination Area Around an Earth Station in Frequency Bands between Space and Terrestrial Radiocommunication Services.
Appendix 29	Appendix 29	Method of Calculation for Determining if Coordination is Required between Geostationary Satellite Networks Sharing the same Frequency Bands.
Appendix 1A	Appendix 1A	Notices relating to Space Radiocommunications and Radio Astronomy Stations.
Appendix 1B	Appendix 1B	Advance Publication Information to be furnished for a Satellite Network.

been changed. Noteworthy are the protection extended to the maritime and aeronautical mobile-satellite services (1.625–1.66 GHz) against primary fixed service footnote allocations, the protection afforded the bidirectionally allocated fixed-satellite service in the bands 10.7–11.7 and 12.5–12.75 GHz, and the protection of the allocation 14.5–14.8 GHz, earmarked for broadcasting-satellite feeder links.

TABLE 7. TECHNICAL RESOLUTIONS AND RECOMMENDATIONS

Designation	Title
Resolution	
AJ	Relating to Information on the Propagation of Radio Waves used in the Determination of the Coordination Area.
AP	Relating to the Use, by Space Stations Operating in the 12-GHz Frequency Bands Allocated to the Broadcasting-Satellite Service, of the Geostationary Orbit and No Other.
BK	Relating to the Division of the World into Climatic Zones for the Purpose of Calculation of Propagation Parameters.
Recommendation	
E	Relating to Studies and Prediction of Radio Propagation and Radio Noise.
J	Relating to the Use of the Term "Channel" in the Radio Regulations.
K	Supplementing the Additional Characteristics for Classifying Emissions and Providing Additional Examples for the Full Designation of Emissions, Both as Given in Appendix 5.
L	Relating to Studies of the Maximum Permitted Levels of Spurious Emissions.
M	Relating to the Provision of Formulae and Examples for the Calculation of Necessary Bandwidths.
O	Relating to Sharing Frequency Bands between the Aeronautical Mobile Service and the Inter-Satellite Service.
P	Relating to the Frequency Tolerance of Transmitters.
T	Relating to the Criteria to be applied for Frequency Sharing between the Broadcasting-Satellite Service and the Terrestrial Broadcasting Service in the Band 620-790 MHz.
U	Relating to the Interdependence of Receiver Design, Channel Grouping, and Sharing Criteria in the Broadcasting-Satellite Service.
V	Relating to the Development of Techniques which would help to Reduce Congestion in High Frequency Bands Allocated to the Aeronautical (R) Service.
X	Relating to the Study of Modulation Methods for Radio-Relay Systems in Relation to Sharing with Fixed-Satellite Service Systems.
Y	Relating to a Study of the Utilization of the Aeronautical Mobile-Satellite (R) Service.
YV	Relating to the Use of the Frequency Band 32-33 GHz Shared between the Inter-Satellite Service and Radionavigation Service.

TABLE 7. TECHNICAL RESOLUTIONS AND RECOMMENDATIONS (continued)

Designation	Title
Recommendation	
YW	Relating to Frequency Sharing by the Earth Exploration-Satellite Service (Passive Sensors) and the Space Research Service (Passive Sensors) and the Fixed, Mobile (except Aeronautical Mobile) and Fixed-Satellite Services in the Band 18.6-18.86 GHz.
Z	Relating to the Coordination of Earth Stations.
ZA	Relating to Carrier Energy Dispersal in Systems in the Fixed-Satellite Service.
ZC	Relating to the Harmonics of the Fundamental Frequency of Broadcasting-Satellite Stations.
ZD	Relating to Transmitting Antennae for the Broadcasting-Satellite Service.
ZE	Relating to Feeder Links for the Broadcasting-Satellite Service.
ZF	Relating to Spurious Emissions in the Broadcasting-Satellite Service.
ZL	Relating to Studies of Propagation at 12 GHz for the Broadcasting-Satellite Service.
ZM	Relating to the Technology for New Spectrum Sharing and Band Utilization Schemes.
ZQ	Relating to Frequency Bands shared between Space Radiocommunication Services and between Space and Terrestrial Radiocommunication Services.
ZR	Relating to Terminology.

ARTICLE 26 (FORMERLY ARTICLE 7, SECTION VIII)

This Article deals with emission constraints on space communications systems in bands shared with terrestrial services. Limits are placed on earth station e.i.r.p. in the horizontal plane, on minimum earth station main beam elevation angle, and on power flux density due to emissions from space stations. Changes include an inter-Regional footnote of the kind mentioned in the paragraph above, and the addition of the frequency range 31-40.5 GHz to the power flux density section.

Present limiting values were retained, but various space services and frequency bands were added to those to which the provisions applied previously, in accordance with the new Table of Frequency Allocations and its various footnote provisions.

In the band 2.5-2.69 GHz, the power flux density for the fixed-satellite service was aligned with that already in existence for the broadcasting-satellite service, providing relief for the fixed-satellite

service. No power flux density penalty was imposed in bidirectionally allocated frequency bands which are also shared with terrestrial services.

ARTICLE 27 (FORMERLY ARTICLE 7, SECTION IX)

The section relating to control of interference between geostationary space systems formerly gave precedence to any geostationary system over non-geostationary systems in the fixed-satellite service. It now gives precedence to geostationary fixed-satellite systems over any non-geostationary space system. A special provision was added by which geostationary fixed-satellite systems have precedence over geostationary systems in the earth exploration-satellite service with links to non-geostationary space stations.

The section on longitudinal stationkeeping of geostationary space stations now imposes on the fixed-satellite service a capability requirement of $\pm 0.1^\circ$ and on other services (excluding the broadcasting-satellite service in the band 11.7–12.7 GHz) a capability requirement of $\pm 0.5^\circ$. Space stations in the broadcasting-satellite service in the band 11.7–12.7 GHz are subject to the provisions of the new Appendix 29A, which were transferred from the Final Acts of WARC-77.

A "prior rights" provision for "old" satellites (put into service prior to January 1, 1987, and advance-notified prior to January 1, 1982) was added.

In the satellite antenna pointing section, the minimum pointing tolerance was tightened to 0.3° , with an exemption added for broadcasting satellites in the band 11.7–12.7 GHz. Article 27 also contains a provision aimed at minimizing earth station transmitted out-of-beam e.i.r.p. density in the direction of the geostationary orbit.

APPENDIX 3

The table of transmitter frequency tolerances applicable to space services is shown below:

Frequency Range	Transmitter Frequency Tolerance Relative to Carrier Frequency	
	Space Stations	Earth Stations
4.0 MHz-2.45 GHz	2×10^{-5}	2×10^{-5}
2.45 GHz-10.5 GHz	5×10^{-5}	5×10^{-5}
10.5 GHz-40 GHz	1×10^{-4}	1×10^{-4}

These tolerances apply to new transmitters installed after January 1, 1985, and to all transmitters after January 1, 1990.

APPENDIX 4

This appendix provides footnotes specifying maximum permitted spurious emission levels for transmitters, as well as a general table giving permitted levels either by frequency range or by mean (carrier) power level. Spurious emissions include by definition harmonic and parasitic emissions, intermodulation products, and frequency conversion products, but exclude out-of-band emissions, *i.e.*, spectral components resulting from a modulation process.

Stations in the space services are exempt from the quantitative provisions of Appendix 4 but are exhorted to minimize their levels of spurious emission.

APPENDIX 28

Appendix 28, which provides for the determination of coordination areas around an earth station with respect to radio relay systems operating in the same frequency band, has been substantively changed to reflect up-to-date CCIR documentation as well as changes to the Table of Allocations.

A provision was adopted which allows the coordination area for a receiving earth station to be smaller than that resulting from the use of values tabulated for that purpose, subject to case-by-case justification. A regulatory provision for the operation of mobile earth stations was added, outlining a method for determining a coordination area which would protect a service area rather than a single service location. Such protection would allow users of mobile earth stations to operate anywhere within the service area, subject to successful prior coordination.

Annex I to Appendix 28 reflects an extension of earth station antenna reference patterns to regions near the main beam including the first sidelobe. Users of antennas with $D/\lambda < 100$ are asked to comply with the reference pattern for $D/\lambda \geq 100$, which is somewhat more stringent.

The auxiliary coordination contours are the subject of a new Annex III. Auxiliary coordination contours may be used by administrations to resolve certain cases of potential interference without recourse to detailed coordination calculations.

APPENDIX 29

This appendix deals with a method for determining whether frequency coordination is required between two geostationary space networks using the same frequency bands. The basic method of the pre-WARC Appendix 29 has been retained, with certain amendments and additions. The most significant amendment changes the "threshold" fractional increase in noise temperature from 2 to 4 percent, while others deal with bidirectional allocations and discretionary polarization isolation provisions.

Revised reference antenna patterns for earth stations, identical to those adopted in Appendix 28, were also incorporated in Appendix 29.

APPENDICES 1A AND 1B

These two appendices contain significant amendments particularly as they relate to Appendix 29. Appendix 1A lists information to be used as a basis for calculations under Appendices 28 and 29, for coordination between administrations, and, ultimately, to be submitted for frequency registration by the International Frequency Registration Board (IFRB). Appendix 1B lists information to be submitted for the advance notification of a space network; such notification is to be the basis for comments by concerned or affected administrations.

Technical Resolutions and Recommendations

WARC-79 generated a large number of Resolutions and Recommendations calling for future action, either to provide lacking information or to test and implement new concepts. Some of these Resolutions and Recommendations were directly aimed at the perceived needs of non-industrialized nations.

Among the Resolutions and Recommendations of primarily technical content listed in Table 7, several deserve a few comments:

RESOLUTION AJ

This Resolution establishes a mechanism for remedying shortcomings of the Appendix 28 propagation model and for introducing new propagation data with a minimum of delay, if desirable. It calls for continuous updating of the relevant material by the CCIR. If a CCIR Plenary Assembly concludes that a revision of Appendix 28 is justified, the relevant amendments proposed by the CCIR will be placed, as an extraordinary item, on the agenda of the next WARC.

RESOLUTION BK

This Resolution calls for intensified studies, by administrations and by the CCIR, of propagation above 1 GHz in remote and, so far, relatively unexplored areas of the world, with special emphasis on the effects of sand and dust storms and on the development of a sufficient number of representative "propagation-climatic geographic zones."

RECOMMENDATION L

Space services, which are exempt from the spurious emission provisions of Appendix 4, are nevertheless perceived as ultimately requiring such bounds in the interest of improved spectrum utilization. Recommendation L calls for the urgent study of necessary and acceptable spurious emission bounds above 960 MHz.

RECOMMENDATION T

This Recommendation deals with sharing between the broadcasting-satellite service and the broadcasting service in the frequency band 620-790 MHz. It imposes a provisional PED limit on broadcasting satellite emissions and calls upon the CCIR for further studies relating to sharing between the two subject services.

RECOMMENDATIONS U, ZC, ZD, ZE, ZF, AND ZL

This is a set of Recommendations aimed at the entire field of designing, coordinating, and operating broadcasting-satellite systems around 12 GHz. Subsequent to the development of the WARC-77 Region 1 and 3 Plan, there were questions relating to the validity of the assumptions used, and to the planning of up-links, which had not been undertaken at all at WARC-77. Moreover, since both up- and down-links need to be considered at RARC-83, Region 2 felt a particular urgency for solving all relevant technical problems prior to that date.

RECOMMENDATIONS X, Z, ZM, AND ZQ

This set of Recommendations is aimed at advancing methods and means by which frequency sharing between space and terrestrial services might be enhanced and assessed.

RESOLUTION ZQ

This Resolution deals with feeder links to broadcasting satellites and reaffirms the need for studies of required technical characteristics (see also Recommendation ZE).

RECOMMENDATION O

This Resolution requests the CCIR to carry out studies of sharing between the inter-satellite service and the aeronautical mobile service pursuant to allocations at WARC-79 in bands above 40 GHz.

RECOMMENDATION YV

As above, this Recommendation relates to sharing between the inter-satellite service and the radionavigation service in the band 32-33 GHz.

RECOMMENDATION YW

As above, this Recommendation relates to sharing of services using passive spaceborne sensors with the fixed and mobile, and the fixed-satellite services in the band 18.6-18.8 GHz.

Regulatory Matters

The provisions dealing with the advance publication, coordination, notification, and registration of space radiocommunication services underwent only minor changes in three areas:

- a. the time periods in which administrations are to examine the advance publication information on new space radiocommunication networks and the requests for coordination between networks or between earth stations and terrestrial stations;
- b. the requirement to submit, for publication, additional reports to the IFRB on the progress in resolving problems in the advance publication and coordination states of implementing a space radiocommunication network;
- c. clarification of various provisions to reflect current practices in the Regulations.

The provisions dealing with the coordination and notification of terrestrial stations in bands shared with the space services underwent similar changes.

A new Article was adopted introducing a procedure to be followed when a footnote to the Table of Frequency Allocations requires the agreement of another administration whose services may be affected.

The provisions dealing with the notification and registration of terrestrial services were revised although the concept remains basically unchanged. Many of the existing provisions were revised to clarify

and highlight them. For example, the IFRB is to select frequency assignments of countries in need of special assistance, to assist in identifying the source of interference to stations of countries in need of special assistance, and to review Master Register entries which received unfavorable findings so that these entries may be upgraded when the assignments have not caused harmful interference.

To maintain the accuracy of the Master Register, provisions were adopted whereby the IFRB is to periodically review each section by sending to each administration extracts of its entries for review and necessary revision.

Special Results

A number of results not falling in any of the previous categories relate to those Resolutions calling for planning conferences. While planning conferences are not new, they have been resisted in the FSS because of the fear that *a priori* assignment of orbital positions and frequencies to individual countries would result in severe limitation of the development and growth of the service. Such planning was discussed before the WARC-71(ST) but not considered by that conference. At WARC-79, however, many more countries advocated such planning, and although no specific type of planning was prescribed for the FSS, resolutions to convene future conferences dealing with planning issues were adopted.

Most important to the FSS was Resolution BP, which proposed a conference in 1984 to "determine which space services and which frequency bands should be planned." The proposed date for this conference allows adequate time for serious study of the merits and problems of planning. This Resolution will result in a higher level of CCIR activity than usual—and the results of such work will be crucial to future assignment of frequencies and orbital positions to space services. Similar efforts will be required to prepare for the Region 2 BSS Planning Conference (RARC-83), whose detailed objectives are given in Resolution CH.

Concluding Remarks

The work at a general WARC is incredibly complex, even under the best of circumstances, and a thorough assimilation of all the results will take time. However, it is not difficult to identify the most important

results and to make some judgments on the relative success of WARC-79.

With respect to frequency allocations, preparations in the U.S. began in early 1975 with COMSAT an active participant. Such work was painstakingly slow because of the many parties involved and it was with great difficulty that a U.S. position responsive to the oftentimes conflicting requirements of these parties was developed. In retrospect, it should be noted that the majority of important results affecting the FSS adopted by the WARC-79 were contained in the proposals presented by COMSAT to the FCC in 1976. At that time, COMSAT also submitted proposals about allocations around 12 GHz for the FSS and the BSS, which were adopted as the U.S. position in 1978 and ultimately adopted by the WARC. The importance of these changes has grown because of recent active U.S. and Canadian interest in broadcasting-satellite systems. The results include more than 1 GHz of new spectrum allocated in both the up and down directions for the FSS below 15 GHz, and at least doubling the orbit space available to the FSS and BSS in the 12-GHz band in Region 2.

While the allocation results were probably the most important outcome of WARC-79 in terms of the space services, there also were many new technical and regulatory results of varying significance. Of these, the most important were those dealing with coordination and the associated frequency sharing criteria, where improvements have been made to increase flexibility in the use of the geostationary satellite orbit and in the various coordination procedures.

Finally, the WARC adopted several very important resolutions setting up a number of planning conferences in the future. In the case of the space services, these conferences will deal specifically with orbit/frequency planning for the BSS in Region 2 (the western hemisphere) and up-link planning for the BSS in Regions 1 and 3, and will determine the need for planning, *i.e.*, *a priori* orbit/frequency allotments, in the other space services including the FSS. This last was viewed as an acceptable alternative to the threat of an unconditional decision at WARC-79 to adopt *a priori* planning at future space conferences.

The results of WARC-79 have to be judged as very good [1] and will permit the continued growth and development of all space services. The space community must now meet the new challenges of wisely using the resources available.

Reference

- [1] J. B. Potts, "WARC-1979: Its Meaning and Impact on the Fixed Satellite Service," *IEEE Communications Magazine*, September 1979, pp. 18-24.

C. Dorian received a B.S. in Engineering from the U.S. Coast Guard in which he served for 30 years before retiring as a Captain. He served as Chief of Communications, U.S. Coast Guard, and as Deputy Director, Office of Telecommunications, Department of Transportation. He has spent eight years in COMSAT/COMSAT General in the field of maritime satellites, and currently serves as Director, Technical Planning, in the Office of MARISAT System Management. Mr. Dorian is a member of the Editorial Board of COMSAT Technical Review, a fellow of the Radio Club of America, and a member of the Veterans Wireless Operators Association. He has received the Legion of Merit, the VWOA Marconi Memorial Gold Medal of Service, and the National Marine Electronic Association's Reginald A. Fessenden Award for services to marine communications.



James B. Potts received B.S.E.E. and M.S.E.E. degrees from Drexel University in 1953 and 1958. He served in the U.S. Navy during World War II as an aviation electronic technician and worked as a Systems Engineer with RCA in Camden, New Jersey, from 1950 to 1963. He joined COMSAT in 1963 and has held a number of positions in engineering and operations. He is presently Division Director and Chief Engineer for the Systems Technology Services organization.

Mr. Potts has been active in the CCIR since 1966, serving on United States delegations at international meetings. In 1970, he was named Chairman of the U.S. National Study Group 4, concerned with the Fixed Satellite Service. He was a member of the U.S. delegation to the 1971 WARC-ST and had headed the U.S. delegation to Study Group 4 meetings and CCIR Plenary Assemblies since 1972. He has participated in the U.S. preparations for the WARC-79, acting as Chairman of the Allocations Task Force of the Fixed Satellite Service Working Group, organized in 1975 by the Federal Communications Commission.



Edward E. Reinhart, Manager of the System Planning and Development Department at COMSAT, has just completed a two-and-a-half year assignment coordinating COMSAT's participation in U.S. preparations for the 1979 WARC, serving as a delegate to the CCIR Special Preparatory Meeting (SPM) in 1978, and as a member of the U.S. WARC Advisory Committee. He was a member of the U.S. Delegation at the WARC, working primarily on the regulatory and allocations committees.

Prior to joining COMSAT, Mr. Reinhart was a communication systems engineer at the Rand Corporation and at the Jet Propulsion Laboratory, where he specialized in the planning and analysis of satellite communications systems for commercial and military applications. This work included participation in the 1971 Space WARC and the 1977 Broadcasting Satellite Planning Conference.

Mr. Reinhart's academic work was in physics, electromagnetic wave propagation, and radio astronomy at the University of California, Berkeley, and at Cornell University. As a naval officer, he also studied and served as an instructor at the MIT Radar School.

Hans J. Weiss received an M.Sc. (Physics) from Karlsruhe Technical University in Karlsruhe, Germany. From 1955 to 1959, he was design engineer and later technical director with RCA Victor and Elmer Ltd., both in São Paulo, Brazil. In 1960, he joined the Surfcom Division of RCA in Camden, New Jersey, as a system engineer. In 1964, Mr. Weiss became a staff member at COMSAT in Washington, where, from 1969-1974, he headed the Spectrum Utilization Department. Since 1974, he has been Director of Systems Engineering.



Mr. Weiss' group was instrumental in the specification and design of the INTELSAT V spacecraft and in the definition and analysis of the basic INTELSAT VI design options. Since 1968, Mr. Weiss has been active in the CCIR and has represented the U.S. at many CCIR meetings and ITU Administrative Conferences. He is the author of numerous publications, and many of his analyses and concepts are reflected in CCIR texts and in the radio regulations.

Mr. Weiss attended the WARC 79 Conference as a member of the U.S. delegation.

Index: protocol, computer communication, satellite network

An international experiment in high-speed computer networking via satellite

W. COOK, A. KAUL, G. HODGE,* AND J. MARCHESE*

(Manuscript received November 8, 1979)

Abstract

An experimental 4-node computer network was established to investigate system design issues related to computer communications via satellite and to demonstrate high-speed data processing applications between widely separated computing facilities. The network consisted of four main frame computers at separate sites in the United States and Europe, communicating in a time-division multiple-access (TDMA) mode. The fixed assignment TDMA system was composed of two 1.544-Mbit/s subnetworks operating in separate transponders of the SYMPHONIE satellite. Each site could access both transponders to provide complete interconnectivity.

The experimental results demonstrated the influence of various transmission system and data processing system parameters on the achievable data throughput and response times. These parameters included channel bit-error rates (BERS), TDMA frame sizes and burst patterns, block sizes and choice of error recovery technique, as well as the processing and storage capabilities of the computers in the network. The wideband satellite channels made possible a number of data processing applications, such as load sharing and remote job entry, which otherwise would not have been feasible.

* IBM System Communications Division, Gaithersburg, Maryland.

Introduction

An experimental program in high-speed computer-to-computer communications has been conducted jointly by IBM System Communications Division; COMSAT Laboratories; the French Postal, Telegraph and Telephone Ministry (PTT); the German Aerospace Research Establishment (DFVLR); and the Deutsche Bundespost (DBP). The first phase of the experiment involved full-duplex transmission at 1.544 Mbit/s through the SYMPHONIE satellite between computers located at IBM facilities in Gaithersburg, Maryland, and La Gaude, France. The objectives of the first phase were to demonstrate the feasibility of high data rate point-to-point communication between computers at distant locations, and to investigate the impact of data link control protocol design on throughput and computer resource utilization. The Phase 1 experimental program began on April 5, 1977, and was completed by July 1, 1977 [1].

This paper describes a second phase in which the network was expanded to include additional earth terminals at COMSAT Laboratories in Clarksburg, Maryland, and the DFVLR site in Weilheim, Federal Republic of Germany. The IBM computers located at these sites (a System 360/65 at COMSAT and a System 370/158 in Weilheim) were then able to communicate with the two computers already involved in the program (both System 370/158) and thus form a completely interconnected 4-node computer network. This experimental 4-node configuration permitted an evaluation of newly developed communications control protocols and data processing techniques. In addition, computer-to-computer load sharing and file transfer applications were investigated in a high-speed data network environment. Phase 2 experiments were conducted from October 1978 through March 1979 [2].

The second phase of the computer/satellite communications experiment has two overall objectives:

- a. to demonstrate that distributed data processing systems (both existing and new) can benefit from the availability of a high-speed computer/satellite network, and
- b. to measure the overall system performance of a specific computer/satellite network under realistic operating conditions.

The first objective deals with data processing applications that can potentially benefit from the use of high-speed satellite networks, and

the second objective deals with systems required to provide efficient computer/satellite communications networks.

The Phase 2 experimental system development effort focused on the design requirements associated with interconnecting multiple host systems through a high-speed satellite communications system, specifically, the computer/communications interface, network and link control protocols, and transmission subsystems design. Additionally, functional capabilities for experimenting with new data processing applications (such as network job entry, load sharing, and file transfer) were developed to demonstrate the feasibility of these new systems.

System description

Figure 1 shows the network configuration for the Phase 2 experiments. The network topology consisted of four nodes connected by six duplex communications links.

Figure 2 gives the configuration for each operational site. IBM 370/158 computer systems were employed at each site except COMSAT Laboratories, which used an IBM 360/65 computer. The earth terminals at both the IBM Gaithersburg and COMSAT Laboratories sites were provided by COMSAT Laboratories. The IBM La Gaude earth terminal was provided by the French PTT, and the antenna at Weilheim was installed by the DFVLR.

Special hardware elements, including 2701 data adapter units, 1.544-Mbit/s modems and forward error correction (FEC) codecs, satellite network multiplexers, and special interface assemblies, were installed at all four sites. The satellite network multiplexer (SNM), which controlled the earth terminal access to the satellite, was developed by IBM. The modems at three of the sites were DCC Model 4007 series units employing rate 3/4 FEC coding. The COMSAT Laboratories site used a COMSAT-designed modem and codec which were compatible with the DCC units.

The space segment of the communications link was provided by the SYMPHONIE satellite. This satellite provides a global up-link receiving beam and two down-link transmitting beams, one covering the European and African continents and the other covering the eastern coast of the United States and a major portion of South America (see Figure 3). Consequently, to fully interconnect all four nodes of the network, each earth terminal had to be capable of accessing each of the two satellite transponders with their associated down-link spot beams.

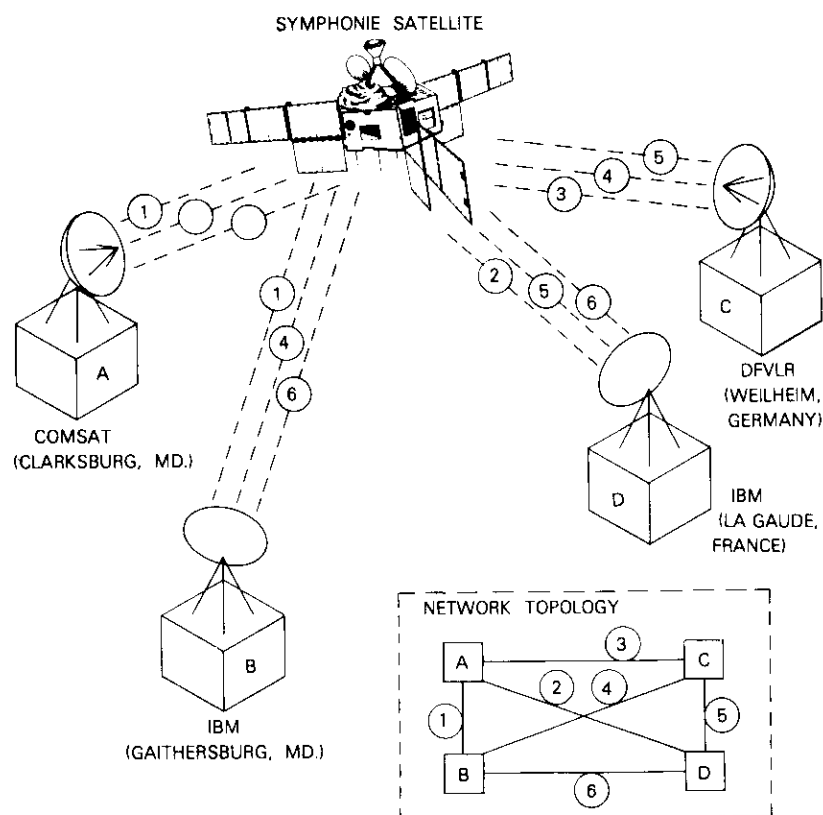


Figure 1. High-Speed Data Network Configuration

Each network node transmitted on two different up-link frequencies, one to communicate with the station in its own down-link coverage pattern, and the second to communicate with the other two stations in the transatlantic down-link spot beam coverage pattern. Since a station receives only transmissions that are directed to the coverage pattern in which the station is located, simultaneous transmissions in both down-link spot beam zones can be accommodated without interference. However, since all stations require access to both up-link frequencies for complete network interconnectivity, a time-division control mechanism is required to synchronize transmission on the two up-link frequencies and hence avoid "collisions" in the down-link channels.

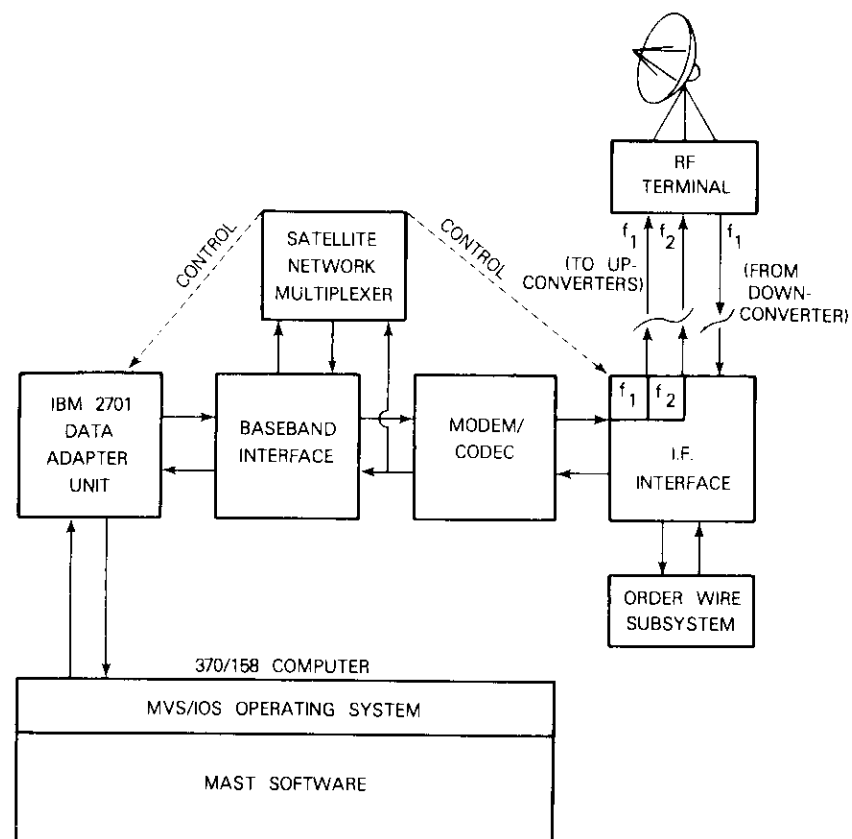


Figure 2. Site System Configuration

The required control functions were incorporated into a time/frequency-division controller developed by IBM. This controller, referred to as the satellite network multiplexer, was located at each earth station and synchronized burst transmissions into fixed time intervals to achieve full utilization of both satellite transponders without mutual interference between transmitting earth stations.

Several major new software packages were required to implement the data link control and network level protocols, to provide the interface between the computer and special hardware systems, and to control and monitor the various applications tests. In addition, the existing IBM network job entry system (JES2 NJE) software product was modified to accommodate the specialized load sharing experiments.

SYMPHONIE COVERAGE PATTERNS

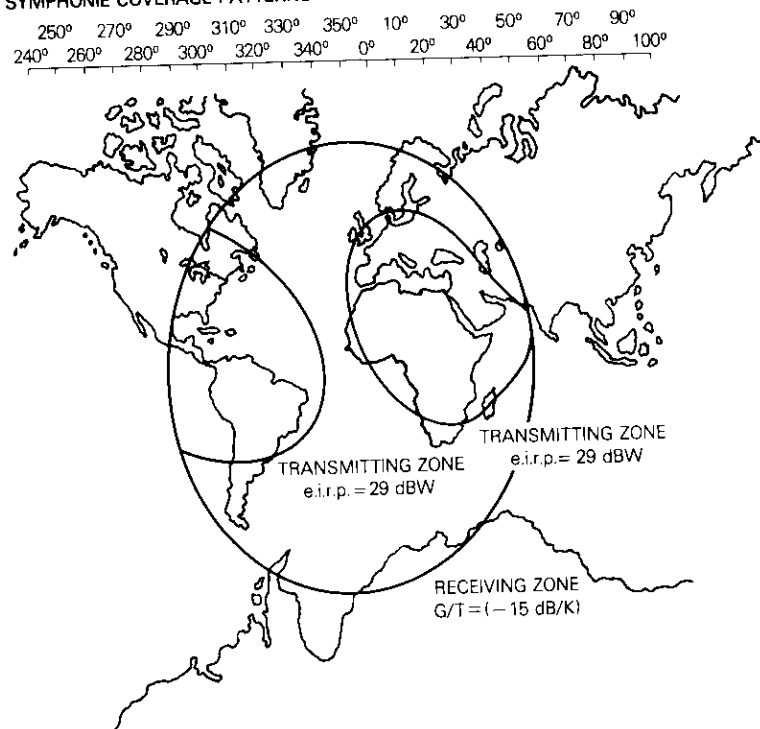


Figure 3. *Symphonie Coverage Patterns*

Hardware description

Symphonie satellite

The SYMPHONIE satellite [3], [4] is equipped with two 90-MHz bandwidth transponders. The main IF amplifier offers a choice of three gain steps, yielding an overall transponder gain at saturation of 108, 110, or 118 dB, respectively. Figure 4 shows the frequency plan of the two flight models. Flight model 2, which was used in the experiment, consists of two bands, A and C, covering the up-link frequency regions, 5940 to 6030 MHz and 6195 to 6285 MHz, respectively.

Table 1 summarizes the important transponder performance characteristics. The values are valid for both satellites and have been

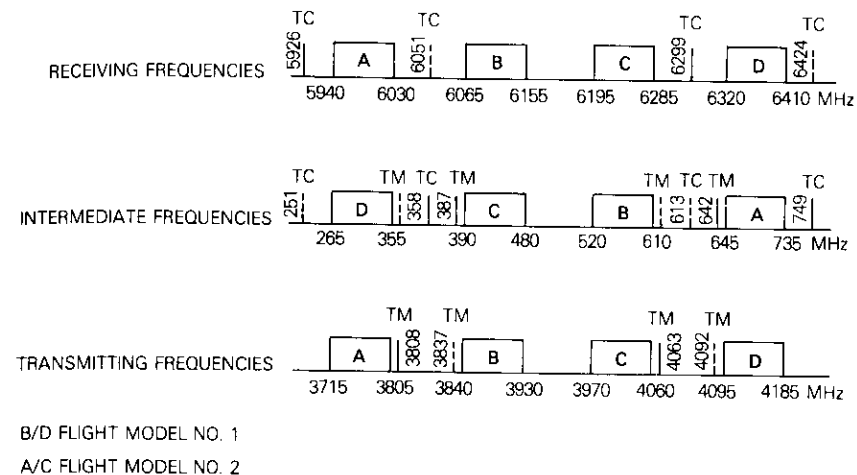


Figure 4. *Symphonie Frequency Plan*

TABLE 1. TRANSPONDER CHARACTERISTICS

Saturation Flux Density at Beam Edge	
High Gain	-87 dBW/m ²
Medium Gain	-79 dBW/m ²
Low Gain	-77 dBW/m ²
Figure of Merit (G/T) at Beam Edge	-13 dB/K
e.i.r.p. at Beam Edge	30 dBW
Transfer Characteristics	
Frequency Response Ripple	1 dB
Gain Slope	0.03 dB/MHz
Group Delay	
Maximum	8 ns
Mid-frequency ±30 MHz	0.35 ns/MHz
Local Oscillator Frequency Stability	3 × 10 ⁻⁶ (25 hr)
Gain Stability	0.5 dB/24 hr
Intermodulation at Saturation	-11 dB
Maximum AM/PM Conversion	5.5/dB
Intelligible Crosstalk	60 dB

confirmed by measurements on the ground and in orbit. Figure 5 gives the TWTA transfer characteristic for single carrier operation, with satellite e.i.r.p. plotted as a function of transmitting earth station e.i.r.p. (measurements made at Pleumeur Bodou, France).

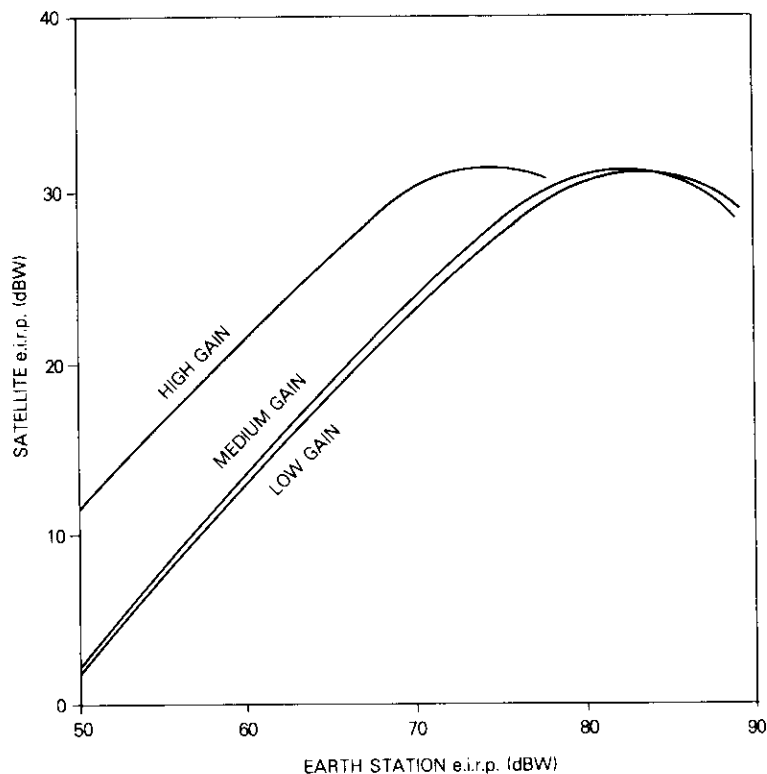


Figure 5. TWTA Transfer Characteristics

Earth terminals

Four separate earth terminals using three different antenna diameters with widely varying performance characteristics were used at the experimental sites. The U.S. sites at Clarksburg and Gaithersburg used 4.6-m diameter antennas. Larger size stations at La Gaude (11.8 m) and Weilheim (8.8 m) permitted an increase in transponder sharing in the European or East spot beam. Table 2 lists the technical parameters of all four stations.

Figure 6 is a general block diagram of the Clarksburg station. After the spacecraft signals are received by the 4.6-m antenna and passed through the polarizer, orthomode transducer (OMT), and transmit reject filter, they are amplified 50 dB by the low-noise receiver (LNR). The

TABLE 2. EARTH STATION PARAMETERS

	Clarksburg	Gaithersburg	La Gaude	Weilheim
Antenna Diameter	4.6 m	4.6 m	11.8 m	8.8 m
Type	Gregorian	Cassegrain	Cassegrain	Cassegrain
Efficiency	55%	55%	55%	55%
Transmit Gain (6 GHz)	46.4 dB	46.1 dB	54.6 dB	52.4 dB
Receive Gain (4 GHz)	43.5 dB	42.6 dB	51.2 dB	48.9 dB
Polarization	Circular	Circular	Circular	Circular
Sidelobe Levels	32-25 log θ	32-25 log θ	32-25 log θ	32-25 log θ
Receiver System Noise Temperature	123 K	135 K	89 K	115 K
Figure of Merit (G/T)	22.6 dB/K	21.3 dB/K	31.7 dB/K	28.3 dB/K
Transmitter Saturated Output Power	350 W	400 W	400 W	400 W
Saturated e.i.r.p.	71.8 dBW	72.1 dBW	80.6 dBW	78.4 dBW

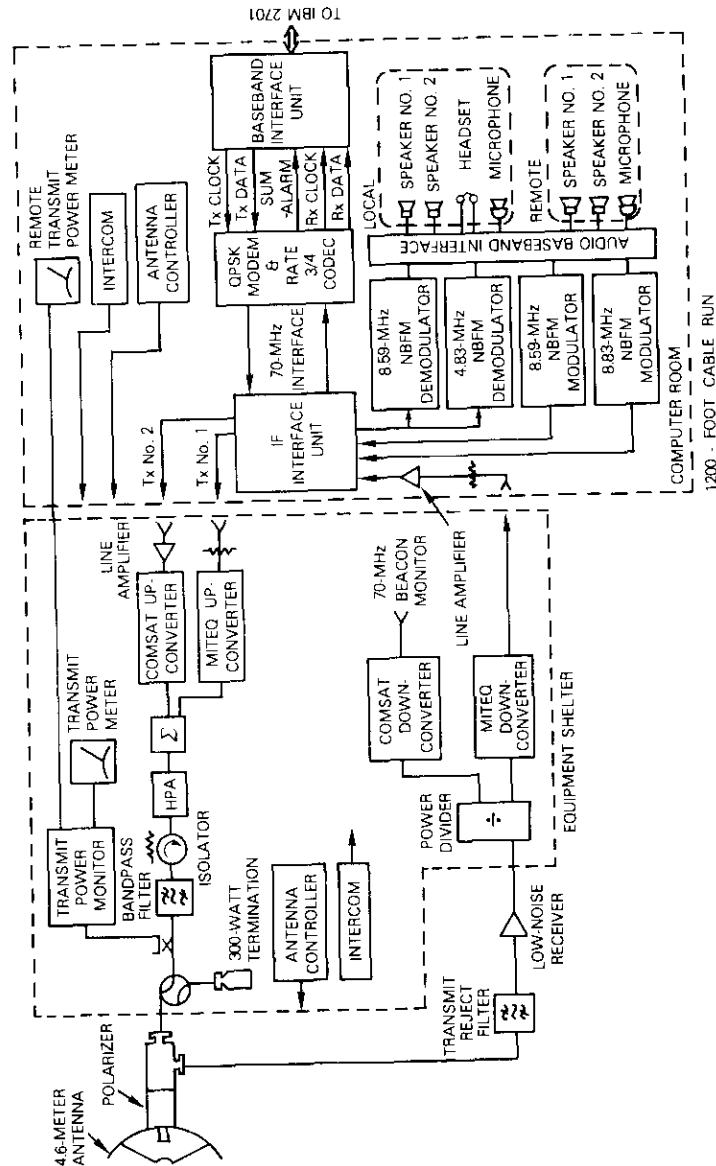


Figure 6. Clarksburg Earth Station Block Diagram

output of the low-noise receiver feeds two down-converters; one is used to monitor the beacon and the other to translate the communications signals to the 70-MHz IF. After a 400-m cable run, the signals enter the computer room through the earth station interface rack containing the IF interface unit, QPSK modem, baseband interface unit, and associated order wire equipment. The interface to both the IBM 2701 data adapter unit and the order wire system is provided by this rack.

The station is equipped with two up-converters using 70-MHz IF. The data signal is modulated onto the IF carrier and then fed through the appropriate cable (under satellite network multiplexer control) to an up-converter. After the signal passes through the high-power amplifier (HPA), bandpass filter, orthomode transducer, polarizer, RF filter, and antenna, it is transmitted to the spacecraft. The order wire IF carriers are sent simultaneously to both up-converters when the circuit is activated. The data and order wire circuits operate as independent communications systems.

Modems and FEC codes

Modems manufactured by Digital Communications Corporation (DCC) were used at the Gaithersburg, La Gaude, and Weilheim sites, and a COMSAT-developed modem was employed at Clarksburg. Although these modems are compatible and functionally equivalent, differences in implementation are evident in both appearance and performance.

The DCC modem system consists of a modulator/demodulator, error-correction codec, and data scrambler. The equipment can handle input data rates of either 1.544 or 6.312 Mbit/s; however, only the 1.544-Mbit/s mode was used for these experiments. Following rate 3/4 FEC encoding of the scrambled input, the coded data at a 2.05867-Mbit/s rate are used for quadriphase shift keyed (QPSK) modulation of a 70-MHz IF carrier having a frequency stability of one part in 10^5 .

The demodulator is specified to acquire carrier and clock recovery within 50 ms with up to ± 10 kHz of frequency offset. A maximum bit error rate of 3×10^{-7} is guaranteed at an E_b/N_0 of 11 dB. The FEC codec employs rate 3/4 convolutional encoding. The systematic, self-orthogonal code has a constraint length of 80 combined information and parity bits and a minimum distance (d_m) of five. This code guarantees that all combinations of two errors in one constraint length

are correctable. In addition, some patterns with more than two errors are correctable.

Although the COMSAT modem is compatible with the DCC modem, it is implemented differently. It consists of two separate hardware components: the modulator/demodulator, and the FEC codec and scrambler. The low-speed version of the COMSAT universal modem [5], which is designed for transmission rates of 60 kbit/s to 10 Mbit/s, was employed. Filter parameters are the only major item which must be changed to accommodate different transmission rates. The conventional modulator processes the input into two parallel streams to drive matched low-pass filters. The filter outputs provide two baseband inputs to two double-balanced mixers driven in quadrature by the carrier frequency oscillator. The mixer outputs are summed, providing a QPSK output signal whose spectral characteristics are determined by the characteristics of the low-pass filters.

In the demodulator, coarse filtering provides thermal noise rejection before the AGC circuit. The constant-level signal is then coherently demodulated by in-phase and quadrature components of the recovered carrier.

The COMSAT FEC codec and scrambler utilize the same basic algorithms as the DCC hardware and have similar bit-error-rate performance. However, the COMSAT rate 3/4 codec includes experimental techniques for reducing ambiguity resolution search time, as well as built-in BER measurement and display circuitry.

Satellite network multiplexer

The satellite network multiplexer controlled the network operation of the four transmitting stations to provide complete interconnectivity of all network nodes. Since two transponders of the SYMPHONIE satellite were used, one for U.S. coverage and the other for coverage of the European sites, each earth station was required to transmit at two separate carrier frequencies. The satellite network multiplexer controlled the transmit time intervals so that each station's bursts were synchronized within an overall transmission frame format.

The satellite network multiplexer transmit format consists of fixed time-duration bursts for each of the four earth stations; the burst sequence assignment is shown in Figure 7. During the first half of the frame interval, two stations in separate down-link coverage zones simultaneously transmit fixed time-duration bursts (each on a different transponder up-link frequency to a separate down-link spot beam)

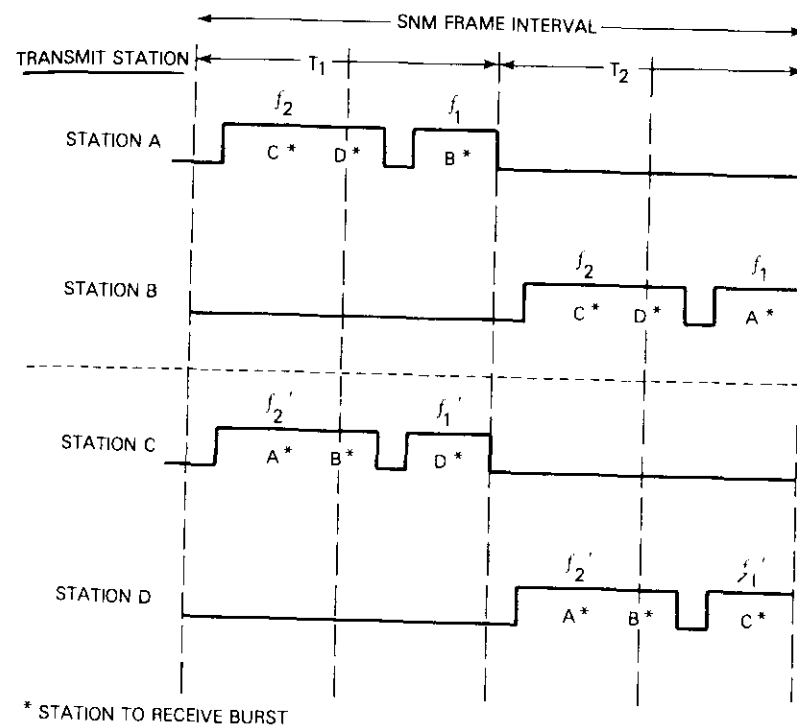


Figure 7. Satellite Network Multiplexer Frame Format

while the other two stations are quiescent. During the second half of the frame interval, the other two stations (also in separate down-link coverage zones) transmit fixed time-duration bursts on separate up-link frequencies. Each station's transmission period is subdivided into two burst intervals (one double burst and one single burst), two modem acquisition delays, and two guard times.

Each burst (either double or single) is composed of a unique word, a transmitting station address, and user data, as shown in Figure 8. The first part of the transmission signal (*i.e.*, the double burst) is always sent to two other stations in the opposite zone using frequency f_2 . The second part (*i.e.*, the single burst) is always sent to the other station in the same zone using frequency f_1 , and is also received by the transmitting station.

Each burst begins with a unique word which is detected at each receiving station within a gated time window generated by logic

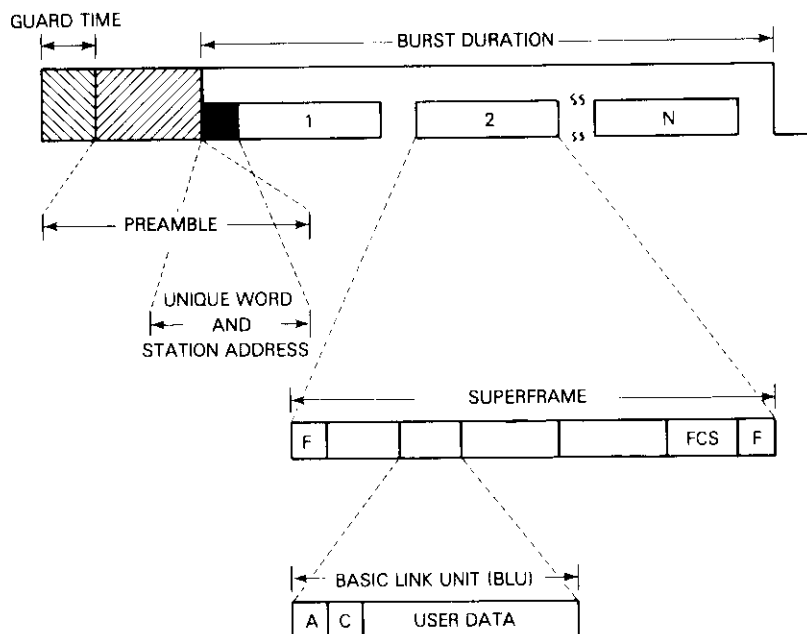


Figure 8. *Satellite Network Multiplexer Burst Format*

associated with the carrier detector. The unique word is followed by the address of the transmitting stations, which causes one of the four interval timers to be initiated.

During normal operation, if all stations in the network are transmitting, four unique words and station addresses are detected within each satellite network multiplexer frame period, the four interval timers are started at every receiving station. Due to variable propagation times and time inaccuracies, the four interval timer stopping points may not be concurrent; therefore, the timer outputs are configured in an "OR" circuit. Thus, the start of the next transmission burst is triggered by the fastest of the four timers, and the other three counters are inhibited (see Figure 9).

This approach maintains synchronization of the network even if one or more transmitting stations stop operation. Even if only one station remains, it will start transmission on its own detected address. The network is also self-synchronizable, since the operator manually

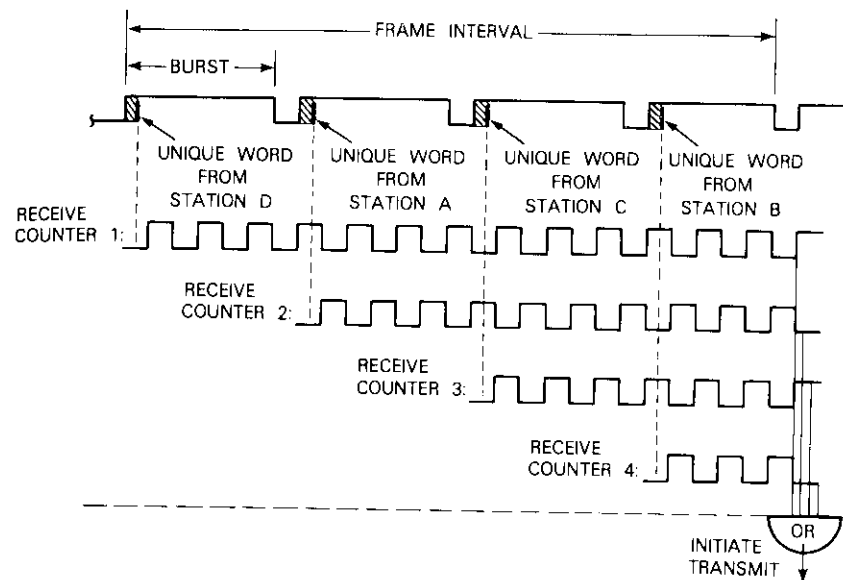


Figure 9. *Satellite Network Multiplexer Synchronization*

enables the four interval timers when a new station is ready to transmit and the new station synchronizes to the currently operating stations.

IBM 2701 data adapter unit

The IBM 2701 enabled the transfer of data between the System/370 and the 1.544-Mbit/s modem. For the experimental program, a modified version of the IBM 2701 with expanded buffering, satellite network multiplexer interfaces, and additional command functions was attached to two dedicated block multiplexer channels of the System/370 (one channel for transmit and one for receive). A special feature permitted the attachment of two channels on the same processor. The IBM 2701 provides the input/output (I/O) channel interface controls and line driver terminations necessary for attachment of the modem terminal device to the CPU system.

The IBM 2701, which uses a standard System/370 channel interface, exchanges data with the System/370 channel in a serial-by-byte, parallel-by-bit fashion; and with the 1.544-Mbit/s modem device serially-by-bit. It performs all necessary bit/byte conversions, word/byte conversions, data buffering control, frame error control

(i.e., frame check sequence generation and detection), zero bit insert/delete in the data sequence, frame synchronization, and interface matching.

Software description

The experimental software system provides a reconfigurable control system to initiate and operate the various network experimental modes. This software package, functionally diagrammed in Figure 10, is known as the method for accessing satellite telecommunications (MAST) and controls all queuing, blocking, routing, error recovery, and data link control (DLC) functions necessary for operating each of the data links within the network under the various experimental configurations.

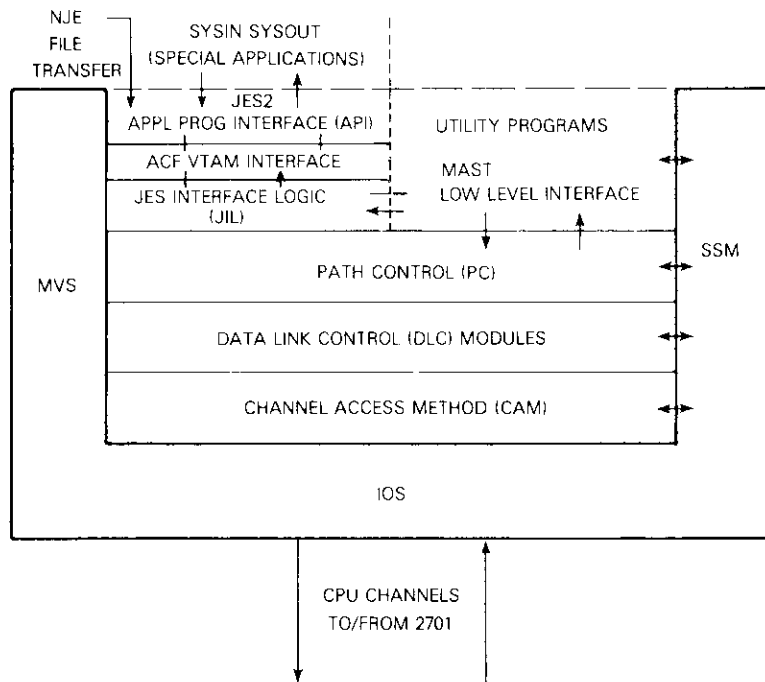


Figure 10. Software Structure

MAST is a communications access method based on a structured architecture that consists of three levels: path control (PC), data link control (DLC), and CPU channel access method (CAM). The user's

interface for sending and receiving data is at the path control level. The satellite system manager (SSM) initializes network control parameters in the MAST software. Additionally, the IBM virtual telecommunications access method (VTAM) provides a transmission control level for the job entry system (JES2) through the applications program interface (API), which was included for the load sharing applications.

Each layer in the MAST software has its own data format. It accepts a binary bit stream from the higher layer and precedes it with its own header. The highest layer in MAST is path control, which accepts basic information units (BIUS) from users (application programs) and prefixes each with a transmission header, thus building a path information unit (PIU). The next layer, data link control, receives path information units from the path control layer and prefixes them with a link header which contains an address and control field, thus building a basic link unit (BLU). The channel access method receives basic link units from data link control and blocks one or more of them into a channel access method buffer, prefixing each with a channel access method local header (CLH) and the first local header with a channel access method global header (CGH), thus building a CAM frame. The IBM 2701 generates a superframe by prefixing each CAM frame with a leading flag, inserting zero bits into the data stream, calculating and appending the frame check sequence (FCS), and appending a trailing flag. The network control layers and their corresponding data formats, which are diagrammed in Figure 11, are summarized as follows:

Layer	Format
User Programs	Basic Information Unit
Path Control	Path Information Unit
Data Link Control	Basic Link Unit
Channel Access Method	CAM Frame
IBM 2701 (hardware level)	Superframe

Path control/data link control

The MAST logic that supports the lower level user interface includes two layers: path control and data link control. Path control is divided between outbound and inbound data. The functions of the outbound path control logic are as follows:

- a. get a MAST buffer;
- b. move the user data into the MAST buffer;
- c. build a transmission header;

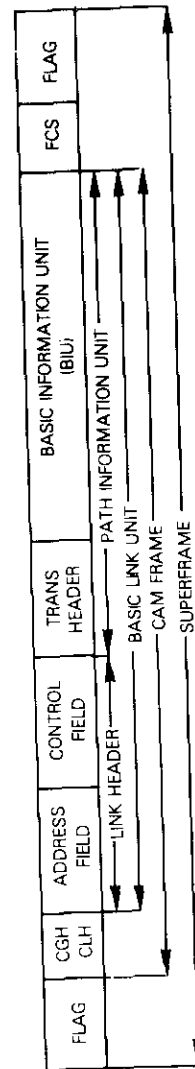


Figure 11. Data Formats

- d. assign a path control sequence number;
- e. store the addresses of the session interface block (SIB) and the data link control block into the MAST buffer prefix; and
- f. place this buffer on a high- or low-priority transmit queue for data link control.

The inbound path control functions are as follows:

- a. find the session interface block for each path information unit;
- b. discard out-of-sequence path information units;
- c. queue path information units for this session in a session interface block queue;
- d. post the user (indicating that there are data for this session);
- e. move the data and system noise figure field into a user-designated area when requested; and
- f. release the MAST buffer to the MAST pool of free buffers.

Data link control follows the International Standards Organization (ISO) HDLC standards [6], using the asynchronous balanced mode extended (ABME) for point-to-point links. This mode requires the data link control module to operate as both a primary and secondary station; the link can operate in either the two-way simultaneous (TWS) mode or the two-way alternate (TWA) mode.

Data link control receives and passes a binary bit stream to path control; it builds the basic link unit by creating and prefixing a link header onto the data received from path control. The basic link units are the data units passed between the channel access method and the data link control.

Channel access method

The channel access method provides a set of macroinstructions to each of the data link control modules operating within the network mode. The channel access method output logic has two main functions:

- a. to block the basic link units formatted by the data link control modules into single transmission frames whenever possible to minimize CPU I/O activity and maximize transmission link throughput, and
- b. to monitor the satellite network multiplexer windows and transmit frames whenever the appropriate frequency window opens.

The channel access method input logic has two main functions:

- a. to store the frames sent over the satellite link in the computer main storage as they are received at the local node, and
- b. to unblock those frames into single basic link units and make each available sequentially on request by the user.

In summary, the channel access method module provides to each data link control module within the network node the ability to transmit and receive user records which have been formatted into basic link unit frames by data link control. The channel access method blocks these basic link units by destination to minimize CPU I/O operations and to maximize link throughput performance. Also, it synchronizes transmissions with the appropriate frequency windows provided by the satellite network multiplexer so that the path control/data link control modules can operate asynchronously with respect to the TDMA frame timing.

Satellite system manager

The satellite system manager is the software module which manages the network operation, enables the local operator to address requests to the local satellite system manager and to exchange messages with the remote operators for experiment coordination. The operator may enter commands at the system console to initiate any of the following actions:

- a. start, restart, or stop a network data link operation;
- b. start or stop application programs;
- c. start or stop sessions between applications programs;
- d. display the status of network configuration, network data links, local applications and active sessions; and
- e. exchange nonformatted messages between operators.

The satellite system manager task, which is started by a command from the operator's console, is created in one MVS address space (or MVT region) by the control program as a result of initiating execution of a job step. It manages the MAST software subsystem including the attachment of the data link control subtask. The satellite system manager resides in all four CPUs and allocates to each operator a share of the subsystem control by providing procedures for initiation, termination, and restart of network data links and application programs that use the satellite communications facility.

Load sharing software

Conceptually, a load sharing network is equivalent to a multiple-input, multiple-server system with a common queue. Unfortunately, the implementation of such a system is subject to the practical difficulties of maintaining a common system job queue and to the transmission system delays encountered in transferring jobs to remote servers. There is no dynamic load-sharing system operating with IBM system control program software that supports widely separated processors. The closest approximation to such a system is JES2 or JES3, operating in a loosely or tightly coupled environment. These systems share a common queue, but the processors must be physically located in proximity. The JES2 NJE provides load sharing across multiple, widely separated establishments, but not on a dynamic basis, and not with a common queue (each establishment has its own job queue).

In standard JES2 processing, jobs enter the system through an input processor, are queued in an execution queue, executed, queued for output, and finally processed on an output device. The left-hand diagram of Figure 12 shows the job flow in such a system. The NJE extension to JES2 adds the network capability as shown in the middle of Figure 12. Jobs may be input at one node, and transmitted to another for execution, and the output may be returned to the originating node. Job routing is performed under operator control or by explicit user specification. Additional JES2 facilities required are the JOB and SYSOUT transmitter/receivers and a network path manager.

The load sharing modifications extend JES2/NJE by adding the functions required to support automatic load sharing. These include the routing decision function and network status management. The former applies a routing criterion to each incoming job, and the latter maintains information about the status of local and remote throughput and delay values at the job and transmission queues, and manages the exchange of this information among the nodes. A schematic of the load sharing NJE is shown on the right of Figure 12.

The load sharing algorithm which was implemented applies a routing decision to each job as it enters the system. The routing decision is based upon two criteria: the estimated job turnaround time (including transmission delay) and the communications overhead on the processor required to support the network. It is necessary for all nodes in the network to exchange information about the status of job and transmission queues so that routing decisions can be made.

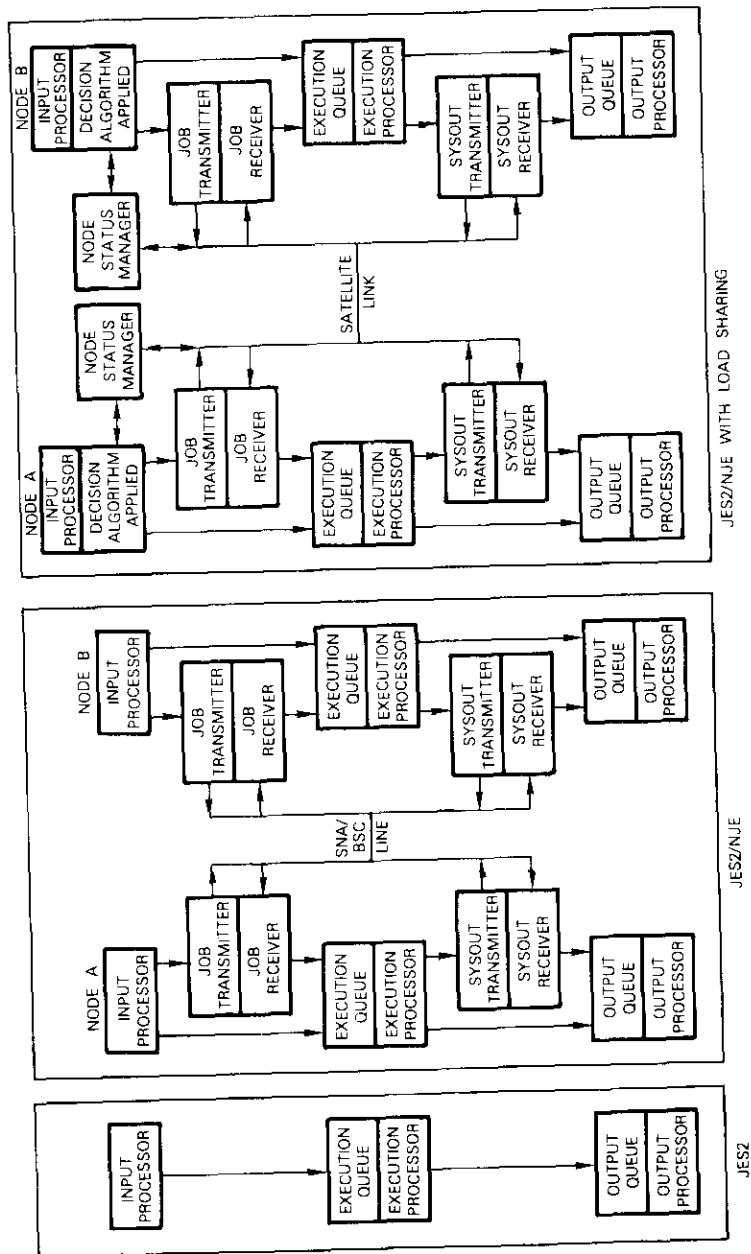


Figure 12. Job Flow

The decision on a job of a specified class (determined by CPU time, memory requirements, etc.) is based solely on the latest information on turnaround times for those jobs and the size of the associated input job stream and expected output (for printer) stream. This is accomplished by computing a decision function D for the job entering at node N , if assigned to each processor ' i '. The decision function for class J has the form

$$D_{ij}^N = a_{1j}T_{ij} + a_{2j}B(1 - \delta_{Ni}) \quad , \quad i = 1, 2, 3$$

where B = sum of input and output stream sizes for incoming job

T_{ij} = latest estimate of average turnaround times for jobs assigned to processor ' i '

$$\delta_{Ni} = 0, \text{ if } N \neq i; \\ = 1, \text{ if } N = i.$$

The actual assignment is made to the processor associated with the lowest value of D_{ij}^N .

The parameters a_{1j} and a_{2j} serve to determine the relative importance that should be given to the balancing of turnaround times (first term) and the communications overhead (second term).

One projected benefit of the algorithm which was developed is that it will operate on job classes independently of one another. The algorithm is also independent of the number of initiators (servers) processing a queue of a specified job class. For unbalanced class loads at various processors, the algorithm will result in equal job turnaround times within each class at each network processor, if all processors structure their class service algorithms similarly, and also balance the mix of job classes over the network.

Experimental program

Three categories of experiments were conducted during the testing period:

- transmission system performance evaluation,
- network control protocol evaluations, and
- distributed data processing applications evaluations.

The purpose of the transmission system performance experiments was to study the relationships of the various transmission subsystem

parameters and their mutual effects on TDMA system performance in terms of transmission efficiency, bit- and frame-error rates, throughput delay, and the variations in these performance parameters under different operating conditions.

The protocol evaluation experiments examined the impact of various link level and network level protocol design parameters on high-speed computer-to-computer data transmission in a TDMA environment. The work in this second category included the design of the necessary software for implementing the link level and network level protocols, and measurements of computer/satellite communications network performance under various modes and conditions.

The data processing applications experiments demonstrated new capabilities which can be supported by high-speed satellite communications networks, and measured computer system performance. The data processing capabilities included high-speed network job entry and load sharing functions. A controlled experimental environment was provided by using application jobs and job streams with specifically chosen characteristics (CPU time and I/O operations) and by operating with controlled CPU and I/O resources dedicated to each experiment.

Transmission system performance

The parameters which affected the network performance were the data transmission rate, bit- and superframe-error rate, propagation delay and its variations, and the parameters of the SNM frame format. The latter include the synchronization and guard time durations, frame period, and preamble size. These parameters were varied to observe the effects on transmission characteristics.

Prior to the establishment of communications links through the SYMPHONIE satellite, a series of tests was performed at COMSAT Laboratories and at IBM Gaithersburg to determine the bit-error-rate performance of each modem. These tests were performed in both a back-to-back configuration and in loopback tests through the SYMPHONIE satellite. They were used to verify the predicted performance curves of the DCC and COMSAT modems and FEC codecs, and to determine the additional degradation, if any, introduced by the nonlinear and dispersive characteristics of the satellite communications channel.

The back-to-back BER performance of the COMSAT modem with FEC is shown in Figure 13. An additional loss of approximately 1.0 dB was incurred when operated over the satellite link (the frequency offset was 4.6 kHz). With either the COMSAT or DCC modem, a bit-error rate

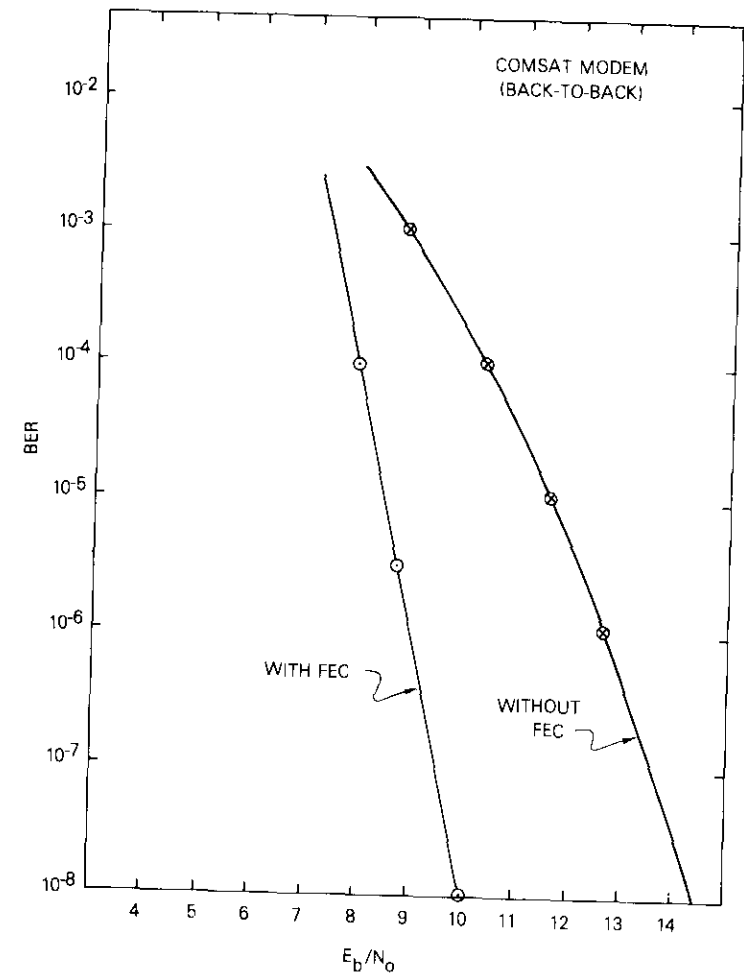


Figure 13. COMSAT Modem Performance

of 10^{-8} could be achieved over the satellite link with a ratio of energy per information bit-to-noise density (E_b/N_0) of 11.0 dB.

Point-to-point measurements of modem performance (in a "continuous" mode, *i.e.*, without satellite network multiplexer burst operation) through the satellite commenced with the installation of the earth terminals at La Gaude and Gaithersburg. Additional tests were conducted as each additional earth station became operational and at the

beginning of each daily test period, so that eventually all twelve simplex links between the four stations were evaluated in a continuous mode.

Records were kept of the measured C/N for each signal received by both the Clarksburg and Gaithersburg stations during the experiments. The unmodulated signal power was measured with a power meter using a receiving filter of known noise bandwidth. The transmitted signals were then removed by request via the order wire channel and the noise level N was measured. The resulting values of C+N and N were then converted to C/N and plotted as shown in Figures 14 and 15 for Gaithersburg and Clarksburg respectively. The shaded portion of each figure indicates the region where the bit-error rate exceeds 10^{-8} . Note that the curves show a considerable variation in performance from day to day, which may be attributed to variations in transmitted power level, antenna pointing or satellite position, atmospheric conditions, etc.

Superframe error rates were measured in the continuous mode for each network link. Frame error rates included frames lost due to receive buffer overruns (caused by contention for CPU and I/O channel resources) and frames rejected due to detected transmission errors. Table 3 shows the average superframe error rates for the twelve transmitter/receiver pairs in the network.

TABLE 3. SUPERFRAME ERROR RATES (PERCENT) FOR CONTINUOUS LINKS

Transmitter	Receiver			
	Gaithersburg	Clarksburg	La Gaude	Weilheim
Gaithersburg	—	2.5	0.6	0.98
Clarksburg	1.5	—	0.5	1.0
La Gaude	1.7	2.5	—	0.5
Weilheim	1.7	2.7	0.4	—

As expected, the La Gaude node had the lowest frame error rate (0.5 percent) since the largest earth station antenna was located there (11.9 m in diameter), and the computer (370/158 CPU Model 3) had the greatest processing capacity in the network (one million instructions per second). The Clarksburg node had the highest frame error rate (2.5 percent) since its earth station antenna was only 4.8 m in diameter and the 360/65 CPU located there had the smallest processing capacity.

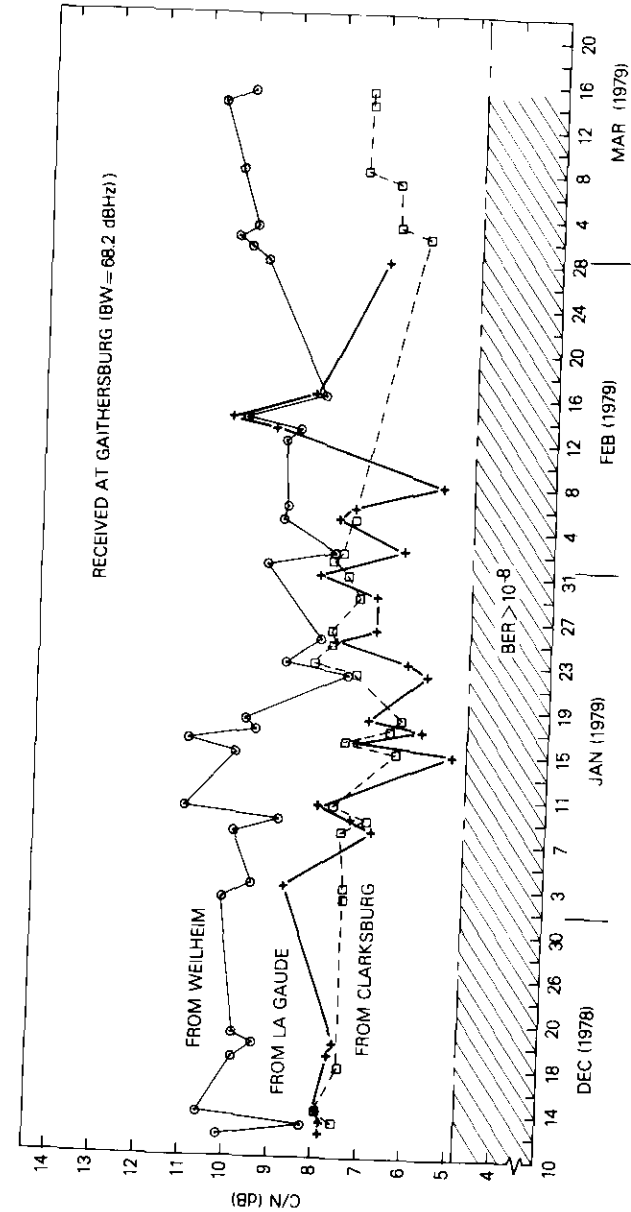


Figure 14. Received Signals at Gaithersburg

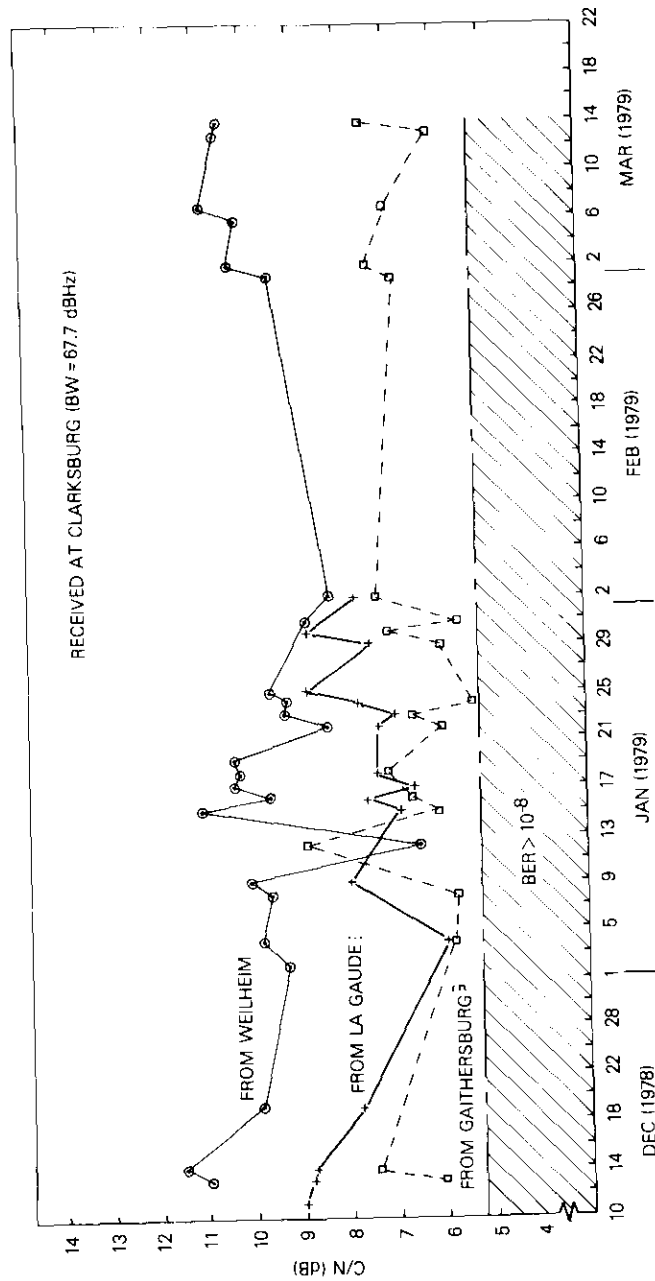


Figure 15. Received Signals at Clarksburg

In general, these frame error rates remained constant over frame sizes ranging from 1 to 16 Kbytes. This may be attributed to the offsetting effects of the inverse relationship of buffer overrun errors and frame size, and the direct relationship of transmission errors and frame size.

The remaining transmission system performance tests were conducted in a "burst" mode, *i.e.*, with the satellite network multiplexer operating. The experimental network consisted of six full-duplex point-to-point links, each with different transmit/response round-trip delay characteristics due to the relative spacing of bursts within the satellite network multiplexer frame period. Three types of links were measured:

- intracontinental, with sequential transmission of bursts between two stations (one station transmits while the receiving station transmitter is turned off, and then the transmit/receive functions are reversed between stations);
- intercontinental, with simultaneous transmission of bursts between two stations; and
- intercontinental, with sequential transmission of bursts between stations.

Preliminary tests showed that a 60-ms preamble at the beginning of each burst was sufficient to ensure a high probability of receive modem acquisition and data reception.

The burst duration was varied over a range of 174 to 1,100 ms to empirically determine its functional relationship to transmission channel capacity. (Hence, the satellite network multiplexer frame size varied from approximately 1 to 7 s.) In Figure 16, which shows the maximum achievable capacity for each type of link, the effect on capacity of the 60-ms preamble is more pronounced with burst durations of less than 374 ms. However, with burst durations of 750 ms or greater, the 60-ms overhead has minimal effect on channel capacity.

With the burst size selected as an integral multiple of the superframe size, sequential superframes were transmitted from a source location and received at a destination which retransmitted them to the original source location. Transmit and receive time tags were recorded by the source location for each frame. The experiment was repeated for various ratios of burst size to superframe size.

Table 4 gives the measurements of round-trip response delays for each of the three link types for various burst durations (and hence satellite network multiplexer frame durations). These round-trip delays

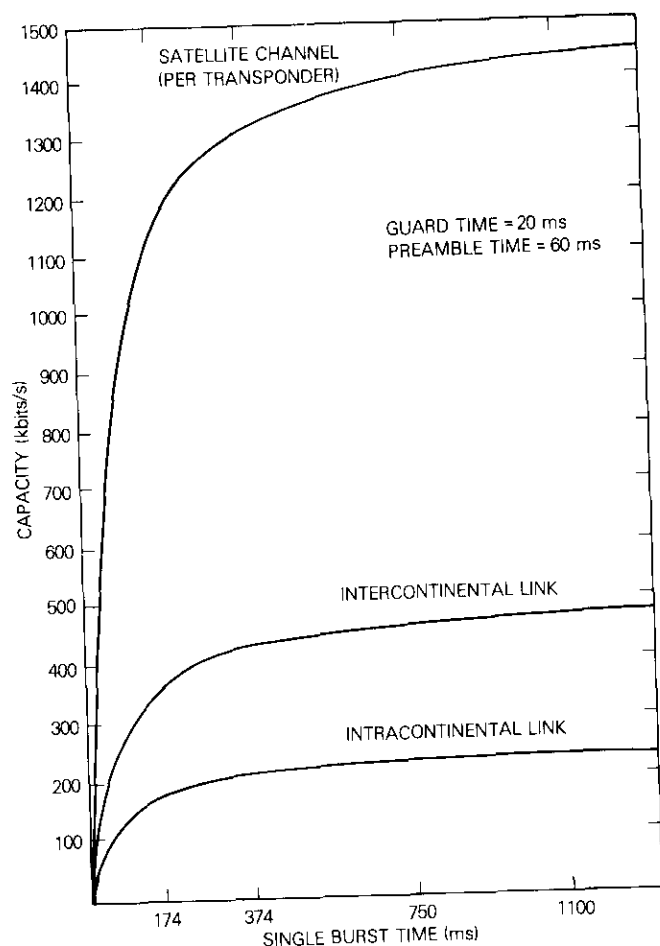


Figure 16. Transmission Capacity vs Burst Duration

include the transmit queuing delay for approximately 10 messages and the processing time at the originating station, the transmission time for a 4-Kbyte superframe, the processing and queuing delays at the destination station, the retransmission time, and the receiver processing and queuing delay at the originating station when the returned frame is received. No delays for HDLC protocol control or error recovery are included in these measured intervals.

The superframe error rates were also measured for the burst mode

TABLE 4. AVERAGE BURST MODE ROUND-TRIP RESPONSE TIMES* (MS)

Link Type	Burst Interval/SNM Frame Period (ms)			
	174/3725	374/2584	750/4840	1100/6940
Intracontinental (noncoincident transmission)	3725	3850	4250	4700
Intercontinental, Type 1 (coincident transmission)	1550	1950	2175	3500
Intercontinental, Type 2 (noncoincident transmission)	3750	3890	4650	5800

* Round-trip response measurements include average processing times, queuing delays, and transmission delays for two-way round-trip transmissions of 4-Kbyte superframes.

of operation, and the results did not differ perceptibly from the superframe error rate measurements recorded for continuous link operation (see Table 3). Therefore, it can be concluded that the 60-ms preamble was adequate to attain a stable receiver lock condition equivalent to a continuous link mode of operation within the time interval of the burst.

Protocol evaluation

The objective of the protocol evaluation experiments was to evaluate the hierarchical network control subsystems (*i.e.*, access methods, data link control, path control, error recovery, and transmission control) in a TDMA environment. The data links provided by the TDMA network were characterized by intermittent transmission periods rather than the continuous transmission typical of most HDLC applications. Therefore, HDLC throughput performance measurements were made for both modes of operation (continuous and burst) and the results were compared.

Selected point-to-point links in the data network configuration were operated in the continuous mode using the HDLC asynchronous balanced mode extended with the reject and selective reject error recovery protocols. The performance of each error recovery protocol was evaluated separately in unidirectional and bidirectional traffic modes. The basic control variables were the superframe size (1 to 16 Kbytes, with one basic link unit per superframe) and the maximum number of outstanding (without acknowledgment) transmitted basic link units

(BLU "maxout" of 31 and 127). The measured variable was the link throughput.

THROUGHPUT FOR CONTINUOUS MODE OPERATION

The objective of these tests was to measure throughput performance for the asynchronous balanced mode of HDLC on a full-duplex continuous satellite data link for bit-error rates ranging from 10^{-8} to 10^{-6} . Throughput measurements were made for all of the test configurations shown in Table 5.

TABLE 5. CONTINUOUS LINK THROUGHPUT TEST CONFIGURATIONS

Superframe Frame Size (Kbytes)	Maxout Value	Error Recovery Mode	Traffic Flow
1, 2, 4, 8, 16	31	Reject	Unidirectional
1, 2, 4, 8, 16	31	Reject	Bidirectional
1, 2, 4, 8, 16	127	Reject	Unidirectional
1, 2, 4, 8, 16	127	Reject	Bidirectional
1, 2, 4, 8, 16	31	Selective Reject	Unidirectional
1, 2, 4, 8, 16	31	Selective Reject	Bidirectional
1, 2, 4, 8, 16	127	Selective Reject	Unidirectional
1, 2, 4, 8, 16	127	Selective Reject	Bidirectional

Figures 17 and 18 show sample results of the bidirectional data flow tests. Three separate sets of data appear on these figures. The dashed curves represent the predicted functional relationship between throughput efficiency and transmitted frame size derived from an analytical model of the HDLC link control process (see the appendix). These predictions were made for variable frame sizes using constant bit-error rates of 10^{-5} , 10^{-6} , and 10^{-7} . The circles (O) indicate the predicted throughput value for a frame size used in an experimental test run for the measured bit-error rate; and the plus signs (+) represent the measured data throughput values. As can be observed from these plots, the measurements of throughput corresponded closely to the model predictions, with an average error of 4.2 percent.

Another format for presenting these test results has been used for Figure 19, which compares the throughput efficiency in the reject and selective reject modes as a function of link bit-error rate. This plot reveals that selective reject provides approximately a 15-percent maximum throughput improvement over reject for a bit-error rate ranging from 5×10^{-6} to 10^{-7} . Outside of this bit-error rate range,

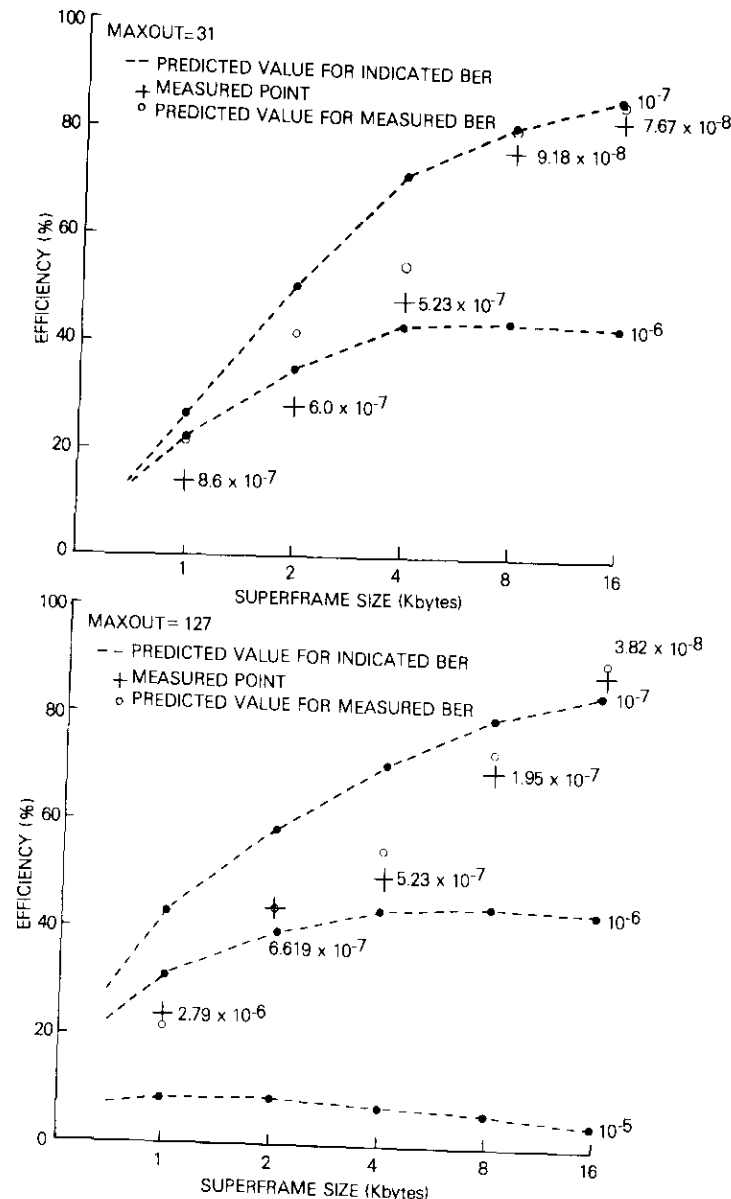


Figure 17. Throughput Efficiency for Reject Mode

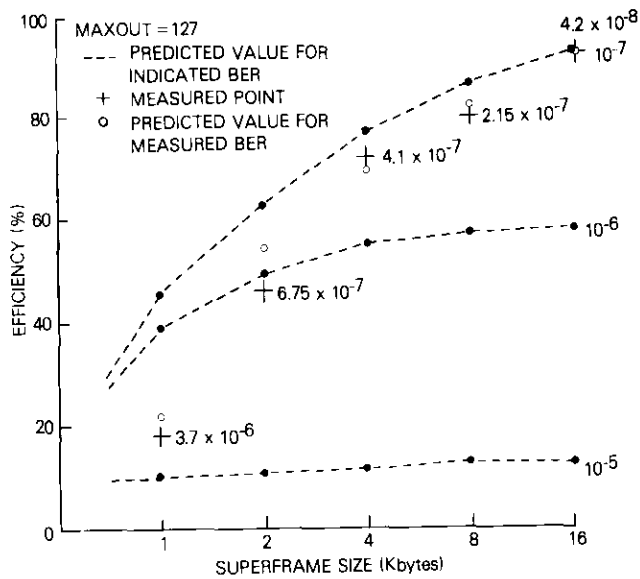
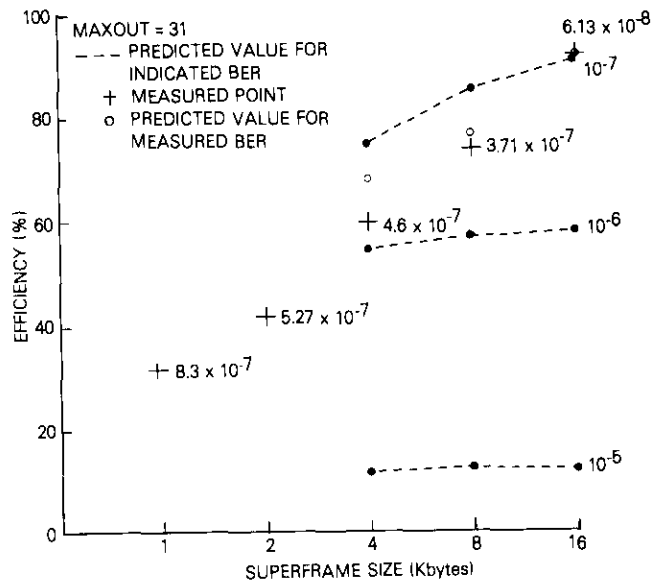


Figure 18. Throughput Efficiency for Selective Reject Mode

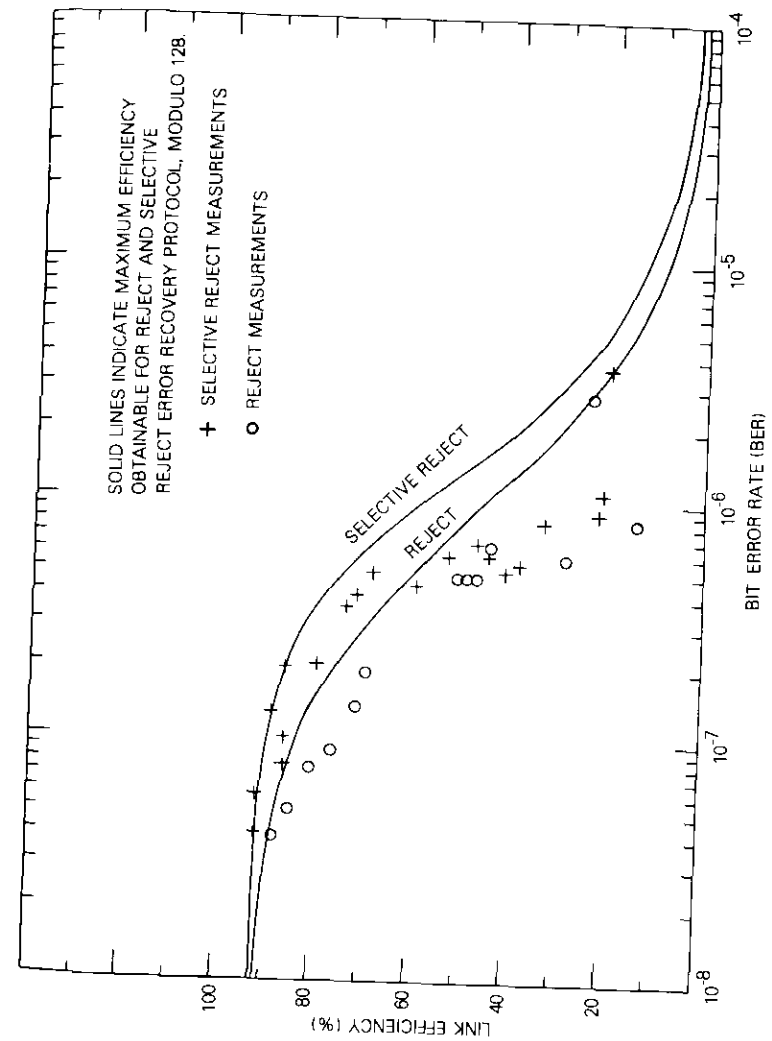


Figure 19. Reject vs Selective Reject, Bidirectional

there is no substantial difference between the throughput performance of the reject and selective reject error recovery protocols defined by the ISO and ANSI standards.

In Figure 19, the test points with the higher effective bit-error rates (approximately 5×10^{-6}) were associated with test runs which used the smaller frame sizes (*i.e.*, 1 and 2 Kbytes). This was due to a higher percentage of lost frames caused by "read overruns" which occurred when smaller frame sizes were employed. The added CPU overhead required to handle these smaller frame sizes increased the interframe gap (or processing delay) between transmitted frames. Hence, the throughput efficiency measured for tests with 1- and 2-Kbyte frames showed the greatest deviation from the predicted maximum throughput performance.

THROUGHPUT FOR BURST MODE OPERATION

The objective of these tests was to collect throughput performance data for the HDLC protocol for all links provided by the TDMA data network. The effects of the burst mode operation, using different values for SNM frame size and link control protocol parameters, were measured and compared with the predicted throughput values derived in the appendix. The predicted values include the effects of all overhead associated with the data processing and satellite network multiplexer subsystems (*i.e.*, interframe gaps between transmitted HDLC frames, preamble size, guard time, etc.).

Figures 20, 21, and 22 show samples of throughput measurements obtained from the tests for 1-, 2-, and 4-Kbyte superframe sizes, respectively. These results were obtained for the link between Weilheim and Gaithersburg, which is the double-burst noncoincident type. Predicted throughput efficiencies for error rates of 10^{-8} , 10^{-7} , and 10^{-6} are superimposed on the measured values for tests using 1-, 2-, and 4-Kbyte superframe sizes. Additionally, predicted values for each test using the error rate measured during each test run are shown.

Throughput efficiency measurements correlate well with predicted values for 1- and 2-Kbyte superframes with double burst sizes of 348 and 748 ms (corresponding to satellite network multiplexer frame sizes of 1.364 and 2.564 s, respectively). However, for the larger double burst sizes of 1,500 and 2,200 ms (corresponding to satellite network multiplexer frame sizes of 4.820 and 6.920 s, respectively), test results with the 1- and 2-Kbyte superframes show a more significant discrepancy between measured and predicted values. This discrepancy was

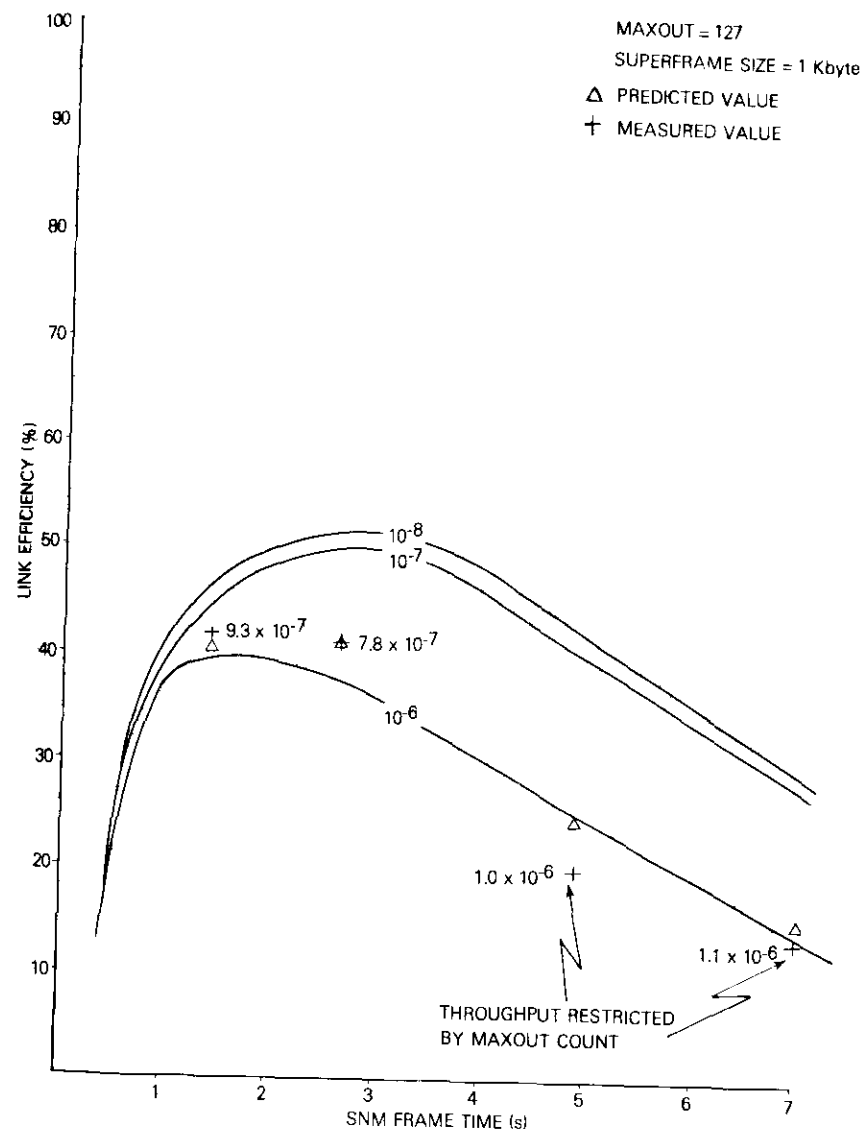


Figure 20. Throughput Efficiency for 1-Kbyte Frames

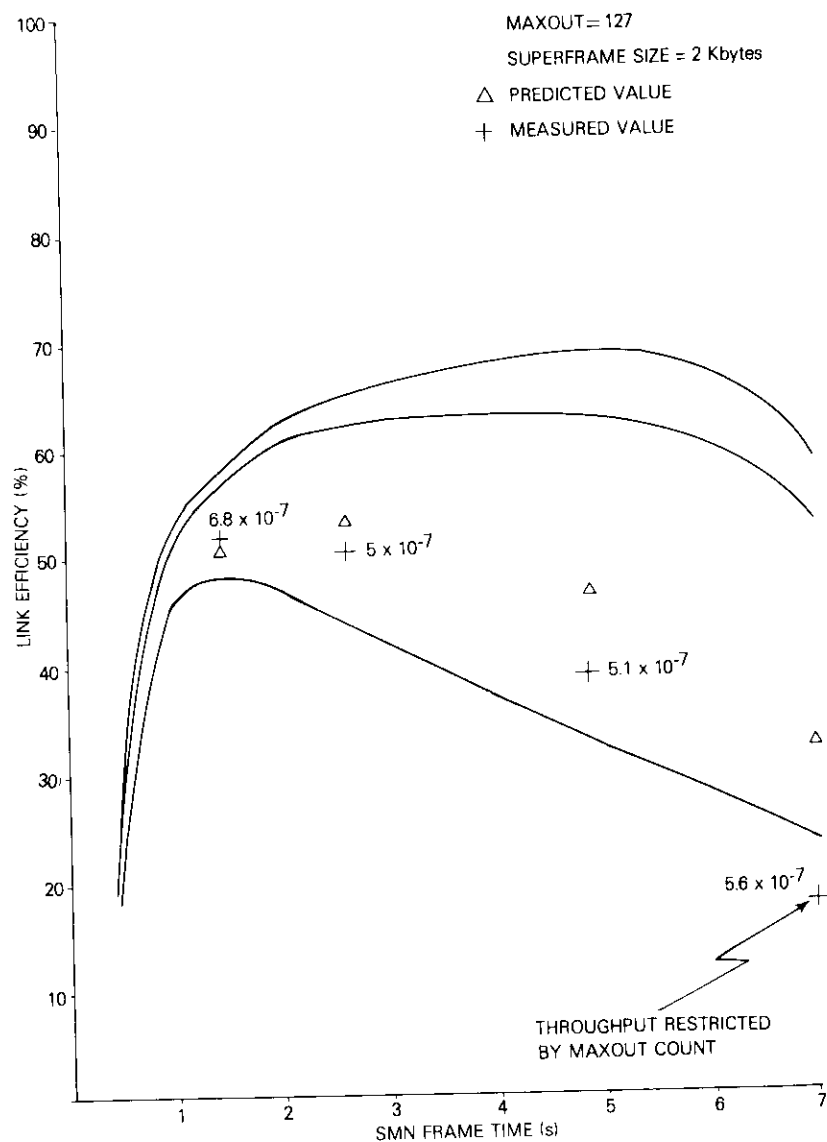


Figure 21. Throughput Efficiency for 2-Kbyte Frames

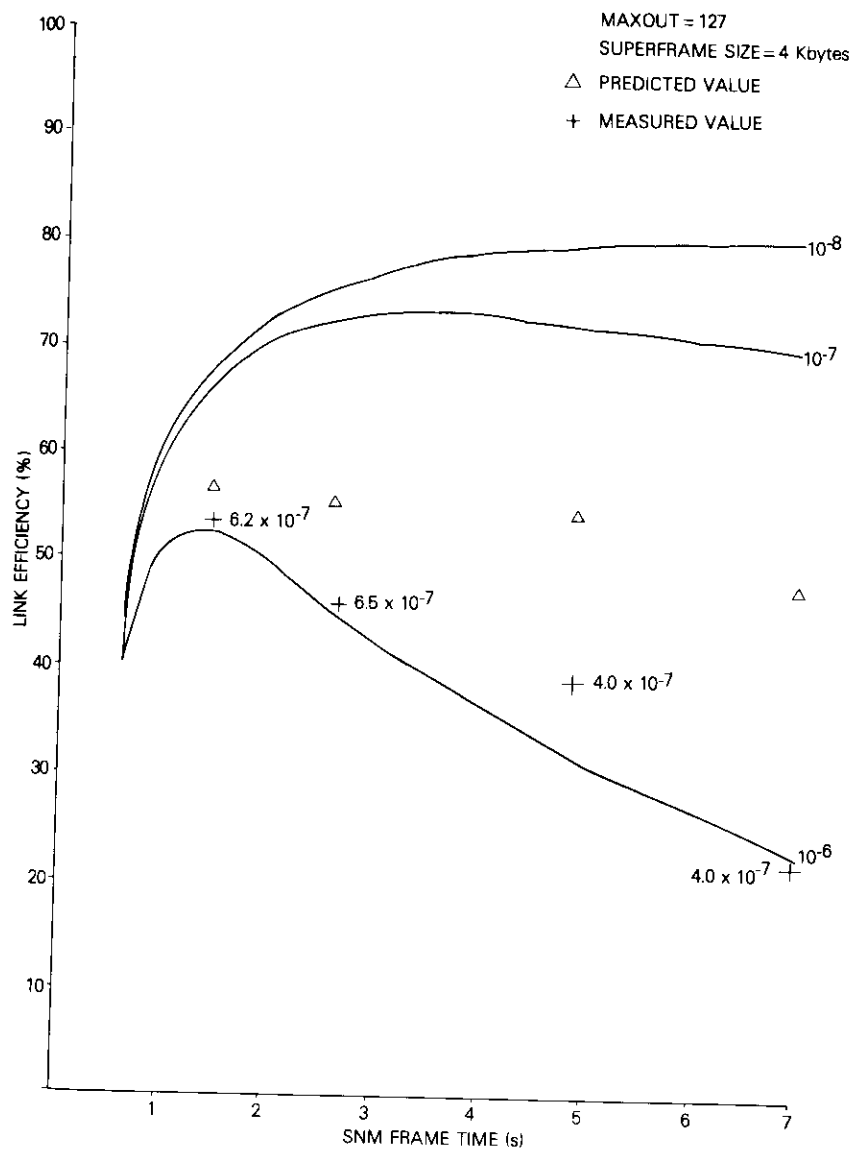


Figure 22. Throughput Efficiency for 4-Kbyte Frames

probably due to a larger interframe gap interval (the time between successive transmitted superframes caused by software overhead) than that assumed in the models used to generate the predicted values. Additional degradation may be attributed to the inability of the system to use the entire transmission capacity of the larger double burst intervals because of the HDLC protocol maxout limit. This limit restricts the amount of data that can be transmitted without acknowledgment to 127 frames.

The test runs which employed 4-Kbyte frames experienced no throughput degradation due to maxout limitations for the entire range of burst intervals used in the experiment. However, Figure 23 shows a difference between measured and predicted throughput results which can be attributed to the increased CPU paging overhead associated with processing the larger 4-Kbyte frame sizes when a 2-Mbyte core limitation is imposed. The degradation was eliminated on test runs in which the CPU was configured to operate with 4 Mbytes of core.

In general, the tests have demonstrated a solution to the complex problem of synchronizing transmissions operation through a shared multiple-access satellite channel. Furthermore, test results indicate that the HDLC protocol can be effectively employed as the link control mechanism for transferring data through such intermittently available channels.

Distributed data processing applications

Networking represents one facet of computer communications which attracts wide interest. Computer networks may be used to provide system capabilities that surpass those of a single isolated computer. The following capabilities are among those that combined satellite communications and computer systems can provide:

- a. sharing computer files and resources,
- b. load sharing among computers, and
- c. emergency backup in case of computer failure.

The availability of satellite facilities offering high-data-rate, low-error-broadcast channels which are insensitive to distance will accelerate the development of such networks.

The purpose of the distributed data processing applications experiments was to demonstrate the function and measure the performance of new data processing capabilities which can be supported by these high-speed data satellite communications networks. The data process-

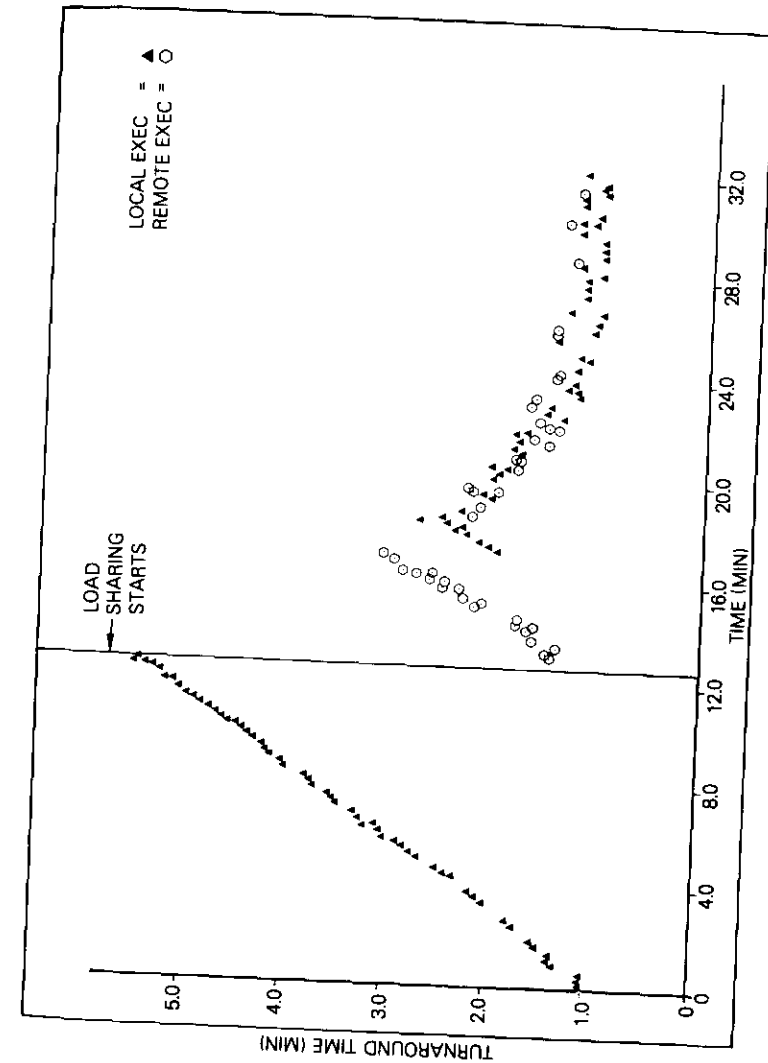


Figure 23. Turnaround Time at Gaithersburg

ing capabilities included load sharing and high-speed network job entry. A controlled experimental environment was provided by using applications jobs and job streams with specifically chosen characteristics (CPU time and I/O operations) and by operating with controlled CPU and I/O resources dedicated to each experiment.

LOAD SHARING

The load sharing experiments were conducted between the IBM 370/158 computers at Gaithersburg and La Gaudé, using the full 1.544-Mbit/s communications capacity in a full-duplex continuous mode. Table 6 shows the parameters used for jobs submitted in a representative experiment. Figure 23 shows the measured turnaround time for jobs submitted at Gaithersburg vs the local clock (0 is the start of the experiment) and Figure 24 shows the measured turnaround time for those submitted at La Gaudé.

TABLE 6. EXPERIMENT PARAMETERS

Parameter	Gaithersburg	La Gaudé
Number of Cards Per Job	Fixed: 100	Fixed: 100
Number of Printed Lines Per Job	Fixed: 1000	Fixed: 1000
Execution Time	Fixed: 1 min.	Fixed: 1 min.
Job Submission Rate (1 job at a time)	Fixed: 6/min.	Fixed: 1/min.
Overload Threshold	5 jobs/min.	5 jobs/min.
Local Processor Load	Overload	Underload

As expected, when load sharing is off, a queue builds up at Gaithersburg since there is an overload at this site. After 12 min. the turnaround time is longer than 5 min. for each individual job. Load sharing was switched on 12.5 min. after the start of the experiment. Then, for almost 9 min., all incoming jobs were sent to La Gaudé to be executed; during that period, the queue at Gaithersburg was reduced and jobs were again executed locally. This process continued until a steady state was reached about 29 min. after the start of the experiment.

The job turnaround time is the main performance criterion from a user point of view. However, load sharing also results in greater system-wide job throughput, especially under unbalanced loads. This is demonstrated in Figure 25, which shows the job submission rates for the entire system as well as for individual nodes, and in Figure 26,

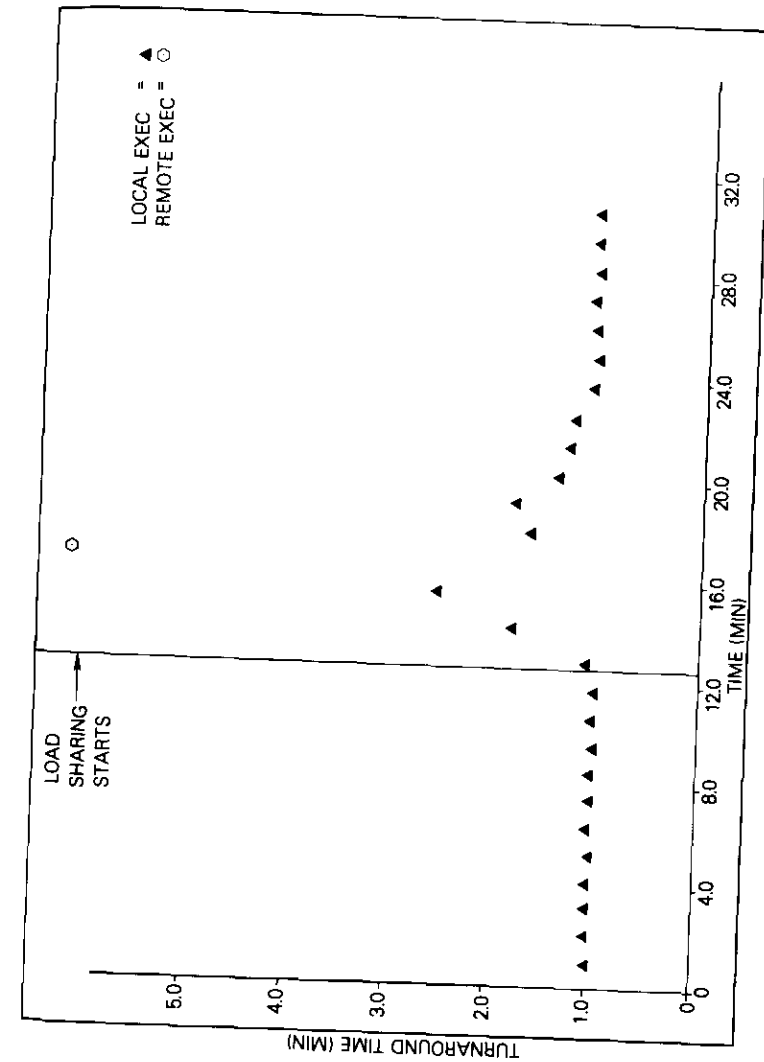


Figure 24. Turnaround Time at La Gaudé

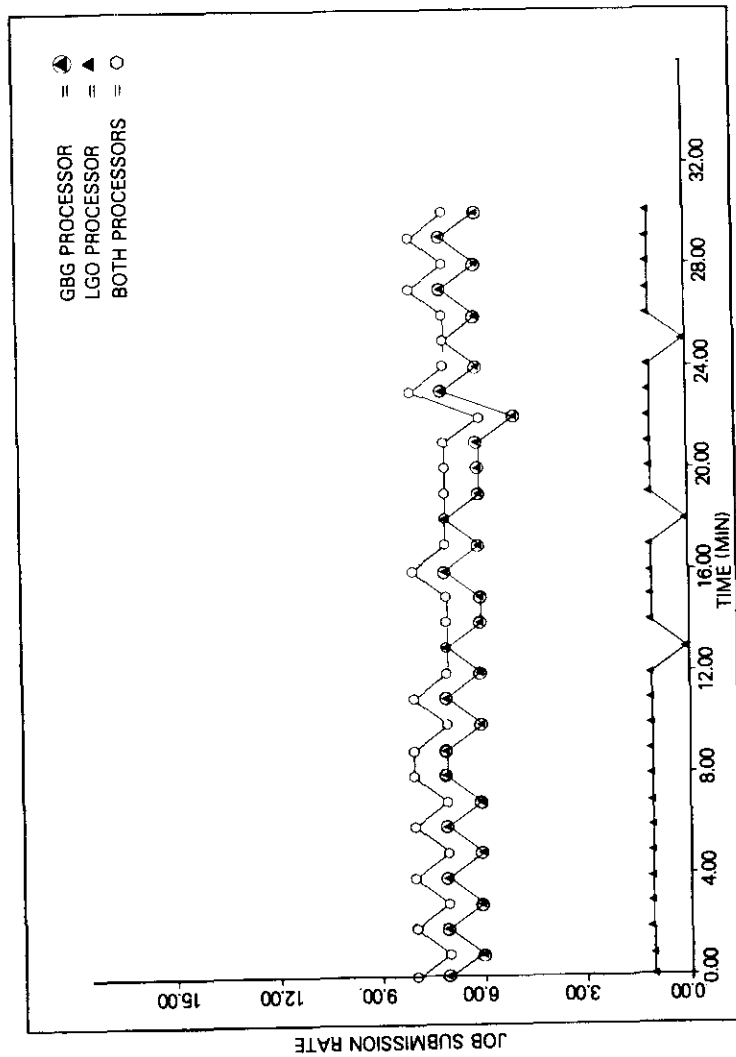


Figure 25. Job Submission Rate

which shows the job output rate before and after load sharing has reached a steady state. As shown in Figure 26, the total job throughput for the system of 6 jobs/min. without load sharing increases to about 8 jobs/min. with load sharing, mainly because the unsaturated La Gaude processor is given a higher job load while the saturated Gaithersburg processor continues at its peak capacity.

Load sharing also yields a better utilization of system-wide resources, in this case, the job initiators. Figure 27 shows that the system initiators have a high average idle time without load sharing, which is reduced if the system is in the load sharing mode.

NETWORK JOB ENTRY

The test objective was to demonstrate the functional benefits of a network job entry system combined with a network of high-speed multiple-access satellite communications channels. The Network Job Entry (NJE) facility in JES2 is designed for users with multiple CPUs that are geographically separated. The NJE facility provides for the transmission of selected jobs, operator commands, messages, SYSOUT data, and accounting information between communicating nodes in the experimental network.

The submitter of a job (or the CPU operator) specified the node at which it was to be executed and the destination of the output. A job could be entered into the network from any JES2 controlled local input device, any remote terminal, or through any internal interface at a given node, and could be queued for transmission to any node in the network.

When transmission to the execution node was completed, the job was placed on the queue. Output data sets generated by its execution were stored at the executing node. If the output was intended for a node other than the executing node, the output was transmitted when execution was completed.

The NJE system was used to demonstrate that significant operational benefits could be derived through the application of NJE functions together with a high-speed satellite communications network. The NJE facility was employed to perform experimental software system updates for Gaithersburg via the satellite communications network on a daily basis.

Source modules were transmitted (0.5- to 2.47-s transmission times) from a central software maintenance facility (Gaithersburg) and executed at the remote nodes to upgrade the experimental software.

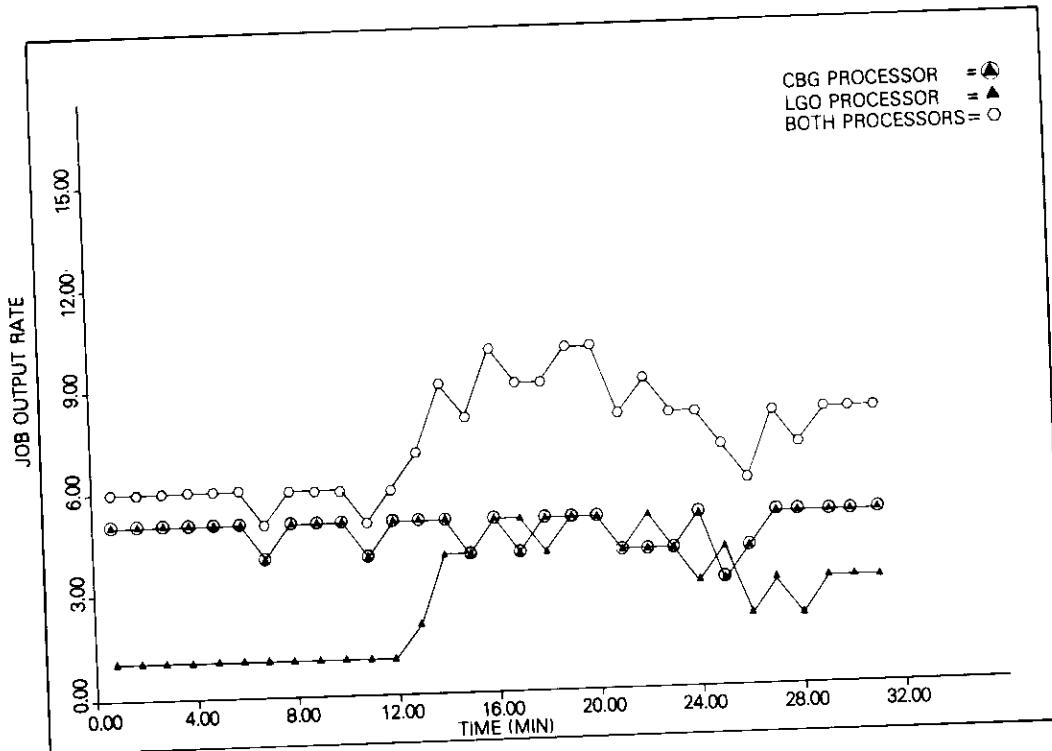


Figure 26. Job Output Rate

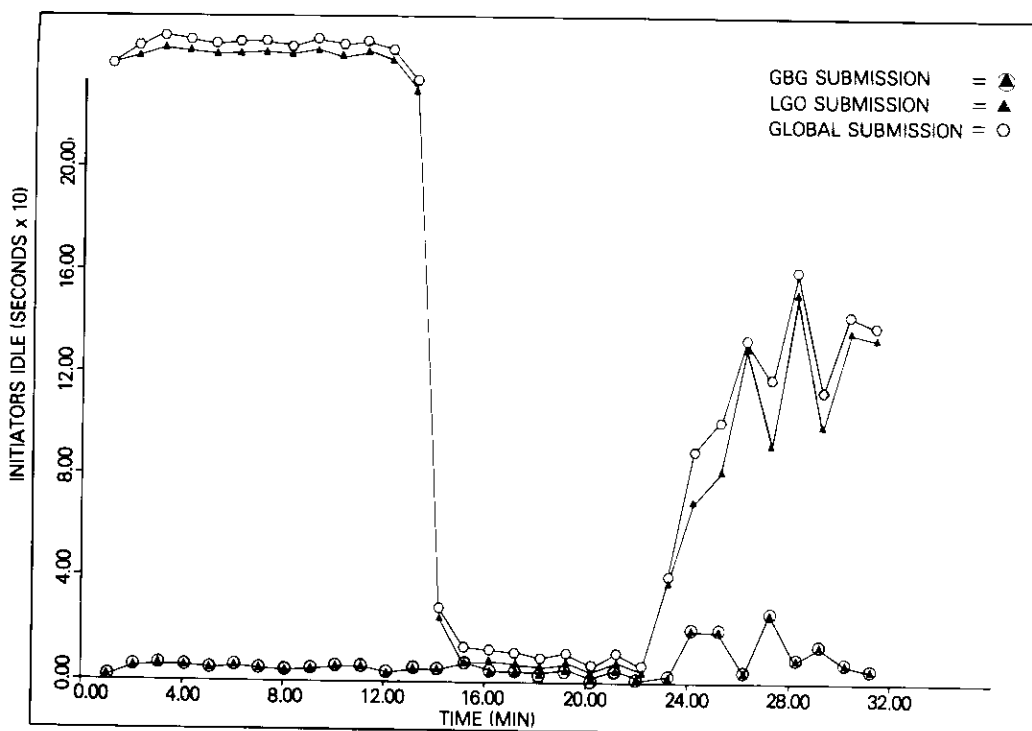


Figure 27. Initiators Idle

Results of job execution were retransmitted to the originating site and the success (or failure) of the software update was evaluated. If the job was executed properly, the remote node operator was instructed to install the new software module in the operational system. This process was completed in minutes. Although such network usage had been envisioned, the initial use dramatically demonstrated the possibilities for software installation and updating between widely separated sites.

Conclusions

Future high-speed satellite communications networks will permit geographically distributed computers and resources to be economically operated as integrated data processing facilities. These computer-to-computer networks (with links operating in the range of CPU channel speeds) and pervasive terminal-to-computer subnetworks, which provide large user populations access to extensive data processing resources, can facilitate the development of new user applications that heretofore were not possible. To achieve this goal, new techniques for accessing satellite transmission channels and new methods for employing data processing facilities must be developed.

In these experiments, a computer-to-computer network based on multiple access to a high-speed satellite broadcast channel was empirically evaluated and demonstrated to have operational value for high-speed data processing applications. The multiple-access technique provided a fully interconnected 4-node network and enabled efficient sharing of a segment of the satellite's transmission capacity by the four earth stations.

An important feature of the data-only TDMA controller was the long frame time employed (of the order of 1 to 7 s). Frame lengths of this duration can result in equipment cost savings in network synchronization and burst acquisition, since interburst guard times and preamble sizes can be relatively large without introducing significant overhead. These experiments demonstrated that not only can very simple data-only TDMA systems be implemented, but that, through proper choice of HDLC protocol parameters, the impact on the link throughput can be minimized.

In computer networks characterized by high traffic volumes, where high throughput is more important than short response times, such a long-frame fixed TDMA system would operate quite effectively. It has

an advantage over a terrestrial network in that traffic from a single node to various geographically distributed destinations can be statistically multiplexed into the transmitting station's burst, thereby adapting to variations in network traffic patterns.

The concept of statistical traffic averaging in high-speed satellite communications channels can provide more pervasive and cost effective transmission facilities than those currently available. Such availability is expected to provide far-reaching benefits to users who employ distributed computer resources and dispersed information data bases.

Specific program achievements relative to the development of new data processing methods for employing these future transmission facilities areas follow:

- a. evaluation and demonstration of high-speed satellite communications network support of distributed data processing functions, including network job entry, tape-to-tape and disk-to-disk file transfer, and dynamic network load sharing; and
- b. evaluation of link level (point-to-point and broadcast) and network level protocols in a multihost computer network interconnected by high-speed satellite transmission channels.

As demonstrated in these tests, file transfer applications which previously required hours (and perhaps days) for transmission can now be accomplished in seconds and minutes. Also, it was demonstrated that greater system productivity could be achieved by automatically routing jobs to more uniformly distribute work load over geographically dispersed data processing resources. This concept should provide economies heretofore unavailable to data processing equipment users.

In the future, new data processing applications such as those demonstrated in these experiments should evolve to exploit the high-speed transmission networks that enable distributed computers to communicate at speeds which approach the maximum I/O channel rates.

References

- [1] J. Marchese, W. Cook, et al., "Computer/Satellite Communications Experiment: Phase 1 Final Report," submitted to the FCC in December 1977.
- [2] J. Marchese, W. Cook, et al., "Computer/Satellite Communications Experiment: Phase 2 Final Report," submitted to the FCC in October, 1979.

- [3] "The Symphonie Project" (seven papers in French) which appeared in *La recherche spatiale*, Volume XIII, No. 5, September-October 1974.
- [4] G. Mösl and J. Muller, "In-Orbit Performance and Experimental Utilization of the Symphonie Satellites," *Satellite Communications: Future Systems, Progress in Astronautics and Aeronautics*, Volume 54, David Jarrett, ed.
- [5] C. J. Wolejsza, D. Chakraborty, and V. Uzunoglu, "A Universal Modem Design for Digital Satellite Communications," 1976 International Conference on Communications, Philadelphia, Pennsylvania.
- [6] International Standards Organization, Documents ISO/TC97 SC6 N1464 with revision N1499; and ISO/TC 97SC6 N1463.

Appendix. Data link control throughput performance

All point-to-point links in the TDMA data network were operated in the HDLC asynchronous balanced mode (ABM) using both the reject and selective reject error recovery protocols. The data links provided by the TDMA network were characterized by intermittent transmission periods (within a TDMA frame cycle) rather than continuous transmission which is typical in most HDLC applications. Therefore, HDLC throughput performance predictions were made for both continuous and intermittent links.

HDLC throughput predictions (continuous links)

Analytic models which were used to predict the throughput performance of HDLC protocols over continuous links have been described in detail [A-1]. These models, derived for satellite data communications links, assume that the transmission capacity of the channel is available on a continuous basis.

Throughput efficiencies of computer communications links using HDLC have been derived from these models for the forms of reject and selective reject error recovery protocol used in these experiments. In addition, the models have also been used to estimate the maximum achievable throughput over a wide range of data frame sizes and bit-error rates. Figures A-1 and A-2 show the results of these predictions for reject and selective reject error recovery using Modulo 128.

HDLC throughput predictions (intermittent links)

Recently, a model for data link control protocols operating through a TDMA system was presented along with predictions of throughput and response time [A-2]. The results of this general analysis have been used to derive throughput predictions for the specific response mode and TDMA burst pattern employed in the experimental program.

Since the asynchronous balanced mode which was employed is, in effect, a superposition of two asynchronous response mode links in opposite direc-

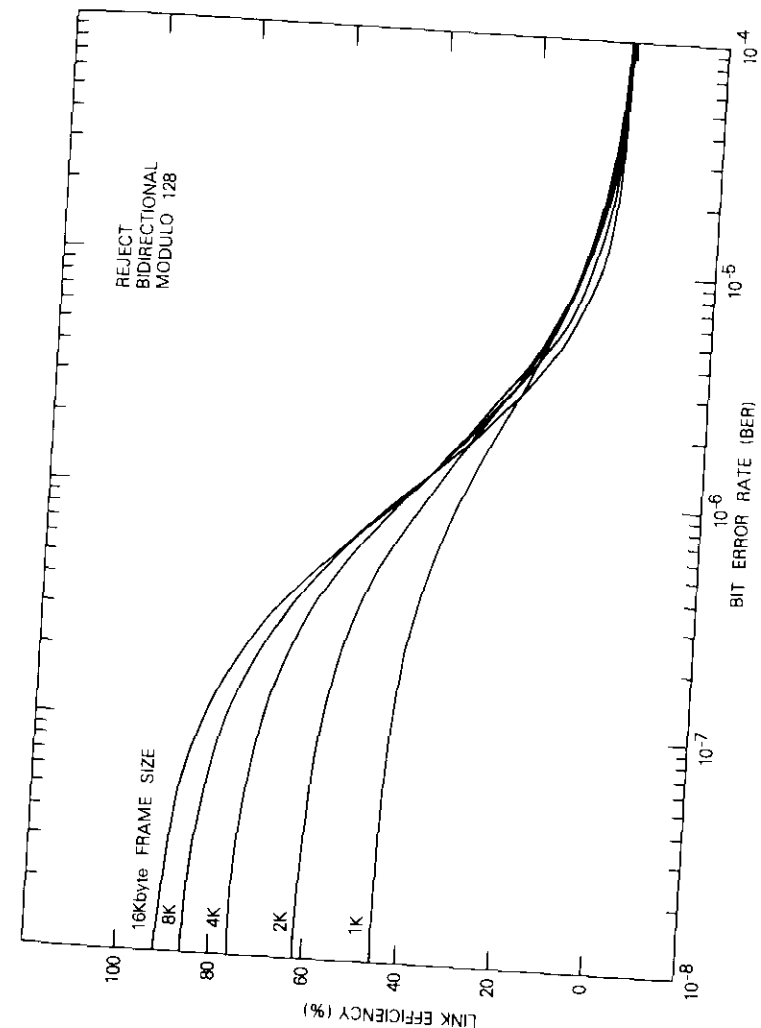


Figure A-1. Link Efficiency vs BER, Reject, Bidirectional

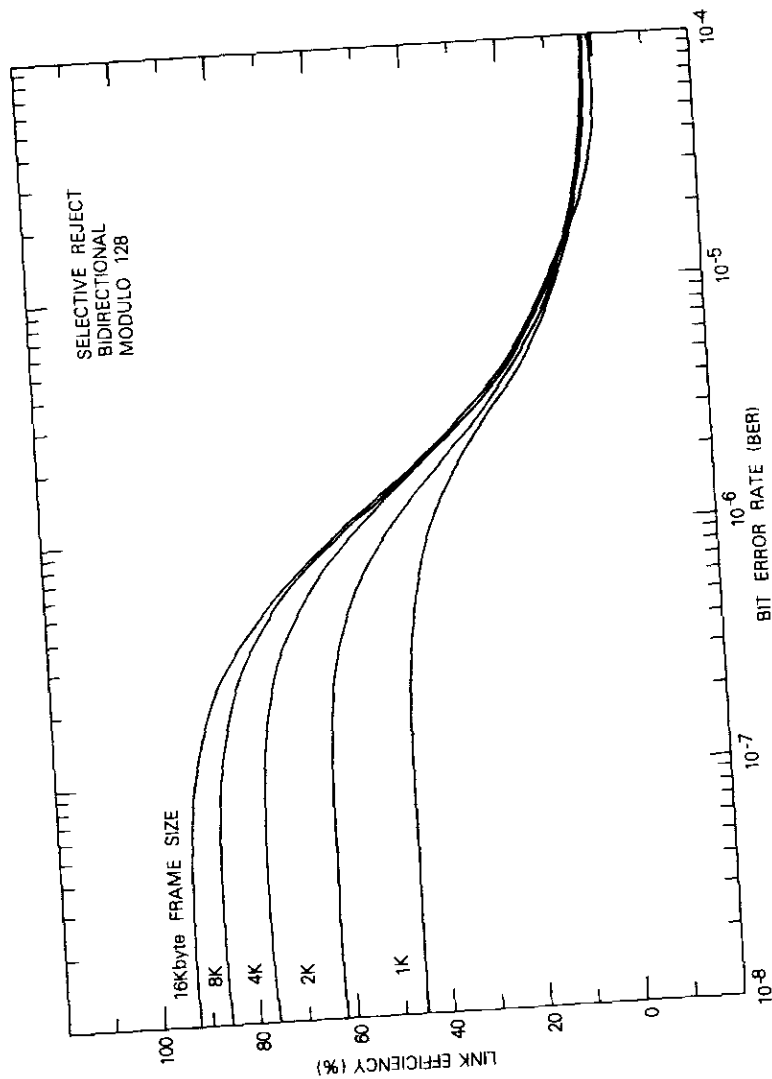
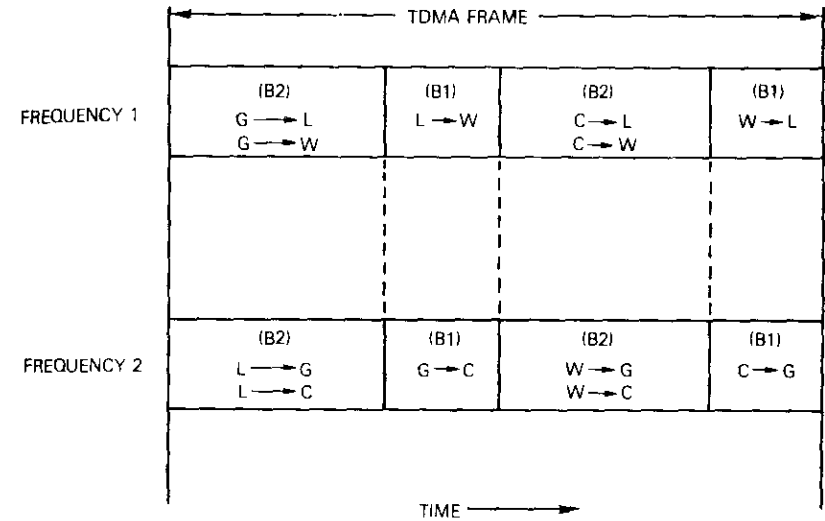


Figure A-2. Link Efficiency vs BER, Selective Reject, Bidirectional

tions, the models are defined for each ARM component link. Figure A-3 shows the burst pattern in a TDMA frame, and Figure A-4 shows the structure of bursts. Two types of bursts are present: single bursts (of duration B_1) containing n_s superframes, and double bursts (of duration B_2) containing $2n_s$ superframes.



G = GAITHERSBURG
C = CLARKSBURG
L = LA GAUDE
W = WEILHEIM

Figure A-3. TDMA Burst Pattern Seen at the Satellite Transponders

Single bursts contain only one logical data link, whereas double bursts may contain up to two logical links. The twelve logical links can be classified into three categories, based upon the separation of the bursts for each link and its complement (the complement of $A \rightarrow B$ is $B \rightarrow A$):

- SB links in which the link and its complement occur in single bursts;
- DB links in which the link and its complement occur in double bursts;
- DBC links in which the double bursts are coincident.

Table A-1 shows the time intervals between each link and its complement for each link type.

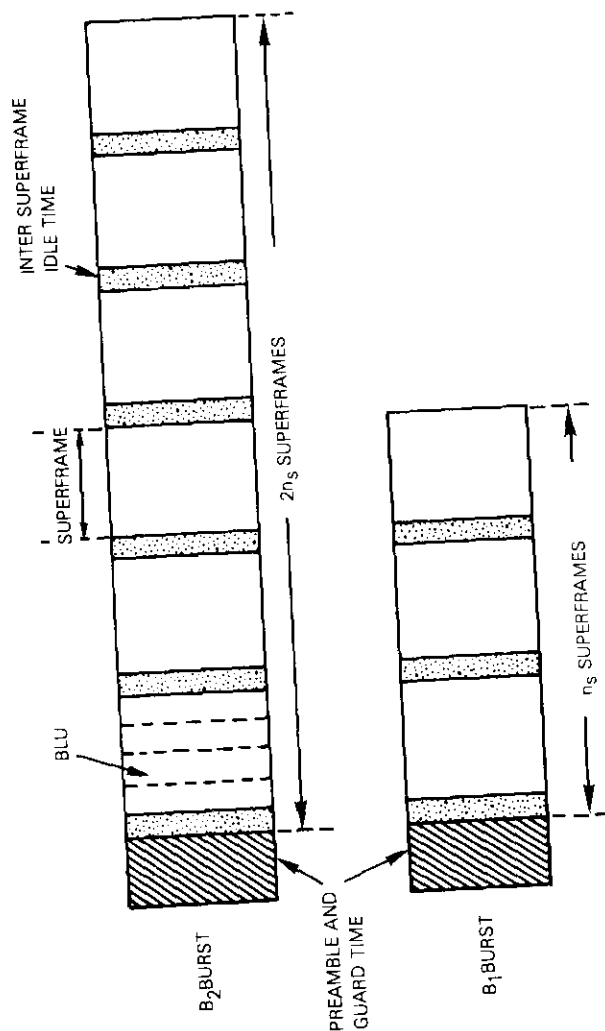


Figure A-4. Structure of Single and Double Bursts

TABLE A-1. LINK CLASSIFICATION

Link Type	d_f^*	d_r^\dagger	Links
SB	B_2	B_2	$L \leftrightarrow W$ $G \leftrightarrow C$
DB	B_1	B_1	$G \leftrightarrow W$ $C \leftrightarrow L$
DBC	$2B_1 + B_2$	$2B_1 + B_2$	$G \leftrightarrow L$ $C \leftrightarrow W$

* The interval (in s) between the burst containing the link and the burst containing the complement.

† The interval (in s) between the burst containing the complement and the burst containing the link.

The throughput (excluding overhead) for any link in the system examined at the superframe level has been derived as

$$\xi = \frac{S}{S + m(1 - S)} \quad (\text{A-1})$$

with

$$m = \text{Min}(N, M) \quad (\text{A-2})$$

where M = maximum number of superframes transmitted per HDLC cycle

N = maximum number of superframes which can be outstanding without acknowledgment (Maxout)

S = probability of a superframe being successfully received over a link.

For the asynchronous balanced mode, an HDLC cycle starts with the transmission or first retransmission in a group of superframes. The length of the HDLC cycle varies depending upon the location of the starting superframe within a burst and on the location of the first transmission error, if any.

When the maximum achievable throughputs are considered, it is assumed that sufficient buffering is available at the transmitter to prevent channel idling caused by a lack of buffering. This implies that the superframe Maxout N is always larger than M ; therefore,

$$\xi = \frac{S}{S + M(1 - S)} \quad (\text{A-3})$$

The quantities S and M must be determined to evaluate this expression; S is governed by the superframe size (b_s) and the error characteristics over the channel. In this case, the random-error model $S = (1 - \text{BER})(b_s)$ has been assumed.

The quantity M , which is more complex to evaluate, depends upon the system implementation (e.g., burst sizes and locations), the starting location of an HDLC cycle within a burst, and the location of the first superframe error (if any) within the HDLC cycle. Figures A-5 and A-6 indicate two of the many possibilities of an effective round-trip delay, and the superframes transmitted between the start of the HDLC cycle and the first frame error. The duration of an HDLC cycle is the time between the start of the first superframe in an HDLC cycle and the start of the first retransmission of the first frame in error. Although this duration is not required to determine throughput, it is required to compute average response time.

The computations are also complicated by the dependence of M , in general, on the relative position of the start of an HDLC cycle within a burst. Hence, throughput must be averaged over the values computed for each starting position. Similarly, the averaged value of M is necessary to compute response time.

For these reasons, the model cannot be used in the closed form, [equation (A-3)], but requires an explicit computation for each set of system parameters for each link. These computations have been implemented in a computer program which was used to predict throughput performance. Sample results for BERS of 10^{-8} , 10^{-7} , and 10^{-6} are shown for double burst (noncoincident) links in Figure A-7, double burst (coincident) links in Figure A-8, and single burst links in Figure A-9.

References

- [A-1] A. K. Kaul, "Performance of HDLC in Satellite Communications," *COMSAT Technical Review*, Vol. 8, No. 1, Spring 1978, pp. 41-87.
- [A-2] A. K. Kaul, "Performance of DLC Protocols Over Synchronous Time-Division Multiplexed Communications Channels," *COMSAT Technical Review*, Vol. 9, No. 1, Spring 1979, pp. 203-231.

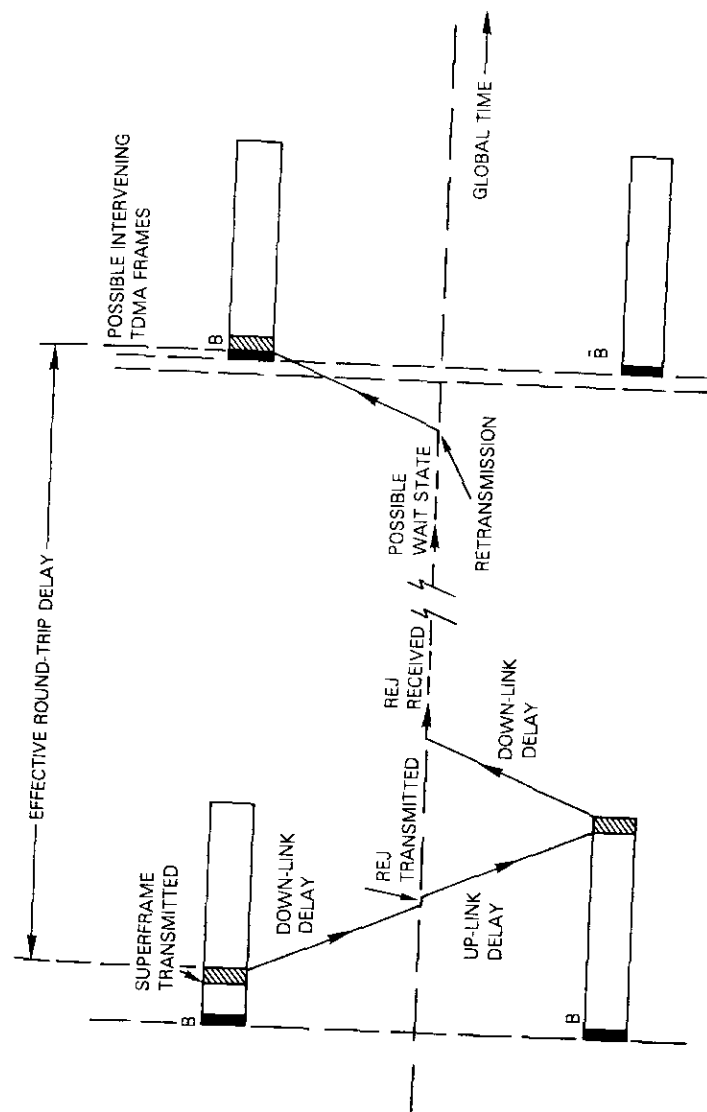


Figure A-5. Example of Effective Round-Trip Delay for a Duplex Link in a Coincident Double Burst

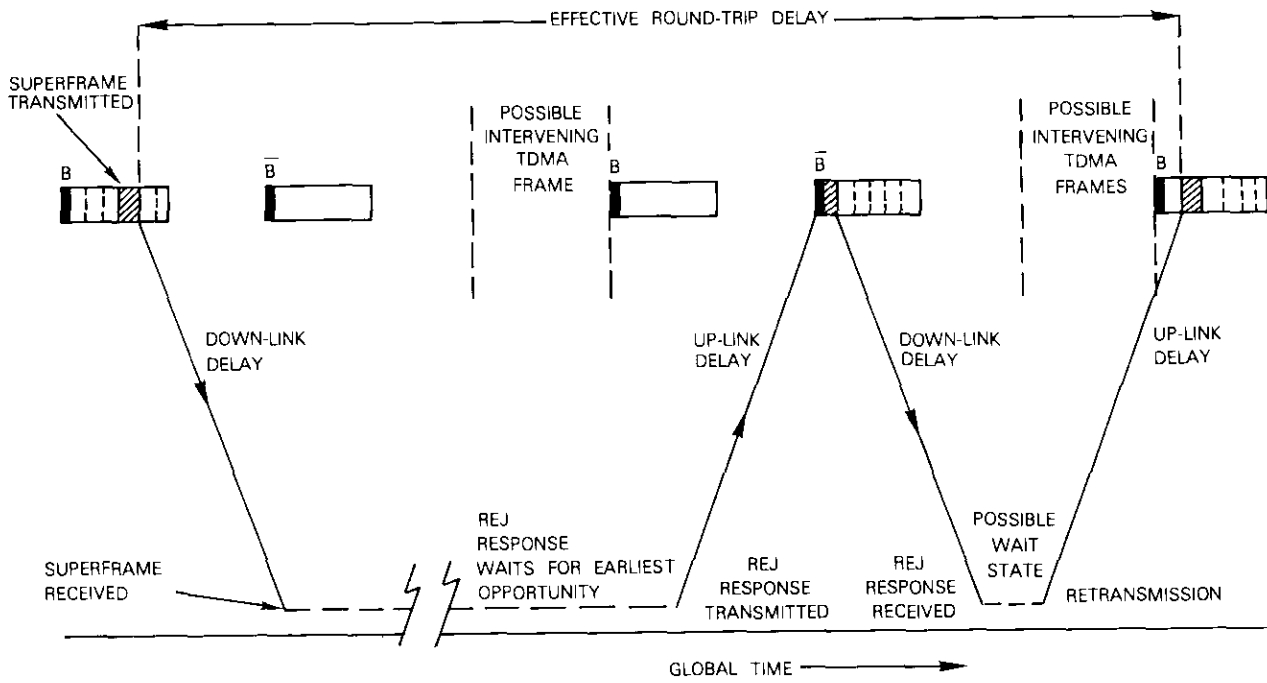


Figure A-6. Example of Effective Round-Trip Delay for a Duplex Link in a Single Burst or Noncoincident Double Burst

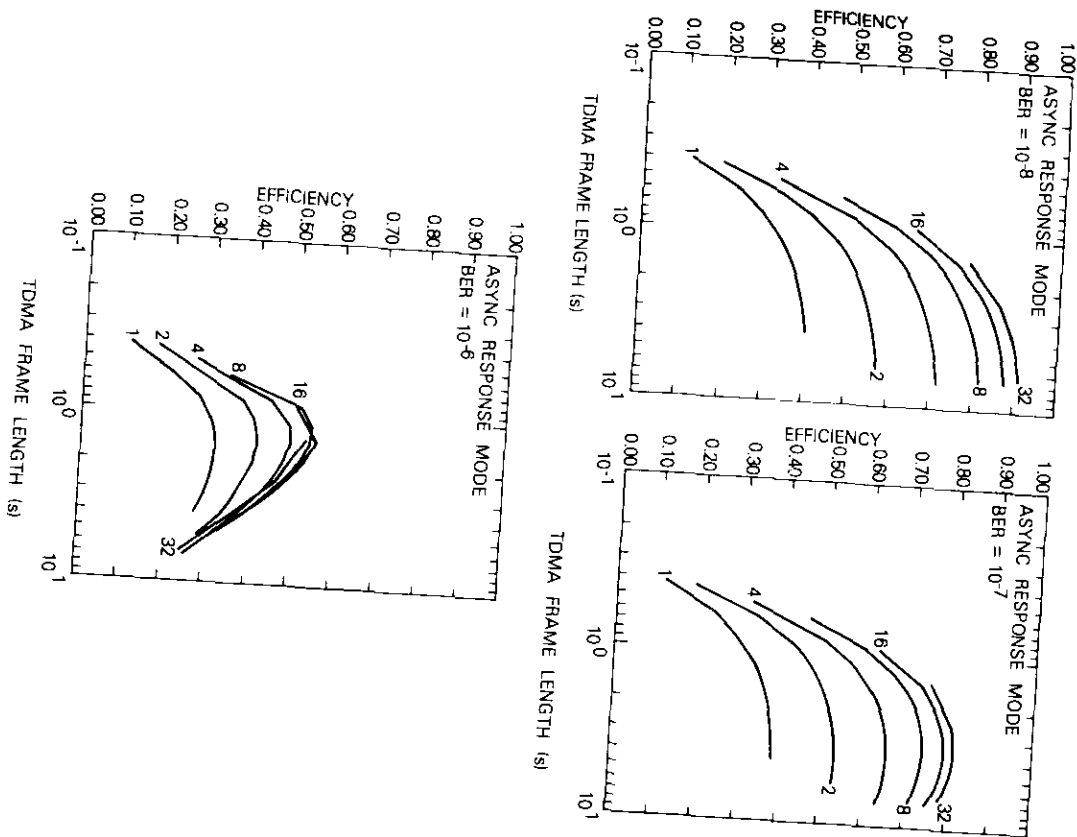


Figure A-7. TDMA Throughput Efficiency vs TDMA Frame Duration at BER of 10^{-8} , 10^{-7} , and 10^{-6} for Double Burst (noncoincident) Links

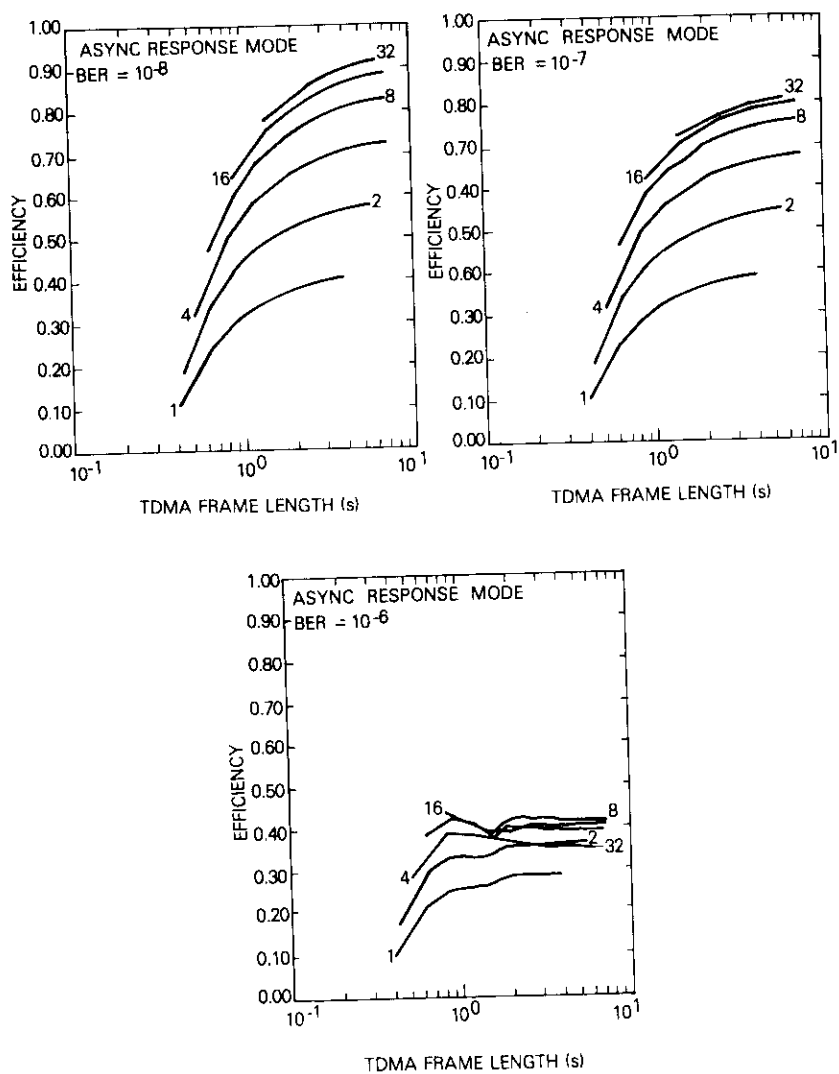


Figure A-8. TDMA Throughput Efficiency vs TDMA Frame Duration at BER of 10^{-8} , 10^{-7} , and 10^{-6} for Double Burst (coincident) Links

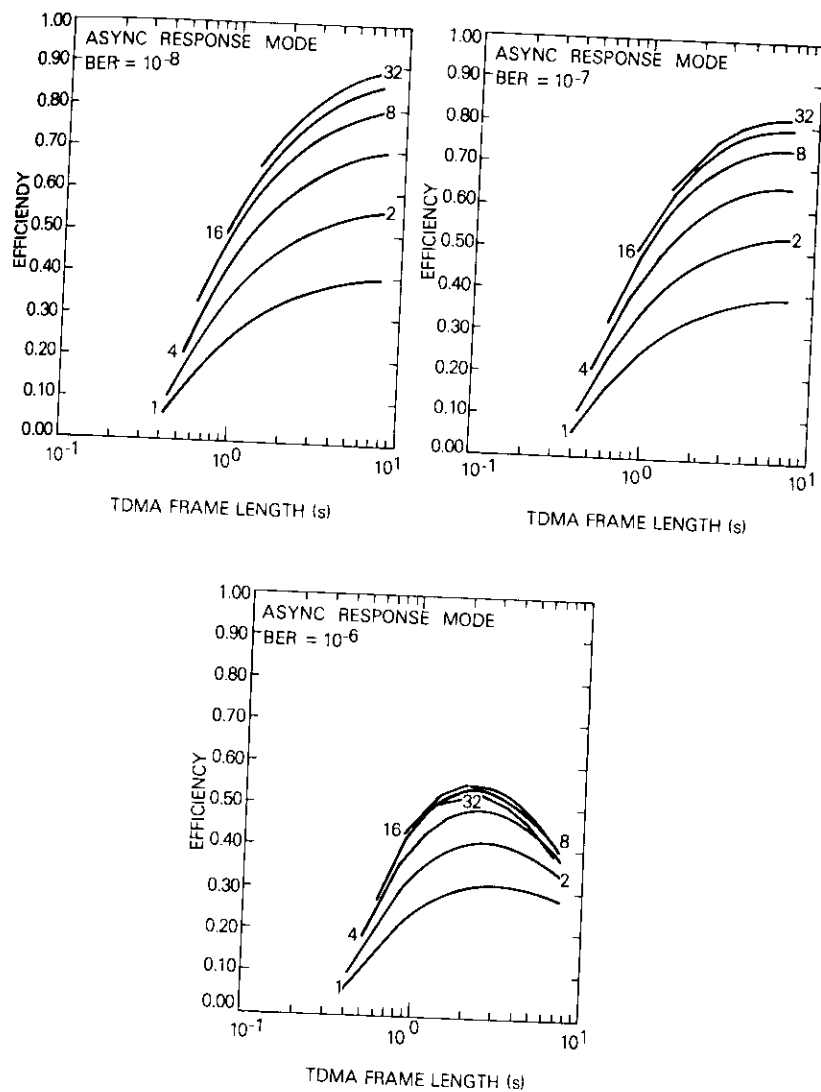
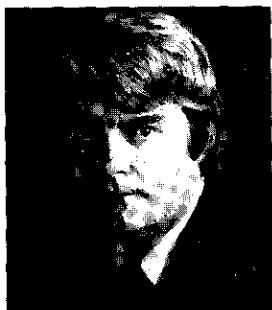


Figure A-9. TDMA Throughput Efficiency vs TDMA Frame Duration at BER of 10^{-8} , 10^{-7} , and 10^{-6} for Single Burst (noncoincident) Links



William L. Cook received a B.S. in Engineering Mechanics from Lehigh University, an M.S. in Engineering Sciences from Purdue University, and a D.Sc. in Computer Sciences from George Washington University. Dr. Cook is currently Assistant Director of the Transmission Systems Laboratory at COMSAT Laboratories, where he is responsible for R&D programs in computer communications and system software development.

Ashok K. Kaul received B.Sc. and M.Sc. degrees in physics from the University of Jammu in Kashmir, India, and a Ph.D. in physics from the University of Maryland. In 1973, he joined COMSAT Laboratories, where he is currently Manager of the Computer Communications Department of the Transmission Systems Laboratory, responsible for directing research and experiments in computer communications.



Gene D. Hodge, Manager of the Advanced System Development Department in IBM's System Communications Division, received a B.S.E.E. from Illinois Institute of Technology, a B.S. in Math from the University of Texas at El Paso, and an M.S.E.E. from George Washington University. He is responsible for advanced development activities in the field of computer communications via satellite. Recently, he provided technical direction to the IBM design team responsible for development of test objectives and system components required for implementation of the Joint Computer/Satellite Communications experiments (Phases 1 & 2). Mr. Hodge has published several papers and holds several patents related to satellite communications systems.

Joseph F. Marchese received a B.S.E.E. in 1956 from Duke University and an M.S.E.E. in 1964 from Drexel University. He is Manager of Advanced Technology at IBM's System Communications Division in Gaithersburg, Maryland, responsible for evaluation and development of advanced communications technology for data information systems, with special emphasis on satellite communications networks.



Fast algorithms for the computation of binary logarithms

O. A. HORNA

(Manuscript received November 6, 1979)

Abstract

The amount of digital signal processing is limited by the speed of available logic hardware, especially when complex multiplications or divisions are required. The speed of these operations can be substantially increased by logarithmic encoding which permits independent adjustment of the dynamic range and resolution of digitized signals.

Simple approximations for the computation of binary logarithms and anti-logarithms are analyzed and formulas for the derivation of errors are presented; properties of certain 1-, 2-, and 3-segment approximations are tabulated. As an example of the hardware implementation of a logarithmic encoder and its arithmetic unit, the block diagram of an echo canceller adaptive filter is included.

Introduction

Sophisticated signal processing methods can provide substantial bandwidth reduction and/or an improvement in the signal-to-noise ratio for speech [1] and video transmissions. For example, good-quality speech has been transmitted over 1.2-kbit/s channels [2], and a 1-bit-per-pel rate appears adequate for TV transmission [3]. Although these schemes have been computer simulated, hardware implementation is

usually cumbersome and difficult because the speed of digital circuits limits the amount of computation which can be performed in real time. This is especially the case when complex multiplication and division are required, as in Fourier transformations and adaptive digital filters. However, provided that a fast algorithm for computing logarithms and antilogarithms is available, the speed can be substantially increased by using a 16th century invention by John Napier. This paper analyzes certain fast methods of finding the binary logarithms.

Floating point format

A binary number b can be expressed in a floating point sign and a magnitude format as

$$b = \text{Sgn}(b) 2^a (1 + m) \tag{1}$$

where the exponent a is an integer and the mantissa m is by definition $0 \leq m \leq 1$. In binary notation, the number $b = 10111.01$ can also be expressed as

$$b = \text{Sgn}(b) 10^{100} (1 + 0.011101) .$$

The number of bits A assigned to the exponent a determines the range of b , and the number of bits M in the mantissa m determines the resolution. (In the example above, $a = 4$, $A = 3$, and $M = 6$.)

The relative precision, *i.e.*, the round-off error, or the signal-to-quantization-noise ratio, S/N_q , is equivalent to a binary number with B bits, where

$$B = M + 2 \tag{2}$$

For a TV signal with a resolution equivalent to 8 bits, $B = 9$ or $M = 7$ is sufficient, even for complex processing. Good-quality speech requires $S/N_q \approx 50$ dB (*i.e.*, $M = 6$) and high-fidelity music with total harmonic distortion less than 0.1 percent and/or $S/N = 60$ dB requires $M = 7$. In all these cases, a binary logarithm with a 6- to 7-bit mantissa (*i.e.*, a relative error less than 0.01) is sufficient.

Binary logarithms and antilogarithms

The binary logarithm, \log_2 , of the number $|b|$ is

$$\log_2 |b| = a + \log_2 (1 + m) \tag{3}$$

The McLaurin series can be used to express $\log_2 (1 + m)$ and 2^m approximately as follows:

$$\log_2 (1 + m) = m + \epsilon(m) \tag{4a}$$

$$\text{antilog } m = 2^m = 1 + m - \epsilon(m) \tag{4b}$$

The error $\epsilon(m)$ in these approximations is

$$\epsilon(m) = \log_2 (1 + m) - m \tag{5a}$$

$$\epsilon(m) = (1 + m) - 2^m \tag{5b}$$

as shown in Figure 1 for $0 \leq m \leq 1$. The maximum value of this error is

$$\epsilon_{\max} = \epsilon(m = 0.442695) = 0.0860713 \tag{6}$$

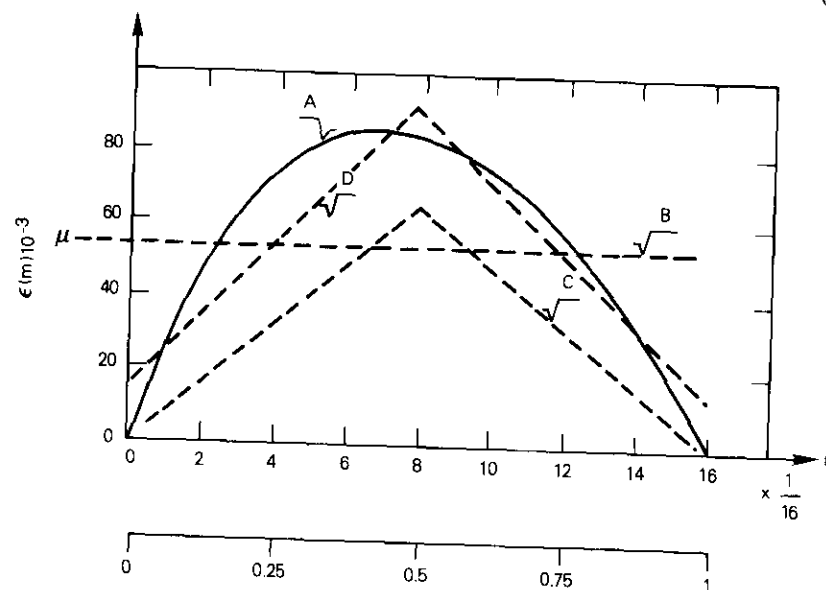


Figure 1. Error $\epsilon(m)$ of the \log_2 Approximation (A) as a Function of Mantissa m and 1-Segment (B) and 2-Segment (C, D) Corrections

which is more than eight times the value required for $M = 7$. Dill [4] suggested that the maximum error could be halved by adding or subtracting a constant $\epsilon(m) = \epsilon_{\max}/2$ [see equations (3) and (4)]. Slightly better results (see Table 1) can be obtained by adding the average value $\mu = E[\epsilon(m)] = 0.0573049$. These corrections can be used if a resolution of $B = 6$ is sufficient, as in the case of certain adaptive filters [5] and "vocoders" [1].

Logarithm approximations

Several methods of improving the \log_2 approximation were suggested [4]. The simplest is to read $\epsilon(m)$ from an ROM table. However, the access speed of presently available 1-kbit memories is still inadequate for certain applications.

In terms of speed, two algorithms seem to be attractive. The simpler one divides the 0 to 1 range of m into two parts. For $0 \leq m < 0.5$, the following relationship is used

$$\log_2(1+m) \doteq m + k_1 m + \gamma_1$$

$$2^m \doteq 1 + m - k_1 m - \gamma_1 \quad (7)$$

and for $0.5 \leq m < 1$,

$$\log_2(1+m) \doteq m + k_1(1-m) + \gamma_1$$

$$2^m \doteq 1 + m - k_1(1-m) - \gamma_1 \quad (8)$$

where $k_1 = 2^{-n}$, n is an integer, and $\gamma_1 \ll 1$ is a constant (see Table 1). Equations (7) and (8) usually require only one addition or subtraction to compute \log_2 or 2^m .

For $\gamma_1 = 0$, the maximum error for $m < 0.5$ occurs if

$$m_1 = \frac{\alpha}{1+k_1} - 1 < 0.5 \quad (9)$$

and for $m \geq 0.5$ if

$$m_2 = \frac{\alpha}{1-k_1} - 1 \geq 0.5 \quad (10)$$

TABLE 1. SELECTED \log_2 APPROXIMATIONS EASILY IMPLEMENTABLE IN HARDWARE AND SOFTWARE AND THEIR ERROR ANALYSIS

Figure Curve	No. of Correction Segments	Coefficient		Error				
		k	γ	Mantissa, m_1, m_2	Maximum, ϵ_{\max}	Average, μ	rms, r	Variance, σ
1-A	0	0	0	0.4427	0.08607	0.05730	0.06279	0.02568
1	1	0	5×2^{-7}	0.4427	0.04575	0.01156	0.03079	0.02853
1-B	1	0	7×2^{-7}	0 ; 1	-0.03645	0.000853	0.02569	0.02568
1-C	2	2^{-3}	0	0.2824	0.04115	0.02605	0.02808	0.01048
1	2	2^{-3}	3×2^{-7}	0 ; 1	0.02419	0.00186	0.01064	0.01046
1-D	2	5×2^{-5}	2^{-6}	0.2477	0.03286	0.00262	0.00904	0.00866
2-B	3	2^{-2}	5×2^{-6}	0.1542	0.01414	0.00359	0.00718	0.00622

where

$$\alpha = \frac{1}{\ell n_2} = 1.442695 \quad (11)$$

The average error is

$$\mu = E[\epsilon(m)] = 0.0573049 - \frac{1}{2}k_1 - \gamma_1 \quad (12)$$

and the rms error can be determined from

$$r^2 = E[\epsilon^2(m)] = p_1 - p_2k_1 + p_3k_1^2 + p_4k_1\gamma - p_5\gamma_1 + \gamma_1^2 \quad (13)$$

The coefficients p_i have been computed:

$$p_1 = 0.0039432$$

$$p_2 = 0.0356475$$

$$p_3 = 0.0833333$$

$$p_4 = 0.5$$

$$p_5 = 0.1146100$$

The variance σ^2 is $r^2 - \mu^2$. Values of these errors for several values of k_1 and γ_1 are given in Table 1, and corrections are shown in Figure 1 (dotted lines).

Approximations (7) and (8) provide satisfactory resolution for values of B equal to 7 or 8. A higher precision can be achieved by a 3-segment approximation shown in Figure 2. For $0 \leq m < 5 \times 2^{-4}$, $k_2 = 2^{-2}$, and $\gamma_2 = 0$,

$$\log_2(1+m) \doteq m + \frac{m}{4} \quad (14)$$

$$2^m \doteq 1 + m - \frac{m}{4} \quad (15)$$

for $5 \times 2^{-4} \leq m < 11 \times 2^{-4}$, $k_2 = 0$, and $\gamma_2 = 5 \times 2^{-6}$,

$$\log_2(1+m) \doteq m + \frac{5}{64} \quad (16)$$

$$2^m \doteq 1 + m - \frac{5}{64} \quad (17)$$

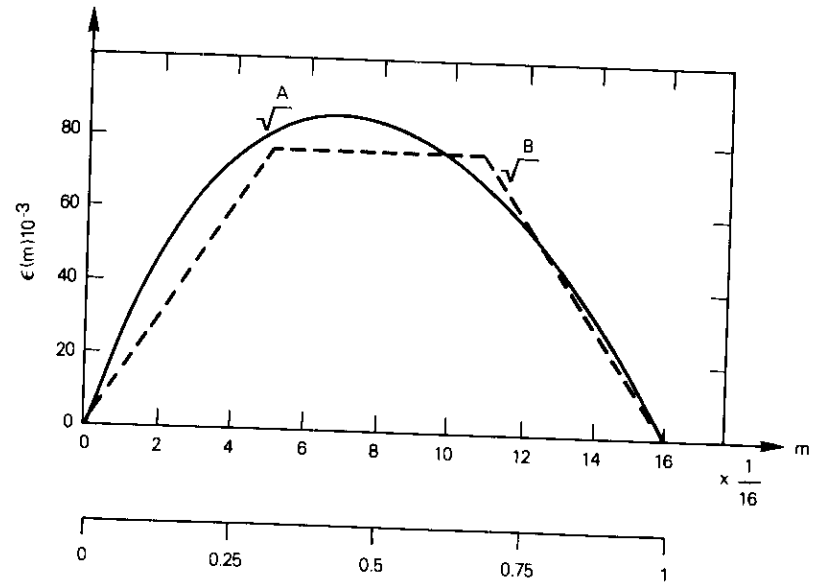


Figure 2. Error $\epsilon(m)$ and 3-Segment (B) Correction of \log_2 Approximation

and for $11 \times 2^{-4} \leq m < 16$, $k_2 = 2^{-2}$, and $\gamma_2 = 0$,

$$\log_2(1+m) = m + \frac{1-m}{4} \quad (18)$$

$$2^m = 1 + m - \frac{1-m}{4} \quad (19)$$

The errors ϵ_{\max} , μ , r , and σ are given in Table 1. Because the maximum error $\epsilon_{\max} \doteq 0.014$, this approximation is sufficient for a $B = 9$ -bit resolution. A small 16×1 or 16×2 bit read only memory can be used to increase the resolution by one or two bits by reducing ϵ_{\max} by an additional correction.

Hardware implementation

Hardware for the conversions is very simple. For example, a \log_2 3-segment approximation can be implemented by the circuit shown in

Figure 3 [6]. The most significant bit of $1 + m$ is truncated, and the next four bits of m are decoded to command the multiplexer (MPX) and inverter. Either the constant $5 \cdot 2^{-6}$ or the product $m \cdot 2^{-2}$ is added to m . Because $1 - m$ and $\bar{m} - 1$ differ only in the least significant bit (which is truncated), a correction $(m - 1)/4$ is used for $m > 11 \times 2^{-4}$. There is no carry into the exponent a . Multiplication by 2^a [see equation (1)] can be performed by a static or dynamic shifter [6].

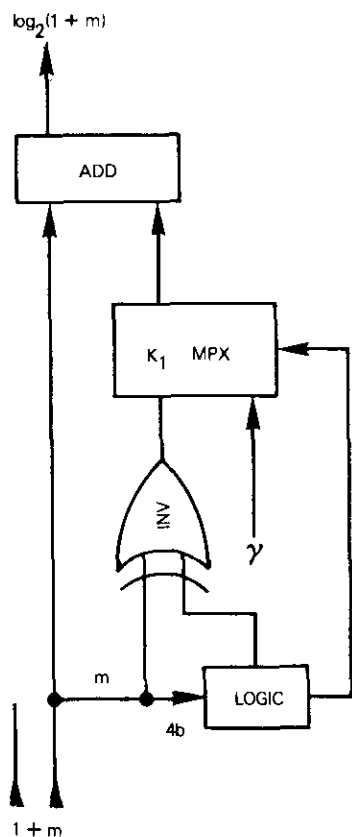


Figure 3. Block Diagram of Hardware Implementation of 3-Segment \log_2 Approximation

The speed of a complex computation involving many multiplications and divisions can be increased substantially if the corrections are

processed and stored in a separate accumulator (ACC) and the total added to the resulting mantissa m_3 (see Figure 4). Two numbers, m_1 and m_2 , are processed in the arithmetic logic unit (ALU); at the same time two corrections are computed (see Figure 3) and the same operation is performed on them in a separate correction accumulator unit (COR.ACC). The resulting mantissa, m_3 , is a sum of the content of ALU + ACC and of all corrections (MPX1). This operation can generate carry C_a into the exponent processor.

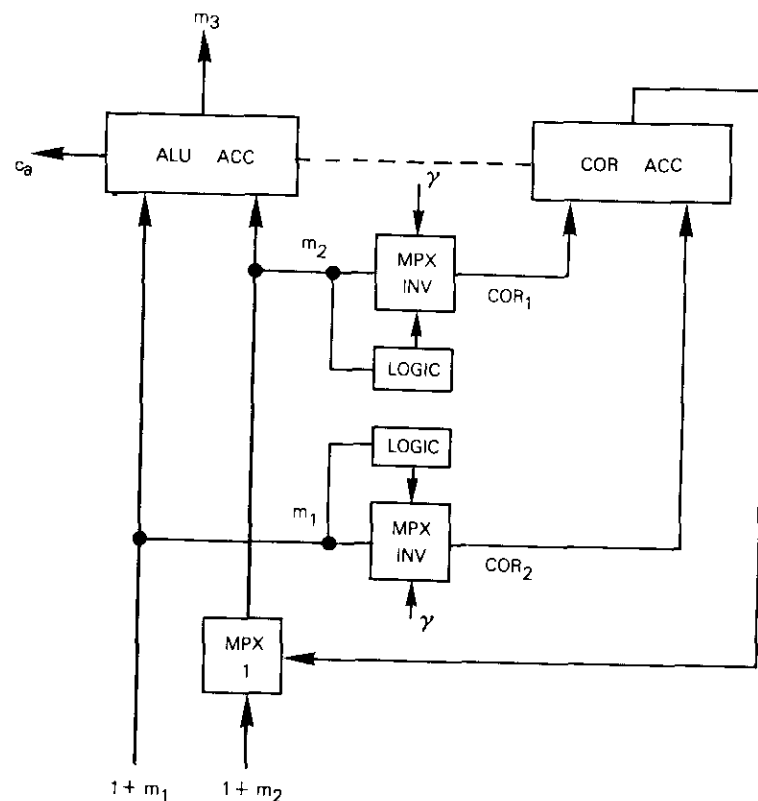


Figure 4. Arithmetic Unit with Separate Correction Accumulator (COR.ACC)

Conclusion

Simple algorithms which can be easily implemented in hardware and software are used to compute the binary logarithm of a floating point binary number with resolution sufficient for speech and video digital signal processing. These algorithms substantially increase the speed of computations and/or simplify hardware. This approach was successfully employed in the design and construction of adaptive filters used for echo cancellation in long-distance telephone circuits [5], [6], where several hundred multiplications are performed during every sampling period (125 μ s).

The problem of "zero crossing," which exists in sign plus logarithm of magnitude format, was solved by linearly encoding a narrow segment around zero [6].

References

- [1] *Record of the IEEE International Conference on Acoustic, Speech and Signal Processing*, Washington, D.C., 1979, Session 2, pp. 44-81.
- [2] S. Amadi and A. G. Constantinides, "Linear Prediction of Formants for Low Bit Rate Digital Speech Transmission," *Record of the IEEE International Conference on Acoustic, Speech and Signal Processing*, Washington, D.C., 1979, pp. 48-51.
- [3] T. S. Huang et al., "Image Processing," *Proc. IEEE*, Vol. 59, No. 11, November 1971, pp. 1586-1609.
- [4] G. D. Dill, Private Communication.
- [5] O. A. Horna, "Echo Canceller Utilizing Pseudo-Logarithmic Coding," *NTC'77 Conference Record*, Los Angeles, California, 1977, Vol. 1, pp. 4:7-1-4:7-8.
- [6] O. A. Horna, "Echo Canceller with Adaptive Transversal Filter Utilizing Pseudo-Logarithmic Coding," *COMSAT Technical Review*, Vol. 7, No. 2, Fall 1977, pp. 393-428.

Otakar A. Horna studied at various European Universities and received an M.S. degree in electrical engineering from the Czech Institute of Technology, a Ph.D. in electronics from the Institute of Radio Technique and Electronics, and a State Diploma in Mathematical Logic from Charles University in Prague.

He was Senior Scientist and Secretary of the Scientific Council of the Research Institute for Mathematical Machines in Prague in charge of the Computer Technology Division, and later became Senior Engineer with Multronics Corporation, Rockville, Maryland. He joined COMSAT Laboratories, in 1969 and is presently a Senior Staff Scientist of the Communications Processing Laboratory.

He is the author of five books, more than 30 U.S. and foreign patents, and numerous scientific and technical articles. His work was awarded a Gold Medal at the Brussels World Fair in 1958, and a Gold Medal at the Brno Fair in 1967. He received the first COMSAT Research Award for his echo canceller design. He is a Senior Member of IEEE.



Index: interference reduction, television transmission, wave dispersion

New TV energy dispersal techniques for interference reduction

S. E. YAM

(Manuscript received June 8, 1979)

Abstract

FM television signals are strong sources of interference in satellite communications systems because of the high-density spectral spikes in the signal's power spectrum. Interference is most serious when the FM TV carrier shares a given channel with a narrowband carrier such as SPADE or SCPC. Although the use of TV energy dispersal techniques reduces the interference effect, the degree of reduction with the presently used frame-rate triangular dispersal waveform appears inadequate.

This paper investigates alternate TV energy dispersal techniques for further reduction of co-channel interference. It is shown that the line-rate sawtooth and half-line-rate triangular waveforms are effective alternatives. The co-channel interference mechanism is analyzed by computer simulation, and laboratory simulation experiments are performed. Experiments have shown that the two above-mentioned new methods can further reduce interference by 9 to 11 dB. Subjective tests indicate that the picture impairment due to the dispersal waveforms can be reduced well below the level of perception. Comparative tests with digital TV interference show an additional 9-dB interference reduction.

Introduction

The high-density spectral components in the power spectrum of FM TV carriers produce strong co-channel interference with other trans-

missions. Co-channel interference may occur between the channels of a satellite system which employs frequency reuse (dual polarizations and/or spatial beam isolation) between adjacent satellites having overlapping coverages, or between satellite and terrestrial services sharing the same frequency bands. Interference is particularly serious when the affected carrier is characterized by low power and narrow bandwidth.

Carrier energy dispersal techniques are used to reduce co-channel interference in fixed satellite services [1]. For instance in the INTELSAT system, a triangular waveform at the TV frame rate synchronized with the field blanking intervals is used for this purpose. The triangular waveform is added to the baseband video signal at the transmitting end and, at the receiving end, it is removed to recover the original video signal. This approach was adopted based on the result of a previous C.C.I.R. study on TV energy dispersal techniques [2], in which several low-frequency waveforms including field-rate, frame-rate and half-frame-rate triangular, and sawtooth waveforms were evaluated in terms of subjective effects on television pictures. The frame-rate triangular waveform was judged to produce the least impairment.

Energy dispersal results in the lowering and flattening of the high-density spectral spikes in the power spectrum of an FM TV signal and consequently reduces its interference potential. However, the degree of reduction achieved with this technique is inadequate, especially in the case of SCPC/PSK or SPADE as the wanted carrier [3], [4]. SCPC and SPADE transmissions are characterized by relatively narrow bandwidths (38 kHz). When co-channel interference exists, a high-density spectral component of an FM TV carrier, which is deviated by the slowly changing dispersal signal, may periodically traverse the narrow band of the SCPC or SPADE channel at the rate equal to the frequency of the dispersal waveform (e.g., 30 Hz for the NTSC standard) and with a duty cycle determined by the peak-to-peak deviation designed for energy dispersion. Thus a pulse-like interference affects the SCPC or SPADE transmission with a resulting high bit-error rate in the case of SCPC/PSK and degraded telephone voice quality for SPADE. In more severe situations, intermittent loss of carrier recovery in the PSK demodulator may cause long and high-density bit-error bursts and disturbing audible "clicks." Clearly, alternative energy dispersal techniques are desirable for a more effective reduction of the interference.

This paper reports on a study of new TV energy dispersal techniques. The merit of a dispersal technique is judged on the basis of five factors:

capability for reducing the peak spectral components, interference effect with respect to SPADE and SCPC/PSK channels, potential impairment of TV pictures, simplicity of implementation, and bandwidth economy. A survey of alternative concepts has indicated that the line-rate sawtooth waveform and the half-line-rate triangular waveform, synchronized to the video line blanking intervals, are promising alternatives. A fixed-amplitude line-rate technique is simple to implement while an adaptive technique offers the advantage of bandwidth economy at the expense of implementation complexity. By exploiting the time constant effect of the SPADE channel filter, the line-rate dispersal can substantially reduce interference to a SPADE channel, compared to the frame rate dispersal. Interference is caused when a spike of an FM TV carrier falls within the narrow bandwidth of the SPADE channel. At the TV frame rate, this interfering spike appears in full strength within the channel. As the sweeping rate is faster and the time that the spike dwells within the channel is short relative to the time constant of the channel filter, the interfering spike is attenuated by the filter.

This study explores the feasibility of the line-rate sawtooth waveform and the half-line-rate triangular waveform as energy dispersal methods for FM television. Interference problems and orbit utilization have been investigated extensively [5], [6]. Theoretical and experimental studies on multiple co-channel interference into PSK channels are reported in References 4 and 7-10. Previous studies on energy dispersal methods are given in References 2 and 11-13. The objective of this study is the evaluation of the merits of the above two waveforms as FM TV energy dispersal methods, as compared to the conventional frame-rate waveform.

An analysis and computer simulation study was first conducted to assess the energy dispersion and interference reduction effects of the selected line-rate and half-line-rate waveforms. Laboratory experiments were subsequently performed to evaluate the performance of the two waveforms as compared to the conventional frame-rate waveform under different assumed conditions. These experiments included SCPC/PSK average bit-error-rate tests, SCPC/PSK bit-error distribution tests, SPADE PCM voice channel impulse noise measurements, signal-to-noise ratio measurements, and voice subjective evaluations. The experimental results were compared with the results obtained from the analysis and computer simulation. Some aspects of a dispersal waveform suggested in Reference 13 were addressed, and

a TV picture subjective test was performed to assess the impairment effect of the dispersal waveforms on the video signal. Techniques for dispersal waveform addition and removal were investigated. Since digital transmission is an alternative to FM transmission of television signals, the interference potential of digital television was investigated.

Computer simulation of the sweep interference mechanism and the dispersion effect

A preliminary analysis and computer simulations were performed to gain a basic understanding of the sweep interference mechanism and the spectral energy dispersion effect of the triangular waveforms. The objectives were to investigate the characteristics of co-channel interference experienced by a narrowband SPADE channel as the result of a dispersed FM TV carrier, and to verify the hypothesis that the interference effect with respect to the SPADE transmission can be reduced using the line-rate dispersal waveform instead of the frame-rate dispersal waveform.

The digital simulation program CHAMP (*Channel Modeling Program for satellite systems*), developed at COMSAT Laboratories, was modified and used as the basic tool for the computer simulation, which was performed on an IBM 360/65 computer.

Sweep interference mechanism

The addition of a triangular dispersal waveform to the baseband video signal causes the spectral components to sweep back and forth at a rate equal to the fundamental frequency of the triangular waveform. The sweep deviation is determined by the amplitude of the triangular waveform and the sensitivity of the FM modulator. In the INTELSAT system, for example, the peak-to-peak deviation is 1 MHz for a modulated FM carrier and 2 MHz for an unmodulated carrier. Consequently, a spectral spike may periodically traverse a narrowband (38-kHz) SPADE channel located within the sweep bandwidth and produce a pulse-like interference to the SPADE channel. For the sawtooth dispersal waveform, a similar interference phenomenon exists except that the sweeping is essentially in one direction instead of back and forth.

Figure 1 illustrates the mechanism of sweep interference for triangular sweeping. The following parameters are defined:

- f_s = sweep frequency (Hz)
- Δf = peak-to-peak dispersal deviation
(span of sweep) = 1 MHz for INTELSAT IV-A
- B = SPADE channel bandwidth \cong 38 kHz
- δ = percentage time during which the sweep component dwells within the SPADE channel ("duty cycle")
- T = sweep period (s)
- τ = time during which the sweep component dwells within the SPADE channel per traversal(s).

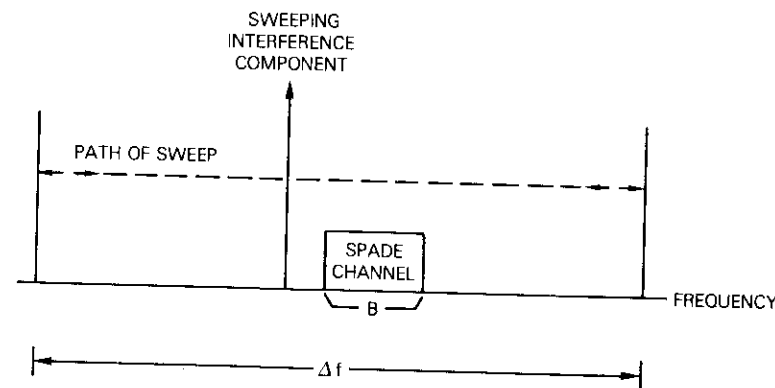


Figure 1. Sweep Interference Model

Then

$$\delta = \frac{B}{\Delta f} \tag{1a}$$

$$T = \frac{1}{f_s} \tag{1b}$$

for both triangular and sawtooth sweeping. Furthermore,

$$\tau = \frac{T}{2} \delta = \frac{1}{2f_s} \frac{B}{\Delta f} \tag{2a}$$

for triangular sweeping, and

$$\tau = T\delta = \frac{1}{f_s} \frac{B}{\Delta f} \quad (2b)$$

for sawtooth sweeping.

Interference as a function of τ or f_s

The triangular sweep interference mechanism was simulated using a time-domain model. Pulse trains were generated to simulate different sweep timings. The pulse width corresponds to the time during which the interfering component dwells within the channel filter. The pulse period, which equals one-half of the sweep period, was set at 26.3 times the pulse width ($\Delta f = 1$ MHz and $B = 38$ kHz). Pulse trains for the values of τ ranging from $2.5 \mu s$ (half-line-rate sweeping) to $650 \mu s$ (frame-rate sweeping) were generated.

Figure 2 is a block diagram of the simulation program. The generated pulse trains, simulating the envelopes of amplitude modulated carriers, were fed into a filtering software module with parameters selected to

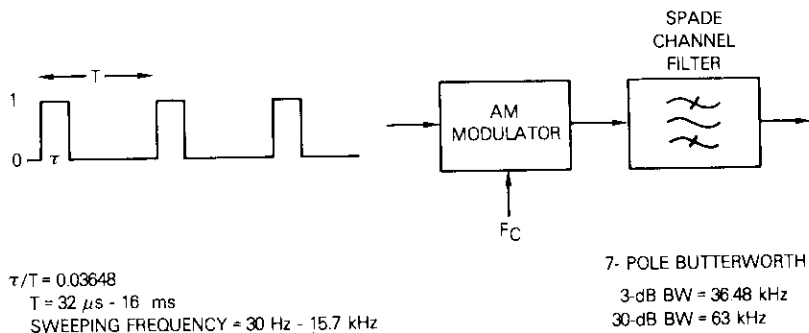


Figure 2. Block Diagram of Pulse Response Simulation

simulate a standard SPADE channel filter (7-pole Butterworth filter with a 3-dB bandwidth of 36.48 kHz and a 30-dB bandwidth of 63 kHz) which is shown in Figure 3. The interference reduction effect was assessed in terms of the power reduction as a result of filtering, computed using a standard CHAMP software module (POWMET).

Figure 4, which shows power as a function of τ , indicates that a noticeable power reduction (0.5 dB) occurs at about $\tau = 3 \times 10^{-4}$ s.

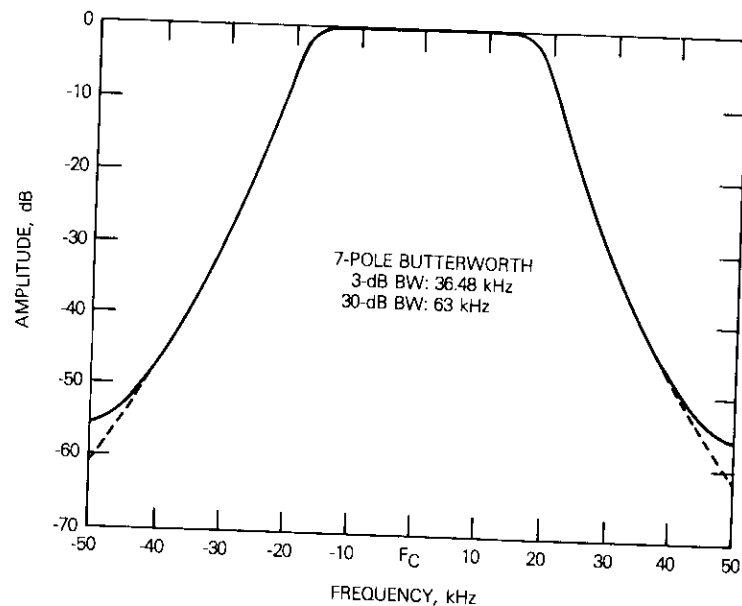


Figure 3. Filter Frequency Response

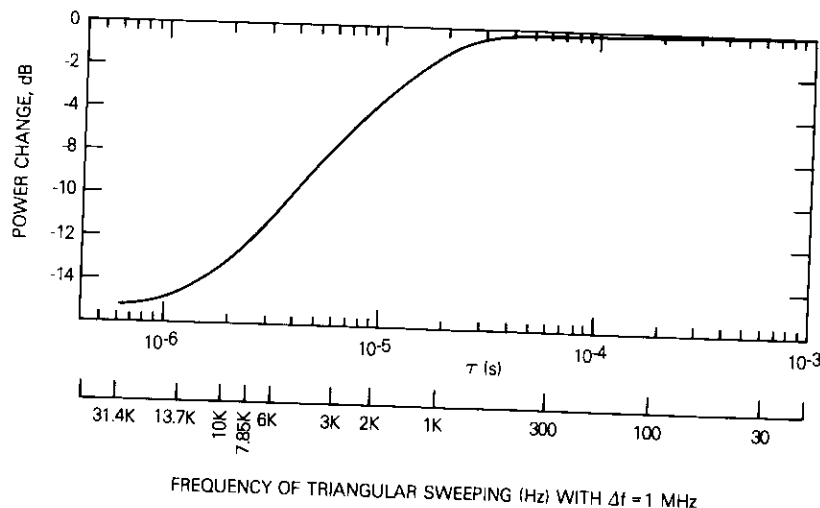


Figure 4. Power Change as a Function of τ or f_s

From that point, power decreases with decreasing τ . The power reduction reaches 11 dB at $\tau = 2 \times 10^{-6}$ s, and then levels off. Clearly, power reduction is a nonlinear function of τ .

Since a one-to-one relationship between τ and f_s exists for a fixed Δf , the curve in Figure 4 can be replotted to express the power change as a function of sweep frequency, f_s , with a fixed Δf . From equation (2), and with $\Delta f = 1$ MHz,

$$f_s = \frac{0.019}{\tau} \quad (3)$$

A second horizontal axis in Figure 4 shows the corresponding values of sweep frequency, f_s . With the new axis, a sweep frequency of 1 kHz is roughly equal to the threshold frequency above which an appreciable reduction in interference power can be obtained. At the frame rate ($f_s = 30$ Hz), there is no power reduction. At the half-line rate ($f_s = 7.88$ kHz), power is reduced by 10.5 dB.

Interference as a function of Δf

It is of interest to study the variation of interference power experienced by the SPADE channel as a function of sweep deviation, Δf , with the sweep frequency fixed, for example, at the TV frame rate and at the half-line rate. Such information is useful for the derivation of interference criteria.

The level of interference power experienced by the SPADE channel in Figure 1 is affected by Δf through two types of effects: the duty cycle effect and the time constant effect. The duty-cycle effect reflects the fact that the interfering components are within the channel for only a fraction of the total time. The SPADE channel is thus exposed to a fraction of the total interference power, which is determined by the duty cycle $\delta = B/\Delta f$. Note that the duty cycle increases, the sweeping component will traverse the channel more frequently; however, it will dwell in it for a shorter time. Thus, in terms of the duty cycle effect alone, the interference power variation experienced by the channel is the same for both frame-rate and half-line-rate sweeping, and can be expressed in dB by the factor $10 \log (B/\Delta f)$.

The time constant effect reflects the band-limiting action of the SPADE channel filter. Substituting $f_s = 30$ Hz and 7.85 kHz and $B = 38$ kHz into equation (2a) yields

$$\tau = \frac{633.3}{\Delta f}, \text{ frame-rate triangular sweeping}$$

$$\tau = \frac{B}{2f_s \Delta f} = \frac{2.42}{\Delta f}, \text{ half-line-rate triangular sweeping.}$$

Figure 5 shows the power change as a function of τ due to the time constant effect. Values of Δf ranging from 0.25 to 2.5 MHz appear beneath the corresponding values of τ for both frame-rate and half-line-rate triangular sweeping. It is clear from Figure 5 that, for frame-rate triangular sweeping, the practical range of Δf falls entirely within the flat 0-dB region of the curve where no power attenuation is present. However, for half-line-rate triangular sweeping, the practical range of Δf falls in a region of the curve where power attenuation is encountered with a strong dependence on Δf . For Δf ranging from 0.25 to 2.5 MHz, power attenuation ranges from 3.5 dB to 13 dB, and at $\Delta f = 1$ MHz, a 10.5-dB attenuation is experienced.

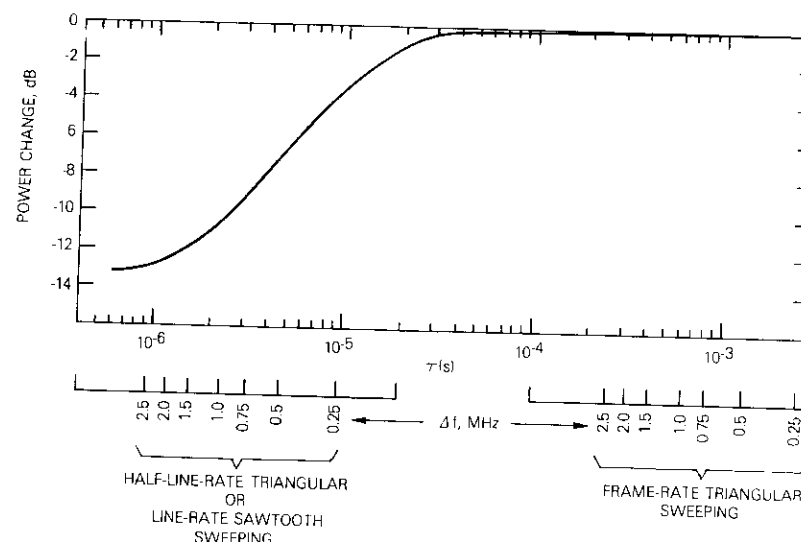


Figure 5. Power Change as a Function of τ or Δf

It is then clear that the "improvement" in interference power reduction as a function of Δf obtainable by using half-line-rate sweeping instead of frame-rate sweeping can be represented by the curve for the time constant effect for half-line-rate sweeping. Figure 6 shows the improvement as a function of Δf , which is redrawn from the left-hand portion of Figure 5. This prediction will be verified by experimental data to be presented later in this paper.

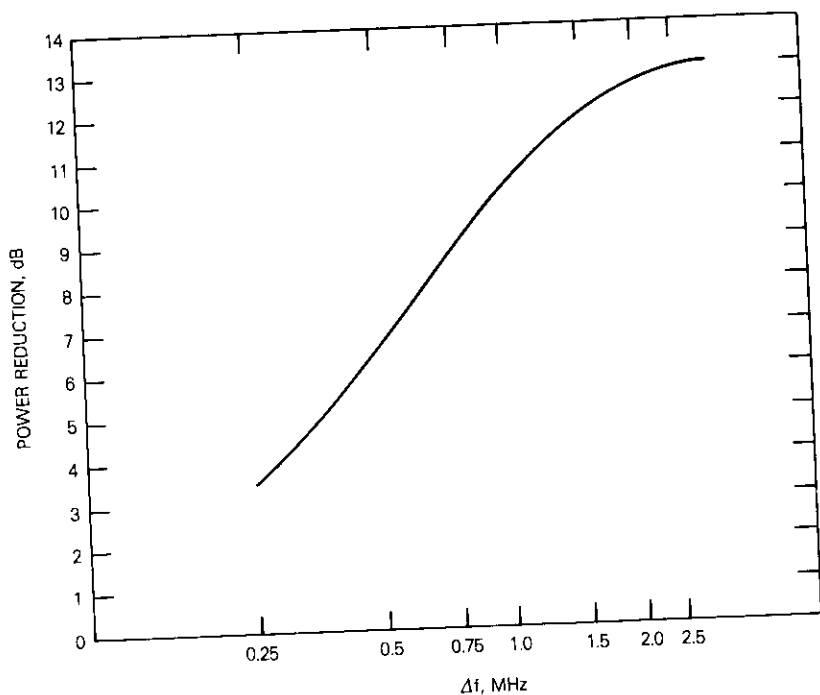


Figure 6. Improvement of Half-Line-Rate Triangular Sweeping over Frame-Rate Triangular Sweeping vs Δf

Simulation of dispersion effects

Computer simulation of the power spectral densities of FM TV carriers was performed. The carriers were modulated with a flat-field video signal processed with different energy dispersal methods.

Figure 7 is a block diagram of the simulation program, which

generates simulated TV and dispersal signals and adds the two signals; the resulting signal frequency modulates a carrier whose power spectral density is computed. Standard INTELSAT IV-A half-transponder NTSC (525/60) TV characteristics were assumed. The peak-to-peak deviation was 4.75 MHz for the low-frequency preemphasized video signal and 1 MHz for the dispersal signal. A pulse train with a duty cycle of 0.1 was generated to approximately simulate the synchronizing pulses and constant intensity intervals of a flat-field video signal (worst-case interfering signal). Dispersal waveforms included frame-rate triangular, half-line-rate triangular, and line-rate sawtooth waveforms. The power spectral density computation provides a spectral resolution of 78 kHz.

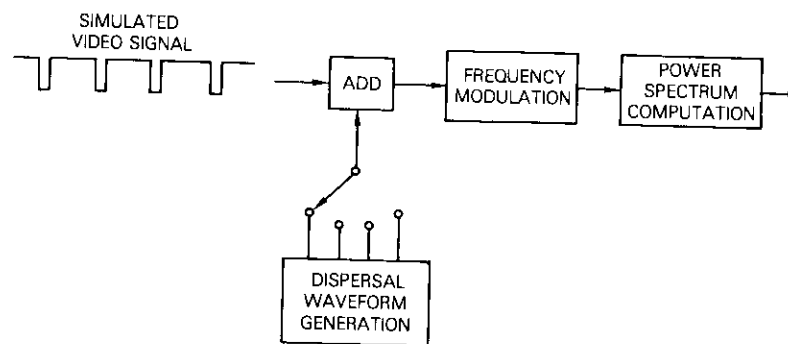


Figure 7. Block Diagram of Dispersal Simulation Program

Figure 8 shows the four combinations of the video and dispersal signals. Figure 9 shows the power spectral density for case 1, in which no dispersal waveform was added to the flat-field video signal. The 0-dB level corresponds to the total power level of the carrier. Two sharp spikes appear in the power spectrum corresponding to the two levels of the video signal. The highest spike is at 1.41 dB below the total power.

Figure 10 shows the power spectral density for case 2, in which a frame-rate (30-Hz) triangular waveform was added to the video signal. In this figure, as compared with Figure 9, the spikes are significantly widened and lowered. The highest spike is reduced to 11.26 dB below the total power. This result was obtained by averaging the energy over a time interval longer than 1/30 second; on a more nearly instantaneous time scale, it can be envisaged that the triangular waveform will cause

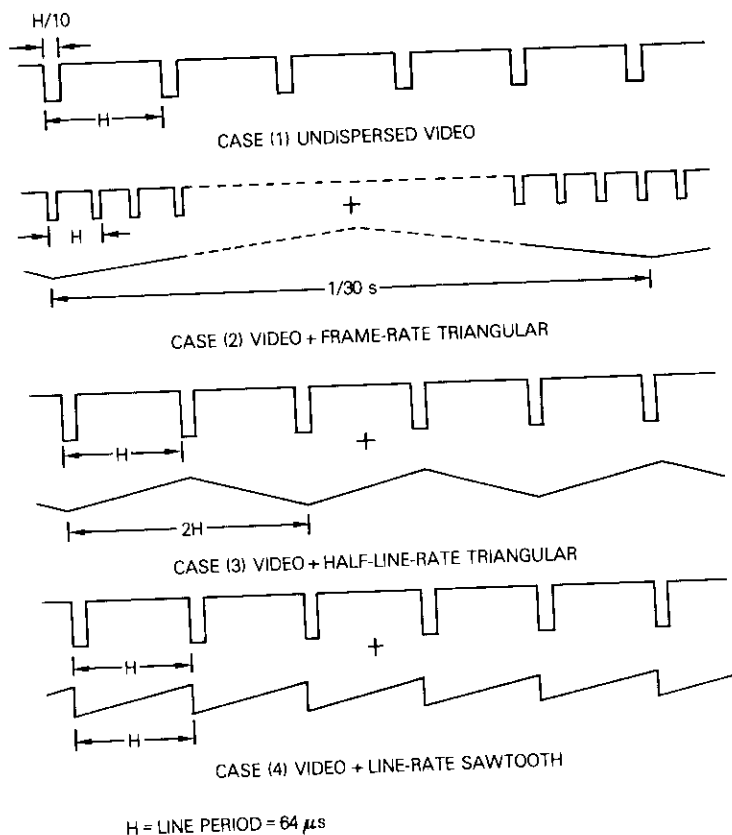


Figure 8. Addition of Dispersal Signals

the spectral spikes to sweep back and forth through the 1-MHz frequency band at the rate of 30 Hz. Computer simulations were performed to observe the more nearly instantaneous power spectral density using an averaging time of 0.83 ms. Figure 11 shows the spectral spikes for the two short time intervals (0.83 ms) corresponding to the two extremes of the sweep. This power spectral density plot shows no significant lowering of the spikes as compared to that for the undispersed case (Figure 9).

Figures 12 and 13 show the power spectral densities for cases 3 and 4, in which the half-line-rate triangular and the line-rate sawtooth waveforms, respectively, are added to the video signal. The results have been obtained by averaging the energy over a 0.83-ms time

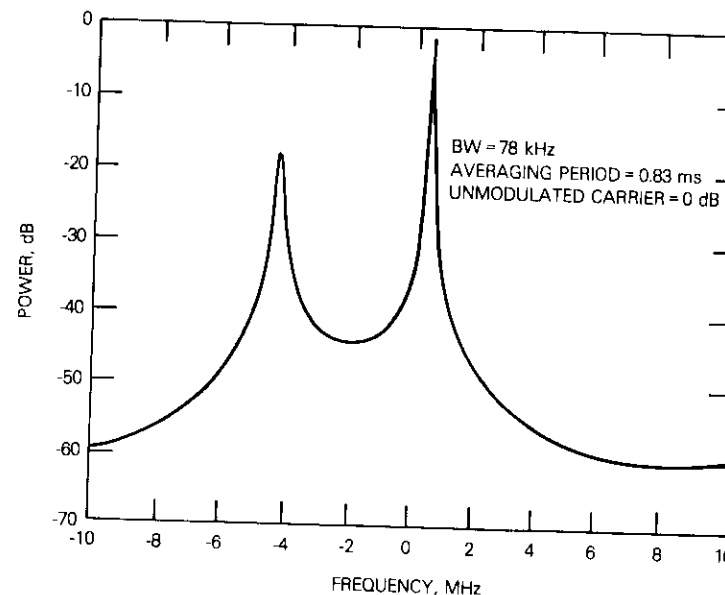


Figure 9. Power Spectrum for Case 1 (no dispersion)

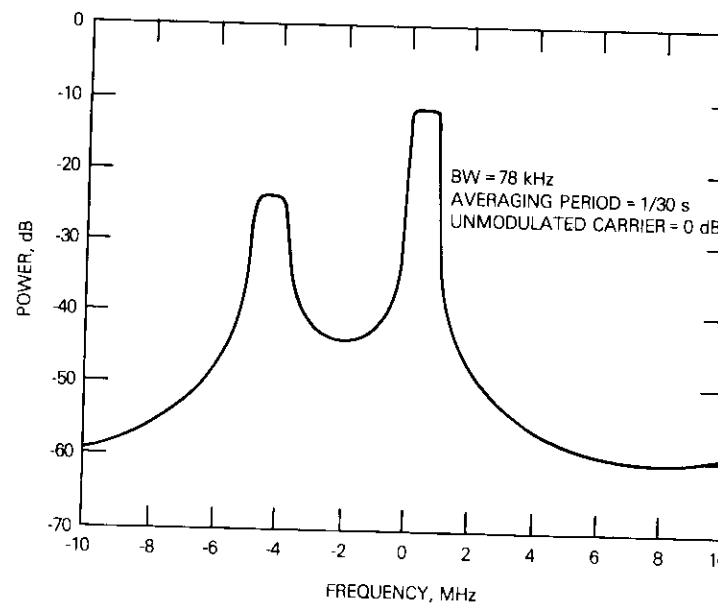


Figure 10. Power Spectrum for Case 2 (frame-rate triangular dispersion)

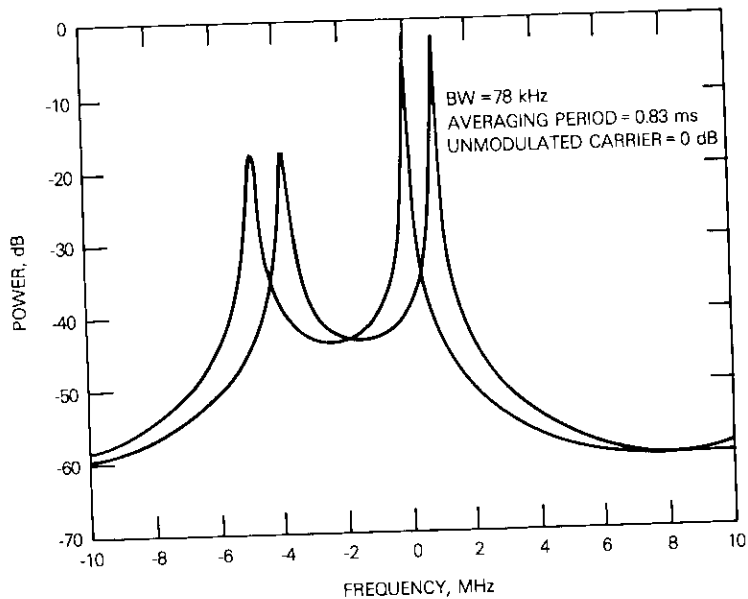


Figure 11. Short Period Power Spectrum for Case 2 (frame-rate triangular dispersion)

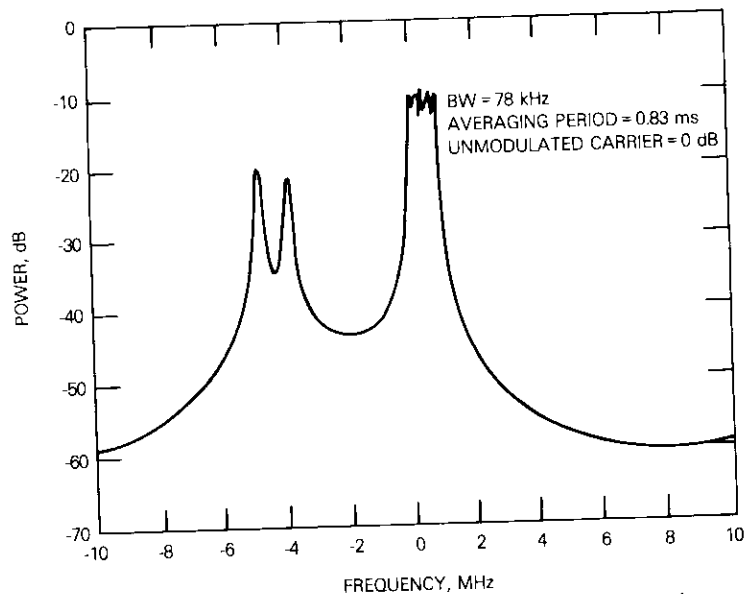


Figure 12. Power Spectrum for Case 3 (half-line-rate triangular dispersion)

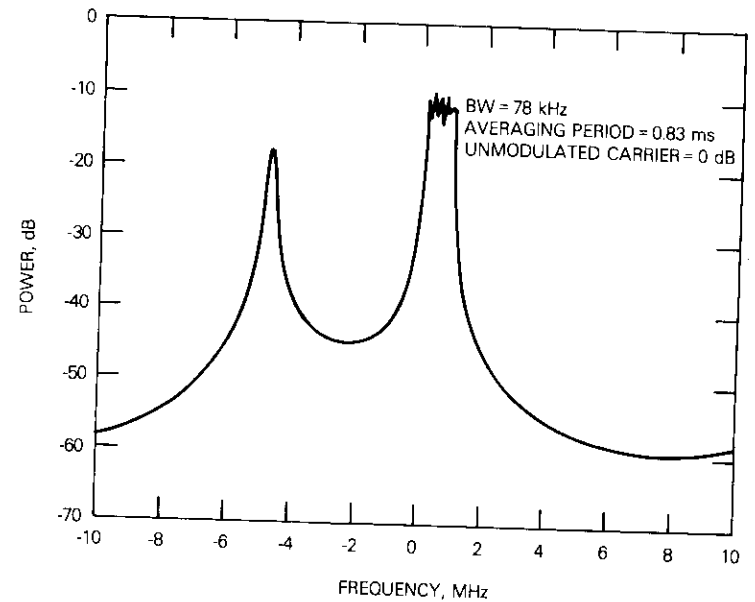


Figure 13. Power Spectrum for Case 4 (line-rate sawtooth dispersion)

interval. In these figures, as compared with Figure 10 for frame-rate dispersal with long averaging time, the spectra have a slightly modified shape, but the reductions for the highest spike remain the same (9.85 dB). Comparing Figures 12 and 13 with Figure 11, all of which have been obtained with the same averaging time of 0.83 ms, indicates that the spectral spike for half-linear-rate triangular or the line-rate sawtooth dispersal is much lower than that for the frame-rate triangular dispersal.

Hardware simulation experiments

The TV energy dispersal techniques using TV line-rate and half-line-rate waveforms were further investigated through a series of laboratory hardware simulation experiments. These experiments studied the effect of co-channel interference into an SCPC/PSK channel caused by a dispersal FM TV carrier under various conditions and the effect of TV picture impairment caused by dispersal waveform additions.

Dispersal waveforms

Three types of dispersal waveforms were included in the hardware simulation studies:

- a. half-line-rate triangular waveform synchronized with the line-blanking intervals (half-line-rate dispersal),
- b. line-rate sawtooth waveform synchronized with the line-blanking intervals (line-rate dispersal),
- c. frame-rate triangular waveform synchronized with the field-blanking intervals (frame-rate dispersal).

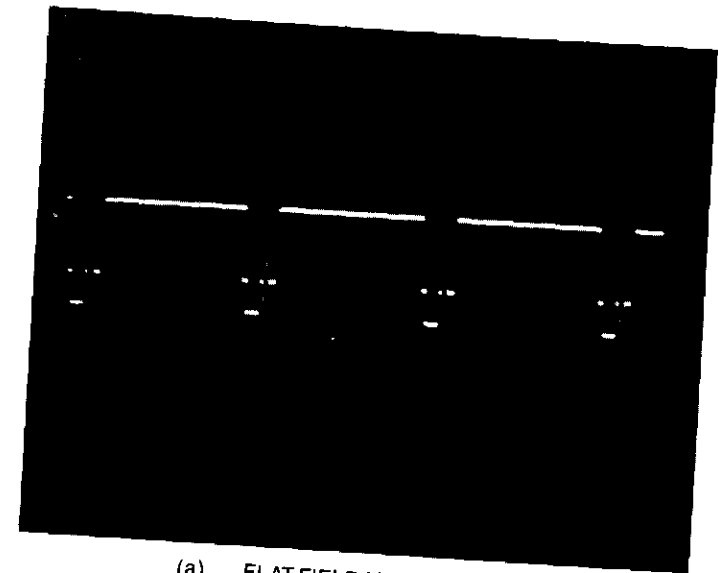
Special circuits for the generation and removal of the half-line-rate triangular and the line-rate sawtooth waveforms were developed. Waveform removal was accomplished using a subtraction scheme. The circuit extracted sync pulses from the incoming video signal, which were then used to synchronize and subtract the dispersal waveform from the composite video signal.

Figure 14a shows the waveform of typical lines of a flat-field video signal. Each line starts with a horizontal sync pulse, followed by the color burst and the constant amplitude representing the flat field. Figure 14b shows the same flat-field video signal with the half-line-rate triangular waveform added in phase with the video signal, starting at the left edge of each horizontal sync pulse. The amplitude of the dispersal waveforms shown is equal to 21 percent of the peak-to-peak amplitude of the video signal, corresponding to 1-MHz dispersion for the INTELSAT IV half-transponder TV. Figure 14c shows the flat-field video signal with the line-rate sawtooth waveform added starting at the right edge of each sync pulse, and Figure 14d shows the frame-rate triangular waveform (present standard) added on a time scale 250 times larger than that in Figures 14a, 14b, and 14c.

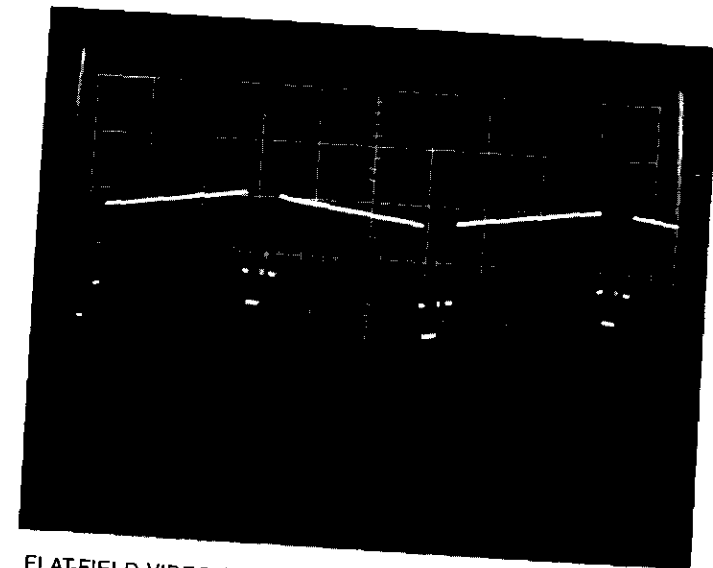
The half-line rate triangular and line-rate sawtooth waveforms exhibit the following features:

- a. The points of inflection of both waveforms fall outside the active portion of the video lines to minimize potential perceptible impairment in the middle of TV pictures.
- b. The line-by-line polarity reversal of the half-line-rate triangular waveform produces an averaging (cancelling) effect. However, the relative vertical positions of the even and odd sync pulses are changed as a result of adding the triangular waveform.
- c. The line-rate sawtooth waveform does not have the averaging effect. However, all the sync pulses are maintained at the same vertical level even after the waveform addition.

A similar line-rate dispersal waveform suggested by Weinberger [13] contains points of waveform inflection which fall within the active

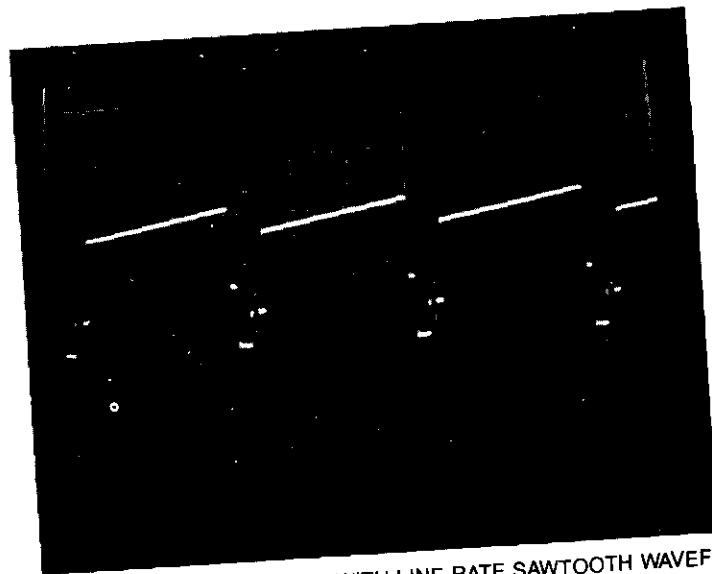


(a) FLAT-FIELD VIDEO SIGNAL

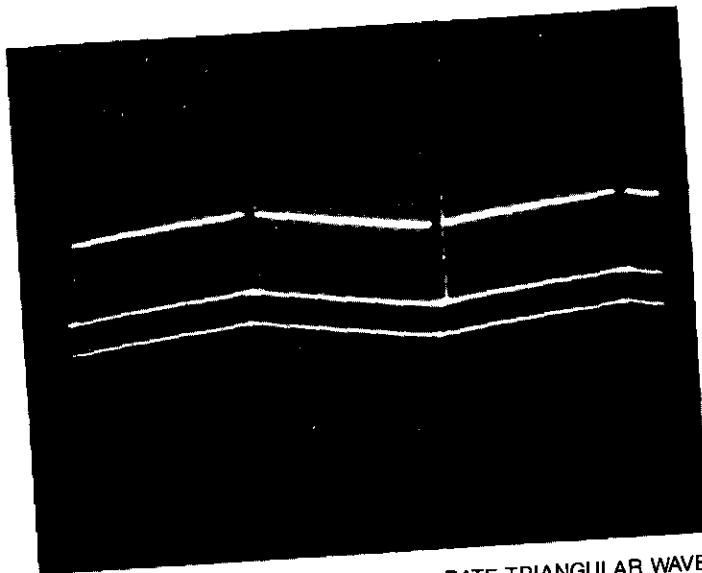


(b) FLAT-FIELD VIDEO SIGNAL WITH ONE-HALF-LINE-RATE TRIANGULAR WAVEFORM ADDED

Figure 14. *Dispersal Waveforms*



(c) FLAT-FIELD VIDEO SIGNAL WITH LINE-RATE SAWTOOTH WAVEFORM ADDED



(d) FLAT-FIELD VIDEO SIGNAL WITH FRAME-RATE TRIANGULAR WAVEFORM ADDED (shown in a time scale 250 times larger than a, b, or c)

Figure 14 (continued). *Dispersal Waveforms*

portion of the video lines. Waveforms of this type have not been considered in this study because of their greater potential for picture impairment and greater implementation complexity.

Experimental tests

The following series of experimental tests was performed to evaluate and compare the dispersal waveforms:

- a. TEST 1: SCPC/PSK average bit-error-rate measurements,
- b. TEST 2: SCPC/PSK bit-error distribution measurements,
- c. TEST 3: SPADE PCM voice channel impulse noise and signal-to-noise (S/N) ratio measurements,
- d. TEST 4: SPADE PCM voice subjective tests,
- e. TEST 5: television subjective tests.

Figure 15 is a block diagram of the experimental setup for these tests. The SCPC/PSK modulator and the demodulator allow manual selection of one 38-kHz SCPC/PSK channel from 108 channels located around 70 MHz. The SCPC equipment is connected to the test equipment by switches labeled 1, 2, 3, and 4 in accordance with the tests listed above. The 7-bit PCM coder and decoder are added to the circuit for tests 3 and 4. Noise and FM TV interfering signals are injected into the 70-MHz IF link between the SCPC/PSK modulator and demodulator.

To generate the FM TV interfering carrier, a baseband video signal from the video source is first fed into a dispersal waveform addition network where one of the three waveforms is synchronously added. The resulting signal is then fed, via a preemphasis network, to the FM modulator. The dispersed FM TV carrier is subsequently injected between the SCPC modulator and demodulator. For subjective tests, the composite video signal is fed into a dispersal waveform removal network where the appropriate type of dispersal waveform is removed. Devices are provided for varying and measuring the amount of residual dispersal waveform. The resulting video signal is fed into a television monitor for subjective evaluation.

The SCPC/PSK modulator-demodulator is the DICOM equipment previously developed at COMSAT Laboratories. This equipment is designed to accept either voice or wideband data signals for transmission using 4-phase PSK modulation. The incoming voice band signals are digitally encoded using the SPADE LSI 7-bit A-law companding PCM codec developed recently at COMSAT Laboratories. The PCM codec produces a data stream at 56 kbit/s, which is subsequently increased to a 64-kbit/s channel rate as a result of added frame synchronization

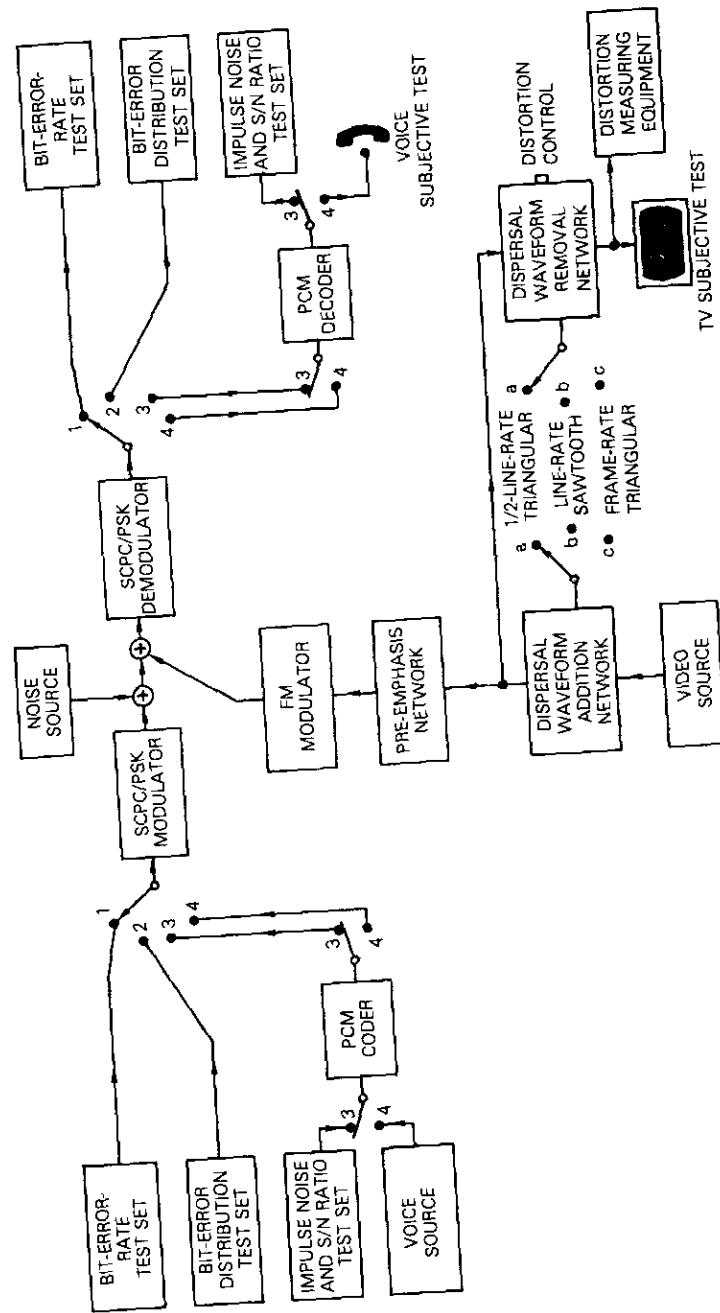


Figure 15. Experimental Setup

bits. The wideband data signals at the baseband rate of 50 kbit/s are interfaced directly into the SCPC channel unit and transmitted at a 66.6-kbit/s channel rate. In this mode, the PCM codec is switched off-line and an R3/4 rate changing forward active error correction codec is switched on-line to provide the necessary interface. At the receiving end, the error correction can be switched on or off.

The bit-error distribution test set is part of the channel monitor hardware and software system at COMSAT Laboratories [14]. The dispersal waveform addition and removal networks were specially developed for this study. The bit-error-rate test set is the HP-1654A error analyzer, and the impulse noise and S/N ratio test set is the H.L.I. model 3901 communication test system.

Standard INTELSAT IV-A half-transponder NTSC (525/60) TV characteristics were assumed for the tests unless otherwise stated. The standard dispersal deviation is 1 MHz, and the preemphasis was in accordance with C.C.I.R. Recommendation 405-1 [15]. For the TV subjective evaluation, color slides, live TV programs, and video test patterns were used as test materials. For the SCPC tests, unless otherwise indicated, a flat-field video signal and an SCPC channel coinciding with the major spike of the FM TV spectrum were selected to create the worst-case interference condition.

Definitions of terms

Throughout this study, the carrier-to-interference (C/I) ratio is defined as the ratio of modulated SCPC carrier power to the power of an unmodulated external FM carrier, measured at the demodulator AGC output (with the AGC turned off) in an SCPC channel coinciding with the unmodulated FM carrier. The carrier-to-noise (C/N) ratio is defined as the ratio of modulated SCPC carrier power to the power of added white noise measured at the same location. The C/I ratios (of the order of +10 to -6 dB) are small because they result from comparing a wideband interference source with a narrowband SPADE channel; they are not a measure of the actual isolation requirement. There are two TV channels per transponder and 800 SPADE channels per transponder; therefore, for an assumed voice activity of 40 percent, there will be 400×0.4 , or 160 active SPADE channels with approximately the same total power as one half-transponder TV channel. Thus, the factor $10 \log 160 = 22$ dB should be added to these C/I ratios to approximate isolation which could create conditions similar to those in the recorded data.

SCPC average bit-error-rate measurements

Modem performance

The experimental setup for the average bit-error-rate measurements is shown in Figure 15 with the test selection switch in position 1. Figure 16 shows the measured average bit-error rate versus C/N, with no added interference, for the SCPC/PSK modem used in the experiment. The modem performance is 1.8 dB below theoretical performance, which is within the modem specification value of 2.8 dB.

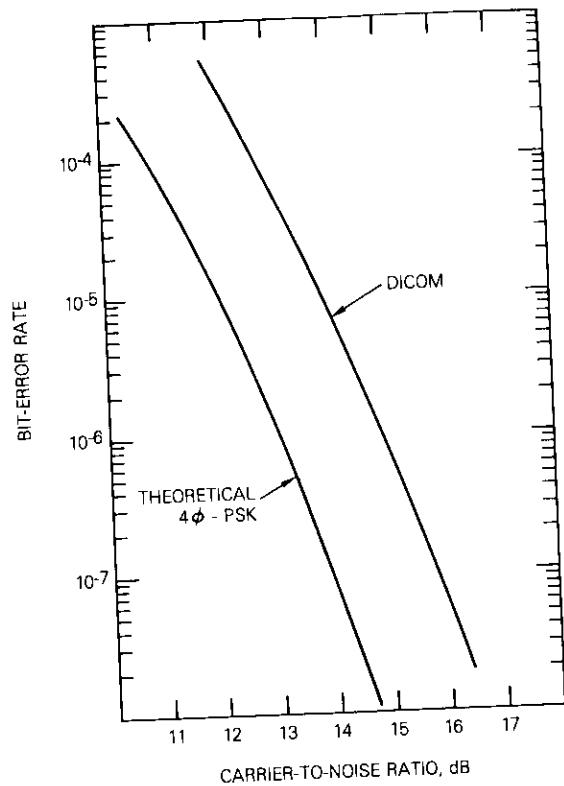


Figure 16. DICOM Modem Performance

Average bit-error rate with standard peak-to-peak dispersal deviation of 1 MHz

Figure 17 shows the measured bit-error rate versus C/I ratio with

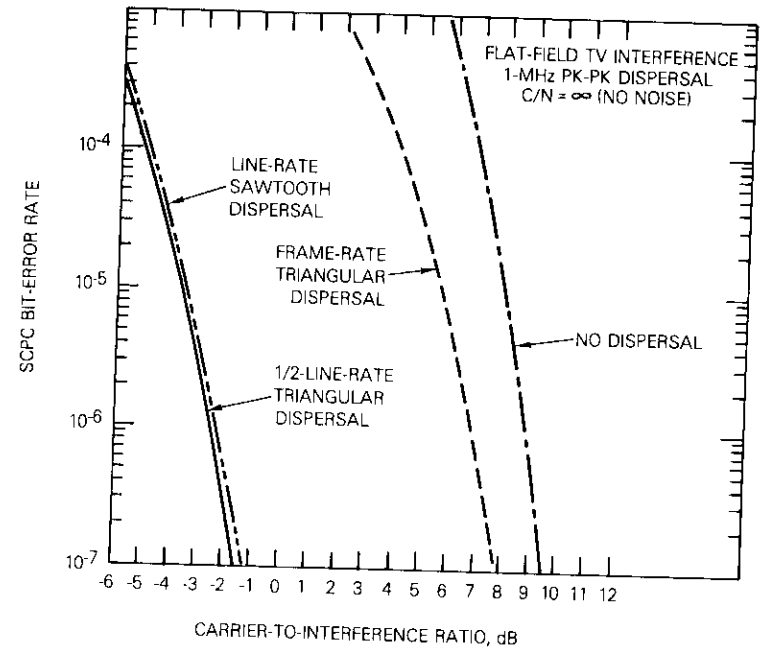


Figure 17. SCPC Bit-Error Rate vs C/I, C/N = infinity

no added noise ($C/N = \infty$). The four curves correspond to half-line-rate, line-rate, frame-rate, and no dispersal, as indicated. The results show that, for bit-error rates ranging from 10^{-4} to 10^{-7} , frame-rate dispersal produced about 2- to 3-dB reduction in interference effect as compared to the case with no dispersal. In the same bit-error-rate range, both half-line-rate and line-rate dispersals produced an 11- to 12-dB reduction as compared to the case with no dispersal or a 9-dB reduction relative to the present frame-rate dispersal. The results for half-line-rate and line-rate dispersals were very similar, with the two curves almost overlapping. Table 1 summarizes the C/I ratios corresponding to $BER = 10^{-6}$ for the three types of dispersal.

TABLE 1. C/I RATIO FOR $BER = 10^{-6}$

Dispersal	C/N = infinity (dB)	C/N = 15 dB (dB)
Frame-Rate Triangular	6.8	16.7
Half-Line-Rate Triangular	-2.4	7.6
Line-Rate Sawtooth	-2.4	7.7

Measurements of SCPC bit-error rate as a function of the C/I ratio were then repeated for $C/N = 15$ dB. Figure 18 shows the measured bit-error rate versus C/I ratio. At a bit-error rate of 10^{-6} , both the half-line-rate and the line-rate dispersals produced about 9-dB reduction in interference effect relative to frame-rate dispersal (see Table 1).

The previous two tests ($C/N = \infty$ and $C/N = 15$ dB) were repeated with rate 3/4 error correction coding in effect for frame-rate and half-line-rate dispersal. Figures 19 and 20 show the measured bit-error rate versus C/I ratio for $C/N = \infty$ and 15 dB, respectively. The results without error correction are also shown for reference. For both cases, error correction coding was found to produce the same relative advantage for half-line-rate dispersal over the standard frame-rate dispersal. For $C/N = 15$ dB (Figure 20), the random bit errors caused by the white noise were corrected, and consequently, a larger improvement due to error correction was obtained.

In summary, the SCPC average bit-error-rate test results show that the bit-error performances of the half-line-rate triangular dispersal method and the line-rate sawtooth dispersal method were extremely similar. In addition, for the four cases ($C/N = \infty$ and $C/N = 15$ dB, with and without error correction), the half-line-rate or the line-rate dispersal method produced a reduction of about 9 dB in interference potential over the present frame-rate dispersal method.

Average bit-error rate as a function of peak-to-peak dispersal deviation

The objective of this test was to compare the interference reduction capabilities of the frame-rate triangular and line-rate sawtooth dispersal techniques for different peak-to-peak dispersal deviations, Δf . Figure 21 shows the measured SCPC bit-error rate versus C/I for line-rate sawtooth dispersal with $C/N = \infty$ for the different values of Δf , ranging from 0.25 to 2.5 MHz. Similarly, Figure 22 shows the results for frame-rate triangular dispersal with Δf ranging from 0.5 to 2.0 MHz.

Figures 23 and 24 show similar results for $C/N = 15$ dB for line-rate sawtooth and frame-rate triangular dispersal, respectively. In this case, the curves appear to be approaching asymptotically for increasing C/I, a bit-error rate of about 7×10^{-7} , which is the bit-error rate of the SCPC modem at $C/N = 15$ dB with no interference.

A comparison of Figures 21 and 22 for $C/N = \infty$ indicates that the SCPC bit-error rate with the line-rate dispersal is more sensitive to changes in Δf than the bit-error rate with the frame-rate dispersal.

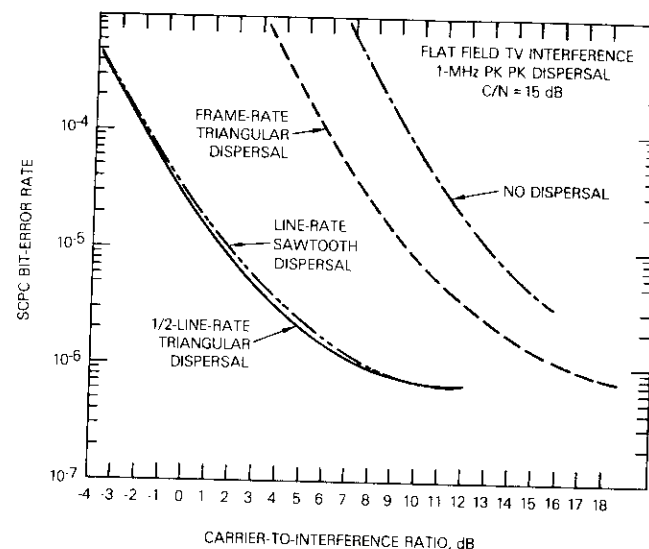


Figure 18. SCPC Bit-Error Rate vs C/I, $C/N = 15$ dB

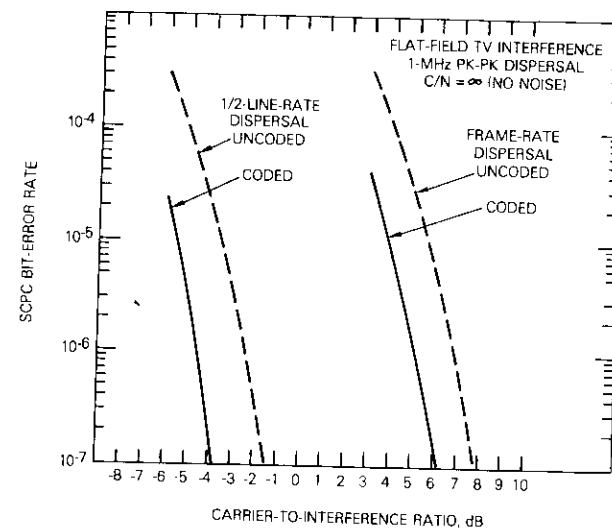


Figure 19. SCPC Bit-Error Rate vs C/I With and Without Error Coding for $C/N = \infty$

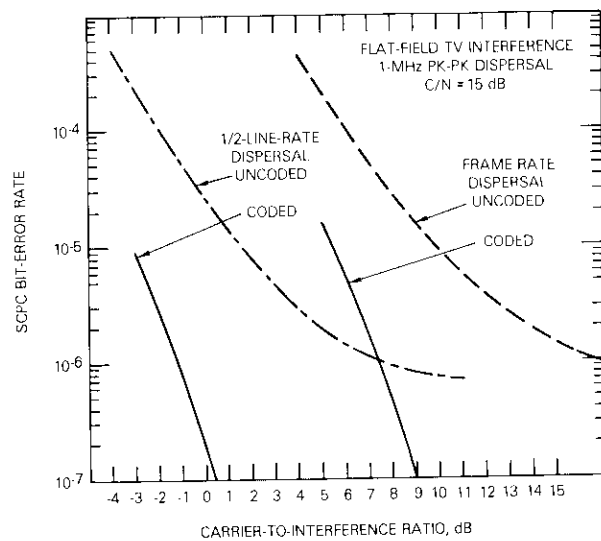


Figure 20. SCPC Bit-Error Rate vs C/I With and Without Error Coding for $C/N = 15$ dB

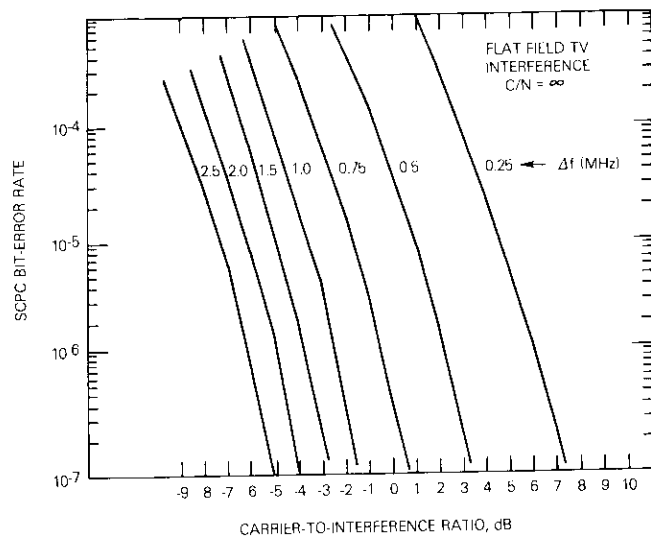


Figure 21. SCPC BER vs C/I With Line-Rate Dispersal for $C/N = \infty$

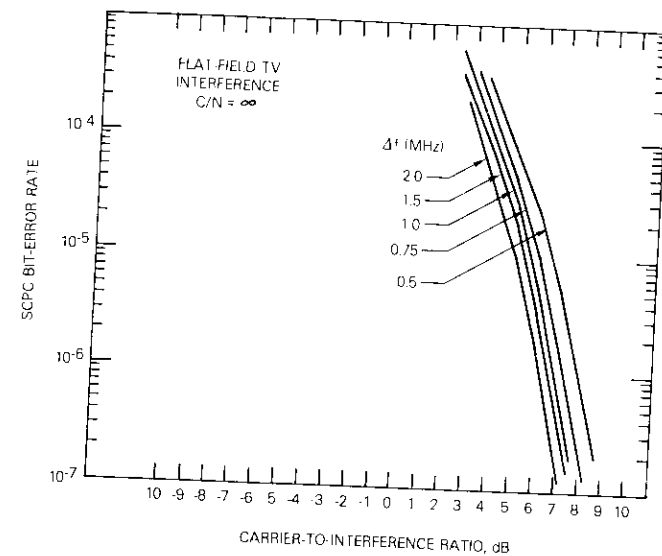


Figure 22. SCPC BER vs C/I With Frame-Rate Dispersal for $C/N = \infty$

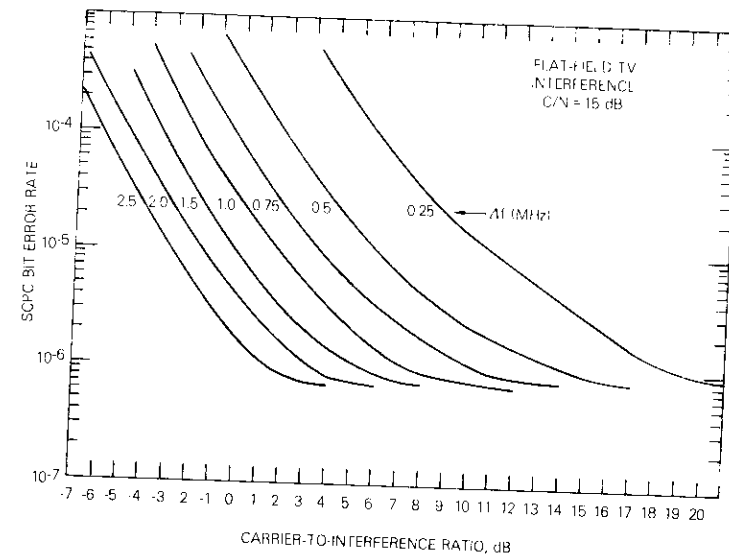


Figure 23. SCPC BER vs C/I With Line-Rate Dispersal for $C/N = 15$ dB

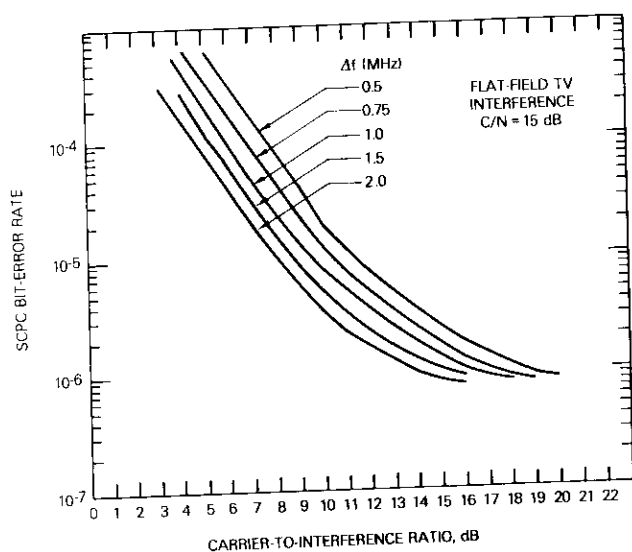


Figure 24. SCPC BER vs C/I With Frame-Rate Dispersal for $C/N = 15$ dB

Figure 25 shows the C/I ratio in dB corresponding to 10^{-6} bit-error rate as a function of Δf (Δf in logarithmic scale). The result shows that the curve for the frame-rate dispersal is roughly a linear function of Δf ,

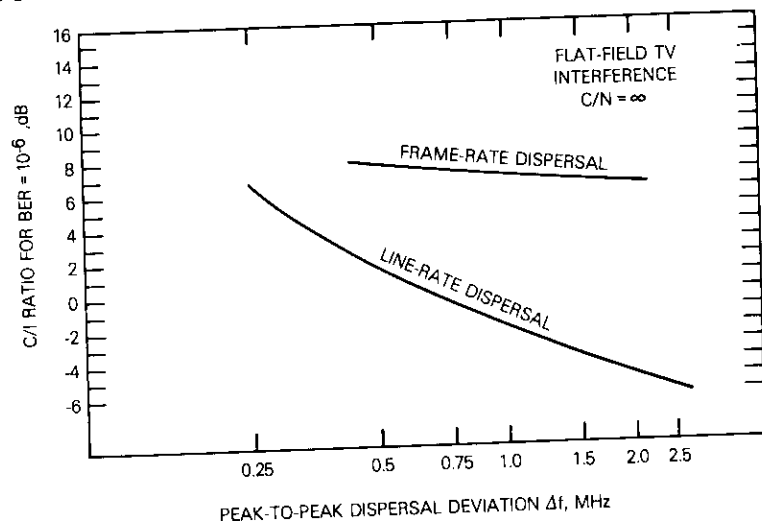


Figure 25. C/I for $BER = 10^{-6}$ vs Δf With $C/N = \infty$

while the curve for the line-rate dispersal is a relatively nonlinear and significantly more sensitive function of Δf . A comparison of Figures 23 and 24 for $C/N = 15$ dB also demonstrates a similar characteristic. Figure 26 shows the C/I ratio for $BER = 10^{-6}$ as a function of Δf for $C/N = 15$ dB.

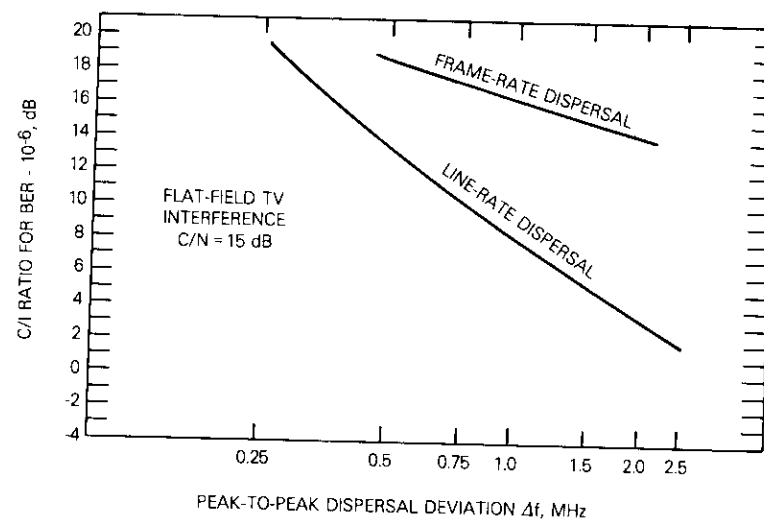


Figure 26. C/I for $BER = 10^{-6}$ vs Δf With $C/N = 15$ dB

The characteristics demonstrated by the above results are as predicted through computer simulation of the sweep interference mechanisms presented previously. Numerical comparison of experimental and analytical results will be presented later in this paper along with other tests.

SPADE voice channel impulse noise measurements

Impulse noise measurements on the SPADE PCM voice channel were performed. Figure 15 shows the test setup with the test selection switch in position 3. The half-line-rate and the frame-rate dispersal methods were tested and compared. The measurements were made with flat-field TV interference and without added noise. Voice activation was not used in the SPADE equipment. Two types of impulse noise measurements were performed:

a. loaded channel measurement, in which a 1004-Hz tone was transmitted and then notched out before the noise measurement was made;

b. idle channel measurement, in which no tone was transmitted and the transmitting end was quietly terminated.

A tone signal level of 0 dBm0 was used for the impulse noise measurements. The impulse counter recorded the occurrences of noise impulses which exceeded preset threshold levels over a fixed time. Two modes of impulse counting were employed. With the first mode, the counter had a maximum counting rate of 7 counts per second (6,300 counts per 15 minutes), which is consistent with C.C.I.T.T. Recommendation V.55 regarding impulse noise measurements [16]. With the second mode, the channel-limited mode, the counter had a maximum counting rate of 180 counts per second (162,000 counts per 15 minutes).

Table 2 shows the recorded impulse counts as a function of C/I for the loaded channel for the two dispersal methods at three present threshold levels. The measuring time was 15 minutes. Table 3 shows the results for the idle channel.

TABLE 2. LOADED CHANNEL IMPULSE COUNT PER 15 MINUTES

Dispersal	C/I (dB)	C.C.I.T.T. Standard			Channel-Limited		
		-1 dBm0	-11 dBm0	-21 dBm0	-1 dBm0	-11 dBm0	-21 dBm0
Half-Line-Rate	-7	2,451	4,857	5,235	3,924	20,958	32,220
	-6	1,125	2,826	3,519	1,179	7,599	11,253
	-5	255	828	1,335	165	1,785	2,457
	-4	63	519	684	36	282	393
	-3	18	69	90	6	75	87
	-2	0	3	9	0	9	12
Frame-Rate	2	2,520	4,686	5,280	4,792	16,673	27,923
	3	1,722	4,617	4,737	1,937	9,073	15,248
	4	912	2,856	3,582	1,203	5,248	10,074
	5	291	1,854	2,418	597	5,113	8,496
	6	147	909	1,227	209	1,219	2,172
	7	21	255	327	9	254	369
	8	3	93	123	5	139	122
	9	0	21	21	0	3	2

Figure 27 shows the 15-minute impulse counts for the threshold level of -21 dBm0 recorded as a function of C/I with the C.C.I.T.T. standard counting mode, with and without a transmitted tone. Based

TABLE 3. IDLE CHANNEL IMPULSE COUNT PER 15 MINUTES

Dispersal	C/I (dB)	C.C.I.T.T. Standard			Channel-Limited		
		-1 dBm0	-11 dBm0	-21 dBm0	-1 dBm0	-11 dBm0	-21 dBm0
Half-Line-Rate	-11	4,035	8,550	5,820	17,835	50,775	81,270
	-10	3,165	4,980	5,730	5,970	20,355	49,875
	-9	358	1,787	4,764	764	4,387	25,750
	-8	16	118	2,760	22	166	5,436
	-7	0	3	686	0	3	19
	-6	0	0	20	0	0	17
Frame-Rate	0	1,800	3,075	3,960	2,040	4,905	8,520
	1	441	1,135	2,734	321	1,381	6,087
	2	30	123	1,138	55	263	1,623
	3	4	14	309	4	9	309
	4	0	1	99	0	0	81
	5	0	0	18	0	0	19

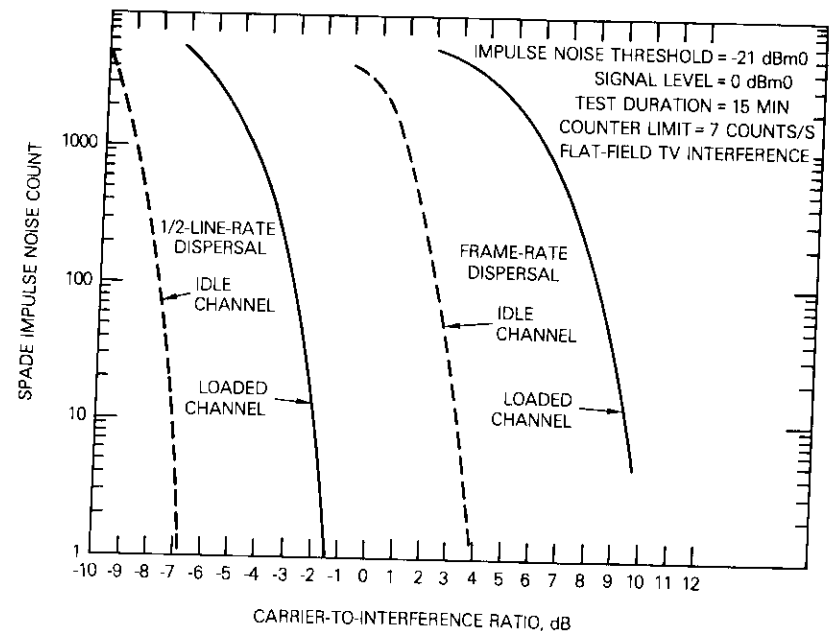


Figure 27. SPADE Impulse Noise Measurement Results

on the value of 15 impulse counts per 15 minutes, which is often considered a standard, Figure 27 shows that the half-line-rate method improved tolerable C/I approximately 10 to 11 dB, as compared with the frame-rate method, for both types of impulse noise measurements. For both dispersal methods, the results measured with and without a transmitted tone had a separation of about 5 to 6 dB in C/I. The pair of curves represents the upper and the lower extremes of impulse noise occurrence for the transmission of a normal level signal. Table 4 summarizes the C/I values corresponding to 15 impulse counts per 15 minutes for the two dispersal methods and for the two types of measurement.

TABLE 4. C/I RATIOS FOR 15 IMPULSE COUNTS PER 15 MINUTES, THRESHOLD = -21 dBm0

Dispersal Method	Measurement Type (dB)	
	Loaded Channel	Idle Channel
Frame-Rate	9	3
Half-Line-Rate	-2	-7

SPADE voice channel signal-to-noise ratio measurement

The S/N on the SPADE PCM voice channel was measured as a function of C/I with flat-field TV interference and no added white noise, for both the half-line-rate and the frame-rate dispersal methods. Voice activation was not used in the SPADE equipment. Similar to the impulse noise measurements, S/N measurements for both the loaded and idle channel were made. A tone signal level of -15 dBm0 was used. The measured results were adjusted to correspond to psophometric noise weighting.

Figures 28 and 29 show the measured S/N as a function of C/I for the loaded and idle channel, respectively. In terms of the 1-dB degradation points of the two curves (e.g., S/N = 49.5 dB in Figure 29), the measured results show that the half-line-rate dispersal method produced about 10-dB improvement in tolerable C/I, as compared with the frame-rate dispersal method, under both the loaded and idle channel conditions.

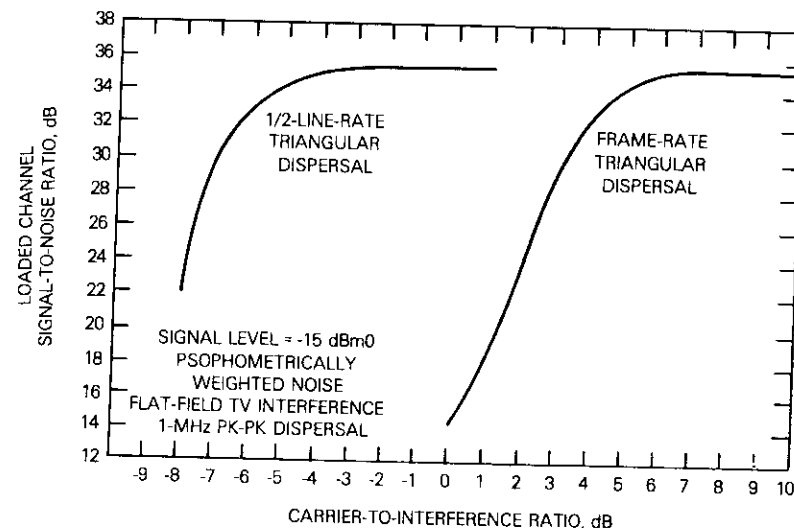


Figure 28. SPADE Loaded Channel S/N vs C/I

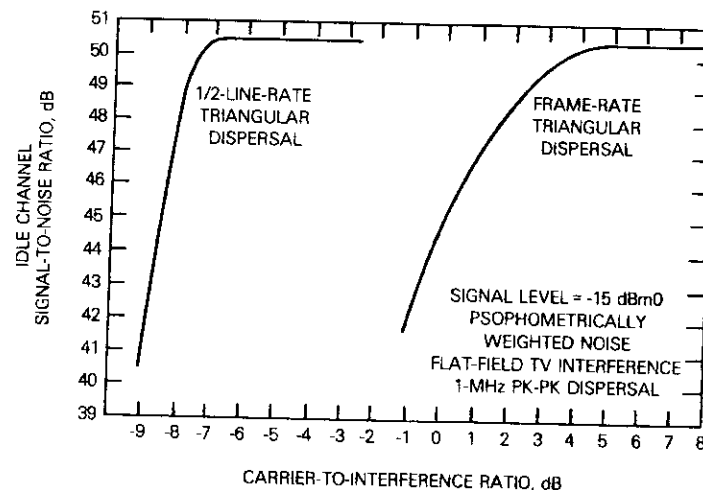


Figure 29. SPADE Idle Channel S/N vs C/I

SPADE PCM voice subjective test

A subjective test was performed to evaluate the SPADE voice quality

as a function of C/I and dispersal method. For each experimental condition, the SPADE voice quality was assessed in terms of an S/N of analog speech, considered to be equivalent by subjective standards. The speech level was set at -15 dBm0. The testing technique, known as the Youden Square experimental procedure, requires participants to evaluate sets of four samples of prerecorded speech by rank ordering them in descending order of quality [17], [18].

Figure 30 shows the equivalent S/N versus C/I for the two dispersal methods as determined by the subjective experiment. Note that the improvement of the half-line-rate technique over the frame-rate technique is of the same magnitude (10 dB) and trend as that experienced for the bit-error-rate measurements.

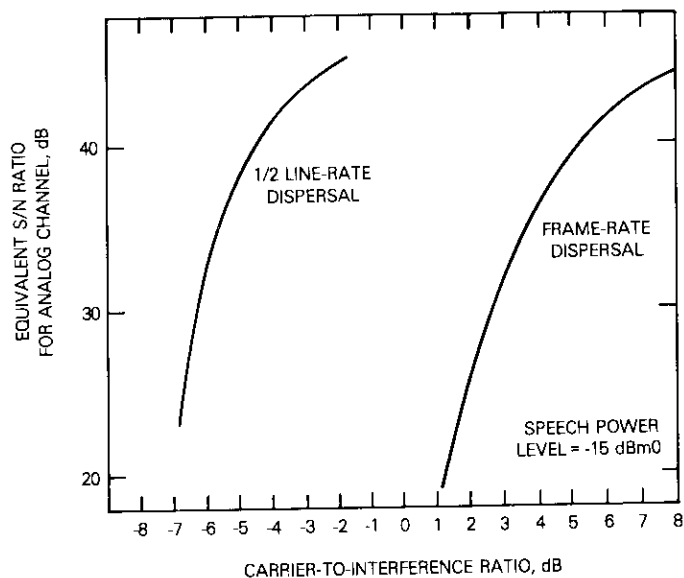


Figure 30. Subjectively Assessed SPADE Voice S/N vs C/I

Comparison of experimental and analytical results

Figure 31 shows a graphical comparison of the experimental results and those obtained from analysis and computer simulation of the sweep interference mechanism. The solid curve in this figure is the analytically predicted improvement in interference power reduction obtained with

half-line-rate dispersal instead of frame-rate dispersal. The data points represent measured results for the different experiments, which include average bit-error-rate tests for different values of peak-to-peak dispersal deviation, as well as S/N test, voice subjective test, and impulse noise tests at the standard deviation of 1 MHz.

The experimental results and the analytical prediction are found to be in agreement within 1.6 dB, which is within the tolerance limits imposed by the experimental conditions and the simulation model.

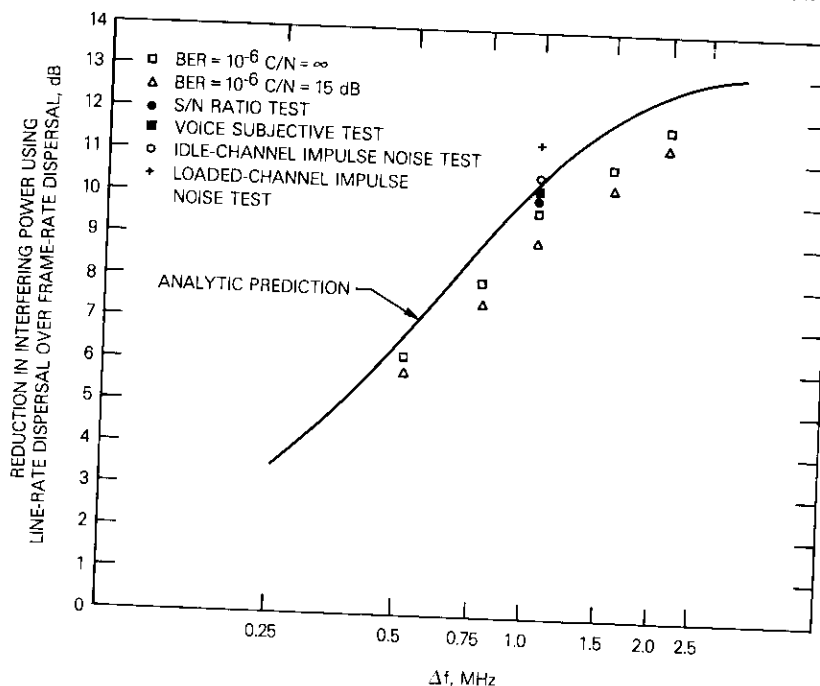


Figure 31. Comparison of Analytical and Experimental Results

Interference with combined frame-rate and line-rate dispersal

This test investigated the interference reduction capacity of a composite dispersal technique which uses a combination of frame-rate and line-rate waveforms [13]. The SCPC/PSK bit-error rate as a function of C/I was measured using a composite waveform consisting of 50-

percent frame-rate dispersal and 50-percent line-rate dispersal. This waveform was generated and added to a flat-field video signal by concatenating two waveform addition circuits. First, the line-rate sawtooth waveform with 0.105-V peak-to-peak amplitude (corresponding to 0.5-MHz peak-to-peak dispersal deviation) was added to the video signal. Then the frame-rate triangular waveform with the same amplitude was added to the resulting signal. The final composite signal was fed, via a preemphasis network, to an FM modulator to generate the interfering carrier at 1F. Observing the power spectrum of the resulting carrier revealed that the major spectral spike had a dispersed width of 1 MHz, as could be expected. An SCPC channel located in the center of the dispersed spike was selected for the bit-error-rate measurement.

Figure 32 shows the measured bit-error rate as a function of C/I for the composite frame-rate plus line-rate dispersal waveform. The curve

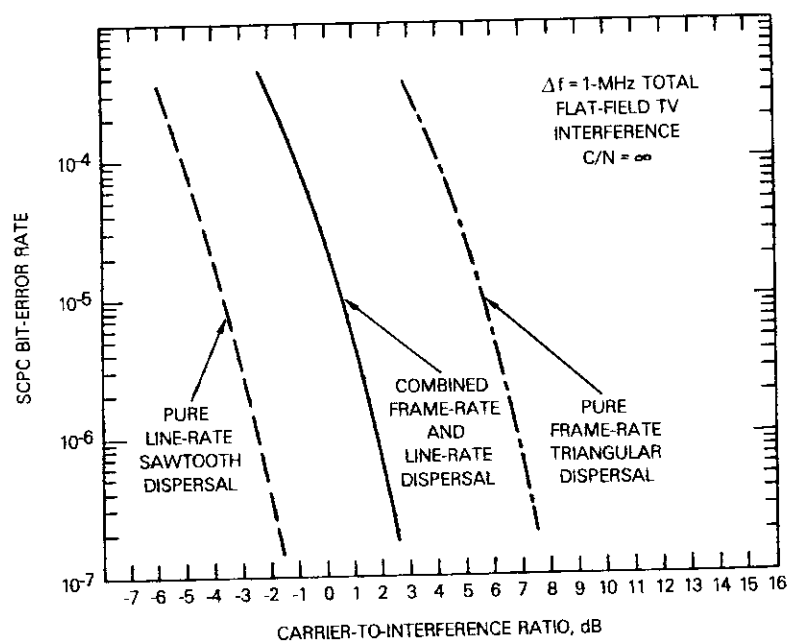


Figure 32. SCPC BER vs C/I for Composite and Pure Dispersals

for the composite dispersal waveform falls approximately midway between the pure frame-rate and pure line-rate curves obtained pre-

viously. At the bit-error rate of 10^{-6} , for example, the C/I for the composite dispersal is 4.2 dB higher than that for the pure line-rate dispersal.

It is also of interest to compare the curve for the composite dispersal in Figure 32 with the curve corresponding to $\Delta f = 0.5$ MHz for the pure line-rate dispersal in Figure 21. The curve for the composite dispersal waveform is only slightly below (better than) that for the pure line-rate dispersal, although the total peak-to-peak dispersal deviation was twice that of the latter.

These results show that the use of the composite dispersal waveform was significantly less effective in terms of reduced bit-error rate than the use of the pure line-rate sawtooth waveform. The deviation (waveform amplitude) for the line-rate dispersal waveform was the controlling factor for the interference reduction. The use of additional frame-rate dispersion produced only minimal additional improvement.

Interference potential of video sync pulses and blanking levels

In the previous studies, measurements were made in a channel located within the dispersed major spectral spikes of a flat-field video signal to obtain data for the worst-case interference condition. The present study was conducted to thoroughly assess the interference potential of the TV carrier outside the major spectral spike.

SCPC/PSK bit-error-rate measurements were made for the two channels which coincided with the two secondary spikes caused by the flat-bottoms of the sync pulses and by the blanking levels. The interfering FM carrier was modulated by a flat-field video signal dispersed by the line-rate sawtooth waveform to a peak-to-peak deviation of 1 MHz. In this signal, no dispersal waveforms were added within the sync pulses. Figure 33 shows the measured bit-error rate versus C/I for the two channels. The curves previously obtained for the major spike with line-rate and frame-rate dispersal are also shown for comparison.

The curves for the two secondary spikes (Figure 33) both fall to the left of the two curves for the major spike, about 3 dB apart from that for the line-rate dispersal and 12 dB apart from that for frame-rate dispersal. This verifies that the data for the major spectral spike were the worst-case. However, the curves for the secondary spikes are below that for the major spike by only 3 dB. Thus, the dispersion of the video sync pulses may be desirable to further reduce the interference

potential, which can be accomplished by minor changes in the waveform addition circuit.

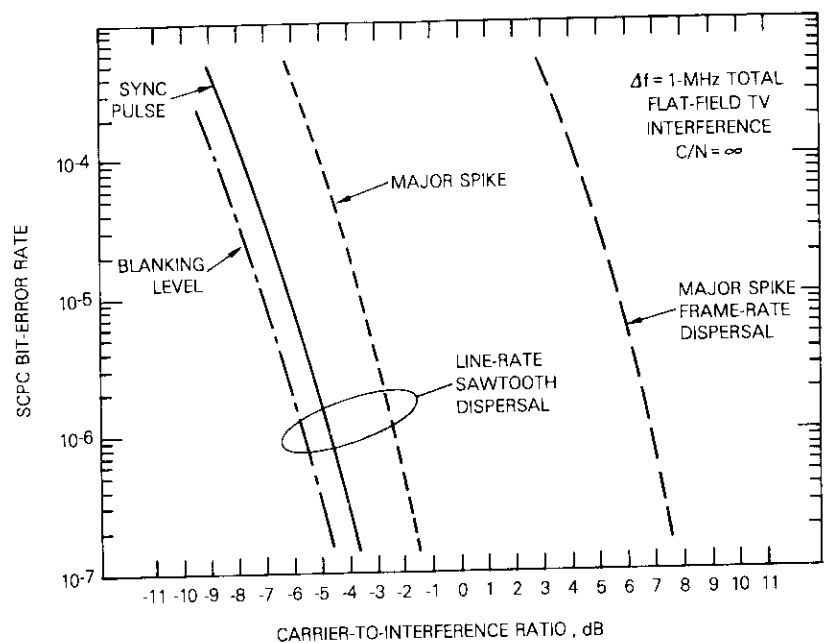


Figure 33. SCPC BER vs C/I for Secondary Spikes

SCPC/PSK bit-error distribution measurements

Bit-error distribution measurements have been performed to study the statistical distribution of bit errors, or the burstiness of bit-error occurrence, while the SCPC/PSK transmission is under the interference of FM TV carriers using different dispersal methods. This information is not obtainable through the average bit-error-rate measurements such as those presented previously.

Figure 15 shows the experimental setup for the bit-error distribution measurements with the test selection switch in position 2. No noise was added into the transmission path ($C/N = \infty$) and error correction was bypassed. The bit-error-rate test set, the channel monitor, recorded exact occurrence of bit errors as a function of time on magnetic tape. Statistical analysis of the data was then performed off-line on an IBM 360/65 computer. Two tests were conducted and have

produced the following observations.

A test was first conducted with a fixed average bit-error rate of 6×10^{-5} , which corresponds to C/I values of +4.5 dB and -4.8 dB for the frame-rate and half-line-rate dispersal, respectively. Under this condition, the frame-rate dispersal was found to be four times more likely to cause complete modem failures (loss of carrier recovery or loss of clock in the demodulator) than the half-line-rate dispersal. The long and high-density error bursts associated with such failures would affect the performance of error correction codes and produce subjective voice impairment in the form of audible clicks. During the intervals in which no modem failure occurred, the error distribution with frame-rate dispersal was found to be only slightly more nonrandom than that with half-line-rate dispersal.

A second test was conducted under the fixed circuit condition of $C/I = 6$ dB and $C/N = 15$ dB which yielded average bit-error rates of 1×10^{-4} and 1.7×10^{-6} for the frame-rate and half-line-rate dispersal, respectively. Under this condition, the error distribution with frame-rate dispersal was found to be drastically more nonrandom than that with half-line-rate dispersal, even during the intervals in which no modem failure occurred. The rate of occurrence of modem failure under this test condition was much higher with frame-rate dispersal than with half-line-rate dispersal (with a recorded ratio of 8:0). Under both test conditions, the characteristics of error distribution for the half-line-rate and the line-rate dispersal methods were found to be extremely similar, as expected.

Television subjective test and dispersal waveform addition and removal

The effectiveness of a TV energy dispersal method is also determined by its potential impairment effect on the video signal itself. The added dispersal waveform should be effectively removable at the receiving end without causing significant perceptible degradation of picture quality. For the presently used dispersal method, the slowly varying (30-Hz) waveform can be adequately removed using the technique of clamping [2], [19]–[21]. Higher frequency dispersal waveforms require alternative waveform removal techniques. The picture impairment and waveform removal aspects of the proposed line-rate sawtooth and half-line-rate triangular waveforms have been investigated.

A television subjective test was performed to determine the corre-

lation between the amount of "residual" dispersal waveform and the picture impairment effects. Using the specially developed waveform addition and subtraction circuits, a dispersal waveform with amplitude corresponding to a 1-MHz peak-to-peak deviation was added synchronously to the video signal. During the subjective evaluation, an observer manually controlled the amount of dispersal waveforms to be subtracted from the video signal and observed the corresponding picture on a TV monitor. Six "expert" observers participated in the subjective evaluation. The test material included color slides, the color bar test pattern, and live TV programs.

Table 5 summarizes the amounts of residual dispersal waveform corresponding to the "just perceptible degradation" determined in the subjective test for the different test materials. Note that the full amplitude dispersal waveform for the 1-MHz dispersal is 29.4 IRE units and the peak-to-peak video signal is 140 IRE units (1 V). The line-rate sawtooth waveform, which produced a shading effect across the TV screen, was found to be less objectionable than the half-line-rate triangular waveform which produced an effect of reduced vertical resolution.

TABLE 5. TV SUBJECTIVE TEST RESULTS

Test Material	Amplitude of Residual Waveform in IRE Units for "Just Perceptible Degradation"	
	Half-Line-Rate Triangular	Line-Rate Sawtooth
Slide of Quiet Scene	5.85	9.4
Slide of Busy Scene	5.95	9.1
Color Bar Test Pattern	6.8	9.3
Live TV Program	6.65	9.3
Overall	6.3	9.3

These results indicate that subtracting the half-line-rate triangular or the line-rate sawtooth waveform poses no critical problem. Automatically adjusted circuitry can remove the waveform to ± 1 IRE unit which is far below the level of perceptible degradation.

Synchronous addition and removal of the half-line-rate triangular and line-rate sawtooth waveforms are accomplished as follows. At the transmitting end, horizontal sync pulses are first extracted from the incoming video signal. With these pulses and a charging-discharging circuit (a current feedback amplifier), a half-line-rate triangular

waveform (or a line-rate sawtooth waveform) is generated. The waveform is added in-phase with the video signal, which is properly delayed to compensate for the processing time. At the receiving end, a similar scheme is used for waveform removal. Sync pulses are first extracted from the composite video signal which contains the dispersal waveform. With these pulses, the appropriate waveform is generated and subtracted in-phase from the composite video signal.

The present implementation permits manual adjustment of the amplitude of the dispersal waveform to be subtracted. In the future implementation, the amplitude will be automatically adjusted by a closed-loop nulling technique. Samples of the composite video waveform will be taken during the intervals of the front and back porch. By adjusting the waveform to minimize the difference between the front and back porch samples, the dispersal waveform can be eliminated with a high degree of accuracy. This technique, which functions on the two different levels, is unaffected by the absolute level of the incoming video signal or the picture content. No special demands are placed on AGC circuitry. The method is also insensitive to sync pulse amplitude or other slight departures from the standard in the composite waveform. An alternative approach would be to utilize the horizontal lines within the vertical blanking interval as the standard reference.

Digital TV interference

For comparison with FM TV, an experimental study was performed to assess the interference potential of digital TV with respect to SCPC/PSK transmission. The digital TV coder used was CODIT (COMSAT digital television) [22] developed at COMSAT Laboratories. CODIT employs intraframe DPCM coding to transmit a high-quality NTSC television signal with a nominal bit rate of 43 Mbit/s. The digital data stream was fed into a 4-phase CPSK modem to generate an IF carrier at 70 MHz. SCPC bit-error-rate tests were performed using the 70-MHz IF digital TV carrier as the interfering carrier. Figure 34 shows a block diagram of the experimental setup. Since the carrier was modulated by a scrambled digital bit stream, the characteristic of the carrier power spectrum (Figure 35) was practically unaffected by the video signal being transmitted. Unlike the case for FM TV, there were no spectral spikes caused by certain characteristics of the video signal. An SCPC channel located near the center of the carrier spectrum was selected for bit-error-rate measurements as the worst-case channel.

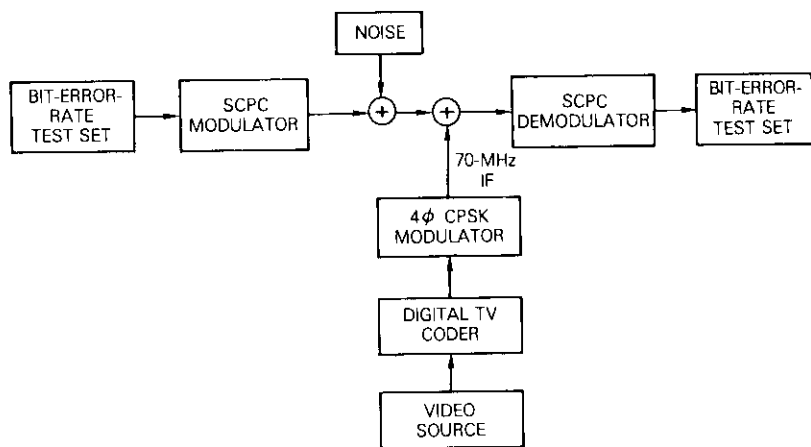


Figure 34. Test Setup for Digital TV Interference Measurement

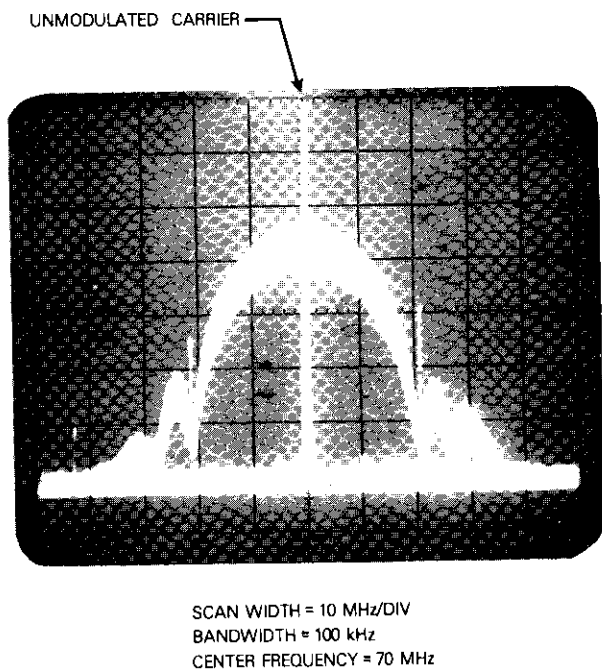


Figure 35. CODIT Power Spectrum

The SCPC bit-error rate was measured as a function of C/I for $C/N = \infty$ and $C/N = 15$ dB. With the presently implemented bit rate of 43 Mbit/s, the required transmission bandwidth for the CODIT carrier was about 25.8 MHz, which was greater than the 17.5-MHz bandwidth for the half-transponder TV for an INTELSAT IV-A satellite. For correct comparison with the previous results for FM TV interference, an adjustment factor of $10 \log (25.8/17.5) = 1.7$ dB was added to the C/I for digital TV interference. Figure 36 shows the measured bit-error rate versus the adjusted C/I with digital TV interference for $C/N = \infty$. Figure 37 shows the results for $C/N = 15$ dB. The curves for the worst-case FM TV interference with frame-rate and line-rate dispersal are also shown for comparison. According to these results, the interference potential of digital TV was 9 dB lower than that of FM TV with the line-rate dispersal technique, or 18 dB lower than that of FM TV with the present frame-rate dispersal technique.

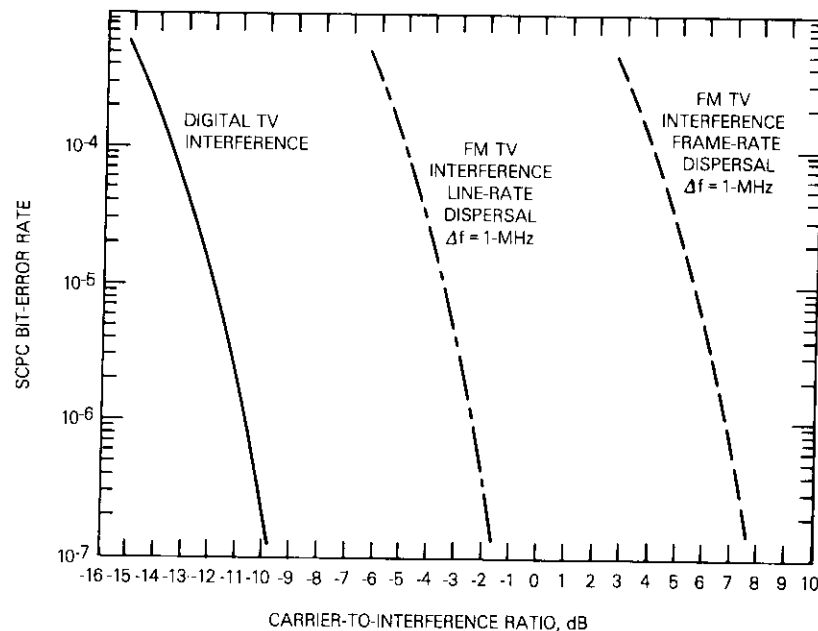


Figure 36. SCPC BER vs C/I for $C/N = \infty$

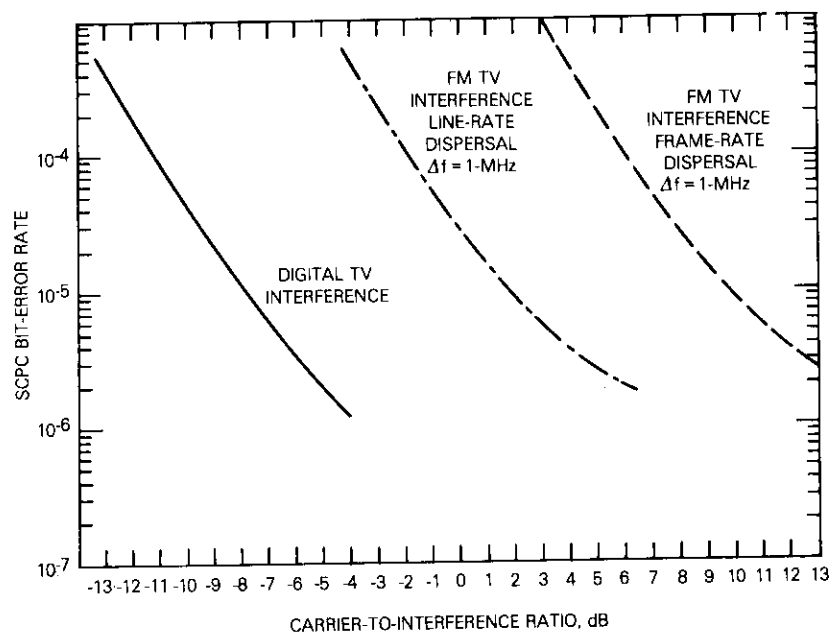


Figure 37. SCPC BER vs C/I for $C/N = 15$ dB

Conclusions

The line-rate sawtooth waveform and the half-line-rate triangular waveform have been studied as alternative FM TV energy dispersal methods to the present frame-rate waveform. The sweep interference mechanism, which characterizes the co-channel interference by a dispersed FM TV carrier into a SPADE channel, was analyzed during computer simulation. The results indicated that, when the line-rate sawtooth or half-line-rate triangular sweeping was used, a significant advantage in terms of reduced interference power could be obtained because of the "time constant" effect of the SPADE channel filter.

A series of hardware simulation experiments was conducted to evaluate the different dispersal methods. These included SCPC/PSK average bit-error-rate tests, SPADE voice channel impulse noise tests, S/N tests, and voice subjective evaluations conducted with the controlled interference of a half-transponder FM TV carrier using different types of dispersal. The experimental results show that with

Δf at the standard value of 1 MHz, a 9- to 11-dB reduction in interference potential could be obtained when the line-rate or half-line-rate dispersal was used instead of frame-rate dispersal. This agrees well with the predicted 10.5-dB value. Furthermore, SCPC/PSK average bit-error rates measured at different values of Δf agree closely with the curve obtained through analysis.

The analysis of the bit-error distribution data shows that the frame-rate dispersal is more likely to cause modem failures than the line-rate dispersal. Under the same circuit conditions, the error distribution with frame-rate dispersal is significantly more bursty than that with line-rate dispersal. The long and high-density error bursts might have an important effect on the performance of error correction codes and subjective voice quality.

The TV subjective test shows that both the line-rate sawtooth and the half-line-rate triangular dispersal waveforms can be removed to well below the level of perceptible degradation with simple circuitry. The subjective effect of the sawtooth waveform is found to be less objectionable than that of the triangular waveform. A closed-loop nulling technique is proposed in which the correct amplitude of dispersal waveform to be subtracted can be automatically determined to a high degree of accuracy.

The above study results indicate that the line-rate sawtooth dispersal waveform is a feasible alternative to the present frame-rate triangular waveform for effectively reducing the interference potential of FM TV carriers.

However, it is not clear that the optimum technique has been developed. In particular, it has been noted that, at the expense of more complex implementation, an adaptive technique might produce equally good or better reduction in interference and at the same time enhance video signal quality. If a line-rate dispersal waveform is added only when needed, or only for the amount needed, it is possible that the amplitude of the composite video signal could be increased. This would result in either a direct increase in the video S/N or an increased margin for overdeviation. Since these two factors are the major contributions to the poor signal quality in half-transponder TV, the improvement could be quite significant even if not large in absolute terms. Furthermore, an adaptive gain technique in which the gain is varied on a line-by-line basis to provide a compandor-like action could possibly produce even greater gain in signal quality while also obtaining interference reduction. These adaptive techniques merit further study.

As a comparison, the interference potential of digital TV is tested. The worst-case interference potential of digital TV is 9 dB lower than that of FM TV using the proposed line-rate dispersal method, or 18 dB lower than that of FM TV using the present frame-rate dispersal method.

Acknowledgments

The author wishes to acknowledge the contribution of A. G. Gatfield to this study. Special thanks are due to B. Merrihew, G. House, S. Lebowitz, D. Weinreich, H. Suyderhoud, and F. Corcoran for their assistance in various parts of the experiment and simulation. The advice of Drs. S. J. Campanella, B. A. Pontano, and others is deeply appreciated.

References

- [1] International Radio Consultative Committee (C.C.I.R.), "Carrier Energy Dispersal in Systems in the Fixed Satellite Service," Recommendation 446-1, Vol. IV, p. 67.
- [2] International Radio Consultative Committee (C.C.I.R.), "Energy Dispersal in Radio Communication-Satellite System," Report 384-2, XIIIth Plenary Assembly, Geneva, 1974 (Study Programme 2D1/4), Study Group 4, Vol. IV, pp. 90-108.
- [3] A. M. Werth, "SPADE: A PCM FDMA Demand Assignment System for Satellite Communications," INTELSAT/IEEE International Conference on Digital Satellite Communications, London, November 25-27, 1969, pp. 51-68.
- [4] D. J. Kurjan and M. R. Wachs, "TV Co-channel Interference on PCM-PSK SCPC System," *COMSAT Technical Review*, Vol. 6, No. 2, Fall 1976, pp. 413-424.
- [5] M. C. Jeruchim, "A Survey of Interference Problems and Applications to Geostationary Satellite Networks," *Proc. IEEE*, Vol. 65, No. 3, March 1977, pp. 317-331.
- [6] D. J. Withers, "Effective Utilization of the Geostationary Orbit for Satellite Communication," *Proc. IEEE*, Vol. 65, No. 3, March 1977, pp. 308-317.
- [7] R. Fang and O. Shimbo, "Unified Analysis of a Class of Digital Systems in Additive Noise and Interference," *IEEE Transactions on Communications*, COM-21, No. 10, October 1973, pp. 1075-1091.
- [8] O. Shimbo and R. Fang, "Effects of Co-Channel Interference and Gaussian Noise in M-ary PSK Systems," *COMSAT Technical Review*, Vol. 3, No. 1, Spring 1973, pp. 183-207.
- [9] J. M. Aein and R. D. Turner, "Effect of Co-Channel Interference on CPSK Carriers," *IEEE Transactions on Communications*, COM-21, July 1973, pp. 783-790.
- [10] D. E. Weinrich and M. R. Wachs, "A Laboratory Simulation of Multiple Unmodulated Interference Source of Digital Satellite Channels," presented at International Conference on Communications, Philadelphia, Pennsylvania, June 1976.
- [11] International Radio Consultative Committee (C.C.I.R.), Conclusion of the Interim Meeting of Study Group 4, Geneva, 18 May-3 June, 1976, Doc. 4/215E, p. 82.
- [12] A. K. Jefferis, "Spectral-Energy Dispersal in Digital Communication-Satellite Systems," *Proc. IEEE*, Vol. 120, No. 5, May 1973.
- [13] H. L. Weinberger, "TV Energy Dispersal Waveform," *NTC '77 Conference Record*, pp. 4:1-1 to 4:1-3.
- [14] W. Snyder, M. Wall, L. Wexler, and A. Gatfield, "A Performance Monitor for Voiceband and Groupband Channels," *EASCON 1974 Record*, pp. 664-669.
- [15] International Radio Consultative Committee (C.C.I.R.), "Pre-Emphasis Characteristics for Frequency-Modulation Systems," Recommendation 405-1, Vol. IX, pp. 194-198.
- [16] International Telegraph and Telephone Consultative Committee (C.C.I.T.T.), "Impulse Noise Measuring Instrument for Data Transmission," Recommendation V.55, Fifth Plenary Assembly, Geneva, 1972, Vol. VIII, pp. 172-175.
- [17] H. G. Suyderhoud, M. Onufry, and J. Sennott, "Subjective Performance Assessment of Delta Modulation in Terms of Equivalent Noise at 16, 24, 32, and 40 kbit/s," Fourth Digital Satellite Conference, Montreal, Canada, October 1978, pp. 243-247.
- [18] B. J. Winer, *Statistical Principles of Experimental Design*, New York: McGraw-Hill, 1971.
- [19] S. Doba and J. W. Rieke, "Clampers in Video Transmission," *AIEE Transaction*, 1950, Vol. 69, pp. 477-487.
- [20] D. C. Savage, "Three Types of TV Signal Stabilizing Amplifier," Report of International Television Conference, June 5, 1962, London, (IEE Paper No. 4027E, June 1963), pp. 251-258.
- [21] K. Miya, ed., *Satellite Communications Engineering*, Tokyo: Lattice Company, 1975.
- [22] A. G. Gatfield, "CODIT, A Digital TV System for Communications Satellite," *INTELCOM '77*, October 1977.



S. Eric Yam received a B.E.E. and an M.S.E.E. from the University of Minnesota in 1969 and 1971, and a Ph.D. from Purdue University in 1976. From 1967 to 1968, he participated in the development of the ARTIC computer at the University of Minnesota. From 1973 to 1974, he worked at the Laboratory for Applications of Remote Sensing of Purdue University, where he was responsible for research and development for machine processing of earth resources data collected via the LANDSAT satellite. From 1974 to 1976, he was engaged in research on robotic visual perception at the Laboratory for Advanced Automation of Purdue. He joined COMSAT Laboratories in 1976, where he is currently a Member of the Technical Staff of the Image Processing Department. His work at COMSAT has included bit-rate compression coding, TV image processing, and trans-multiplexing and advanced digital processing techniques.

Dr. Yam is a member of Tau Beta and Eta Kappa Nu.

Index: voice switch, performance criteria

Voice-activated-switch performance criteria

G. G. SZARVAS AND H. G. SUYDERHOUD

(Manuscript received January 7, 1980)

Abstract

Voice switches which must ensure satisfactory speech quality and noise immunity in SPADE and digital speech interpolation (DSI) systems are expected to be increasingly important in satellite communications networks.

Objective voice-switch performance criteria have been derived from speech characteristics, typical impairments inherent to voice switching, the noise environment of telephone channels, and the relationships between subjective speech quality and measurable voice-switch parameters. These performance criteria have been established for two similar voice switches with level threshold detection, but different threshold requirements. In one case a fixed threshold of -40 dBm₀ has been chosen, while in the other case a continuously variable threshold between -55 and -40 dBm₀, adapted to the long-term level of the terminating telephone channel noise, has been proposed. The voice switches are protected against echo activation by increasing the threshold to -27 dBm₀ when speech is present in the receive channel.

Introduction

Voice-activated switches are required in telephony for a number of applications. Perhaps the oldest known use of voice-activated switching was for the prevention of echo; in this case, the detected receive-side speech signal in a 4-wire circuit activates a switch to block transmission

in the return path. Today, more sophisticated echo suppressors still utilize this principle.

More recently, voice activation has been applied to services which require that a communications channel be enabled upon detection of speech. Examples are speech interpolation systems, such as time-assignment speech interpolation (TASI) and more recently DSI, which depend critically on accurate speech detection to distinguish active speech from silent intervals. Another example is SPADE, in which transmission is permitted only after the presence of speech has been detected.

Ideally, voice switches for this type of application would activate the transmission channel in unison with the vocal effort, while blocking transmission otherwise. In practice, a good voice switch performs this function most of the time, whereas a poor switch fails to activate many times or, conversely, overactivates the channel in the presence of noise and other unwanted signals (such as echo).

The function of the voice-switch designer is to ensure nearly ideal performance without listener awareness of the on-off action which actually occurs in his connection. This implies that initial clipping of the speech signal, the switch-on time at the end of it, and activation by noise and echo must be minimized.

This paper will present voice-switch specifications which will ensure satisfactory performance. These specifications will be objectively quantified in terms of voice-switch parameters and related to subjective effects in terms of quality assessments. Performance criteria analysis and specification are preceded by a review of the speech structure, typical impairments due to voice switching, and the noise environment of the telephone channel.

Speech structure

Voice switching techniques utilize the difference in the amplitude-time structures of speech and noise. Thus, it is appropriate to review some of the speech time-domain characteristics such as long- and short-term power distribution, speech envelope rise and decay rates, phoneme duration, duration of speech bursts and pauses during telephone conversations, and zero crossings of the speech signal. Since the language and the sex of the speaker are important factors, the English language and male speakers will be assumed, unless otherwise indicated.

Speech level is generally measured in volume units (VUs); the mean talker power, P , in dBm0 corresponding to a volume, V , in VU is $P = V - 1.4$ (dBm0) [1]. It is well known that speech-level distributions are Gaussian. Figure 1 shows volume distributions measured by AT&T [2], SIT Siemens [3], and the British Post Office (BPO) [4]. The AT&T measurements were conducted on transatlantic cable telephone circuits, the SIT Siemens measurements at the Acilia (Rome, Italy) International Transit Center on links via satellite and cable circuits, and the BPO measurements were made at the input to the transatlantic cable telephone system in London, U.K. A recent publication [5] indicated that, in the AT&T network, average talker volumes on toll calls in class 5 offices decreased from -16.8 to -21.6 VU (relative to zero transmission level), and from 6.4 dB to 4.5 dB in standard deviation over a 15-year period (1960–1975). This was attributed to telephone set and loss-management improvements. A similar trend can be assumed for international satellite circuits.

Instantaneous amplitude measurements of speech show that it has a gamma distribution [6] as indicated in Figure 2, which also includes the Gaussian and exponential distributions. The peak-to-rms ratio is about 20 dB for a typical continuous talker. (Peak is defined as the amplitude exceeded with 0.001-percent probability.)

Figure 3 shows the short-term root mean square (rms) voltage fluctuations of a typical speech utterance, obtained by linear rectification and smoothing with an RC filter having a 12-ms time constant [6]. Rise and decay rates for various conditions are given in Table 1. Phoneme duration measurements [6] are shown in Table 2.

The on-off pattern of speech utterances during 16 experimental telephone conversations between eight male and eight female talker pairs was measured by Brady [7] using an instantaneous envelope detector (full-wave rectified without filtering) at threshold levels of -45 , -40 , and -35 dBm0. Spurts less than 15 ms were erased to reject impulse noise, and gaps less than 200 ms were filled to eliminate short interruptions due to intersyllabic pauses and stop consonants. Table 3 gives the duration of talk spurts and pauses according to Reference 7, as well as activity factors, a measure related to speech interpolation gain and defined as the ratio of the time that a voice switch is activated by one party's speech to the total conversation time. According to Table 3, a higher threshold increases the number of talk spurts and pauses and decreases the activity factor.

The frequency structure of the speech signal yields a characteristic

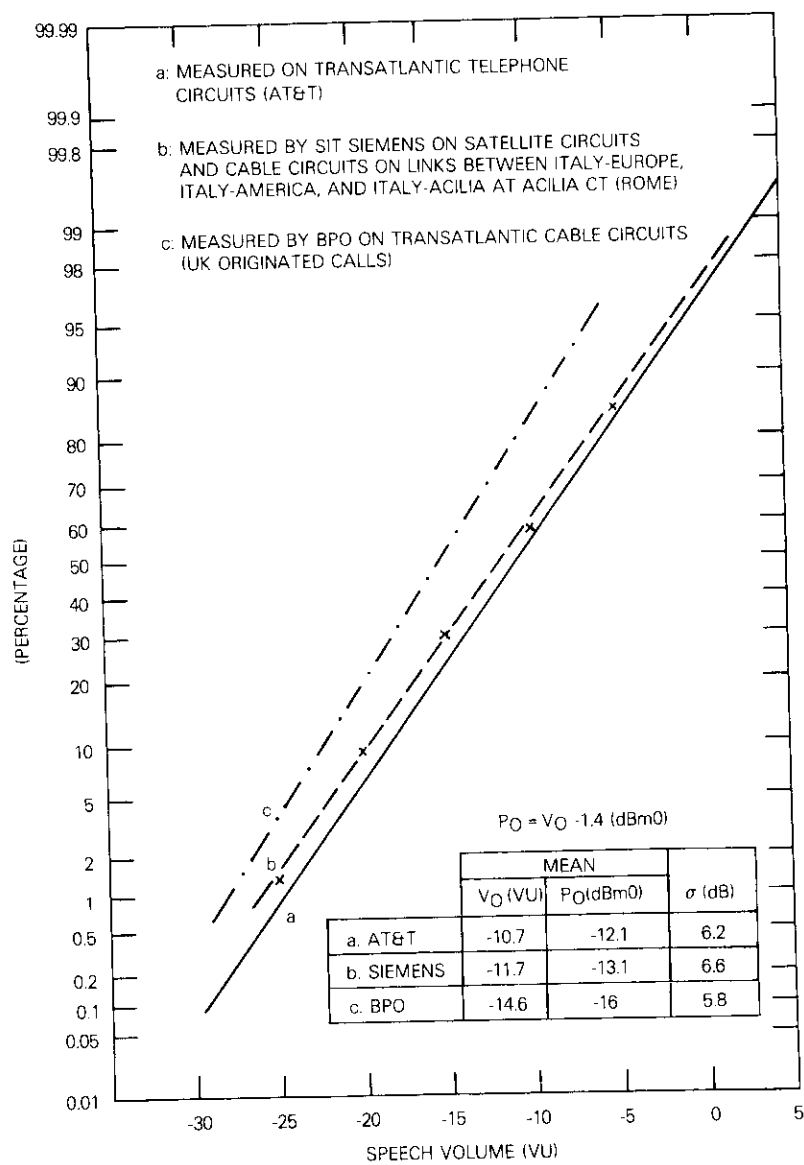


Figure 1. Speech Level Distribution

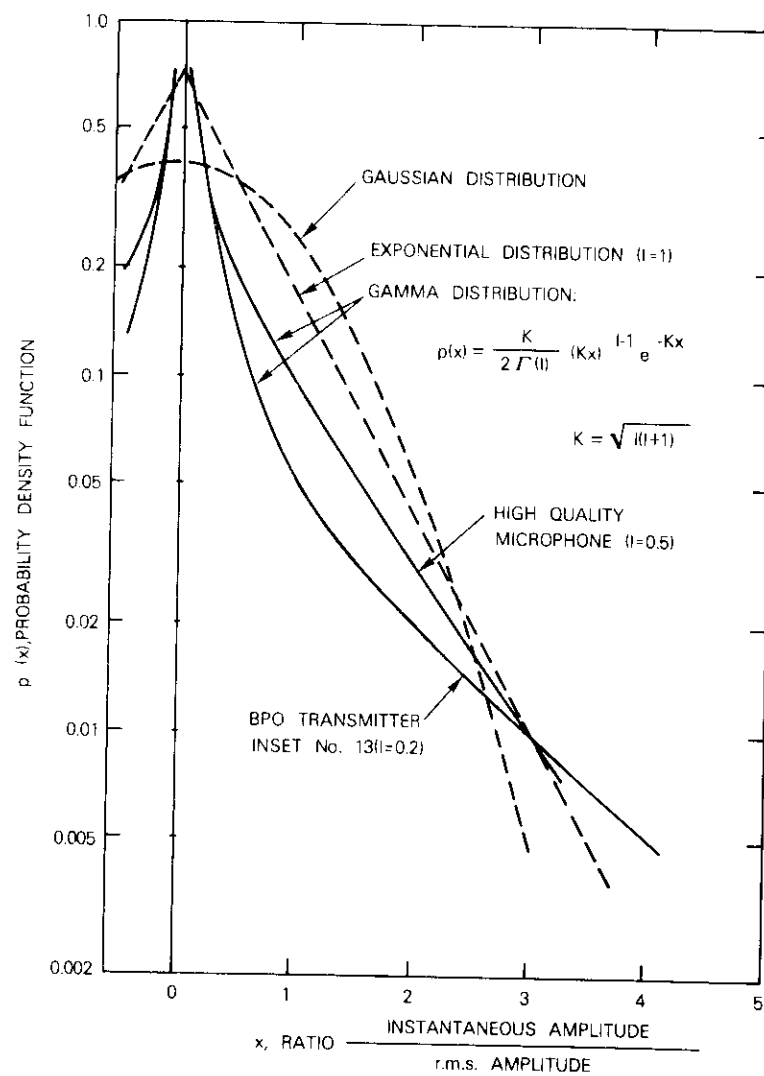


Figure 2. Probability Density Function of Instantaneous Speech Amplitudes

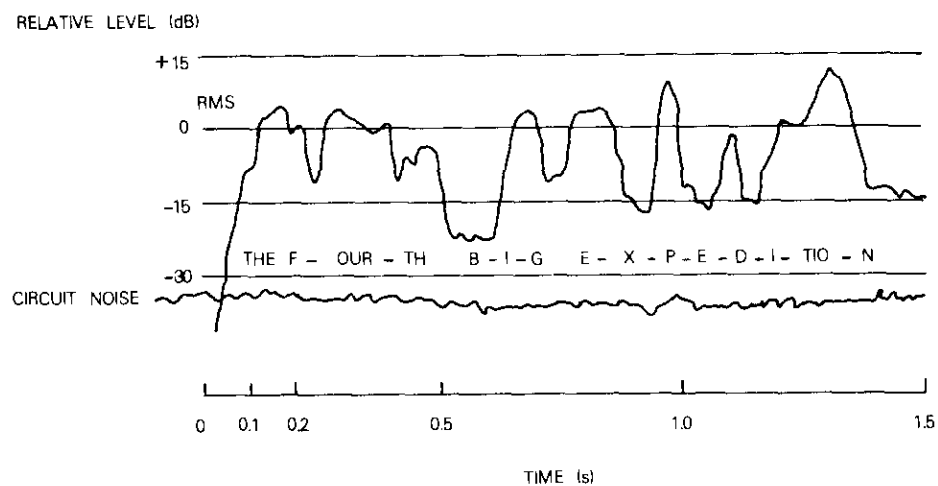


Figure 3. Utterance Envelope Waveform

TABLE 1. SPEECH ENVELOPE RISE AND DECAY RATES (dB/ms)

Condition*	Rise	Decay
a	0.3	0.3
b	1.5	1.5
c	0.6	0.4

* Condition *a* involves initial rise and final decay rates of utterances ranging from 23 to 13 dB below the level of the long-term power of the speech. Condition *b* is within utterances for only a few decibel changes, and condition *c* is within utterances for substantial level changes.

TABLE 2. DURATION OF PHONEMES FROM CONSONANT-VOWEL-CONSONANT (CVC) MEASUREMENTS

Phonemes	Duration Range (ms)	Average Duration (ms)
Initial Consonants	70-250	120
Vowels	150-500	250
Final Consonants	100-350	190

TABLE 3. DURATION OF TALK SPURTS AND PAUSE EVENTS*

Event	Threshold					
	-45 dBm0		-40 dBm0		-35 dBm0	
	Mean (s)	Median (s)	Mean (s)	Median (s)	Mean (s)	Median (s)
Talk Spurt (274.8 min)	1.311	0.775	1.125	0.675	0.902	0.575
Pause (274.8 min)	1.695	0.725	1.721	0.725	1.664	0.675
Double-Talk (137.4 min)	0.296	0.213	0.262	0.185	0.235	0.165
Activity Factor	0.436		0.395		0.352	

* 137.4 minutes of conversation of 274.8 minutes of speech. The activity factor is the ratio of time that a voice switch is activated by one party's speech to the total conversation time.

zero-crossing pattern which can be utilized in special applications [8]. In a voice switch, detection techniques based on the zero-crossing pattern can be used only as a complement to level threshold detection because unwanted signals such as echo and crosstalk are also speech signals, although generally at a lower level. The zero-crossing patterns of speech are characterized by sibilants and fricatives with a relatively high number of zero crossings per unit time and by vowels, semi-vowels, and stop consonants with a relatively low number of zero crossings per unit time.

Speech impairments associated with voice switching

As shown in Figure 4, the major voice-switch parameters influencing performance are switch threshold, attack time, and hangover time. Figure 4a shows the envelope of a speech utterance and a threshold

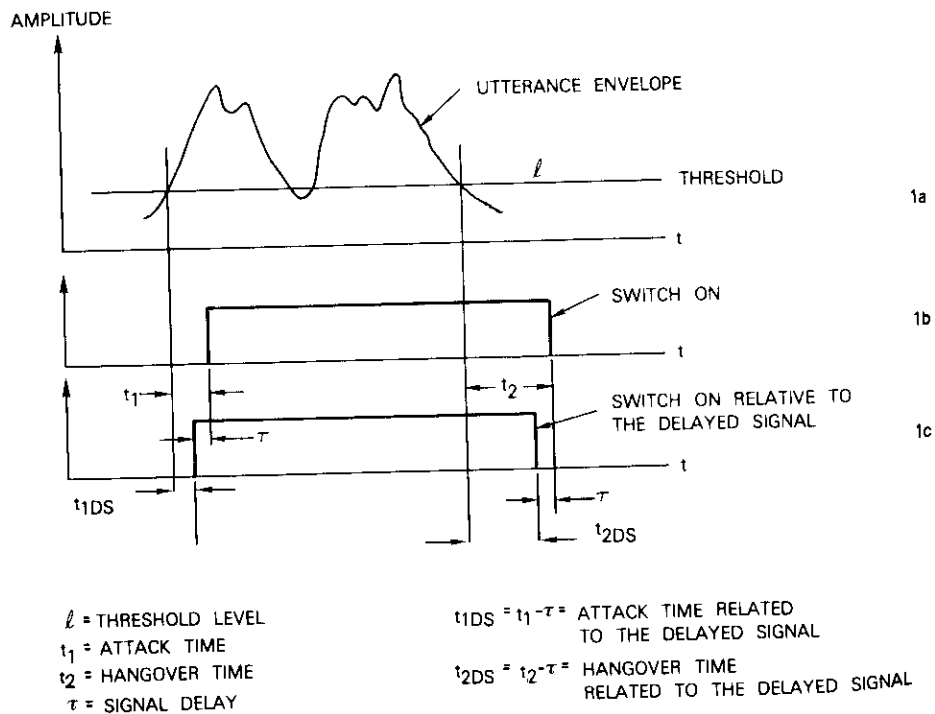


Figure 4. Threshold, Attack Time, and Hangover Time

at level l . Figure 4b shows the voice-switch response; the attack time, t_1 , needed for voice recognition; and the hangover time, t_2 , which is provided to avoid clipping of low-level passages within and at the end of speech utterances.

An excessive attack time may cause perceptible initial clipping of the speech bursts. This clipping may be compensated by delaying the signal by a given interval, τ , before it reaches the switch, as shown in Figure 4c. The hangover time should be sufficiently long to prevent speech clipping. The attack time and hangover time, t_{1DS} and t_{2DS} , related to the delayed signal, and the threshold level jointly determine the quality of the switch. For instance, a low threshold level and a long attack time may result in initial clipping which is similar to that caused by an increased threshold and a reduced attack time. The relationship in this case is determined by the initial rise of the speech envelope (see Table 1). A suitable combination of voice switch parameters based on articulation and subjective listening tests will be presented on a comparative scale.

In logatom tests, voice switch impairments can be characterized by errors in recognizing the phonemes of nonsense syllables (logatoms) in the CVC* format. A logatom test is a valuable analytical and diagnostic tool, but care must be exercised when correlating logatom test errors and conversational speech degradation, in which, for instance, the language structure and redundancy are important factors. The following suggested voice switch parameter values [9] are based on logatom tests:

- a. a threshold level at least 22 dB below the long-term power level;
- b. an attack time (t_{1DS}) not exceeding about 6 ms for a threshold 25 dB below the rms speech level;
- c. hangover time (t_{2DS}) values between 150 and 200 ms for adequate transmission of the final consonants. (For echo suppressor break-in, a hangover time as low as 50 ms has been found adequate, and also prevents excessive echo.)

In the following subjective tests, the hangover time was held constant at 170 ms, and the attack time was inversely proportional to the signal level with a maximum t_{1DS} of about 12 ms. The subjective tests [3] consisted of telephone conversation (in Italian) and CVC scoring. The

* Consonant-vowel-consonant.

10 subjects participating in the tests used the rating categories shown in Table 4 for the conversational tests.

TABLE 4. CATEGORY RATING

Score	Quality	Description
5	Excellent	Voice-switch effect is imperceptible in all listening conditions.
4	Good	Voice-switch effect is just perceptible, but intelligibility loss does not occur.
3	Fair	Degradation is definitely perceptible; some syllables and fricative sounds are clipped.
2	Poor	Degradation is objectionable; some words are clipped and are not intelligible.
1	Unusable	Many words are not intelligible.

Figure 5 shows mean opinion score (MOS) as a function of switch threshold for -60-dBm0 random noise, with VU as a parameter; Figure

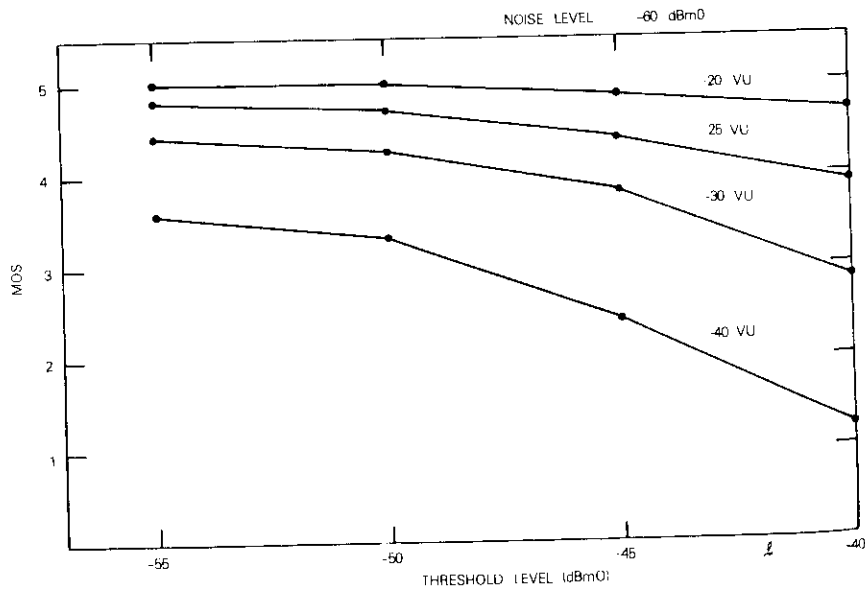


Figure 5. Mean Opinion Score as Function of Threshold with Speech Level as a Parameter

6 shows MOS as a function of VU at random noise levels of -60 and -50 dBm0 and threshold levels of -54 and -60 dBm0, respectively.

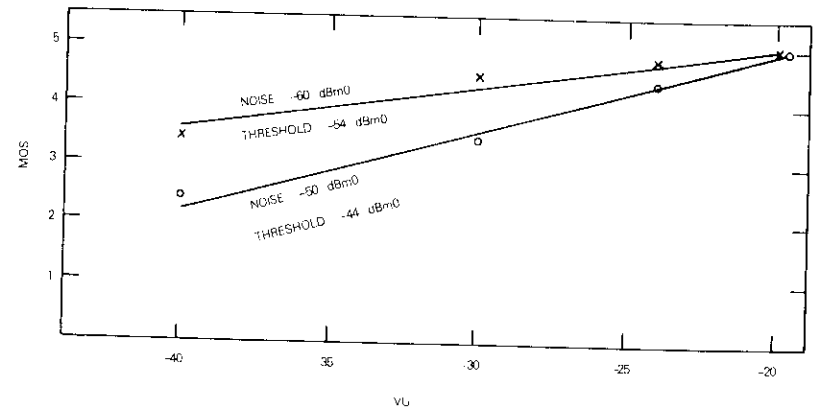


Figure 6. Mean Opinion Score as a Function of Speech Level with Threshold and Noise as Parameters

Figure 7 gives MOS values of Figures 5 and 6 as a function of Δ , the difference between speech volume in VU and voice-switch threshold

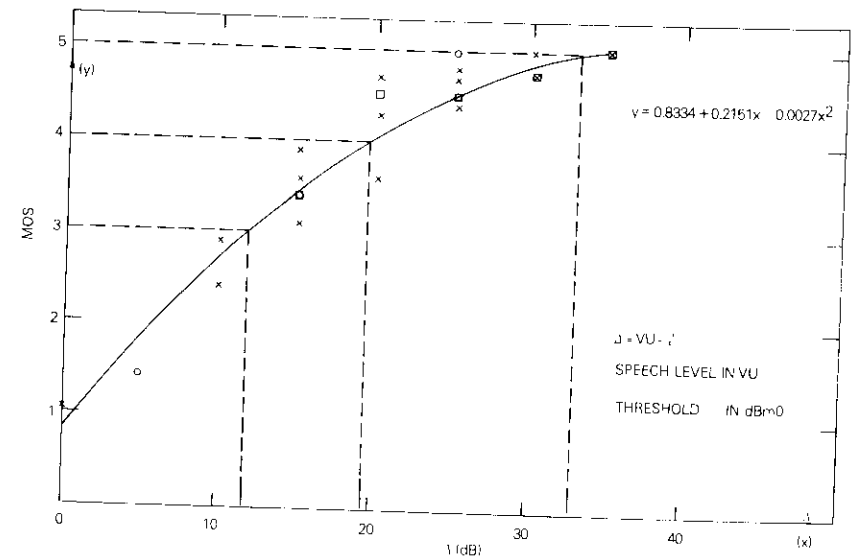


Figure 7. Mean Opinion Score as a Function of Speech-to-Threshold Ratio, Δ

in dBm0. The suggested voice-switch threshold of 22 dB below the long-term rms level of speech in Reference 10 corresponds to a value of $\Delta = 22 - 1.4 = 20.6$ dB. Figure 7 indicates that this corresponds to a quality somewhat better than "good."

In terms of the functional relationship of Figure 7 and the AT&T's voice level distribution of Figure 1, the distribution curves of Figure 8 were obtained showing listener satisfaction as a function of voice-switch threshold. For example, at a threshold of -45 dBm0, the speech quality is excellent for 62 percent and good for almost 100 percent of the listeners. To obtain the same degree of satisfaction at a lower average speech volume, the threshold must be lowered proportionally.

Noise

Speech is often produced at low energy levels comparable to that of noise. Simple voice-switch sensitivity criteria based on energy alone can inadvertently be met by non-speech-like and unwanted signals. Specifically, random noise, impulse noise, echo, and crosstalk are signals which may inadvertently activate a voice switch.

Voice-switch activation by noise in the broad sense degrades system efficiency; for example, it reduces interpolation gain in speech interpolation systems. Voice-switch parameter selection must therefore represent a compromise between system efficiency and switched speech performance.

A voice switch can also influence the subjective noise performance of a system. The suppression of relatively high levels of noise during the "off" periods in a conversation may actually be annoying to the listener. However, when the noise is heard clearly during silent periods but masked when speech is present, a voice switch can be beneficial and improve overall circuit quality [10].

Random noise

Thermal, intermodulation, and crosstalk noise have approximately normal instantaneous amplitude distributions with a peak-to-rms ratio around 13 dB, which is about 7 dB less than the corresponding 20-dB value for the speech of a single continuous talker. This difference between random noise and speech amplitude distributions (Figure 2) is utilized in some speech detectors [11].

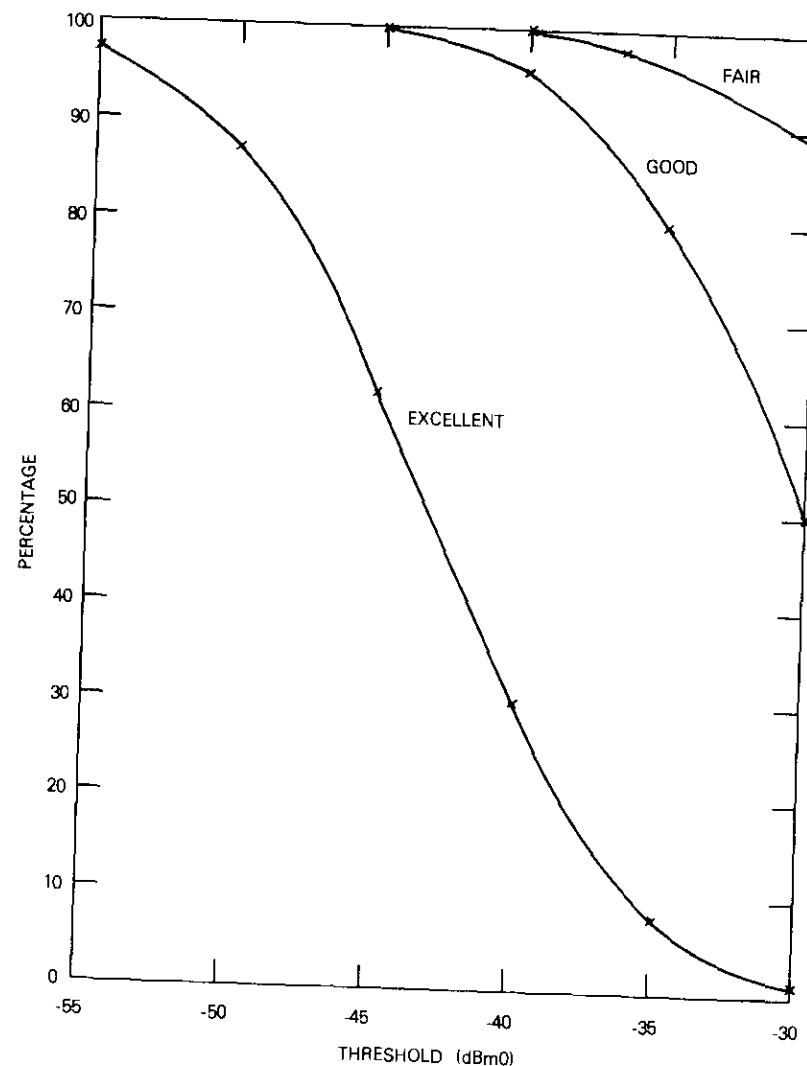


Figure 8. Telephone User Satisfaction as a Function of Voice-Switch Threshold

Measurements of noise at the Acilia Transit Center [3] on 15 terrestrial links for a total of 80 busy hours gave a long-term average of -50.7 dBm0p* with a standard deviation of 2.42 dB and extreme values of -46 and -56 dBm0p. These extreme values correspond to the noise objectives given by CCITT Rec. M580 for circuit lengths from 2,501 to 5,000 km and less than 320 km, respectively.

The long-term number of zero crossings of band-limited random noise corresponds to that of a sinusoid centered in the band. For example, the long-term (average) number of zero crossings of noise in the 300- to 3400-Hz band is 3,700 per second. This is significantly different from that for speech, which has an average of about 500 zero crossings per second. Certain voice-switch designs, such as those used in the SPADE system [12], combine zero-crossing differences with a level threshold criterion for voice detection to obtain good performance.

Impulse noise

Table 5 summarizes the results of 80 hours of measurements of impulse counts on 15 terrestrial links at the Acilia Transit Center [3]. At the average random noise level of -50.7 dBm0p (-48.2 dBm0), the amplitude of random noise exceeds the impulse noise counter threshold levels of -41 and -46 dBm0 with a probability of 10^{-1} and 10^{-2} , respectively, and contributes to the impulse noise counts. For low threshold levels, the impulse noise rate and width distribution may be estimated by extrapolating data measured at high threshold levels.

TABLE 5. LINE NOISE IMPULSE RATES RECORDED ON TERRESTRIAL LINKS (AT ACILIA CT)*

Threshold (dBm0)	Impulses per hour				
	$t_1 \geq 1$ ms	$t_2 \geq 2$ ms	$t_3 \geq 5$ ms	$t_4 \geq 10$ ms	$t_5 \geq 20$ ms
-46	45,485	29,620	13,413	6,034	2,192
-41	12,647	3,218	579	147	41
-36	1,297	236	33	10	4
-31	304	91	22	9	3.5
-26	70	24	5	1.1	0
-21	28	10	1.5	0	0
-16	6	1.8	0	0	0

* The device dead time is 50 ms, and its fill-in is 0.8 ms.

*dBm0p is a psophometrically weighted measure of flat noise (in dBm0), differing from it by -2.5 dB.

Figure 9 shows the observed impulse noise rate as a function of threshold according to the first column in Table 5. For comparison, closely matching results obtained in the U.K. are also shown in Figure 9. Neither data set included circuit-length information. A significantly different impulse count (per 15 min.), reported by

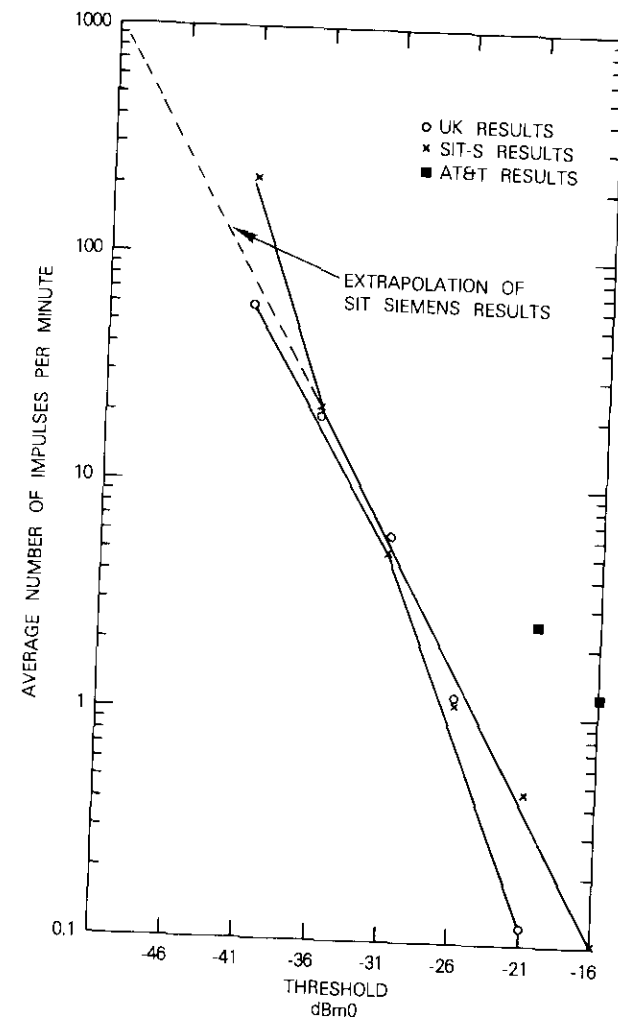


Figure 9. Noise Impulse Rates From Field Measurements

AT&T for circuit distances up to 4,600 km, gives 39 counts for a -20-dBm0 threshold and 18 counts for a -16-dBm0 threshold [13].

Echo

Although echo suppressors are presently used in most long-distance telephony when the round-trip delay exceeds 50 ms [14], in the future, echo cancellers are expected to be generally introduced. Echo spurts inadvertently admitted by an echo suppressor may activate a voice switch. Three modes of echo suppressor operation will be considered:

a. The transition into suppression has an attack time specified not to exceed 5 ms. However, actual attack times may be longer and cause very short but perhaps high-level spurts of echo if the end delay is less than the attack time. The peaks of the spurts may well exceed the voice-switch threshold and thus cause false operation.

b. In the suppression mode, the echo is attenuated with at least 50 dB and cannot activate the voice switch.

c. During the break-in mode of an echo suppressor, echo may well occur during the silent portions of the near-end talker, and a certain amount of unwanted activation may result.

Table 6, which summarizes the results of measurements at the Acilia Transit Center [3], indicates the rate of echo spurts as a function of the threshold level. Echo spurts longer than 5 ms indicate the presence of older echo suppressors, not complying with Reference 14.

TABLE 6. ECHO SPURT* OCCURRENCES PER HOUR

Threshold (dBm0)	$t \geq 1$ ms	$t \geq 2$ ms	$t \geq 5$ ms	$t \geq 10$ ms	$t \geq 20$ ms
-36	364 (100)	138 (38)	36.3 (10)	7 (1.9)	1.3 (0.36)
-31	159 (100)	44 (28)	16 (10)	3.5 (2.2)	0.78 (0.5)
-26	56 (100)	11.4 (20.4)	3.2 (5.8)	0.89 (1.6)	0 (0)
-21	31 (100)	6.9 (22)	2.2 (7.1)	0.67 (2.1)	0 (0)
-16	10 (100)	2.56 (24.8)	0.89 (8.6)	0 (0)	0 (0)

* The total observation time is 36 hours. The numbers in parentheses represent the mean percentage relative to all echo spurts measured on the given threshold level.

Noise influence on switch parameters

As mentioned earlier, it is important to prevent voice-switch activation by unwanted signals including echo. Therefore, the threshold for activation must be related to the rms level of the random noise. Furthermore, noise peaks and impulse noise must not excessively prolong the on-time of the switch needed for speech. This is accomplished by special control of the hangover time. Finally, protection must be provided against activation by echo signals. Except for the rms value, echo signals are indistinguishable from useful speech signals. Echo activity can be predicted by detecting the receive speech signal, which in turn can be coupled with increasing the near-end voice switch threshold.

Figure 10 is a block diagram of a voice switch with echo protection. Voice detector A is part of the voice switch for activation of the transmit side. It has an additional input from voice detector B which controls the threshold of A with the echo protection command (EPC).

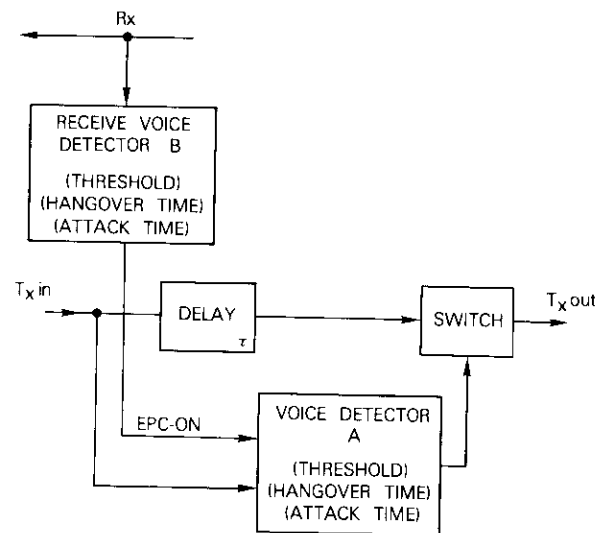


Figure 10. Voice-Switch Block Diagram

As shown in Figure 10, the receive speech detector has the same parameters as the transmit speech detector, but is generally less

sophisticated. The definitions of its attack time, t_{1EP} , and hangover time, t_{2EP} , correspond to those of the transmit detector parameters t_1 and t_2 , shown in Figure 4b.

In general, the input signal to the detector can either be analog or digital for an analog or digital voice switch, respectively. In the latter case, both single-channel (SPADE) or multi-channel (DSI) applications are possible. For the multi-channel case, time sharing is more economical and affords greater design sophistication.

In summary, the voice switch must perform the following somewhat contradictory functions:

- a. recognize useful signals;
- b. minimize switch-on time at the end of the useful signal;
- c. minimize initial clipping of signal; and
- d. minimize activation by noise and echo.

Objective voice-switch parameter requirements

The requirements discussed in the following subsections are applicable to voice switches which attempt to maximize speech quality while minimizing activation by noise. Such switches are used in speech interpolation systems, for example. Prevalent voice switches usually have the following features:

- a. fixed threshold or noise-adaptive threshold;
- b. increased threshold during the presence of speech in the associated receive channel (protection against echo activation);
- c. variable hangover time, *i.e.*, proportional to the interval that the signal exceeds the threshold, thus diminishing the voice-switch on-time which may be caused by short noise spikes.

Objective static and dynamic performance requirements are proposed which define the voice-switch response to sinusoidal and Gaussian noise stimulus signals. Some of the requirements are identical for voice switches with fixed threshold and with noise-adaptive threshold.

Voice switch state diagram and static requirements

Figure 11 shows operational state diagrams for a voice switch with noise-adaptive threshold and fixed threshold. Each area is defined by input signal levels (sinusoidal signal and Gaussian noise) and corresponds to the ON or OFF state of the voice switch, depending on the echo protection command (EPC) status. Table 7 describes the states of

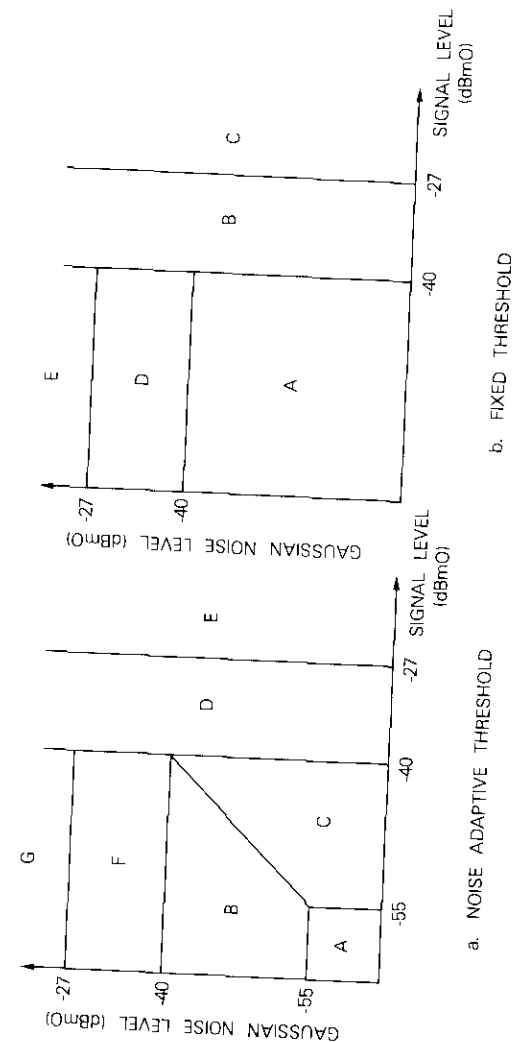


Figure 11. Voice-Switch State Diagrams

the areas shown in Figure 11. The static requirements given by the state diagrams are as follows:

a. For the EPC OFF state the threshold should be -40 dBm0 for the fixed threshold voice switch and 3 dB over the Gaussian noise level for the noise-adaptive voice switch over the noise level range -58 dBm0 to -43 dBm0. The EPC activation threshold (voice-switch receive input) should be -35 dBm0 for both types of voice switches.

b. For the EPC ON state the threshold should be -27 dBm0 for both types of voice switches.

The threshold should be frequency independent over the channel bandwidth. Furthermore, the maximum permissible signal delay should be 12 ms between the voice-switch transmit input port and transmit output port, as will be explained subsequently.

TABLE 7. PROPOSED REQUIREMENTS FOR SWITCH STATE DIAGRAM (FIGURE 11)

Area	Voice Switch State	EPC State*	Gaussian Noise Level (dBm0)	Tone Signal Level (dBm0), 300-3400 Hz	Comments
A	OFF	X	< -55	< -55	Noise Adaptive Voice Switch (see Figure 11a)
B	OFF	X	< -40	S/N ratio < 3 dB	
C	ON	OFF	< -40	S/N ratio > 3 dB	
D	ON	OFF	Any	$< -27, > -40$	
E	ON	X	Any	> -27	
F	ON	OFF	> -40	< -40	
	OFF	ON	< -27		
G	ON	X	> -27	< -40	
A	OFF	X	< -40	< -40	Fixed Threshold Voice Switch (see Figure 11b)
B	ON	OFF	Any	$< -27, > -40$	
C	ON	X	Any	> -27	
D	ON	OFF	> -40	< -40	
	OFF	ON	< -27		
E	ON	X	> -27	< -40	

* EPC ON: the signal level exceeds -35 dBm0 (300 Hz - 3.4 kHz);
X: EPC ON or OFF.

Dynamic requirements

Unless otherwise stated, the signal is assumed to be a sinusoid with a frequency of 1000 Hz. The requirements are given in the form of masks as follows. The requirements for the attack time (t_{1DS}), the EPC attack time (t_{1EP}), and hangover time (t_{2DS}) are shown in Figures 12-14, respectively. The

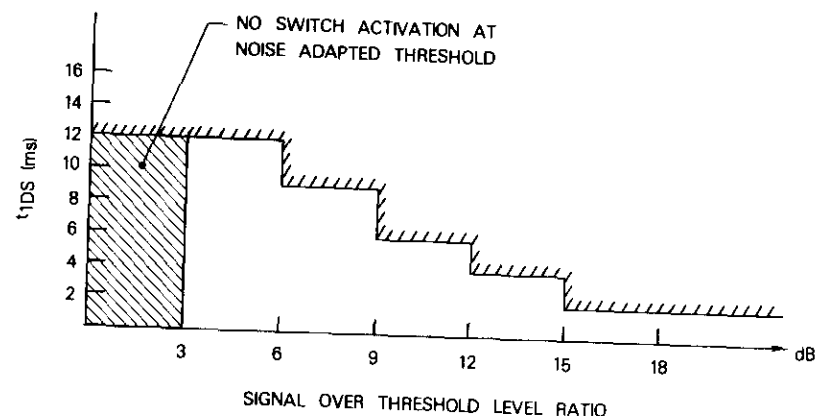


Figure 12. Mask of Permissible Attack Time (t_{1DS})

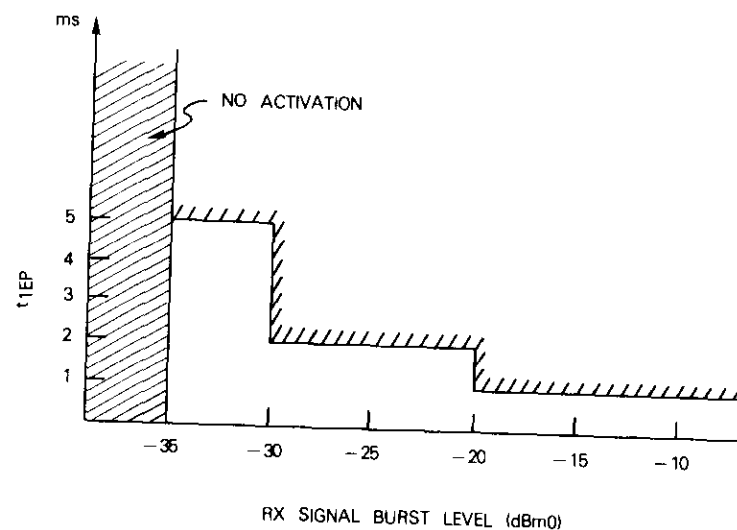


Figure 13. Mask of Permissible Echo Protection Operate Time (t_{1EP})

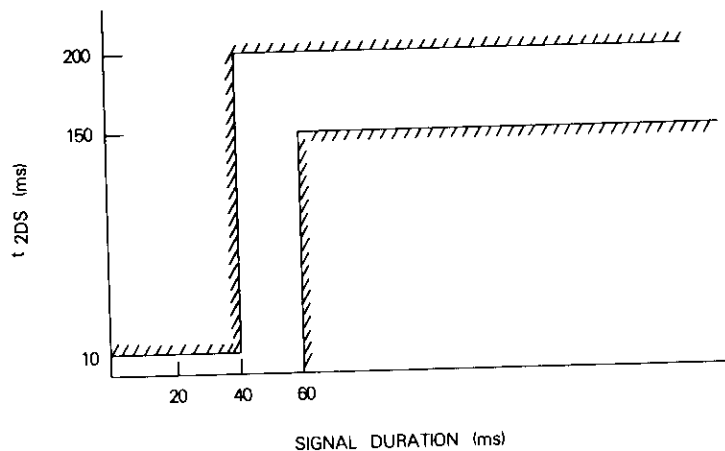


Figure 14. Mask of Permissible Hangover Time (t_{2DS})

impulse noise is simulated with a tone burst of 2000 Hz and the immunity requirement is shown in Figure 15.

The echo protection hangover time should be 60 ms, independent of the length of the stimulus signal. The threshold adjustment time for the noise-adaptive voice switch should be less than 4 s for any change in the random noise level in the range of -58 dBm0 to -43 dBm0.

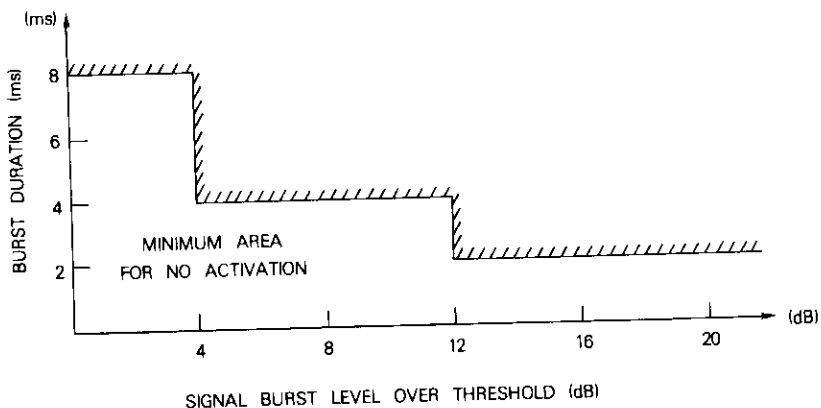


Figure 15. Mask for Tone Burst Immunity

Measurement of the objective characteristics

Figure 16 is a functional block diagram for measurements of objective characteristics of a digital voice switch. For analog voice-switch measurements, the A/D and D/A converters are not included. The input to the transmit port is a summation of a sinusoidal signal and Gaussian noise of both known and adjustable levels. For dynamic measurements, single and repetitive tone bursts of variable length and level must be generated, and may be implemented by gating the continuous tone with the switching pattern generator through switch S1. The input to the receive port is a continuous tone or tone burst at 1000 Hz unless stated otherwise in the requirements.

The measurements can be simplified by providing tape-recorded inputs to the transmit and receive ports and by synchronizing signals for the oscilloscope connected to the transmit output. Implementation can be accomplished, for example, by frequency dividing one or both channels of a stereotape. The transmit and receive inputs are in the low-frequency band of the left and right channels, and the oscilloscope synchronizing signals are in the high-frequency band.

Discussion

Level threshold detection

Because echo and crosstalk are usually low-level unwanted speech signals, speech detection must be based either solely on level detection, or on some other method complementing level detection. For example, autocorrelation techniques for speech detection are very effective but usually too complex and costly in terms of implementation. Therefore, the specified performance recommendations are based on a voice-activated switch with level threshold detection as the fundamental method.

The relationship between the subjective speech quality and the objectively measurable voice-switch threshold, with defined attack and hangover times, is given in Figures 8 and 9. These figures show that a voice switch with a noise-adaptive threshold ensures better speech quality than a voice switch with a fixed threshold selected at the worst-case channel noise. Therefore, a voice switch with noise-adaptive threshold is preferable whenever its additional complexity (and cost) per channel is warranted, as in the case of time-shared voice switches. On the other hand, the generally lower voice-adaptive switch threshold increases the activity factor (see Table 3) and the ON time due to noise activation.

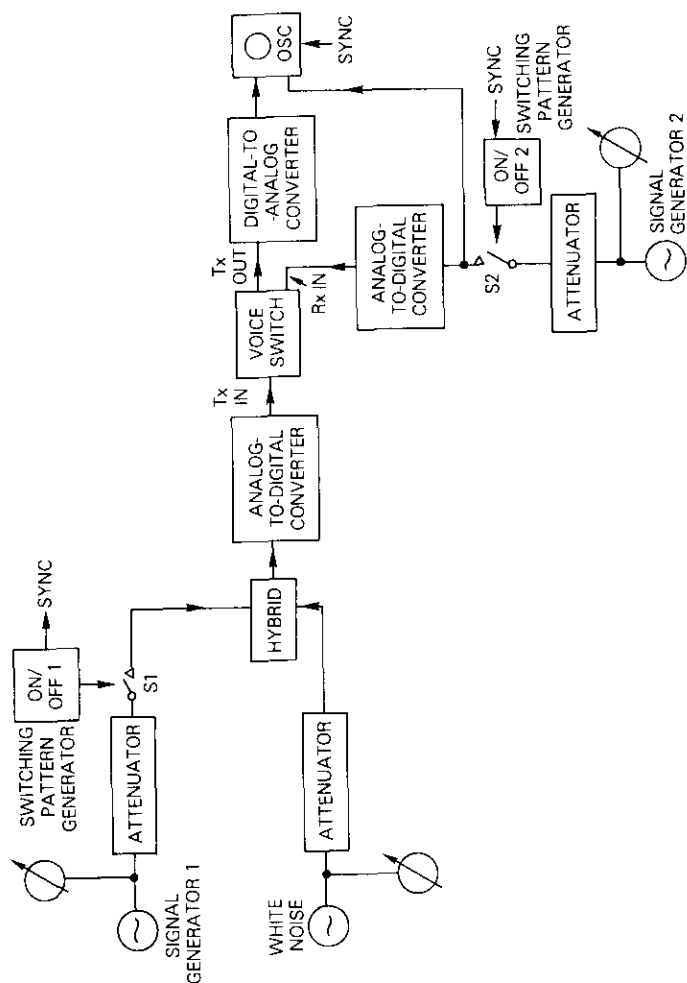


Figure 16. Setup for Objective Parameter Measurements

Comments about the characteristics

The recommended objective characteristics are based on data of implemented voice switches [2], [15]. However, there is a major difference in the threshold characteristics for noise-adaptive voice switches. In Reference 15, for instance, the threshold is 6 dB above the noise level, and no explicit minimum threshold is given. In this paper, a 3-dB threshold-to-noise ratio and a minimum threshold of -55 dBm0 are recommended. The lowering of threshold-to-noise ratio produces a significant increase in the percentage of subscribers rating the speech quality as excellent (shown in Figure 8). It is also shown in Figure 8 that lowering the threshold below -55 dBm0 does not improve speech quality significantly, but would significantly increase the probability of inadvertent triggering due to noise spikes. It may well be possible to implement the more desirable 3-dB threshold-to-noise ratio by utilizing the additional detection time provided by the signal delay increase from 4 ms [15] to 12 ms.

The maximum signal delay of 12 ms is considered an inconsequential increase in end delay. The conservative -27 -dBm0 threshold for avoiding activation by echo complies with the maximum threshold of Reference 2. The consequent decrease in speech quality during the doubletalk mode was neglected.

In the worst case, the noise-adapted voice switch is estimated to be in the ON state one percent of the time due to the impulse noise activation. This estimate is based on the lowest voice-switch threshold of -55 dBm0, the extrapolated impulse noise rate, the noise impulse width distribution at the -36 -dBm0 threshold of Table 6, the tone burst immunity discussed previously, and 10-ms hangover time. The most serious effect of the -55 -dBm0 threshold would be the increased speech activity factor. For instance, a linear extrapolation of the activity factors of Table 3 results in a 20-percent increase for a threshold decrease from -40 to -55 dBm0.

Data transmission and signaling

CCITT Rec. V2 suggests -10 and -13 -dBm0 levels for data transmission, well above the recommended voice-switch threshold levels. Thus, voice-activated switches complying with the recommendations are also appropriate for constant level data transmission (FSK and PSK modulation). Time-assignment speech interpolation (TASI) may be used in CCITT Signaling System No. 5, with restrictions on the number of circuits in tandem. The voice-switch recommendations permit a delay

of 12 ms. The possible consequences of this delay on CCITT Signaling System No. 5 must be investigated.

Conclusions

Voice-activated switch objective characteristics and measurements have been presented to ensure a satisfactory compromise between voice quality and noise immunity in systems such as speech interpolation and single-carrier-per-channel (SCPC) transmission. Two types of voice switches have been considered; one with a fixed level threshold of -40 dBm0, and the other with a variable threshold between -55 and -40 dBm0 adapted to the long-term average of line noise. The other characteristics are identical for both voice switches. The noise adaptive voice switch, which ensures improved speech quality, is recommended whenever additional complexity on a per-channel basis can be justified.

Subjective tests of voice switches have made it possible to establish a relationship between subjective quality and objective performance characteristics. It should be noted, however, that voice switches which satisfy the objective requirements will not necessarily ensure satisfactory subjective performance. Thus, a simplified listening test is always recommended as a complement to the objective test.

Acknowledgment

The work reported in this paper is, to a considerable extent, based on previous work by SIT Siemens of Italy under INTELSAT Contract.

The authors wish to acknowledge the valuable comments and critique by S. J. Campanella and P. L. Bargellini.

References

- [1] *Transmission Systems for Communications*, Bell Telephone Laboratories, Inc., 1970, p. 222.
- [2] H. Miedema and M. G. Schachtman, "TASI Quality-Effect of Speech Detection and Interpolation," *Bell System Technical Journal*, July 1962, pp. 1455-1473.
- [3] Final Report by SIT-Siemens of Italy on INTELSAT Contract IS-777.
- [4] R. W. Berry, "Speech Volume Measurements on Telephone Circuits," *Proc. IEE*, Vol. 118, No. 2, February 1971, pp. 335-338.

- [5] W. C. Ahern, F. P. Duffy and J. A. Mahr, "Speech Signal Power in the Switched Message Network," *Bell System Technical Journal*, Vol. 57, No. 7, September 1978, pp. 2695-2726.
- [6] D. L. Richards, *Telecommunication by Speech*. New York: John Wiley and Sons, 1973.
- [7] P. I. Brady, "A Statistical Analysis of On-Off Patterns in Conversations," *Bell System Technical Journal*, January 1968, pp. 73-91.
- [8] N. C. Geckinli and D. Yavoz, "Algorithm for Pitch Extraction Using Zero-Crossing Interval Sequence," *IEEE Transactions on Acoustics, Speech, and Signal Processing*, ASSP-25, No. 6, December 1977, pp. 559-564.
- [9] G. T. Barnes, "Voice Switching Parameters in Telephony," *Electrical Communication*, Vol. 47, No. 3, 1972, pp. 186-196.
- [10] H. H. Haas, "Syllabic Compandor System for Noisy Fading Channels," *Proc. of National Electronics Conference*, 1968, pp. 539-544.
- [11] E. Fariello, "A Novel Digital Speech Detector for Improving Effective Satellite Capacity," *IEEE Transactions on Communications*, COM-20, No. 1, February 1972, pp. 55-60.
- [12] E. Fariello, "Digital Speech Detector," COMSAT Laboratories Technical Memorandum, CL-46-69, October 31, 1969.
- [13] F. P. Duffy and T. W. Thatcher, Jr., "Analog Transmission Performance on the Switched Telecommunications Network," *Bell System Technical Journal*, Vol. 50, No. 4, April 1971, pp. 1311-1347.
- [14] International Telegraph and Telephone Consultative Committee (CCITT), "Echo Suppressors Suitable for Circuits Having Either Short or Long Propagation Times," Rec. G.161, *Orange Book*, Vol. III-1, Geneva, 1977.
- [15] J. A. Jankowski, Jr., "A New Digital Voice-Activated Switch," *COMSAT Technical Review*, Vol. 6, No. 1, Spring 1976, pp. 159-177.



George G. Szarvas received a Dipl. Eng. Degree in Electrical and Mechanical Engineering from the Technical University in Budapest, Hungary. He has completed postgraduate courses at the Royal Institute for Technology in Stockholm, Sweden. Before he joined COMSAT in 1969, Mr. Szarvas had worked for the Telecommunications Research Institute in Hungary, for L. M. Ericsson and Facit Electronics in Sweden, and for the Swedish Tele-administration. He is currently a Member of the Technical Staff in the Signal Processing Department of the Communications Processing Laboratory. He is a member of the IEE.



Henri G. Suyderhoud received the Ingenieur degree from Delft Technological University in the Netherlands in 1955, and an M.S. degree in applied mathematical statistics from Rutgers, New Brunswick, in 1966. He is currently Manager of the Signal Processing Department of the Communications Processing Laboratory where he is responsible for signal processing research and development using both digital and analog techniques as well as the development of subjective evaluation techniques to assess transmission quality. His experience includes development of echo cancellers and speech processing and encoding techniques for achieving transmission economy. Prior to joining COMSAT, Mr. Suyderhoud worked for 11 years at Bell Telephone Laboratories in the fields of exchange area and toll transmission engineering, echo control, and picture phone. He is a senior member of IEEE and the American Statistical Association.

Index: unattended, data collection platform, seismic data, design criteria

Automatic seismic observatory communications system

K. GREENE, W. SONES, M. GROSSMAN, M. JONES, and N. JACOBUS

(Manuscript received June 8, 1979)

Abstract

The Automatic Seismic Observatory System is a network of unattended, remote platforms which collect data generated from seismic activity detectors. Each platform transmits the data on a BPSK-modulated single-channel-per-carrier (SCPC) satellite link to a central receive terminal.

For transmission control, an FSK-modulated signal from the central terminal is broadcast to all platforms with discrete addressing of commands to specific stations. To minimize the frequency error in the command link, a pilot link from and to the central terminal is used to detect and compensate for frequency shifts caused by the satellite and earth station up-converter.

This paper discusses the system design, link budget, RF implementation and impairments, and the rationale for the choice of the modulation methods adopted in the data and pilot links. Results of a prototype system are presented.

Introduction

The efficient and rapid collection of data from widely scattered geographic points requires a network of remote and preferably unattended platforms which transmit their data via satellite to a central command, collection, and control station. In particular, a communications system which is compatible with the INTELSAT system and

which will provide for the continuous monitoring of seismic data activity, when there is a requirement for immediate recognition of unusual levels of activity, can be realized by an SCPC configuration with each platform transmitting on its own assigned frequency to a dedicated receiver in the central collection station. A low-data-rate command carrier with discrete addressing can be broadcast to the remote terminals to effect control of the individual transmitters, as required by the INTELSAT system.

To demonstrate the feasibility of a seismic data collection system employing two-way asymmetric data communications between a remote unattended platform and a central receive station, a prototype Automatic Seismic Observatory Communications System was designed and fabricated by COMSAT Laboratories. The system was placed in operation in November 1978, using the Atlantic, Major Path I, INTELSAT IV-A satellite with the central receive station located at Andover, Maine, and a remote station located at Clarksburg, Maryland. After the success of this initial satellite operation the remote terminal was moved in December 1978 to McMinnville, Tennessee, an area of continuous low-level seismic activity, for an evaluation period of six months.

The system was subsequently relocated to operate via the Pacific INTELSAT IV satellite with the central receive station placed at the Jamesburg, California, earth station and the remote terminal located near Fairbanks, Alaska. The relocated system became operational in February 1980. The performance of the remote terminal operating in a hostile environment will be evaluated during the subsequent 6-month period.

The prototype system, shown in Figure 1, consists of a single remote terminal transmitting seismic data at an information rate of 4,800 bit/s to the central receive station and a 96-bit/s command link from the central station to the remote platform. In addition, a pilot link in a loopback configuration generated at the central station is used to determine the value of frequency offsets caused by the satellite and up-converter and to precompensate the command link frequency. Hence, the received frequency error of the command link at the remote station is minimized.

The 4,800-bit/s seismic data are rate 1/2 encoded so that the actual transmitted bit rate is 9,600-bit/s. BPSK modulation of the data link carrier is employed. Each of the three carriers in the system is assigned one channel of the SCPC transponder.

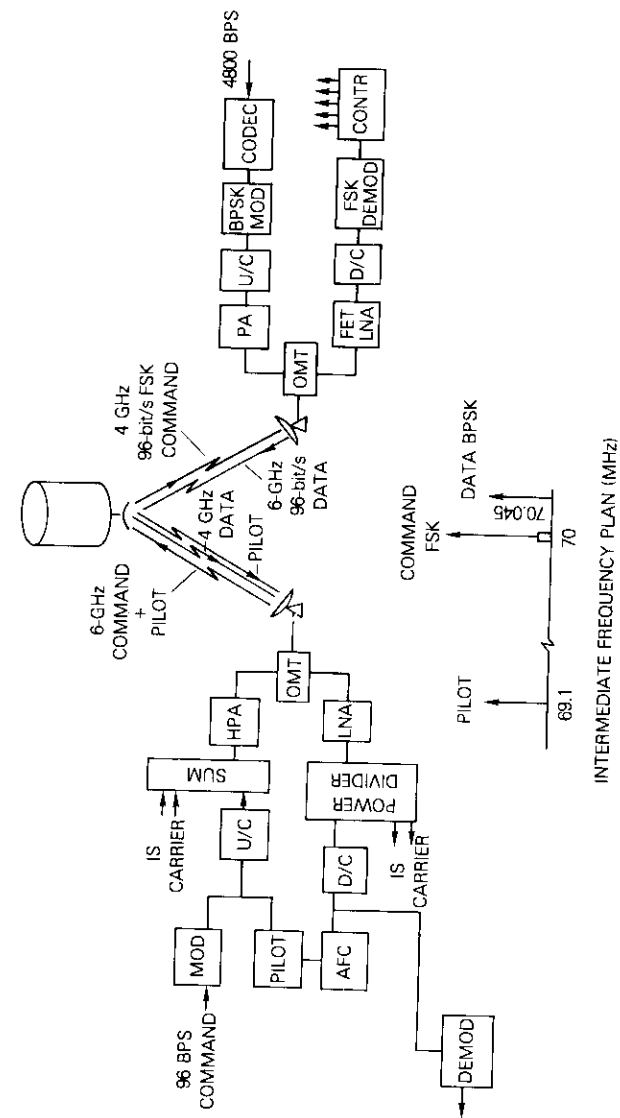


Figure 1. Automatic Seismic Observatory Communications System

A subsidiary purpose of this demonstration was to test low-data-rate (96-bit/s) transmissions via an INTELSAT satellite, operating as closely as possible within the system constraints. This objective involved the investigation of low-frequency phase modulation caused by the high-power amplifier (HPA), frequency stability and phase noise of the satellite translation oscillator, and multiplexing of low-data-rate signals within an operating system handling traditional FDM/FM, TV, and SCPC traffic. The system design was affected by parameters such as size limitations of the collection platform equipment, subsystem reliability, severe prime power constraints and hostile environment at the remote terminal, HPA and oscillator stability requirements, and very low elevation angles of the remote station antenna.

System design and tradeoffs

Theoretical considerations

The principal elements of a digital coherent communications link are depicted in Figures 2 and 3. The sources of link impairment will be oscillator phase noise from sources LO_1 , LO_2 , and LO_3 ; thermal noise (primarily in the down-link); and recovered carrier phase jitter caused by thermal noise in the carrier recovery tracking phase-lock loop of the demodulator. In addition, incidental phase jitter introduced by power supply modulation of the command link HPA could cause bursts of errors.

Given the desired link bit-error-rate performance and oscillator short-term stability data, the carrier recovery phase-lock loop bandwidth must be chosen such that the resulting recovered carrier phase jitter due to the sum of tracked thermal noise and untracked phase noise yields low demodulation loss compared to ideal performance. In addition, the mean time for the loop-to-cycle slip must be sufficiently high.

THERMAL NOISE

After squaring a bandwidth-limited signal plus additive white Gaussian noise (Figure 3), the signal-to-noise ratio [1], α'_{TH} , at the VCO output is

$$\alpha'_{TH} = \frac{R_s E_s}{4B_L N_0} \frac{1}{\left(1 + \frac{1}{2E_s/N_0}\right)} = \frac{1}{\sigma_{TH}^2} \quad (1)$$

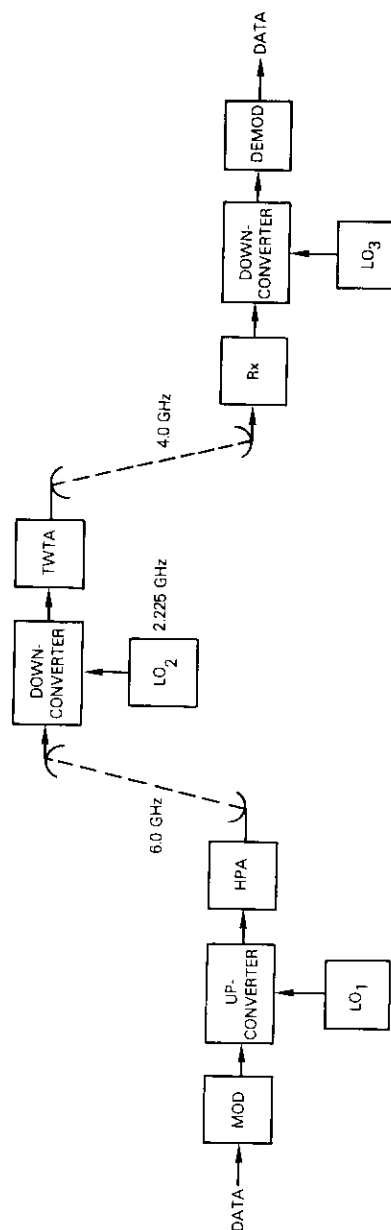


Figure 2. Simplified Communications Link Block Diagram

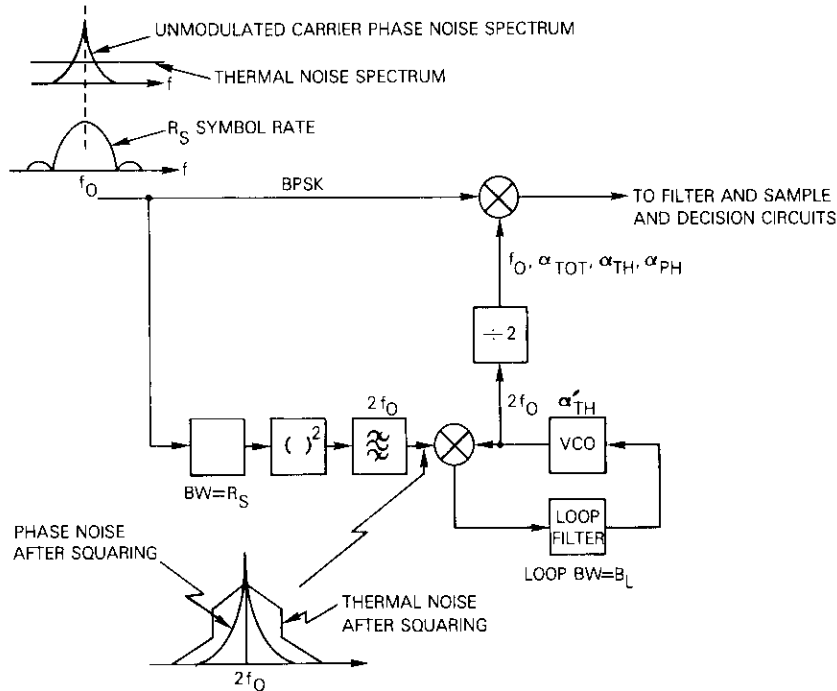


Figure 3. BPSK Demodulator Carrier Recovery and Demodulation Multiplier

where R_s is the BPSK symbol rate, B_L is the single-sided tracking loop bandwidth, and E_s/N_0 is the energy per symbol-to-noise density ratio required for an acceptable link bit-error rate. The quantity σ_{TH}^2 is the variance of the phase jitter out of the loop. The equivalent signal-to-noise ratio after the divide-by-two function at the carrier multiplier input (Figure 3) is

$$\alpha_{TH} = \frac{R_s E_s}{B_L N_0} \frac{1}{\left(1 + \frac{1}{2E_s/N_0}\right)} \quad (2)$$

PHASE NOISE

The effective phase noise jitter, σ_{PH} , can be determined from oscillator short-term stability data expressed as a fractional frequency

departure, $\sigma_{\Delta f}/f_0$, which is a function of measurement averaging time, τ . The carrier recovery loop will track the portion of the phase noise spectrum that falls within the 2-sided loop bandwidth (see Figure 4). Although this portion is of no concern, since it is included as part of the carrier power, the phase noise that falls outside the two-sided loop bandwidth of the tracking loop must be considered as a noise impairment. The untracked phase noise adds to the tracked thermal noise distorted by the carrier multiplier to produce an equivalent phase jitter which degrades the recovered carrier. The value of untracked phase noise jitter is

$$\sigma_{PH} = 2\pi \left(\frac{\sigma_{\Delta f}}{f_0}\right) \tau f_c \quad (3)$$

where $\sigma_{\Delta f}/f_0$ is the fractional frequency departure of the oscillator source normalized by the actual frequency of the oscillator, τ is the averaging time employed to measure $\sigma_{\Delta f}$, and f_c is the actual carrier frequency to which the oscillator source is multiplied. The equivalent signal-to-noise ratio of the untracked phase noise is

$$\alpha_{PH} = \frac{1}{\sigma_{PH}^2} = \left[\frac{1}{2\pi(\sigma_{\Delta f}/f_0) \tau f_c} \right]^2 \quad (4)$$

or in terms of loop bandwidth, B_L ,

$$\alpha_{PH} = \left[\frac{B_L}{\pi(\sigma_{\Delta f}/f_0) f_c} \right]^2 \quad (5)$$

where $\tau = 1/2B_L$ assuming that the oscillator measurement time is equal to the loop averaging time.

The satellite link contains three oscillator sources, each multiplied up to a different carrier frequency, f_c . The satellite translation oscillator, at 2.225 GHz, is the dominant phase noise source in the system. Figure 5 shows typical measured fractional frequency departure data for this oscillator normalized to a 1-Hz oscillator carrier frequency as a function of loop averaging time, τ , and loop bandwidth, B_L , [2]. These data can be employed to calculate α_{PH} using equation (5). For comparison, data for a high-quality 5-MHz oscillator source are also included in Figure 5 [3].

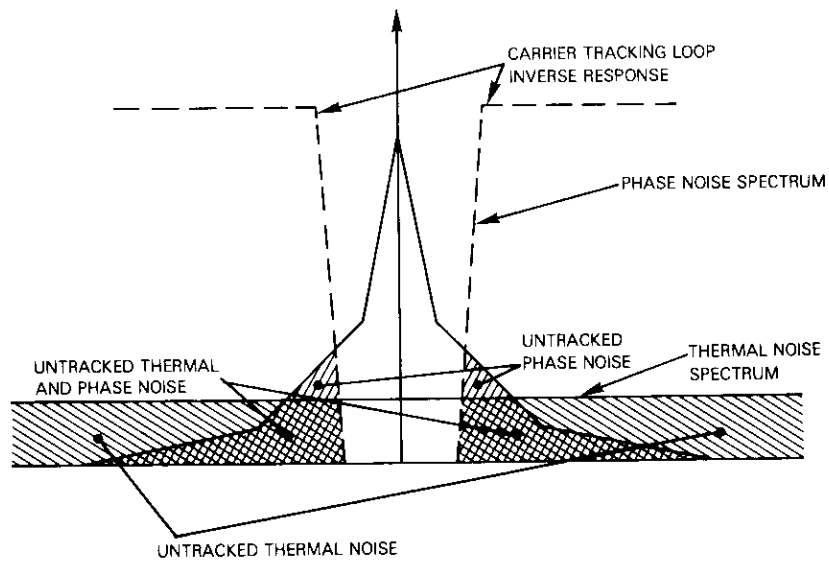
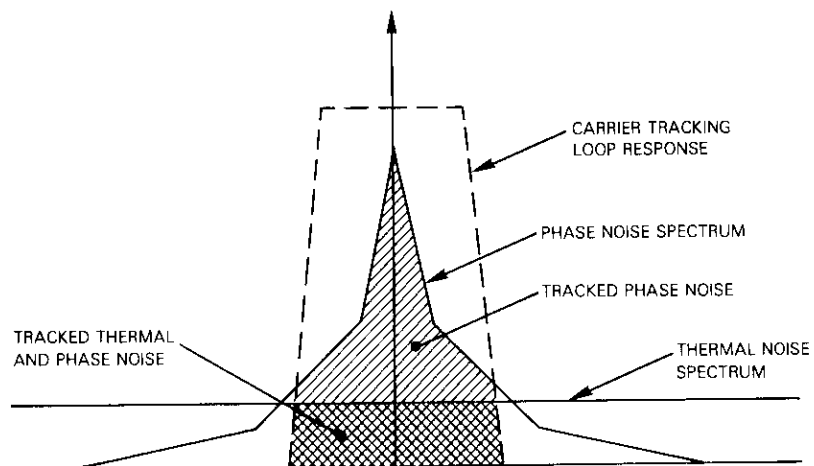


Figure 4. Untracked Phase Noise

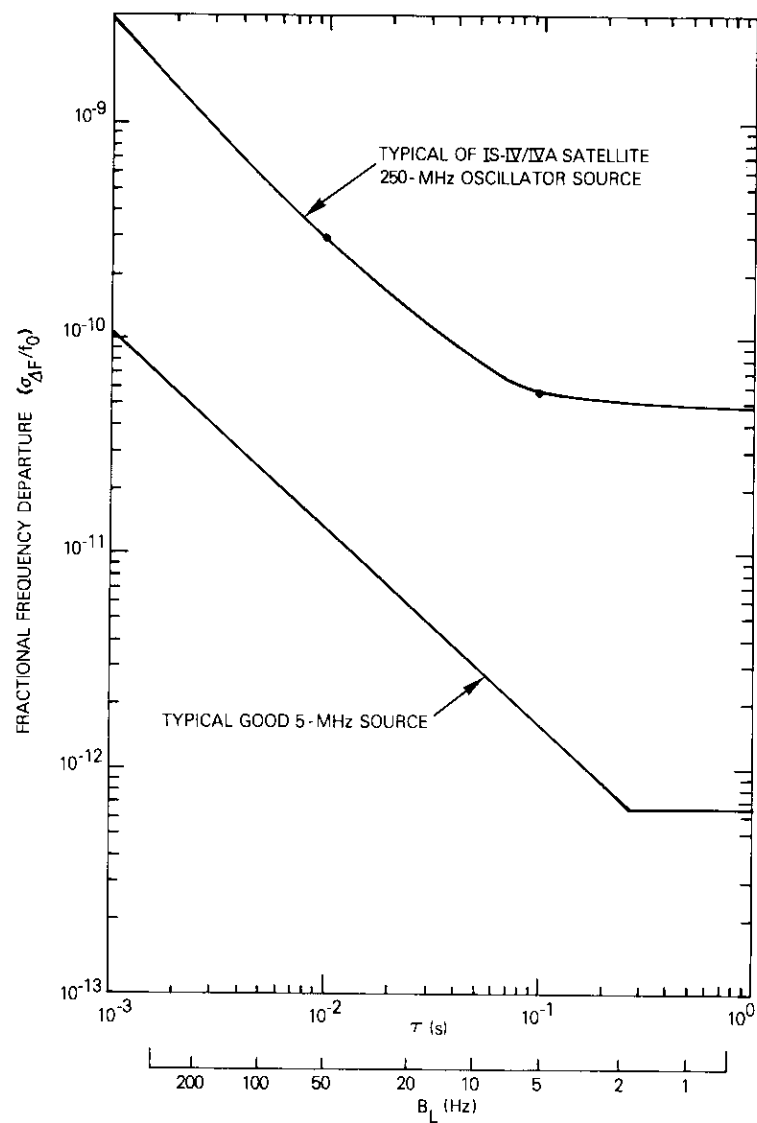


Figure 5. Oscillator Short-Term Stability Data

CYCLE SLIPPING

Second-order phase-lock-loop cycle slipping performance as a function of loop signal-to-noise ratio and loop bandwidth has been adopted from References 4 and 5, where the mean time-to-loop cycle slip, verified using computer simulation analysis, is

$$T_{SL} = \frac{1}{2B_L} \frac{3}{8} \exp[2\alpha_{TH}] \quad (6)$$

In terms of the signal-to-noise ratio, α_{TH} , after the divide-by-two function in Figure 3, the mean time-to-cycle slip is

$$T_{SL} = \frac{1}{2B_L} \frac{3}{8} \exp\left(\frac{\alpha_{TH}}{2}\right) \quad (7)$$

Data link

This link employs rate 1/2 convolutional encoding with soft decision, $Q = 8$, $K = 7$ Viterbi decoding requiring a theoretical E_b/N_0 of 5.8 dB for a bit-error rate of 1×10^{-7} .

The tracked thermal noise and untracked phase noise contributions resulting in a nonideal carrier reference for BPSK demodulation have been determined from equations (2) and (5), respectively, and plotted as a function of loop bandwidth in the lower part of Figure 6. This figure, which also includes the total equivalent reconstructed carrier reference signal-to-noise ratio determined from α_{TH} and α_{PH} components, indicates the tradeoff in terms of loop bandwidth variations. The loop bandwidth that maximizes α_{TOT} is approximately 20 Hz. The demodulation loss due to a noisy carrier phase reference is determined from bit-error rate as a function of E_b/N_0 data with carrier reference signal-to-noise ratio (α_{TOT}) as a parameter. These loss data are shown in the upper portion of Figure 6. With a 20-Hz loop, the demodulation loss will be less than 0.1 dB and the bandwidth could be increased to 100 Hz, resulting in 0.5-dB loss and thermal-noise-limited loop operation.

The final tradeoff that must be considered is mean time-to-cycle slip using equation (7). The 100-Hz loop bandwidth alternative results in a mean time-to-loop slip of 4.57×10^{28} seconds or 1.45×10^{21} years. This loop design is satisfactory and has been adopted for the system. The overall data link budget is given in Table 1.

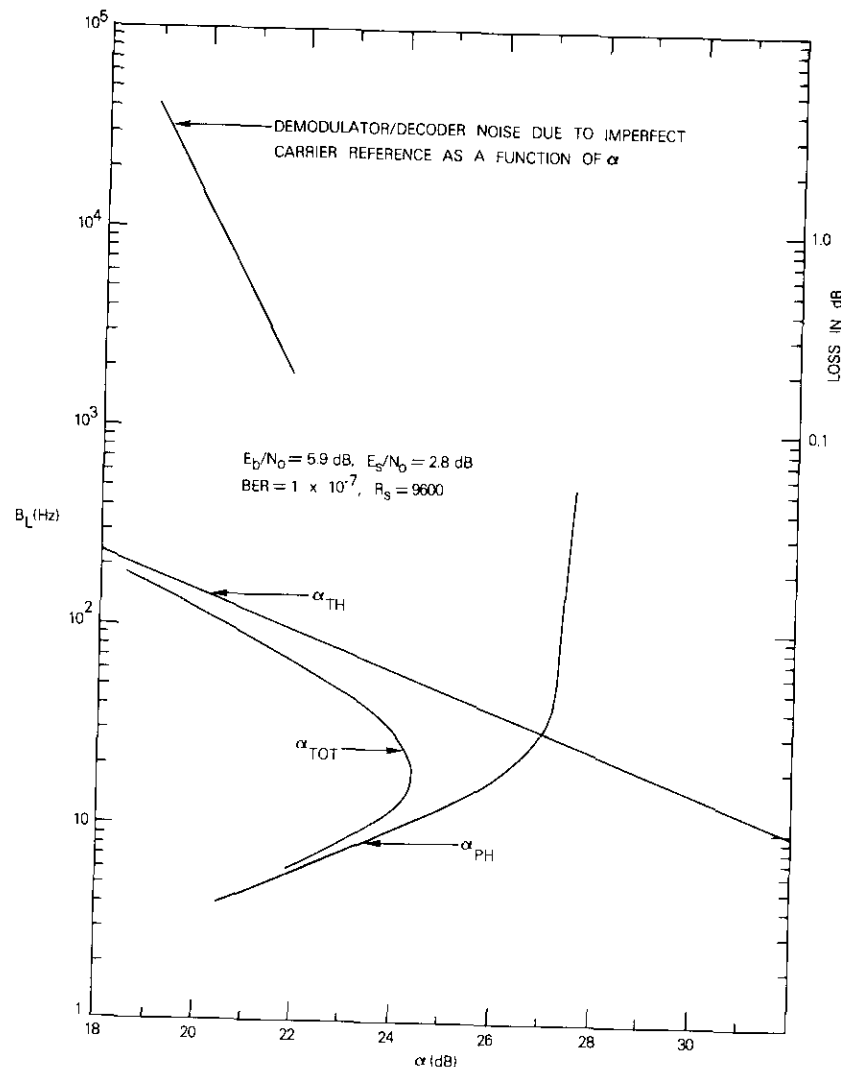


Figure 6. 4,800-bit/s Coded BPSK Link Analysis

TABLE 1. LINK BUDGET FOR DATA LINK

Up-Link (6327.3 MHz)	
Power (HPA Flange)	10.00 dBW
Feed Loss	1.00 dB
Antenna Gain	42.50 dB
e.i.r.p.	51.50 dBW
Radome Loss	0.50 dB
Multipath Loss	1.00 dB
Atmospheric Loss at 6 GHz	1.50 dB
Path Loss (nominal)	200.00 dB
Power on Satellite	-152.00 dBW
Satellite G/T	18.60 dB/K
$(C/N_0)_{up}$	58.00 dB-Hz
Satellite Saturation Flux	-67.30 dBW/m ²
Satellite Flux	-114.53 dBW/m ²
Input Backoff	47.23 dB
Output Backoff	42.23 dB
Satellite Saturated e.i.r.p.	22.00 dBW
Down-Link (4102.3 MHz)	
Satellite e.i.r.p.	-20.23 dBW
Atmospheric Loss at 4 GHz	1.00 dB
Path Loss	196.50 dB
Power at INTELSAT Earth Terminal	-217.73 dBW
Feed Loss	0.30 dB
INTELSAT Earth Terminal Receive Power	-161.03 dBW
Receive G/T	40.70 dB/K
$(C/N_0)_{down}$	51.27 dB-Hz
$(C/N_0)_{total}$	50.43 dB-Hz
Information Bit Rate (4,800 bit/s)	36.82 dB
E_b/N_0	13.60 dB
E_b/N_0 (required BER = 1×10^{-7})	5.80 dB
Implementation Loss	1.60 dB
Margin	6.20 dB

COMMAND LINK

A similar analysis was performed for the 96-bit/s command link using BPSK modulation. The assumption of $E_b/N_0 = 8.4$ dB for a bit-error-rate performance of 1×10^{-4} resulted in the tradeoff analysis shown in Table 2.

A reasonable design choice would be a loop bandwidth of 15 Hz, resulting in a demodulation loss of 0.23 dB and a mean time-to-loop unlock of 2.29×10^7 seconds (265 days). However, because of the

TABLE 2. 100-BIT/S BPSK LINK ANALYSIS SUMMARY

B_L (Hz)	α_{TOT} (dB)	Demodulation		T_{SL} (s)
		Loss (dB)	α_{TH} (dB)	
5	18.0	0.18	21.0	8.15×10^{25}
10	17.0	0.20	18.0	9.42×10^{11}
15	16.0	0.23	16.3	2.29×10^7
20	15.0	0.30	15.0	6.90×10^1
25	14.0	0.50	14.0	2.14×10^0
35	12.6	1.80	12.6	4.79×10^{-1}

long acquisition time (typical of a 15-Hz loop bandwidth design) at the remote terminals, the uncertainty of additional HPA-induced phase noise, particularly at 60 Hz, and the desirability of equipment compatibility with any earth terminal presently in operation, it was decided not to use BPSK for the command link. Instead, FSK, a more conservative approach for which these impairments are not significant, was chosen; the overall link budget is given in Table 3.

TABLE 3. LINK BUDGET FOR COMMAND LINK

Up-Link (6327.3 MHz)	
INTELSAT Earth Station Power at the OMT	4.40 dBW
e.i.r.p.	64.90 dBW
Atmospheric Loss at 6 GHz (due to low look angle)	1.50 dB
Path Loss	200.00 dB
Power on Satellite	-136.60 dBW
Satellite G/T	18.60 dB/K
$(C/N_0)_{up}$	73.40 dB-Hz
Satellite Saturation Flux	-67.30 dBW/m ²
Satellite Flux	-99.13 dBW/m ²
Input Backoff	31.83 dB
Output Backoff	26.83 dB
Satellite Saturated e.i.r.p.	22.00 dBW
Down-Link (4102.3 MHz)	
Satellite e.i.r.p.	-4.83 dBW
Radome Loss	0.75 dB
Multipath Loss	1.00 dB
Atmospheric Loss at 4 GHz	1.00 dB
Pointing Loss (INTELSAT IV-A)	0.50 dB
Path Loss	196.50 dB
Polarization Loss	0.10 dB

(continued next page)

TABLE 3. LINK BUDGET FOR COMMAND LINK (continued)

Down-Link (4102.3 MHz)	
Power on Remote Earth Station	-204.68 dBW
Remote Earth Terminal Antenna Gain	39.50 dB
Receive Noise Temperature	23.00 dB
Receive G/T	16.50 dB/K
Receive Power, Remote Terminal	-165.18 dBW
$(C/N_0)_{down}$	40.42 dB-Hz
$(C/N_0)_{total}$	40.42 dB-Hz
Data Rate (96 bit/s)	19.82 dB
E_b/N_0	20.60 dB
Processing Loss	4.10 dB
E_b/N_0 Available	16.50 dB-Hz
E_b/N_0 Required ($P_e = 10^{-4}$ BER)	12.40 dB-Hz
Margin	4.10 dB

Overall receive terminal equipment

Figure 7 is an overall block diagram of the central terminal. The intermediate power amplifier (IPA/HPA), low-noise amplifier (LNA), combiner, and divider, as well as the antenna and all related peripheral equipment not shown, are portions of a normal Standard A INTELSAT earth station. A system containing multiple remote data platforms would require a separate data demodulator for each platform.

Data link

The data link of the Automatic Seismic Observatory uses one channel of a satellite single-channel-per-carrier transponder to transmit 4,800-bit/s seismic data from the remote station to the central terminal at Andover, Maine. The data are rate 1/2 convolutionally encoded prior to transmission and the resulting 9,600-bit/s data modulate the carrier using biphase PSK modulation. At the central terminal, the doubling technique in conjunction with a phase-locked loop is used for carrier recovery, while a Costas loop is employed for data demodulation.

DATA LINK AFC

The biphase PSK-modulated carrier is received by the data link receiver at 70.045 MHz and down-converted to 5.045 MHz by the 65-MHz voltage-controlled crystal oscillator (VCXO) in the AFC circuit shown in Figure 8. The 5.045-MHz signal is split into two branches: one is applied to the Costas loop demodulator, and the second to the doubler and the AFC loop. The doubler removes the modulation from

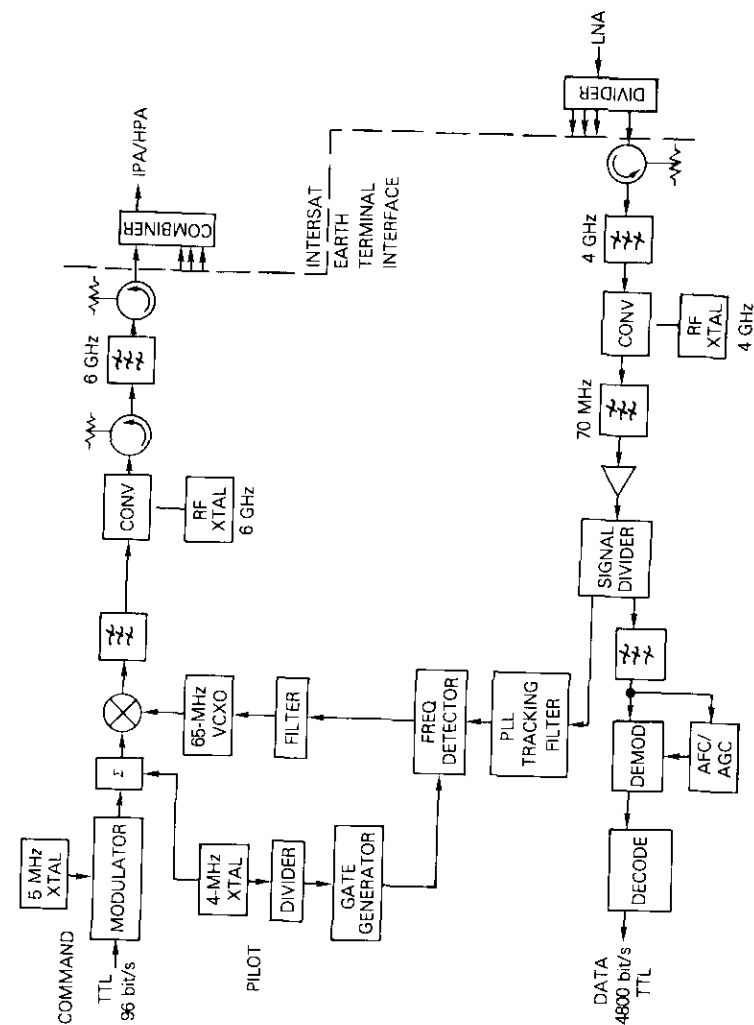


Figure 7. Central Receive Terminal Communications System Block Diagram

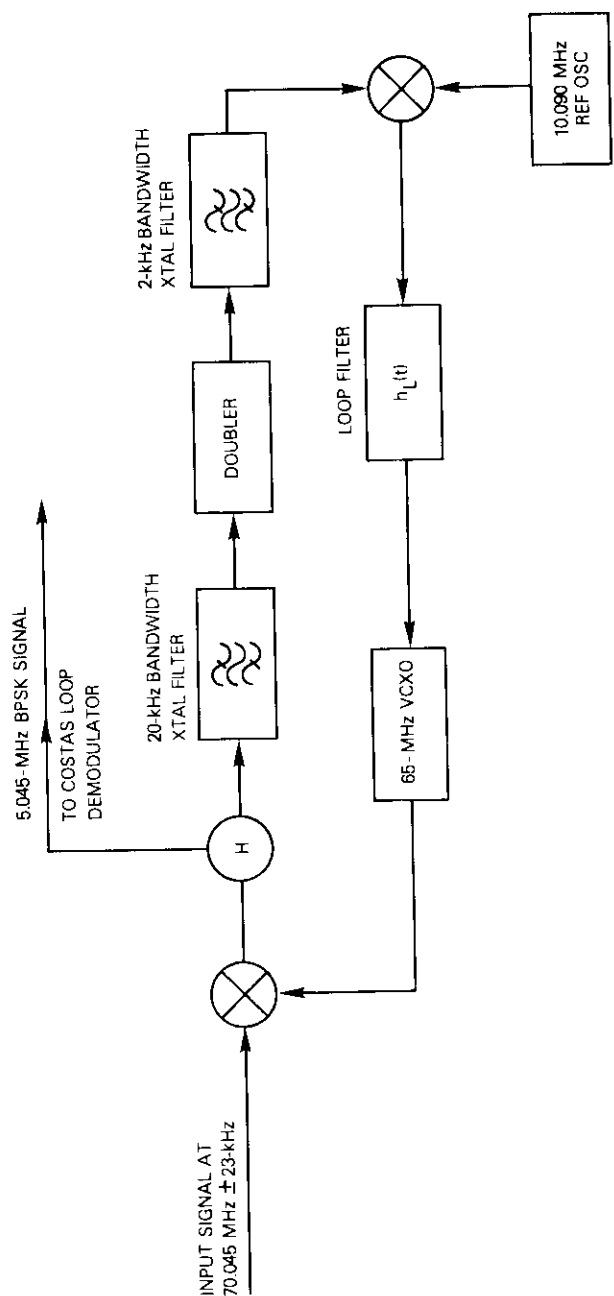


Figure 8. Data Link Receiver AFC Circuit

the signal and the 2-kHz bandwidth crystal filter eliminates a large portion of the noise resulting from doubling. The output of the crystal filter at 10.090 MHz is then phase-compared with a 10.090-MHz reference oscillator; the resultant signal is applied through loop filter $h_L(t)$ to the 65-MHz VCXO to maintain phase lock between the doubled signal and the reference oscillator. Hence, the input to the Costas loop demodulator remains constant at 5.045 MHz for a range of data link receiver input frequency variations up to ± 23 kHz.

COSTAS LOOP DEMODULATOR

The Costas loop demodulator, shown in Figure 9, is essentially a phase-lock loop with signal-dependent gain polarity. Its operation is most easily envisaged by imagining that the loop is phase locked to an unmodulated carrier. Assume that the loop has locked to produce a positive output at the quadrature detector. Now consider the effect of a change in input polarity due to a phase modulation of 180° . The quadrature detector will immediately become negative and, if no further change occurs, the forward loop gain will reverse polarity, causing loop instability and loss of lock. However, as the forward loop gain is multiplied by the quadrature detector output in the Costas loop demodulator, the initial reversal of loop-gain polarity is cancelled and

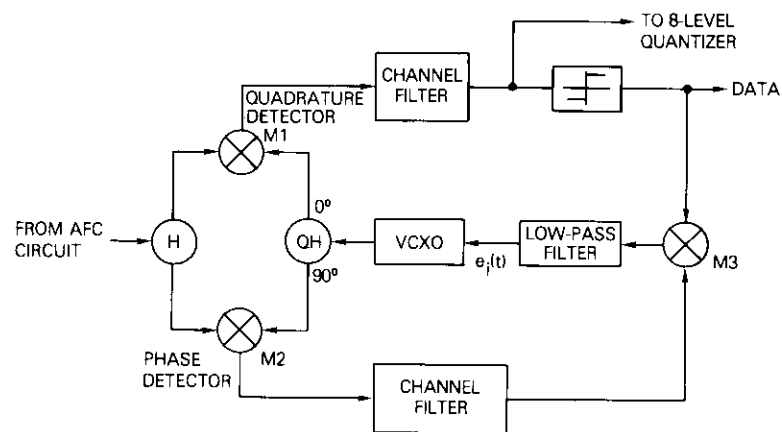


Figure 9. Costas Loop Demodulator Block Diagram

the loop remains stable and phase locked despite random changes of 180° in the input carrier phase. It should be noted that, with this multiplying technique, the loop can lock up in either of two states: the unmodulated carrier may be either in phase or 180° out of phase with the recovered carrier.

DATA CLOCK RECOVERY

It is clear from the preceding discussion that the quadrature detector output reversals conform to data transitions. Thus, the detector output, after leveling, is applied to the clock recovery circuit and relocked by the output of the clock recovery circuit. The resulting data and clock signals at 9,600 bit/s are then applied to the Viterbi decoder. The quadrature detector output is 8-level quantized before being applied to the Viterbi decoder for soft decision decoding. Differential encoding is used in this link so that cycle slipping in the receiver phase-lock loops does not cause long strings of errors.

The clock recovery circuit, which is an all-digital phase-locked loop contained in an LSI chip, is designed to recover a synchronous clock from a random binary data signal. It incorporates acquisition mode circuitry, which provides for rapid phase lock upon initial acquisition.

Pilot loopback link

To reduce the frequency uncertainty of the command link received at the remote station to within the narrow bandwidth of the command link receiver, a pilot loopback link is transmitted and received at the central terminal. Hence, the amount of frequency offset caused by the central station up-converter and satellite translator oscillators can be determined and used to predisplace the transmitted frequency of the command link so that the frequency offsets are cancelled.

LINK DESIGN

The satellite and up-converter can cause frequency offsets of as much as ± 25 kHz in one year, while the command link receiver design can acquire signals with no more than $\pm 1,800$ -Hz deviation. Rather than an AFC loop in each of the remote stations, a single pilot loopback link was used to eliminate the large frequency offsets for all remote stations simultaneously.

With reference to Figure 10, since both the pilot at 4.01 MHz and the 5-MHz FSK-modulated command link carrier are translated by the same 65-MHz VCXO, it should be noted that while their absolute

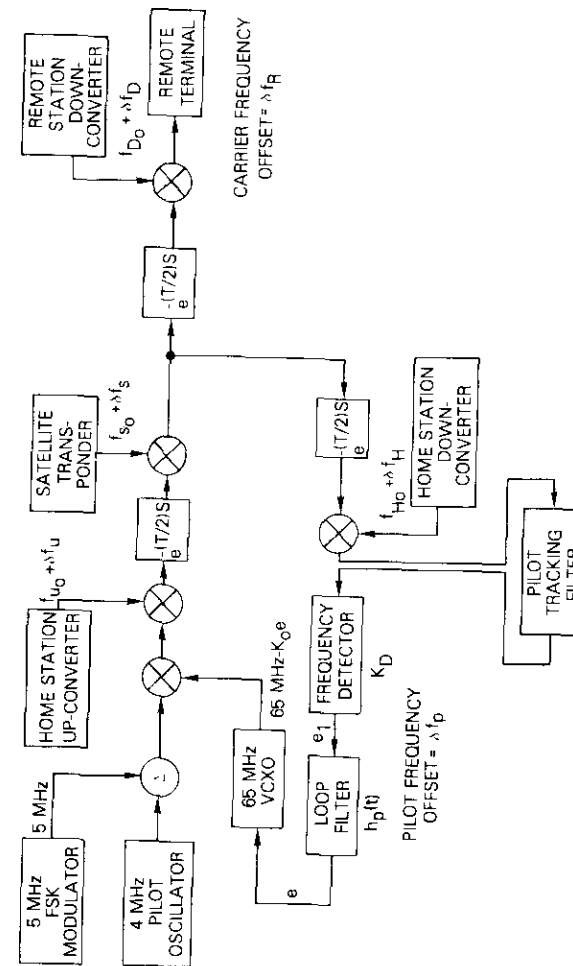


Figure 10. Pilot Loopback Configuration Block Diagram

frequency may vary, their frequency separation remains constant. The variation in frequency of the 65-MHz vxco is that which is required to compensate for the up-converter and satellite translator offsets.

FREQUENCY DETECTOR

The nucleus of the pilot loopback link is a digital frequency detector designed and developed for application in data collection systems [6]. Figure 11 is a detailed schematic of this module.

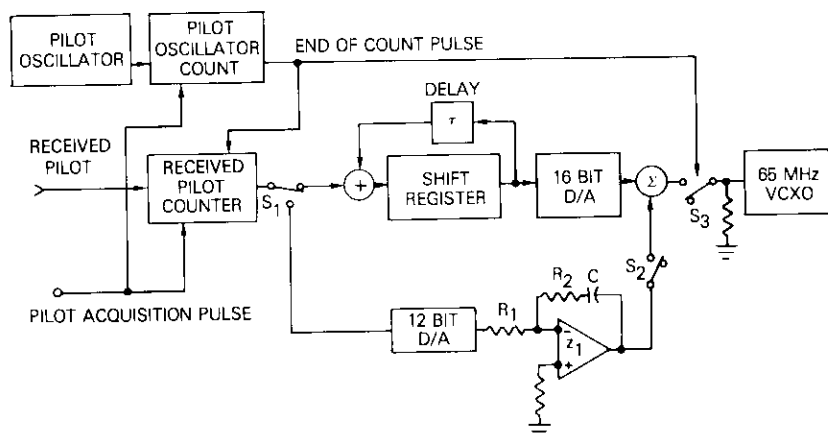


Figure 11. Pilot Frequency Detector and Loop Filter

Because of the wide bandwidth (50 kHz) over which the received pilot may range, it must be acquired by a phase-lock pilot tracking filter. A 100-Hz bandwidth tracking filter yields a carrier-to-noise ratio of 35.8 dB for the pilot at the loop output (see Table 4), resulting in an rms frequency jitter of less than 0.3 Hz.

Frequency detection is performed by counting the cycles of the pilot at the output of the tracking filter over a specific time period. The count time is determined by the 4-MHz pilot oscillator itself with counters applied to both the 4-MHz pilot oscillator and the 69-MHz received pilot at the tracking loop filter output. Start of count is triggered on both counters by the same pulse. When the pilot oscillator count reaches 4,000,000 (equivalent to a 1-second count period), the received pilot counter is stopped; 69,000,000 is subtracted from the count; and the difference is converted to an analog voltage. As shown in the block diagram of Figure 11, the analog voltage is filtered by a

loop filter and applied to the 65-MHz vxco. With an integrating-type loop filter, the offset will theoretically be reduced to zero.

TABLE 4. LINK BUDGET FOR PILOT LINK

Up-Link (6326.3 MHz)	
INTELSAT Earth Station Power at OMT	-5.60 dBW
Antenna Gain	60.50 dB
e.i.r.p.	54.90 dBW
Atmospheric Loss at 6 GHz (due to low look angle)	1.50 dB
Path Loss	200.00 dB
Power on Satellite	-146.60 dBW
Satellite G/T	18.60 dB/K
$(C/N_0)_{up}$	63.40 dB-Hz
Satellite Saturation Flux	-67.30 dBW/m ²
$4\pi/\lambda^2$	37.47 dB/m ²
Satellite Flux	-109.13 dBW/m ²
Input Backoff	41.83 dB
Output Backoff	36.83 dB
Satellite Saturated e.i.r.p.	22.00 dBW
Down-Link (4101.3 MHz)	
Satellite e.i.r.p.	-14.83 dBW
Atmospheric Loss at 4 GHz	1.00 dB
Path Loss	196.50 dB
Power on INTELSAT Earth Station	-212.33 dBW
Feed Loss	0.30 dB
Receive G/T	40.70 dB/K
$(C/N_0)_{down}$	55.67 dB-Hz
$(C/N_0)_{total}$	55.83 dB-Hz
S/N_L (loop bandwidth = 100 Hz)	35.82 dB

Application of the same frequency detector sensitivity to the initial very large frequency offsets (as high as 23 kHz) and the steady-state offsets, which should be held to less than 5 Hz, results in a problem in resolution. As an example, the increment of pilot offset in the loop of Figure 10 can be expressed as

$$\delta f_p = \frac{1}{1 + K_0 K_d H_p(s)} \delta f_L - \frac{1}{1 + K_0 K_d H_p(s)} \delta e_1 \quad (8)$$

where δf_L is the sum of the link-induced frequency uncertainties, and δe_1 is a small voltage error at the detector output.

For an integrating loop filter, it is then possible to write

$$\delta f_p = \frac{s}{s + K_0 K_d K_i} \delta f_L - \frac{K_0 K_i}{s + K_0 K_d K_i} \delta e_1 \quad (9)$$

Two problems are immediately apparent. First, the loop time constant, $1/K_0 K_d K_i$, must be 2.5 seconds to be an order of magnitude greater than the satellite link delay. Thus, for an initial offset of 23 kHz, the loop would require 21 seconds to bring the received pilot to within 5 Hz of the nominal frequency. While this time may be tolerable during the initial setup of the link, it would constitute a serious drawback if periods of pilot loss occurred during operation.

The second problem is due to the offset voltage, δe_1 . The steady-state value of δf_p for initial offsets $\delta f_L = \Delta f_L$ and $\delta e_1 = \Delta e_1$ is

$$\begin{aligned} \delta f_p(t \rightarrow \infty) &= \lim_{s \rightarrow 0} s \left\{ \frac{s}{s + K_0 K_d K_i} \frac{\Delta f_L}{s} - \frac{K_0 K_i}{s_0 + K_0 K_d K_i} \frac{\Delta e_1}{s} \right\} \\ &= \frac{1}{K_d} \Delta e_1 \end{aligned} \quad (10)$$

which is independent of the integrator or vcxo gains. With a voltage range of ± 12 V (corresponding to ± 24 kHz) at the frequency detector output, the ratio

$$\frac{\delta f_p(t \rightarrow \infty)}{\Delta e_1} = \frac{1}{K_d} = \frac{24000 \text{ Hz}}{12 \text{ V}} = 2 \text{ Hz/mV} \quad (11)$$

indicates an excessive sensitivity to noise voltages if δf_p must be held to within ± 5 Hz.

The latter problem is avoided by including the 12-bit digital-to-analog (D/A) converter in the circuit of Figure 11. During acquisition, the 16-bit D/A converter is in the circuit, and the output voltage range of the converter is ± 12 V for an input frequency variation of ± 25 kHz. When the offset frequency has been reduced to less than 120 Hz, switches S1 and S2 are activated and the 12-bit D/A converter replaces the 16-bit converter. The 12-bit converter output range is the same as that of the 16-bit converter and the new frequency offset sensitivity is

$$\frac{\delta f_p(t \rightarrow \infty)}{\Delta e_1} = \frac{1}{K_d} = \frac{120 \text{ Hz}}{12 \text{ V}} = 10 \text{ Hz/V} \quad (12)$$

which indicates insensitivity to noise.

To reduce the long acquisition period associated with the 2.5-second time constant of the feedback loop, the integrator is removed from the circuit during acquisition and replaced by a directed-type step reduction in frequency. The circuit is shown in Figure 11; the counters, one on the pilot oscillator and one on the received pilot, are started by a pulse generated by the pilot acquisition indicator in the pilot tracking filter. At the end of one second, as determined by the pilot oscillator counter, the contents of the received pilot counter are transferred to the shift register through switch S1, which is in the position shown in Figure 11. The 16-bit D/A converter generates an analog signal to correspond to the digital counter at the input. At the end of the count, switch S3, which is initially open so that the vcxo sees a grounded input, is closed. The step change in vcxo voltage changes the transmit frequency in the direction which reduces the received pilot offset.

The counters are immediately restarted. At the end of the second 1-second count period, the output of the received pilot counter is added to the previous count by delay element τ . The 16-bit D/A converter converts the cumulative count to an analog signal which drives the vcxo to further reduce the received pilot offset.

When the received pilot offset has been reduced to less than 120 Hz, the threshold count detector switches S1 and S2 simultaneously; hence, the signal from the received pilot counter is applied to the 12-bit D/A converter and the loop filter, consisting of Z1, K1, C, and R2, for continuous operation of the loop.

Operationally, the total acquisition time has been found to be less than 10 seconds.

LINK FREQUENCY OFFSET MEASUREMENTS

A link diagnostic feature has been incorporated in the pilot link receiver to measure the actual frequency offset due to the satellite translator and up- and down-converter oscillators. A front panel-mounted switch can be repositioned to ground the input to the 65-MHz vcxo, thereby opening the feedback loop. The pilot and command links will then be transmitted at their nominal frequencies without correction and the received frequency, measured by the digital frequency detector and displayed on the front panel, will be the actual variation due to link oscillators, with the largest part due to the satellite oscillator. While the frequency offset is being monitored, the remote stations will normally be unable to acquire the command link.

An experiment was conducted to determine satellite frequency variations over a long period of time. The difference between transmitted and received pilot frequencies was observed at 1-hour intervals from 0000Z, 15 December 1978, to 0000Z, 1 January 1979. Results, shown in Figure 12, indicate that the maximum diurnal variation was less than 700 Hz. The maximum variation over the period of observation was 755 Hz; the mean frequency offset was 2,325 Hz.

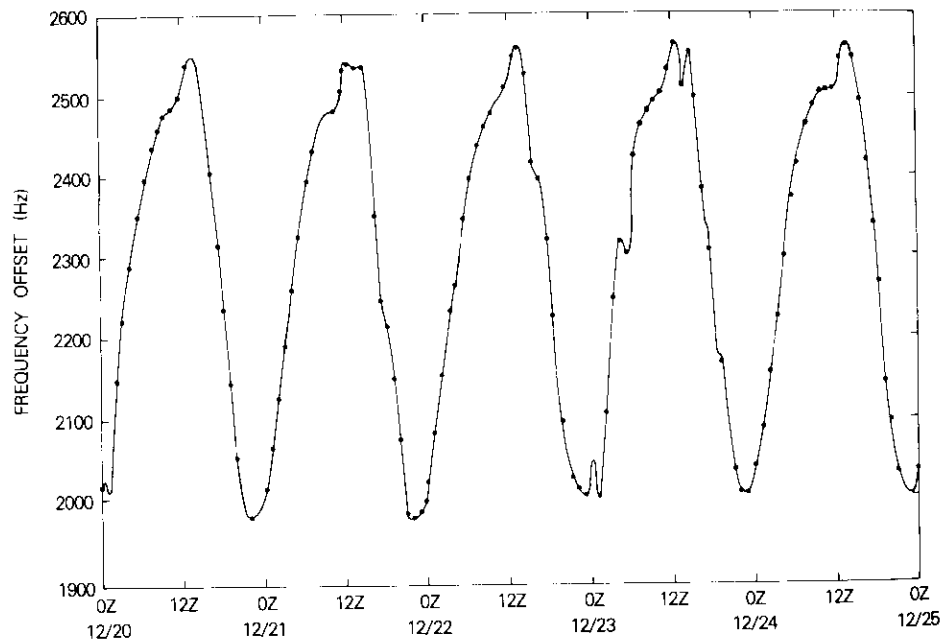


Figure 12. Satellite Frequency Variations, 15 December 1978 to 1 January 1979

Up-converter and local oscillator stability

The up-converter shown in Figure 13 provides the transmit command and pilot carriers, as well as a means for remotely monitoring the transmit input power to the Standard A earth terminal IPA/HPA. A portion of the 6-GHz signal resulting from the initial up-conversion is coupled off, down-converted to 70 MHz, and then detected. The resultant output voltage can be used either for a digital alarm system, as presently constituted, or as an analog indication of transmit power.

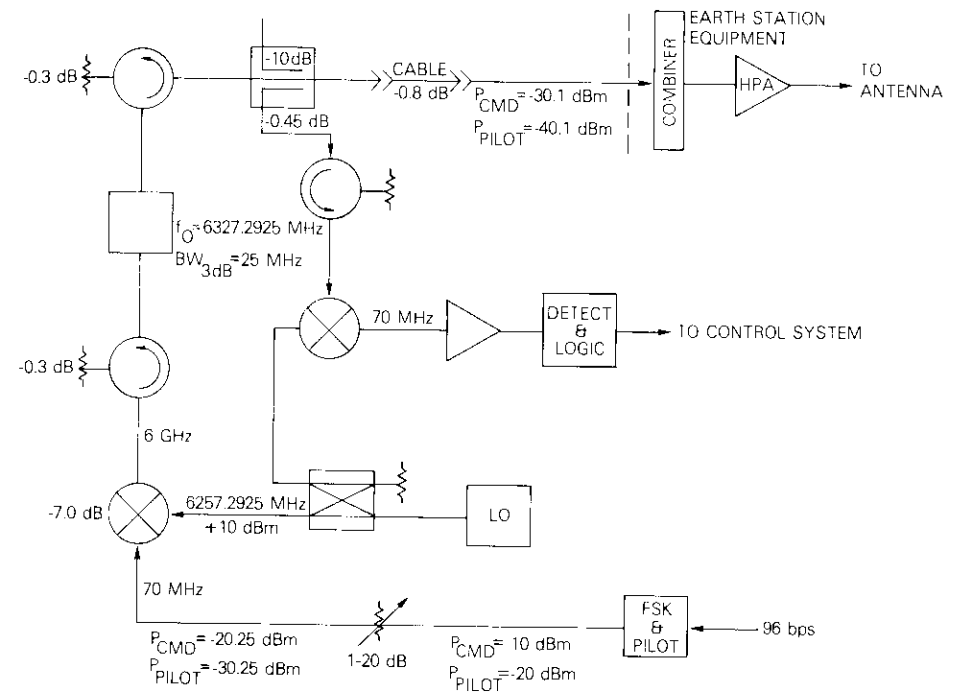


Figure 13. Central Terminal Up-Converter

Either form of information can then be added to the decoded control data from the remote platforms and transmitted to a remote control facility for real-time monitoring.

The up-converter local oscillator, one of four oscillators in the total link, presents a serious stability problem. The pilot link accounts for the satellite instabilities and some of the Doppler shift. Although the local oscillator frequencies could be constantly monitored and reset at the central terminal once a week, this approach would be impractical for the remote platforms except perhaps on a 6-month basis. Also, with identical oscillators at the central and remote sites, fewer interchangeable units are needed as spares.

The second practical constraint is the realizable tracking range of the remote FSK receiver, namely, $\pm 1,400$ Hz. Therefore, based on a 6-month readjustment at the remote platform, a weekly readjustment at the central terminal, and the other frequency perturbation shown in

Table 5, a stability of 1×10^{-9} /day for the local oscillators was chosen. To achieve this, a precision, temperature-controlled, nominal 5-MHz crystal-controlled oscillator was used with a phase-locked multiplier in all the local oscillators in both terminals.

TABLE 5. LOCAL OSCILLATOR FREQUENCY PERTURBATIONS

FSK Demodulator Tracking Range	± 1400 Hz
FSK Deviation	± 150 Hz
Differential Doppler	± 15 Hz
Remote Down-Converter Temperature Variation (2×10^{-8})	± 80 Hz
Remote Down-Converter Aging (6 months)	± 730 Hz
Demodulator 55-MHz Oscillator Stability (1×10^{-6})	± 55 Hz
Demodulator 55-MHz Oscillator Aging	± 3 Hz
Central Up-Converter Temperature Variation	± 80 Hz
Central Up-Converter Aging (1 week)	± 28 Hz
Net Frequency Drift Margin (Tracking range less all deviations and aging)	± 259 Hz

HPA phase noise

The use of a command carrier with very low data rate (96-bit/s) information makes the carrier particularly susceptible to phase jitter produced by the HPAs. Especially detrimental is the 60-Hz hum induced on the carrier by the central station HPA. Figure 14 depicts the baseband

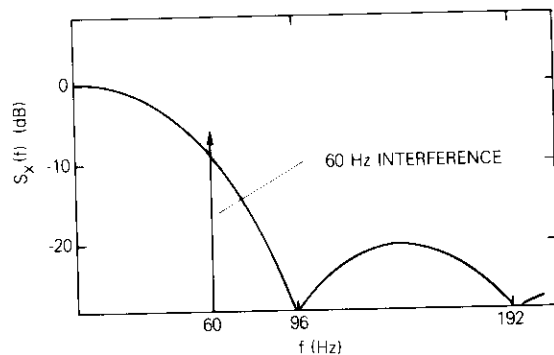


Figure 14. Baseband Spectrum of Command Link Modulation with 60-Hz Interference

spectrum of the data and interference, while the corresponding data sequence, interfering signal, and composite signal are shown in Figure 15. Since the present INTELSAT system does not specify performance

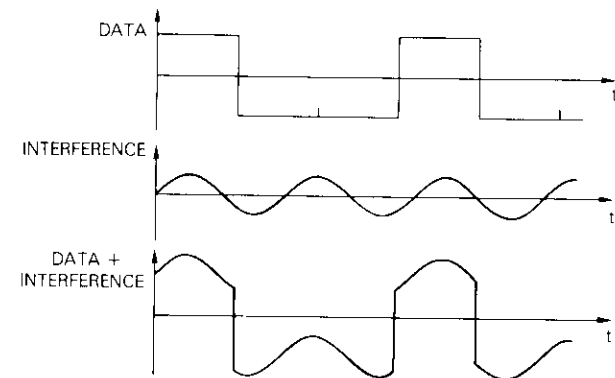


Figure 15. Command Link Data with 60-Hz Interference

below 4 kHz, tests were conducted at the Andover terminal. The results indicated that the interference levels were not high enough to impair operation.

Down-converter

The central terminal down-converter is shown in Figure 16. The 4-GHz local oscillator discussed previously mixes with the incoming signals to produce a nominal 70-MHz IF. A critical design consideration is the separation of the data, pilot, and command signals when the carrier-to-noise ratio is negative. The filter bandwidths represent a tradeoff between frequency and bandwidth, the need to preclude amplifier saturation by noise, and the need to improve the carrier-to-noise ratio as much as possible prior to PSK and pilot demodulation.

Remote data collection platform

Overall block diagram

The overall remote data collection terminal block diagram shown in Figure 17 consists of three assemblies:

- communications package,
- antenna and LNA,
- external HPA.

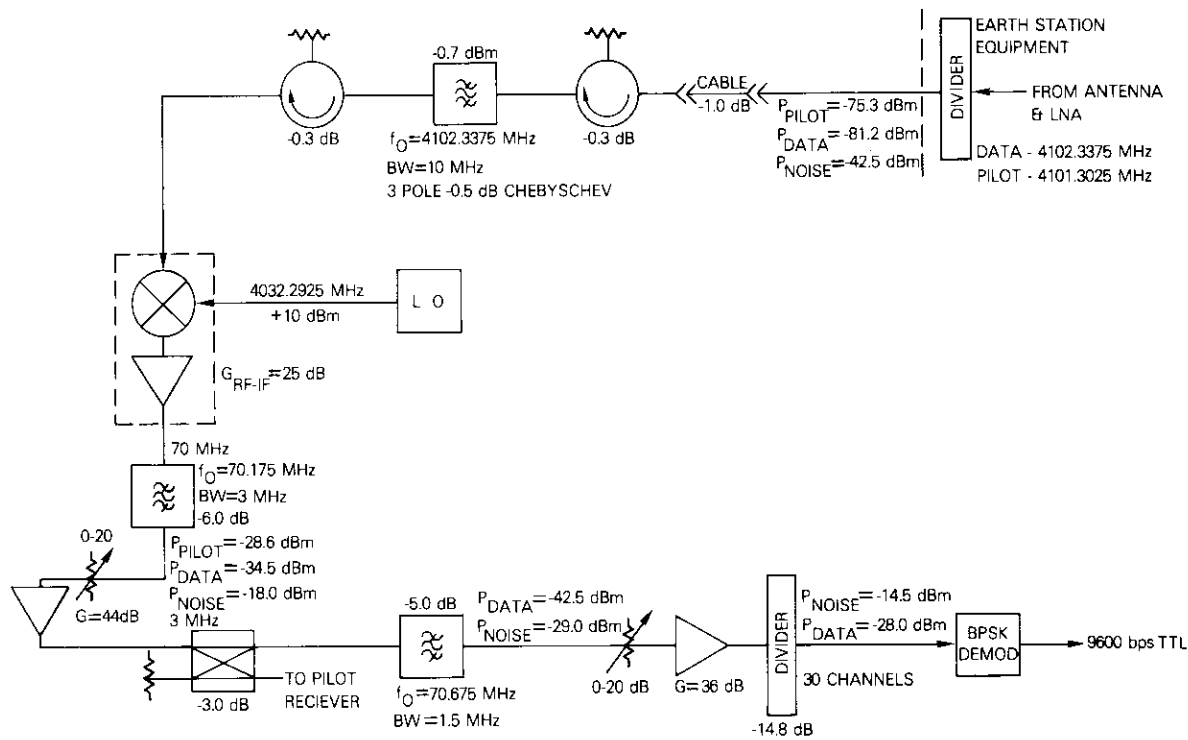


Figure 16. Central Terminal Down-Converter

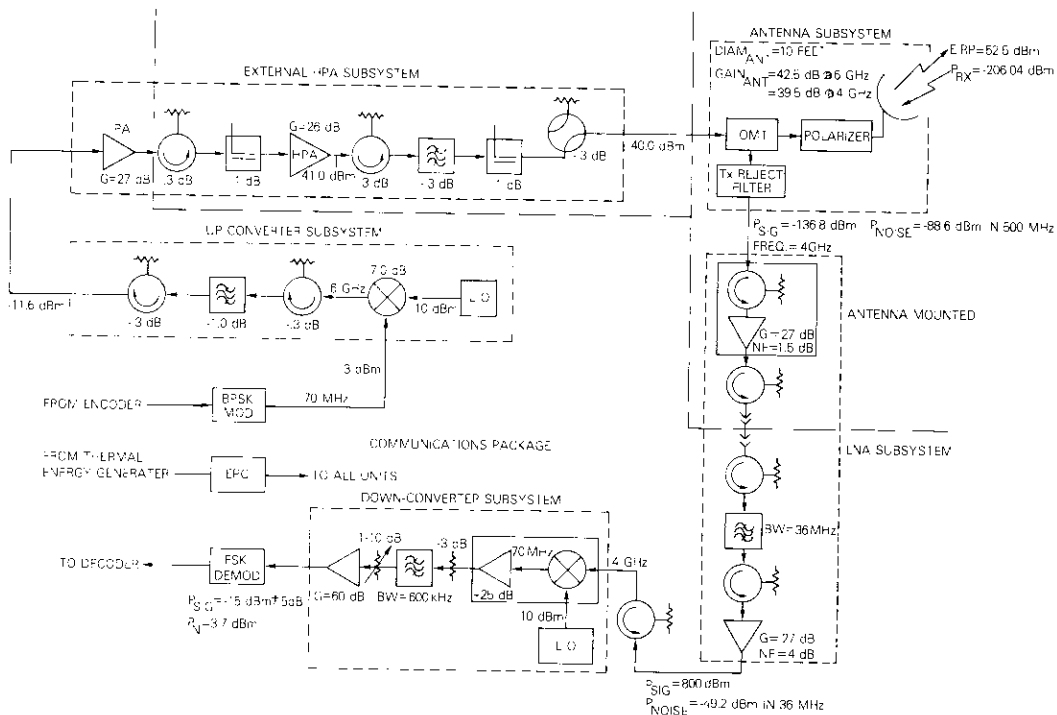


Figure 17. Remote Data Terminal Block Diagram

The LNA, feeds, and polarizer were mounted directly on the antenna. The HPA was a 10-W TWTA (Varian) powered by a thermal energy generator (TEG) separate from those used for the rest of the equipment. This TWTA was used because no comparable solid-state amplifier or other TWTA that could be mounted within the communications package was available. The rest of the equipment was mounted within the package, which was powered by an electronic power conditioner (EPC) fed by the main TEG and constrained to a maximum of 100-W prime power.

A photograph of the remote station communications package is shown in Figure 18. This package contains all of the communications equipment except for the LNA which is mounted directly on the antenna. A photograph of the antenna and its mounting is shown in Figure 19.

Command link receiver

The command link carrier is continuous phase FSK-modulated by 96-bit/s command data with a modulation index of 1.5, chosen as a result of previous experience gathered in data collection systems [6].

The demodulator choice was dictated by the large frequency uncertainties relative to the bit rate (ratios of up to 15) and the available E_b/N_0 (20 dB). Because of these factors, the implementation of a parallel filter-type demodulator is no more attractive than that of the phase-lock loop demodulator, while the latter could be used as a discriminator if the earth station oscillator stability characteristics required 2-tone FM modulation.

Figure 20 is a schematic of the demodulator. The received carrier at 70 MHz is down-converted to 30 MHz and filtered by a 7.8-kHz crystal filter; its frequency variations due to both modulation link offsets are tracked by the phase-lock loop (see Appendix), consisting of the 30-MHz VCXO, loop filter $h_L(\tau)$, and phase detector. The control voltage at the VCXO input varies in proportion to input frequency. Capacitor coupling is used between the control voltage and decision device to eliminate frequency errors due to the satellite link long-term variations.

Up-converter and HPA

Figure 21 is a block diagram of the up-converter and HPA. A 6-GHz local oscillator of the type described in the section entitled "Up-Converter and Local Oscillator Stability" was used. The HPA control circuit was modified to permit remote (central earth terminal) turn on/off.

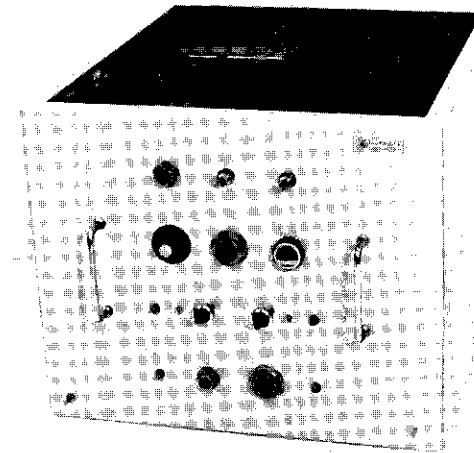


Figure 18. Remote Terminal Communications Package



Figure 19. Remote Terminal Antenna

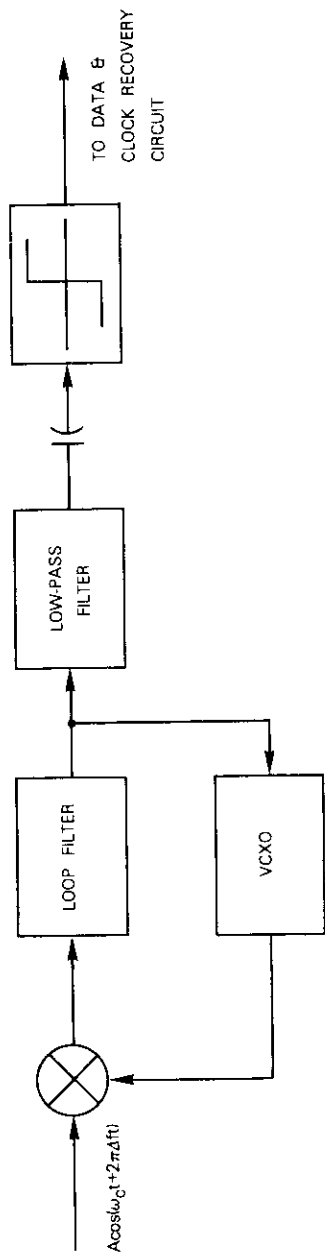


Figure 20. FSK Phase Lock Loop Demodulator

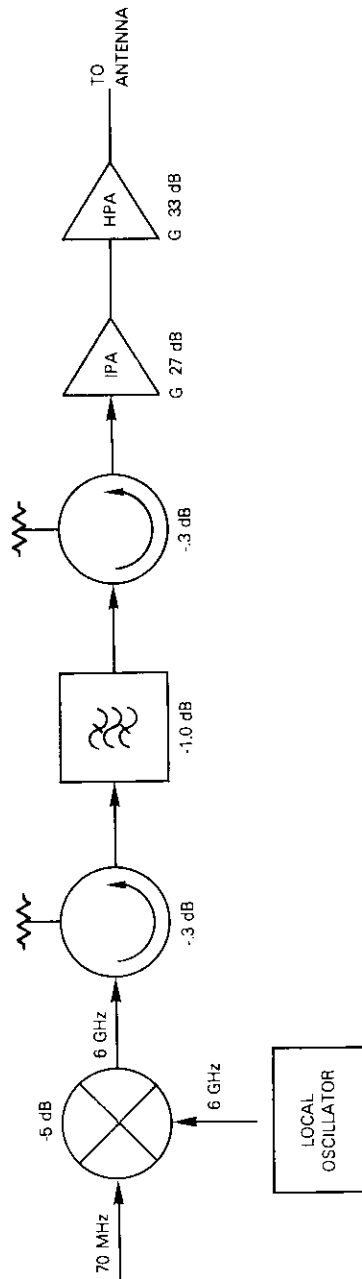


Figure 21. 6-GHz Up-Converter and HPA

Down-converter and LNA

The remote terminal down-converter and LNA are shown in Figure 22. The down-converter is similar to that used in the central terminal except that a series of power splitters is needed since it must process only the FSK command signal. In addition to the stability and phase noise problems previously discussed, the best carrier-to-noise ratio available at the input to the FSK demodulator is -20 dB, hence compounding the remote receive problem.

To achieve a reasonable system noise temperature, a field effect transistor LNA with a 1.5-dB noise figure was used. Since this rugged unit was mounted on the antenna approximately 30.5 cm from the communications package, it was limited to 27-dB gain to preclude oscillations induced by cable mismatches. In all units employed in the remote site, efforts were made to minimize prime power requirements.

Antenna and radome

Since the equipment must operate in various climates, a radome was required. The largest radome that could be used was 4.6 meters in diameter. Also, since INTELSAT IV satellites with 1° stationkeeping might eventually be used, the largest practical antenna was a 3-meter-diameter parabolic dish. The orthomode transducer, polarizer, transmit reject filter, and feed horn assembly developed at COMSAT Labs were easily adaptable to the system.

Power conditioner

The prime power for the system is provided by a thermal electric generator backed up by batteries. A power conditioner provides four regulated outputs with isolation between the prime power and equipment so that ground currents can be controlled. Reliability and low cost are of primary consideration.

Figure 23 is a block diagram of the power conditioner. The low-level switching circuit provides a square wave for driving the main switching circuit. Pre-regulation and maintenance of the low internal impedances provide sufficient regulation for the -15-V, +8-V, and internal power. Output from the +15-V supply is sensed and fed back to the pulse-width modulator. Isolation is provided by transformer coupling to all outputs.

The power conditioner, originally designed for a space application, included cooling through a cold plate; therefore, no change in cooling was required. Telemetry monitors are included.

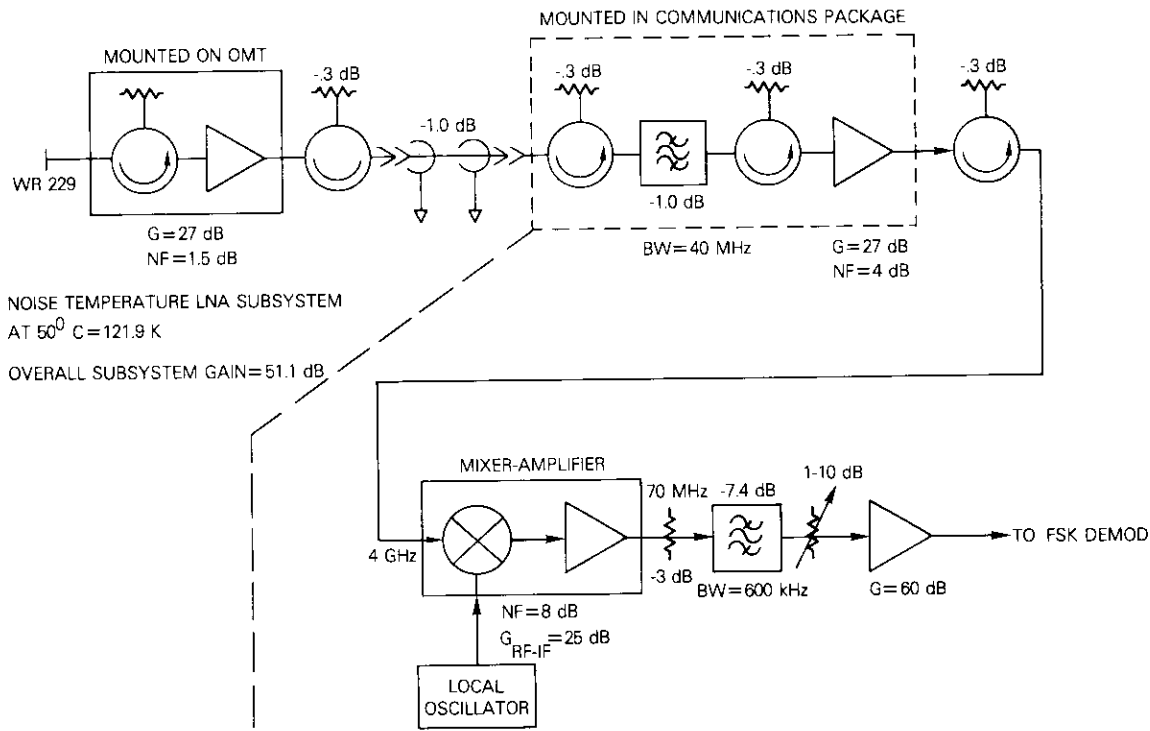


Figure 22. Down-Converter and LNA

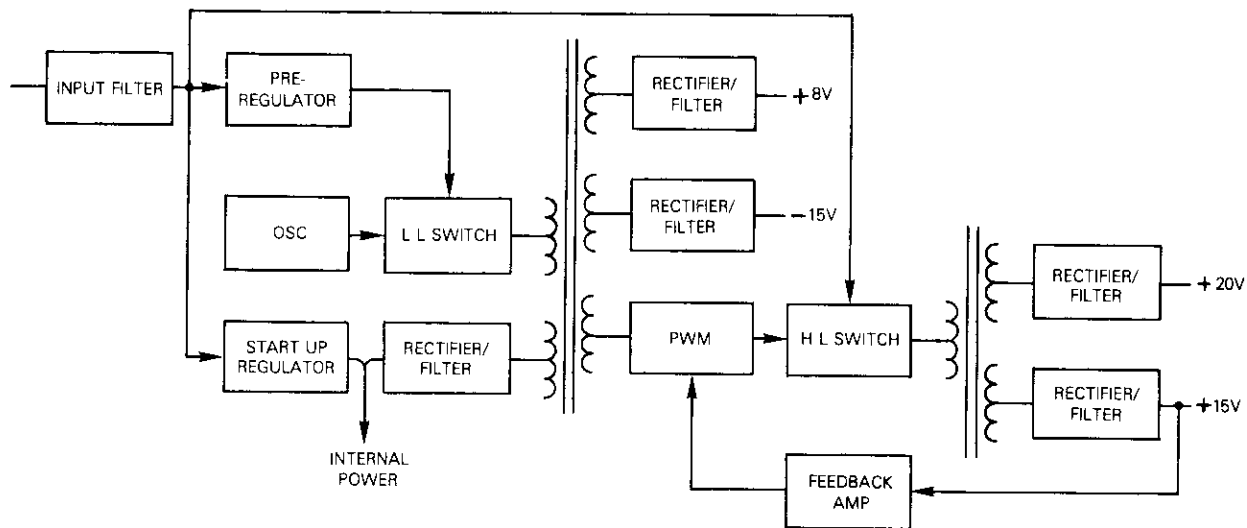


Figure 23. Power Conditioner Block Diagram

Experimental results

Data link receiver performance

The AFC loop has an IF noise bandwidth of 1,100 Hz for acquisition, which is reduced to 100 Hz for normal operation. Acquisition, which is achieved by sweeping the 65-MHz oscillator over the input frequency uncertainty range of ± 23 kHz, occurs in less than 5 seconds. The Costas loop has an IF bandwidth of 68 Hz. Acquisition by the Costas loop occurs rapidly and without sweeping because the input signal has been centered by the AFC loop.

Results of laboratory IF BER tests are shown in Figure 24, which also includes the satellite link bit-error-rate results obtained during acceptance tests of the operational equipment.

Command link demodulator performance

The measured loop characteristics of the demodulator designed for the remote station were found to be

$$\begin{aligned}\omega_n &= 794 \text{ rad/s} \\ \zeta &= 1.0 \\ 2B_L &= 998 \text{ Hz.}\end{aligned}$$

The cycle slipping rate is then (see Appendix)

$$\text{CSR} = 4.135 e^{-0.302E_b/N_0} \quad (13)$$

and the BER due to cycle slipping should be (see Appendix)

$$(\text{BER})_{cs} = 2.067 e^{-0.302E_b/N_0}$$

This rate is plotted along with the actual IF link and satellite link results in Figure 25.

THE IF link experimental results are from 0.5 to 0.8 dB worse than the theoretical bit-error rate caused by cycle slipping, which is consistent with the experimental results for cycle slipping rates discussed in the Appendix. Approximately 0.5 dB is lost over the satellite link.

Effect of modulation index

An apparent alternative to the problem of high bit-error rate as a result of cycle slipping is to reduce the modulation index with a

consequent reduction in demodulator loop bandwidth. In an experiment in which the modulation index was reduced to unity, and the loop

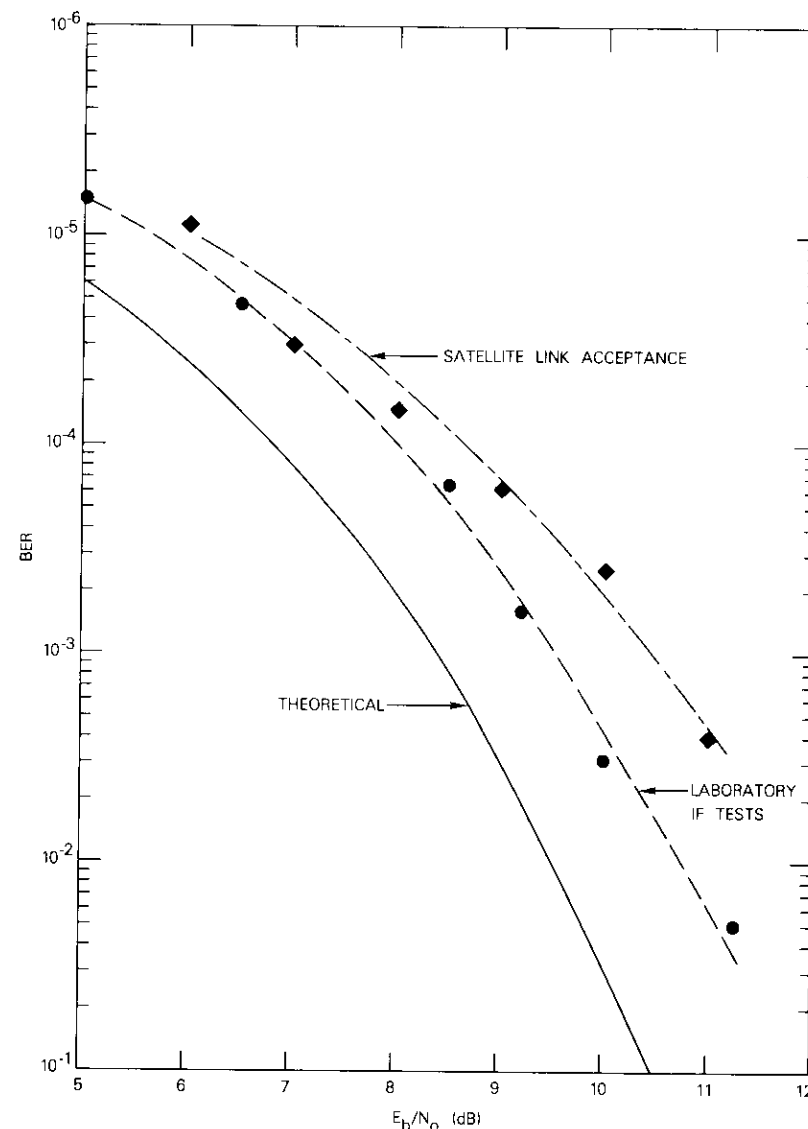


Figure 24. Data Link Receiver vs E_b/N_0

bandwidth reduced proportionately, it was found that cycle slipping was virtually eliminated. However, the reduction in signal-to-noise

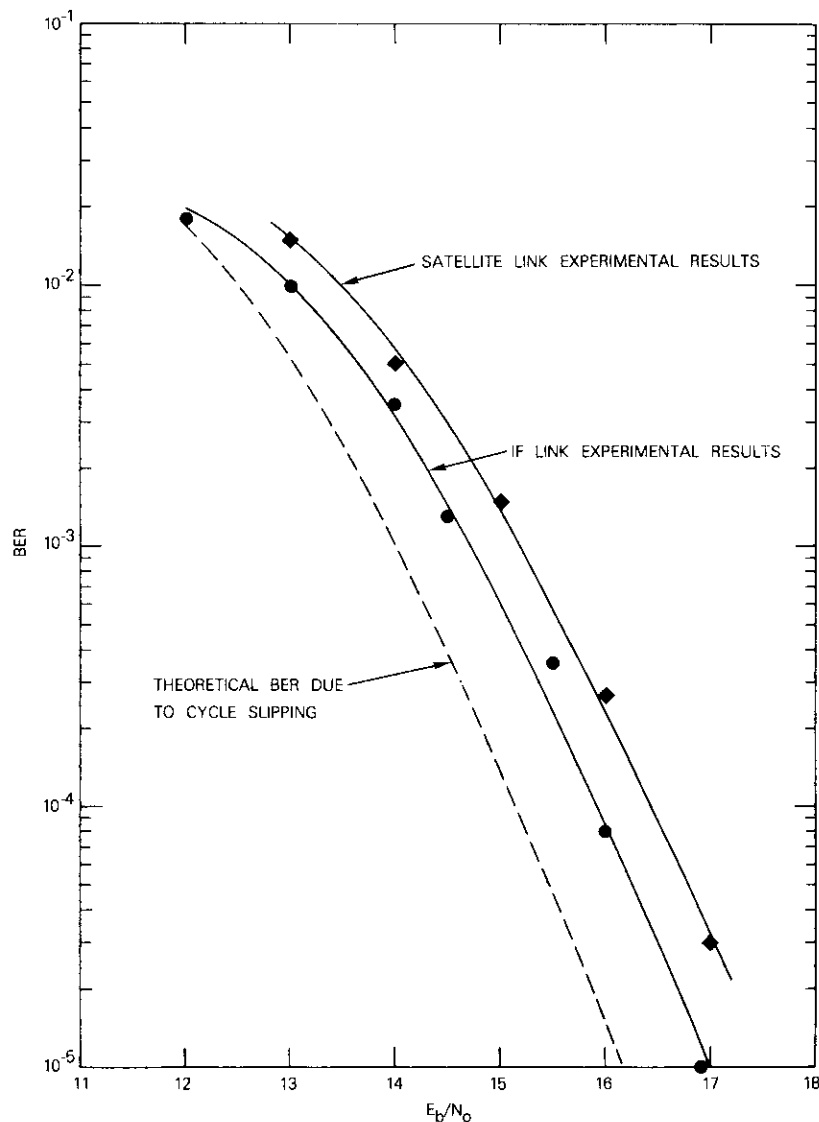


Figure 25. Command Link Demodulator BER vs E_b/N_0

ratio as a result of the reduced deviation yielded only 0.5-dB gain in bit-error-rate performance. Moreover, the signal-to-noise ratio was so sensitive to deviation at the reduced index that it was felt that maintaining the original modulation index of 1.5 would result in a more robust system.

Conclusions

The feasibility of a 2-way asymmetric communications system between a remote unattended data collection platform and a central receive terminal was demonstrated. The feasibility of low-data-rate transmissions via an INTELSAT satellite was also demonstrated, with good agreement between theory and measured data. In addition, areas of concern and possible future study were delineated.

Acknowledgments

The authors would like to acknowledge the efforts of the many people involved in bringing this program to fruition, particularly Messrs. T. P. McGarty for overall program management and many helpful technical suggestions; D. DiFonzo and R. Gruner for the antenna and feed assembly; C. Pentlicki and R. Kessler for the mechanical design; H. Flieger and G. L. Albright for the thermal analysis; J. Talcott for the reliability analysis and quality control; E. Ackermann for his efforts on the remote HPA and other RF assemblies; and R. Hefele for his work on the digital modems.

References

- [1] J. J. Spilker, Jr., *Digital Communications by Satellite*, Englewood Cliffs, NJ: Prentice-Hall, Inc., 1977, p. 387.
- [2] M. Wachs, "Short Term Frequency Stability of ATS-F Propagation Experiment Local Oscillator Source," Private Communication, June 21, 1973.
- [3] Frequency and Time Systems, data supplied for Model 1000 5-MHz oscillator.
- [4] S. Klein and L. Palmer, "A Study of Phase Skipping Phenomenon in Phase Tracking Loops Which Track QPSK Signals," DCA Contract 100-70-C-009, 10 March 1970.
- [5] S. Klein and L. Palmer, "Phase Slipping in Phase-Locked Loop Configurations that Track Biphase or Quadrature Modulated Carriers," *IEEE Transactions on Communications*, October 1972.

- [6] K. H. Greene and R. F. Hefele, "FSK Burst Receiver for Data Collection Systems," *COMSAT Technical Review*, Vol. 9, No. 2, Fall 1979.

Appendix: FSK phase-lock-loop design

PLL design

The second-order type loop must have a bandwidth which is sufficiently wide to track the frequency variations due to modulation. The phase error response of a second-order loop to a step change in frequency, $\Delta\omega$, is

$$\theta_e(\tau) = \frac{\Delta\omega}{\omega_n} \frac{e^{-\zeta\omega_n\tau}}{\sqrt{1-\zeta^2}} \sin \sqrt{1-\zeta^2} \omega_n\tau \quad (\text{A-1})$$

which has a peak value of

$$\theta_e(\tau_p) = \frac{\Delta\omega}{\omega_n} e^{-\zeta/\sqrt{1-\zeta^2} \tan^{-1}(\sqrt{1-\zeta^2}/\zeta)} \quad (\text{A-2})$$

To maintain operation in the linear region, the loop is designed so that $\theta_e(\tau_p) < 30^\circ$. The required loop bandwidth is then

$$\omega_n = \frac{\Delta\omega}{\pi/6} e^{\zeta/\sqrt{1-\zeta^2} \tan^{-1}(\sqrt{1-\zeta^2}/\zeta)} \quad (\text{A-3})$$

While this bandwidth will ensure that the loop operation is reasonably linear, it is found to be large enough so that a rather low loop signal-to-noise ratio results. Gardner [A1] provides an expression for the average rate of cycle slipping in a phase-lock loop:

$$\text{cycle slipping rate (CSR)} = \frac{\omega_n e^{-\pi(S/N)_L}}{2R} \quad (\text{A-4})$$

In a second-order loop, the loop noise bandwidth is

$$2B_L = \omega_n \left(\zeta + \frac{1}{4\zeta} \right) \quad (\text{A-5})$$

so that the loop signal-to-noise ratio is

$$(S/N)_L = \frac{E_b R}{N_0 \omega_n \left(\zeta + \frac{1}{4\zeta} \right)} \quad (\text{A-6})$$

For a loop damping factor of $\zeta = 0.707$, the expressions for ω_n and $(S/N)_L$ become

$$\omega_n = 12\Delta f e^{-\pi/4} \quad (\text{A-7})$$

and

$$(S/N)_L = \frac{E_b/N_0}{12.728 (\Delta f/R)} e^{\pi/4} \quad (\text{A-8})$$

where $\Delta f = \Delta\omega/2\pi$ and $\Delta f/R$ is the modulation index, which in this design is 1.5. The cycle slipping rate is then

$$\text{CSR} = 4.104 e^{-0.361 E_b/N_0} \quad (\text{A-9})$$

It was found experimentally that the pulse due to a cycle slip normally had a duration of the order of one bit. It will therefore cause a bit error if it is in the opposite direction from the data bit. Since cycle slipping may be in either direction with equal probability, the bit error due to cycle slipping will be one half the cycle slipping rate

$$(\text{BER})_{cs} = 2.052 e^{-0.361 E_b/N_0} \quad (\text{A-10})$$

When this value is compared with the bit-error rate due to thermal noise in a bandwidth equal to the bit, which is given by

$$\text{BER} = \frac{1}{2} e^{-E_b/2N_0} \quad (\text{A-11})$$

it is seen that errors due to thermal noise are negligible compared with those due to cycle slipping. Thus, the bit-error rate in this type of demodulator is essentially that due to cycle slipping.

Measured cycle slipping rate

During the development of the remote station modem, experimental measurements of cycle slipping rate were made on a prototype demodulator loop with a bit rate of 75 bit/s. The measured loop dynamics were

$$\omega_n = 714 \text{ rad/s}$$

$$\zeta = 0.7$$

$$2B_L = 750 \text{ Hz}$$

According to equation (A-4), the cycle slipping rate for this loop should be

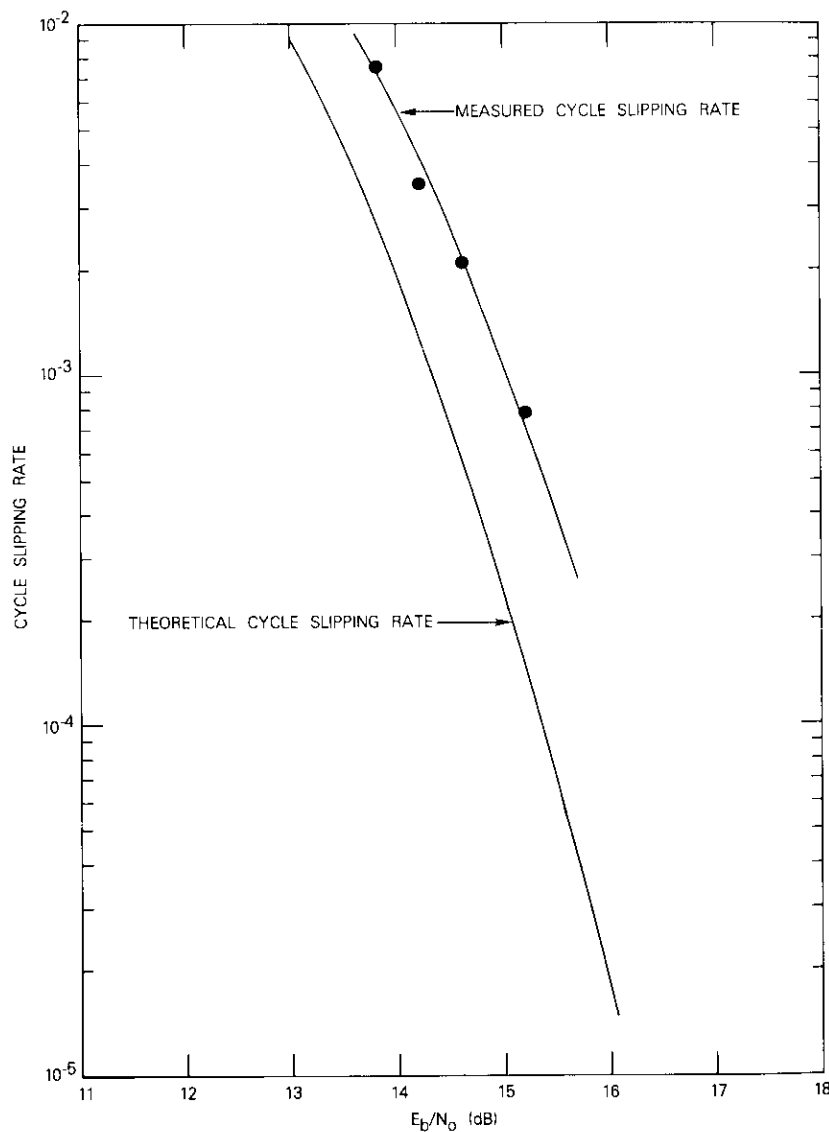


Figure A-1. Cycle Slipping Rate vs E_b/N_0

$$\text{CSR} = 4.76 e^{-0.314E_b/N_0} \quad (\text{A-12})$$

Cycle slipping rates measured on an unmodulated carrier are plotted in Figure A-1, along with the theoretical value given by equation (A-12). It is seen that the actual cycle slipping rate is approximately 0.7 dB worse than the theoretical rate.

Reference

- [A1] F. M. Gardner, *Phase Lock Techniques*, New York, NY: J. R. Wiley, Co., 1966.

Kenneth H. Greene received a B.S. from Polytechnic Institute of Brooklyn in 1959 and an M.S. and Ph.D. from the University of Connecticut in 1964 and 1969, respectively. He joined COMSAT in 1969 as a member of the Systems Simulation Laboratory participating in the simulation of the INTELSAT IV satellite system and supervising simulation of the domestic satellite system. In 1972, he joined the Modulation Techniques Department, where he supervised the field trials and operation of the shipboard terminal for the MARAD Experiment. His principal activities have involved modern development for data collection systems. Dr. Greene is presently a Staff Scientist in the Optical Communication Laboratory.



William K. Sones received a B.Sc. with honors from London University, and an M.S. and a Ph.D. with distinction from Johns Hopkins University. His professional career includes seven years at Westinghouse, Baltimore, where he participated in the design of HF, VHF, and microwave communications systems. At Johns Hopkins University five years were spent jointly as supervisor in charge of the communications and data processing group at their radiation laboratory and as professor in the school of graduate engineering, where his main interests were optimum detection and adaptive maximum likelihood techniques. In the ten years Dr. Sones has been at COMSAT Laboratories he has worked principally on earth terminal design for satellite systems. He is presently a Senior Staff Scientist.

Melvyn Grossman received a B.E.E. from the City College of New York in 1961 and an M.S. from George Washington University in 1974. Prior to joining COMSAT, he was a design engineer with the Space Communications Laboratory, ITT Defense Communications Division, Nutley, New Jersey, where he engaged in PLL and FMFB receiver design. He joined the Microwave Laboratory of COMSAT Laboratories in 1969 and engaged in the design of low-noise amplifiers, FDM/FM modulators, and threshold extension receivers for earth terminal use.



Mr. Grossman is presently involved in the study of nonlinear effects on digital transmission via satellite.

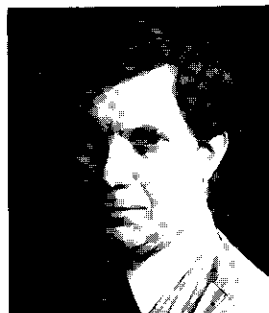
He is a member of the IEEE.



Milton E. Jones received a B.S.E.E. in 1951 and an M.S.E.E. in 1956 from Newark College of Engineering (now New Jersey Institute of Technology). He worked for International Telephone and Telegraph Federal Laboratories where he was involved in missile guidance communications systems. While employed by Computer Sciences Corporation, he performed system studies for the U.S. Defense Satellite Communication System development. In 1975 he joined COMSAT Laboratories as a member of the Systems Applications and

Simulation department where he has been engaged principally in hardware simulation studies for the evaluation of satellite link transmission impairments. He is a member of IEEE and Tau Beta Pi.

Nelson M. Jacobus attended the School of Engineering at Purdue University. Prior to joining COMSAT in 1974, he was a technical instructor for RCA, the range technical contractor at the Atlantic Missile Range. Earlier, he designed the power supply and control circuitry high-frequency back scatter transmitters for ITT Electro-physics Laboratories. He is currently a Member of the Technical Staff of the Spacecraft Laboratory at COMSAT Laboratories, involved with both ground-based and spacecraft power conditions.



Mr. Jacobus holds four patents in the power supply area.

CTR Notes

A model for calculation of rain-induced cross-polarization discrimination at 6/4 GHz

D.J. KENNEDY

Introduction

This note presents a semiempirical model for the calculation of circular cross-polarization discrimination at 6/4 GHz for earth-space propagation paths as a function of climate and elevation angle. For comparison with measurement results and other models, a simple benchmark model is provided that includes only fairly well accepted concepts, principally from the C.C.I.R., for each of the major areas of rain rate distribution, effective path length, and differential phase shift. Each of these areas is compartmentalized to easily accommodate future improvements. The restriction of the model to 4 and 6 GHz reflects the assumption that differential attenuation effects are small compared with those of phase. This restriction could be lifted with some penalty in complexity. The calculational model is sufficiently simple to be programmed for a small personal electronic calculator. Some typical results based on the model are included.

Overview of calculational procedure

The objective of the model is to predict, with a minimum essential set of inputs, the circularly polarized cross-polarization discrimination occurrence distribution for radiowave propagation on slant paths at 4 and 6 GHz at any world-wide location. The available information must include some characteristics of the local rainfall and path geometry. In this note, the two parameters (M and β) of the Rice-Holmberg [1] distribution are used to characterize the distribution of rain rates. The

David J. Kennedy is a member of the technical staff of INTELSAT and a former member of the technical staff in the Transmission Systems Laboratory of COMSAT Laboratories.

third parameter necessary is the path elevation angle, ϵ , which impacts both the effective path length through the rainfall and the cross-sectional shape which individual raindrops present to the impinging radiation. This latter factor significantly affects the observed differential phase shift.

For a given occurrence level, p (given in percent), a knowledge of M and β allows a determination of the rain rate R that is exceeded p percent of the time. In turn, the rain rate and elevation angle determine an effective path length L over which rain is assumed to fall at a uniform rate R . The rate and path elevation angle also determine the differential phase shift per unit path length, ϕ_s . From the combination of effective path length with specific differential phase shift, the cross-polarization discrimination for circular polarization may be calculated [2]:

$$XPD = -20 \log_{10} \left(\tan \frac{\phi}{2} \right) \text{ dB} \quad (1)$$

where $\phi = \phi_s L$.

Rain rate distribution

The rain rate distribution can often be well modeled by the Rice-Holmberg distribution [1]. Figure 1 is an example of the comparison between a measured and a Rice-Holmberg distribution for data collected at Lario, Italy [2]. M is the total mean annual rainfall in millimeters and β is the ratio of thunderstorm ("Mode 1") rain accumulation to total rain accumulation. Usually M can be determined from climatological data for the earth station location. Generally β is more difficult to estimate if rain rate data are unavailable and it is often necessary to rely on the world-wide contour map of β [1]. In such cases, it is good practice to bracket the estimates thus obtained by adjoining β values.

The Rice-Holmberg distribution is given by a sum of three exponentials, each being the predominant component in a different range of R :

$$p(R) = ae^{-0.03R} + be^{-0.258R} + ce^{-1.63R} \quad (2)$$

where

$$a = \frac{0.03 M \beta}{87.66} = \frac{M \beta}{2922} \quad (3)$$

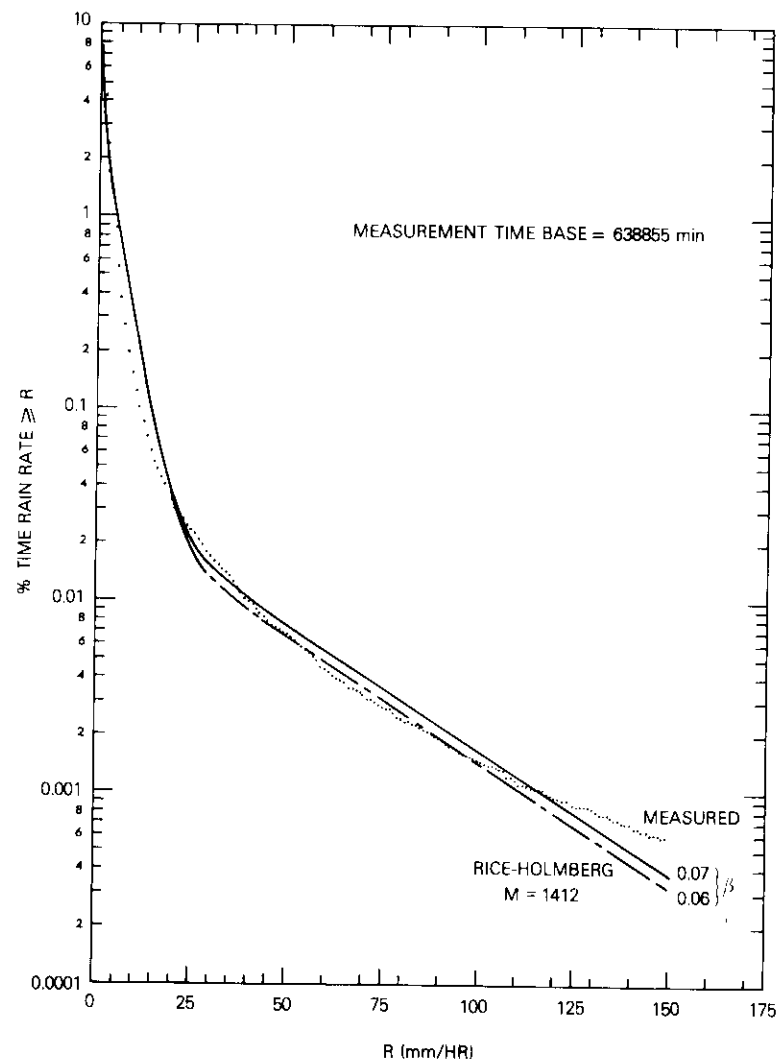


Figure 1. Rice-Holmberg Rain Distributions

$$b = \frac{0.2 M(1 - \beta)}{87.66} = \frac{M(1 - \beta)}{438.3} \quad (4)$$

$$c = 1.86b = \frac{0.372 M(1 - \beta)}{87.66} \quad (5)$$

The rain rate R is exceeded p percent of the year. Further calculation requires the inverse of the Rice-Holmberg distribution with an adequate match determined to be

$$R(p) = 11.37 \ln \left[\left(\frac{a}{p} \right)^{2.93} + \left(\frac{b}{p} \right)^{0.341} + 0.1 \left(\frac{c}{p} \right)^{0.054} \right] \text{ mm/hr} \quad (6)$$

In general, equations (2) and (6) vary less than 1 mm/hr for the same percentage of time. Near the point of inflection, the error increases to just over 2 mm/hr. Such errors are generally inconsequential for the rain rates under consideration.

Effective path length

Effective path length is a physically fictitious quantity which nevertheless has strong intuitive appeal. At a given rain rate and path elevation angle, it is the distance along which a uniform rain rate R must be assumed in order to yield a net path effect in agreement with observations. The rain rate R is taken to be that measured at a single surface point rain gauge near the terrestrial terminal of the path.

For attenuation measurements, an effective path length is thus defined as

$$L(p) = \frac{A(p)}{A_s[R(p)]} \text{ km} \quad (7)$$

where A is the attenuation exceeded p percent of the time and A_s is the specific attenuation for a rain rate R (which is exceeded p percent of the time). Alternatively, for depolarization at 4 and 6 GHz, an effective path length may be defined as

$$L(p) = \frac{\phi(p)}{\phi_s[R(p)]} \text{ km} \quad (8)$$

where ϕ is the observed differential phase shift exceeded p percent of the time and ϕ_s is the specific differential phase shift for a rain rate R . When both depolarization and attenuation are measured, the experimentally derived values for effective path length from equations (7)

and (8) in general will not agree. Some measurements have indicated that the values of effective path derived from attenuation measurements exceed those from the differential phase [3]; others demonstrate the reverse [2]. For this note, the path lengths from C.C.I.R. [4] will be adopted; however, future models will seek to refine this important area.

The assumed effective path lengths are of the form

$$L(R, \epsilon) = [7.413 \times 10^{-3} R^{0.766} + (0.2323 - 1.803 \times 10^{-4} R) \sin \epsilon]^{-1} \text{ km} \quad (9)$$

for a rain rate R and path elevation angle ϵ . It is noted that the functional dependence of L upon elevation angle is not simply $\csc \epsilon$. Figure 2 shows this relationship for L as a function of rain rate with elevation angle as a parameter.

Specific differential phase shift

Rain-induced depolarization is produced by the nonsphericity of falling raindrops. For linearly polarized waves, depolarization is also caused by the nonspherical drops being canted or tilted with respect to the polarization direction. For circular polarization, only the raindrop shape and the distribution of the canting angles are important. The absolute canting angle is immaterial, although it will affect the tilt angle of the received polarization ellipse. At 4 and 6 GHz, the principal depolarization mechanism is the differential phase shift experienced between the field components with polarization aligned with the major and minor axes of the approximately oblate spheroidal drops. At higher frequencies, above 10 GHz, differential attenuation effects become more important and ultimately predominate.

Although the depolarization for circular polarization is affected by the canting angle distribution, the error caused by assuming that all drops are equi-oriented is small for the modest standard deviation ($\sim 10^\circ$) normally observed. This assumption is conservative because it overestimates the depolarization effect; that is, the cross-polarization discrimination calculated assuming all drops are equi-oriented will be lower than if a distribution with non-zero variance is assumed. In this note, an equi-canting angle model is adopted with the differential phase shift given by the results of Oguchi [5] and shown in Figure 3. These 4- and 6-GHz curves are for an elevation angle of 0° . For other elevation angles, the depolarization effect is reduced since the drops

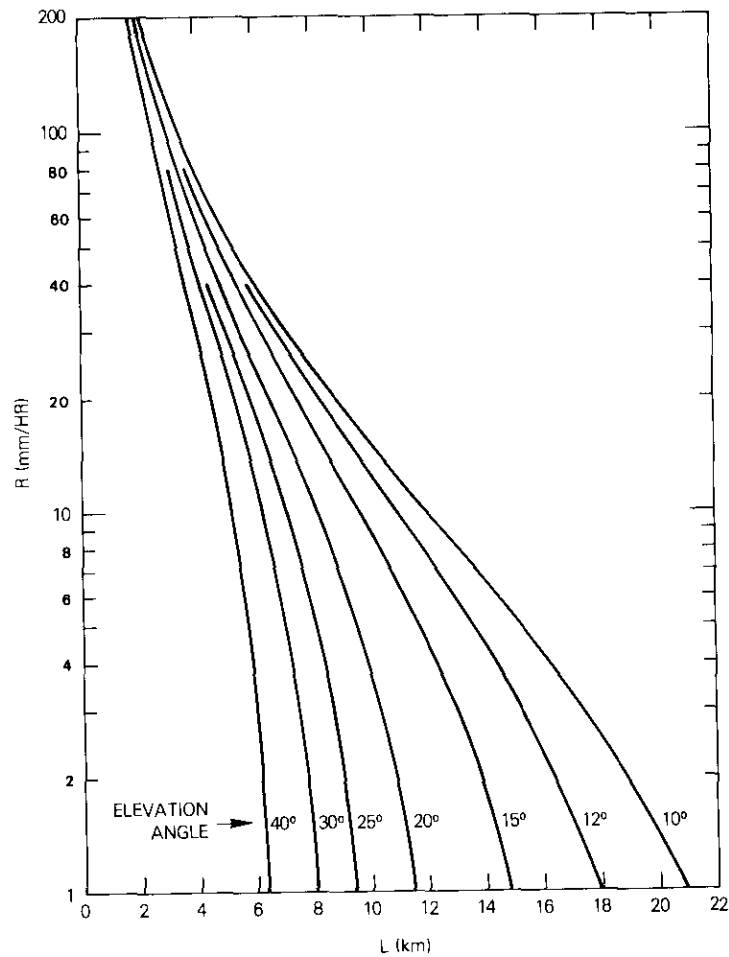


Figure 2. Effective Path Lengths

present a more nearly spheroidal shape. It can be shown [6] that approximately

$$\phi_s(\epsilon) = \phi_s(0) \cos^2 \epsilon \quad (10)$$

In the calculator procedure, ϕ_s for a zero elevation angle is input with an internally applied correction for a non-zero elevation angle.

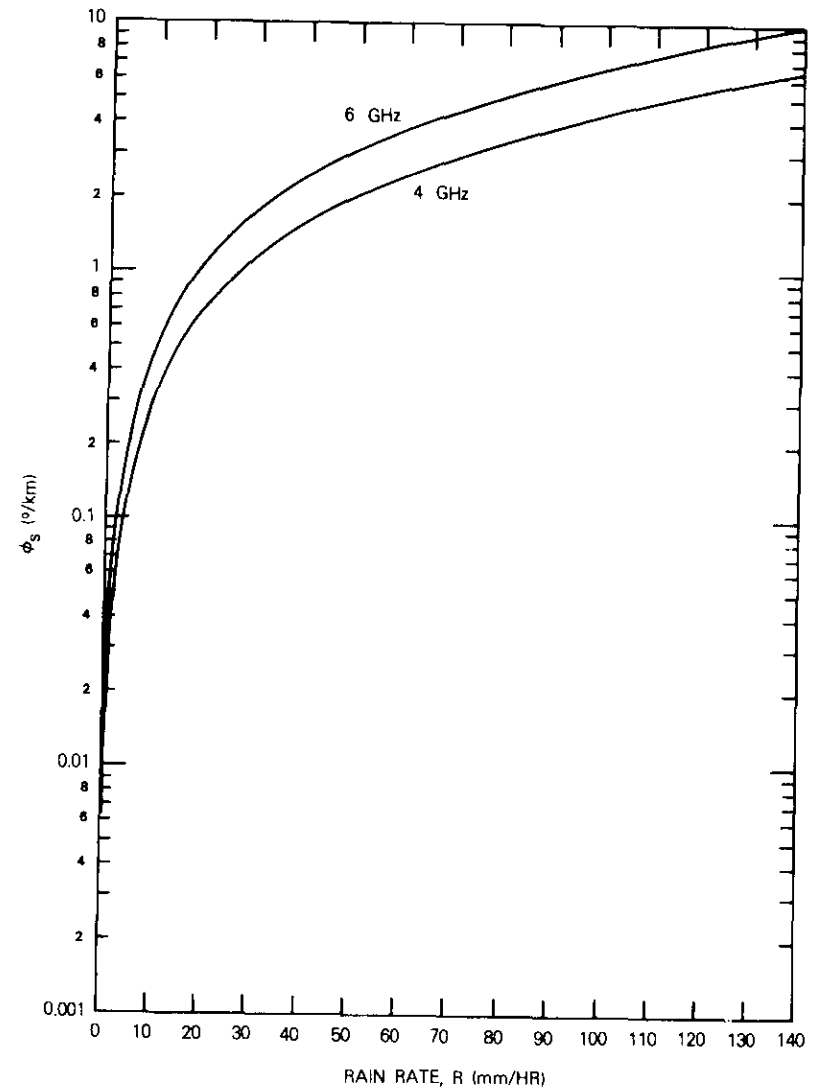


Figure 3. Specific Differential Phase Shifts at 4 and 6 GHz

Calculator program

A review of this computational approach (the relationships given for the inverse Rice-Holmberg distribution, the effective path length, and

the elevation angle dependence of ϕ_s) evidences that the procedure is sufficiently compact for application to programmable electronic calculators. This has been accomplished for Hewlett Packard HP-67 and Texas Instruments SR-52 calculators, and the resulting programs are available to interested readers.

Typical results

The application of this procedure is illustrated in Figure 4 which shows cross-polarization discrimination calculations for 4 GHz at $p = 0.01$ percent for several combinations of M and β . These vary from a worst case (M, β) of (3000 mm, 0.5) to a minimum effect case of (500 mm, 0.1). The results are plotted as a function of the elevation angle, and the marked dependence is apparent. Similarly, other families of curves can be generated for 6 GHz and for other occurrence levels. In the usual application to a particular site, M, β and ϵ will be established and the results calculated as a function of p . An example at 4 GHz for the hypothetical case in which $M = 2000, \beta = 0.1, 0.15, \text{ and } 0.2$, and $\epsilon = 25^\circ$ is shown in Figure 5.

Conclusions

A simple model has been presented for rapidly estimating the circularly polarized cross-polarization discrimination for a given occurrence probability, a Rice-Holmberg rain distribution of specified M and β , and a given elevation angle. The inverse relationship for the Rice-Holmberg distribution [equation (6)] may be useful and also serve as a starting point for rapid convergence in iterative solutions to $p(R)$.

References

- [1] P. L. Rice and N. R. Holmberg, "Cumulative Time Statistics of Surface Point-Rainfall Rates," *IEEE Transactions on Communications*, COM-21, No. 10, October 1973.
- [2] D. J. Kennedy, "Rain Depolarization Measurements at 4 GHz," *COMSAT Technical Review*, Vol. 9, No. 2, Fall 1979, pp. 629-668.
- [3] M. Yamada et al., "Rain Depolarization Measurement by Using INTEL-SAT-IV Satellite in 4-GHz Band at a Low Elevation Angle," Proceedings of URSI Committee F, La Baule, France, April 1977.
- [4] International Radio Consultative Committee (C.C.I.R.), XIVth Plenary Assembly, Kyoto, 1978, Doc. 5/1049-E, December 1977. The analytic form is from C.C.I.R. Doc. 5/(Can 4, 15 April 1977).

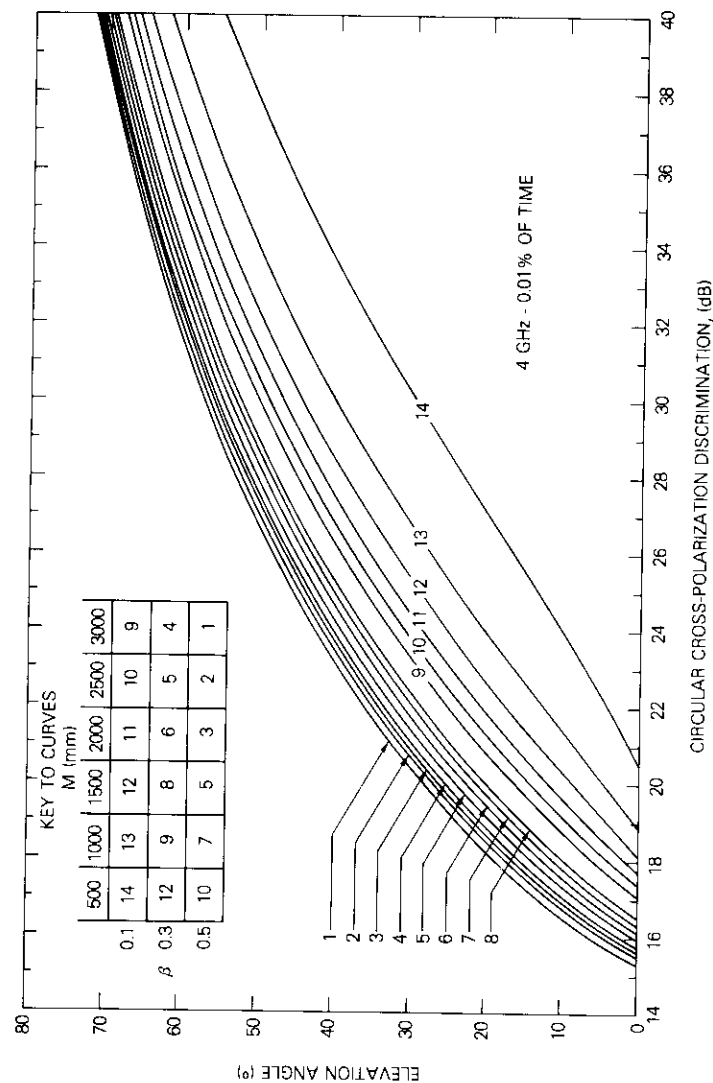


Figure 4. Typical Results for 4 GHz at 0.01 Percent

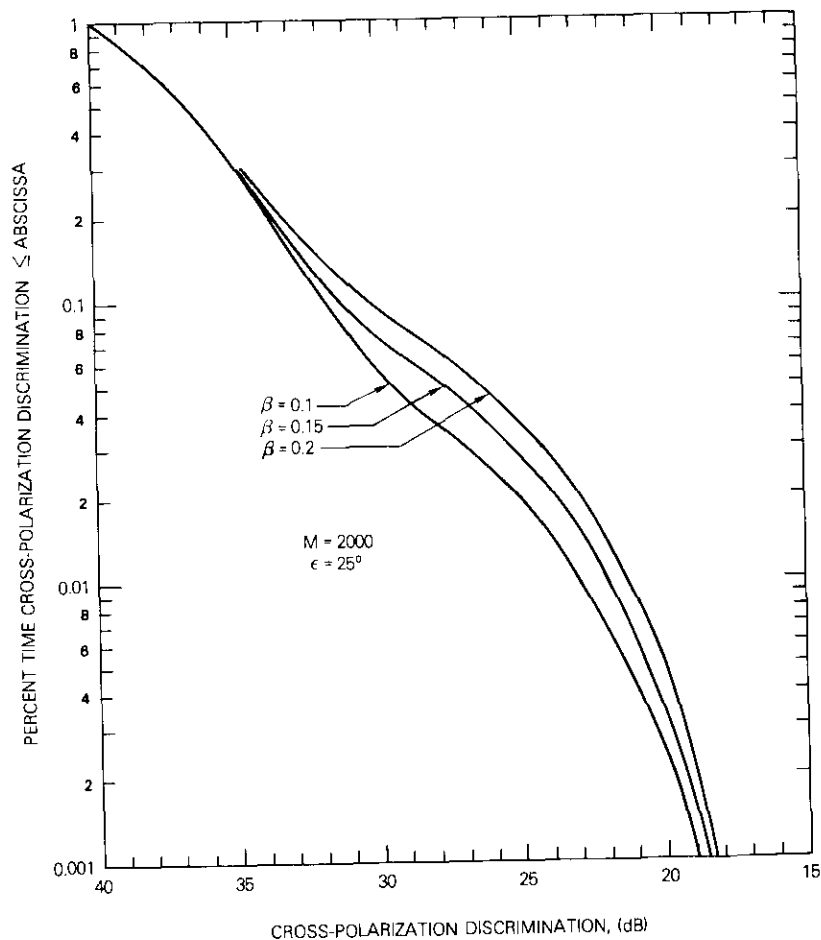


Figure 5. Results for $M = 2000$ mm, $\beta = 0.1, 0.15, 0.2$, and $\epsilon = 25^\circ$

- [5] T. Oguchi, "Rain Depolarization Studies at Centimeter and Millimeter Wavelengths: Theory and Measurement," *Journal of the Radio Research Laboratory (Japan)*, Vol. 22, No. 107, pp. 165-211. Differential phase-shift and amplitude coefficients by private communication.
- [6] N. K. Uzunoglu, B. G. Evans, and A. R. Holt, "Scattering of Electromagnetic Radiation by Precipitation Particles and Propagation Characteristics of Terrestrial and Space Communication Systems," *Proc. IEE*, Vol. 124, No. 5, May 1977.

Geosynchronous Satellite Log for 1980

WALTER L. MORGAN

(Manuscript received January 16, 1980)

In the two years since the last Geosynchronous Satellite Log was published [1], several additional satellite missions have been announced. Growth is particularly evident in the direct broadcast satellites and domestic systems operating in the 11-, 12-, and 14-GHz bands. The number of multiple-mission satellites is also increasing. Examples of these are INSAT, ARABSAT, GORIZONT, and the combination of STATIONAR-5 and LOUTCH-2.

In 1970, there were approximately 92 active and future entries [2]. By 1978 [1], this number had increased to about 140. Tables 1, 2, and 3 are representative of the situation today; they contain over 280 active, future, and inactive entries. Additional pieces may be present, but the locations are unknown. Figure 1 shows the number of satellites in the geosynchronous orbit vs time. As of January 1, 1980, there were approximately 80 operational geosynchronous satellites (over 80 percent primarily intended for communications).

The information reported in this log has been obtained from a wide variety of public and private sources, and has been cross-checked as much as possible. Information on contemporary launches may often be found in *Spaceflight*, the ITU's *Telecommunication Journal*, the *NASA Satellite Situation Report*, and a United Nations' document [3].

Table 1 gives detailed geosynchronous satellite data. The first column gives the longitude in degrees East up to 180° , and beyond that in degrees East and West. The longitudinal values are nominal with tolerances up to 1° or more. The satellite positions are affected by orbital perturbations due to the earth, moon, and sun. They are also subject to relocation to satisfy specific system traffic requirements and changes.

Walter L. Morgan is a Senior Staff Scientist on the Project Staff at COMSAT Laboratories.

Column 2 shows the year of launch (or anticipated launch), and Column 3 the nominal satellite lifetime based on predictions at the time of launch. Although there may be substantial variations, the combination of launch date and nominal lifetime indicates when a replacement satellite must be launched.

The fourth column provides the satellite name. For given families (networks), the names of individual satellites are indented. Column 5 identifies the sponsoring organization, and Column 6 gives the function. In a few instances, satellites are owned by one entity and commanded by another.

The frequency bands are shown in the last column with the numbers before the slash mark designating the earth-to-space (up-link) frequencies followed by the space-to-earth (down-link) frequencies.

Satellites for which locations have not been determined are listed in Table 3. Many of these have completed their missions and expended the stationkeeping propellant. They will drift back and forth across the orbit with the amplitude of the oscillation determined by the position at which control ceased (e.g., if abandoned at one of the stable points, 79E and 255E or 105W, there would be no drift). INTELSAT has recently used the remaining fuel in INTELSAT III F-3 to propel it into a higher orbit; thus this satellite is not included in this log.

References

- [1] W. L. Morgan, "Geosynchronous Satellite Log," *COMSAT Technical Review*, Vol. 8, No. 1, Spring 1978, pp. 219-237.
- [2] W. L. Morgan, "Satellite Utilization of the Geostationary Orbit," *COMSAT Technical Review*, Vol. 6, No. 1, Spring 1976, pp. 195-205.
- [3] Committee on the Peaceful Uses of Outer Space, "Physical Nature and Technical Attributes of the Geostationary Orbit," United Nations Document A/AC.105/203/Add. 3, May 22, 1979.

TABLE I. GEOSYNCHRONOUS SATELLITE DATA

Longitude	Launch Date	Life (yr)	Satellite Name	Sponsor	Function	Up/Down-Link Frequency (GHz)
0E	1977		Meteosat 1	European Space Agency	Meteorological	0.148,0.402, 2.1/0.137, 0.468,1.7
0E	1980		Meteosat 2	European Space Agency	Meteorological	0.148,0.402, 2.1/0.137, 0.468,1.7
0E	1983		Nordsat	Nordic Nations	Regional	14/12
0E	1983		EBS (European Broadcasting Satellite)	European Broadcasting Union	Direct Broadcast	14/11
0E-29E ^b	1978		GEOS-2	European Space Agency	Experimental	0.149/ 0.137,2.3
10E	1978	5	OTS-2 (Orbital Test Satellite)	European Space Agency	Experimental	0.149,14/ 0.138,1.1
10E ^c	1983	7	ECS-1 (European Communications Satellite)	European Conference of Post & Telecommunications Administrations (CEPT)	Regional	14/11
10E ^c	1982	7	ECS-2 (spare)	European Conference of Post & Telecommunications Administrations (CEPT)	Regional	14/11
15E	1983	7	Arabsat	Arab Satellite Communications Organization	Regional Direct Broadcast	6/4 6/2.5
20E	1982	7	Arabsat	Arab Satellite Communications Organization	Regional Direct Broadcast	6/4 6/2.5

TABLE I. GEOSYNCHRONOUS SATELLITE DATA (continued)

Longi- tude	Launch Date	Life (yr)	Satellite Name	Sponsor	Function	Up/Down-Link Frequency (GHz)
26E			Zohreh-2	Telecommunications Company of Iran	Domestic	14/11,12
34E			Zohreh-1	Telecommunications Company of Iran	Domestic Direct Broadcast	14/11
35E			Statsionar-2 Network (uses Raduga)	Ministry of Posts & Telecommunications (USSR)	Domestic	6/4
35E	1977		Raduga-3 ^e	Ministry of Posts & Telecommunications (USSR)	Domestic	6/4
35E	1978		Raduga-4 ^e	Ministry of Posts & Telecommunications (USSR)	Domestic	6/4
40E	1980	5	Marecs-A	European Space Agency	Maritime ^f	1.6,6/ 1.5,4
44E	1975		Cosmos-777	USSR		Inactive
45E	9		Gals-2	Ministry of Posts & Telecommunications (USSR)	Government	8/7
45E	1980		Volna-3	Ministry of Posts & Telecommunications (USSR)	Land Aeronautical Maritime	0.3-0.4/0.2-0.3 1.6/1.5 1.6/1.5
45E	1980		Statsionar-9 Network	Ministry of Posts & Telecommunications (USSR)	Domestic	6/4

45E	1981		Loutch-p ^{2h}	Ministry of Posts & Telecommunications (USSR)	Domestic	14/11
47E			Zohreh-3	Telecommunications Company of Iran	Domestic	14/11
49E	1974	5	Symphonie-1	France & Federal Republic of Germany	Experimental	6/4
53E			Statsionar-5 Network (uses Ekran & Gorizont)	Ministry of Posts & Telecommunications (USSR)	Direct Broadcast Domestic Government	6.2/0.714 6/4 8/7
53E	1979		Ekran-3 ⁱ	Ministry of Posts & Telecommunications (USSR)	Direct Broadcast	6.2/0.714
53E	1979		Ekran-4 ⁱ	Ministry of Posts & Telecommunications (USSR)	Direct Broadcast	6.2/0.714
53E	1979		Gorizont-3 ^j	USSR	Domestic Government	6/4 8/7
53.0E	1981		Loutch-2 ^{h,k}	Ministry of Posts & Telecommunications (USSR)	Domestic	14/11
54E ^c	1973	5	DSCS-2 F4 (Defense Satellite Communica- tions System II)	DOD (USA)	Government	2,8/2,7
54E ^c	1983	10	DSCS-III (Defense Satellite Communica- tions System III)	DOD (USA)	Government	2,8/2,7
55.5E			Later Loutch-2 ^h	Ministry of Posts & Telecommunications (USSR)	Domestic	14/11

TABLE I. GEOSYNCHRONOUS SATELLITE DATA (continued)

Longitude	Launch Date	Life (yr)	Satellite Name	Sponsor	Function	Up/Down-Link Frequency (GHz)
57.0E			INTELSAT Indian Ocean Network (spare & lease)	INTELSAT	International Maritime ^f	6,14/4,11 1.6/1.5
57.0E	1972	7	INTELSAT IV F-5 (spare)	INTELSAT	International	6/4
58.0E			Volna-4	Ministry of Posts & Telecommunications (USSR)	Aeronautical Maritime ^f	1.6/1.5 1.6/1.5
60.0E			INTELSAT Indian Ocean 2 Network (spare & major path)	INTELSAT	International Maritime ^f	6,14/4,11 1.6/1.5
60.2E	1978	7	INTELSAT IV-A F-3	INTELSAT	International	6/4
63.0E			INTELSAT Indian Ocean 1 Network (primary)	INTELSAT	International Maritime ^f	6,14/4,11 1.6/1.5
62.9E	1978	7	INTELSAT IV-A F-6	INTELSAT	International	6/4
65E	1984		PRC-1	Radio Management Bureau (Peoples Republic of China)	Domestic Direct Broadcast	6/4 17/12
66.0E			INTELSAT Indian Ocean (spare)	INTELSAT	International Maritime ^f	6,14/4,11 1.6/1.5
70E	1980		GOMS (Geostationary Operational Meteorological Sputnik)	USSR	Meteorological	λ

70E ^c	1981		STW-2	Radio Management Bureau (Peoples Republic of China)	Experimental	6/4
73E	1976	5	Marisat Indian Ocean	COMSAT General Corporation (USA)	Maritime	0.3-0.312,1.6, 6/0,248-0.26, 1.5,4
74.0E	1981	7	Insat-1A (Indian National Satellite)	Indian Space Research Organization (India)	Domestic Direct Broadcast Meteorological	6/4 6/2.5 0.46/4
75E ^c	1980	5	Fltsatcom-2 Indian Ocean	DOD (USA)	Government	0.29-0.32,1.8, 8/0.24-0.27, 2.2,7
75E ^c			Leasat Indian Ocean	DOD (USA)	Government	0.24-0.40,8/7
77.0E	1977	7	Palapa-A2	Perumtel (Indonesia)	Domestic	6/4
80E			Stasionar-1 Network (uses Raduga)	Ministry of Posts & Telecommunications (USSR)	Domestic	6/4
80E	1975		Raduga-1 ^e	Ministry of Posts & Telecommunications (USSR)	Domestic	6/4
80E	1979		Raduga-5 ^e	Ministry of Posts & Telecommunications (USSR)	Domestic	6/4
80E	1984		PRC-2	Radio Management Bureau (Peoples Republic of China)	Domestic Direct Broadcast	6/4 17/12
83.0E	1976	7	Palapa-A1	Perumtel (Indonesia)	Domestic	6/4

TABLE I. GEOSYNCHRONOUS SATELLITE DATA (continued)

Longitude	Launch Date	Life (yr)	Satellite Name	Sponsor	Function	Up/Down-Link Frequency (GHz)
85.0E	1980		Volna-5	Ministry of Posts & Telecommunications (USSR)	Land Aeronautical	0.3-0.4/ 0.2-0.3 1.6/1.5
85E			Stasionar-3 Network (uses Raduga)	Ministry of Posts & Telecommunications (USSR)	Domestic	6/4
85E	1976		Raduga-2 ^e	Ministry of Posts & Telecommunications (USSR)	Domestic	6/4
85.0E	9		Gals-3	Ministry of Posts & Telecommunications (USSR)	Government	8/7
85.0E	1980-81		Loutch-P3	Ministry of Posts & Telecommunications (USSR)	Domestic	14/11
90E ^c	1974		Molniya-1S (Raduga prototype)	Ministry of Posts & Telecommunications (USSR)	Experimental	Inactive
90E	1979-80		Stasionar-6 Network	Ministry of Posts & Telecommunications (USSR)	Domestic Direct Broadcast	6/4 6/4
90.0E	1981		Loutch-3 ^h	Ministry of Posts & Telecommunications (USSR)	Domestic	14/11
90E	1984		PRC-3	Radio Management Bureau (Peoples Republic of China)	Domestic	6,14/4,12

94E	1982	7	Insat-1B (Indian National Satellite) (standby)	Indian Space Research Organization (India)	Domestic Direct Broadcast Meteorological	6/4 6/2.5 0.46/4
98E ^m		7		Ministry of Posts & Telecommunications (Australia)	Domestic Direct Broadcast	? 14/12
99E			Stasionar-T Network (uses Ekran)	Ministry of Posts & Telecommunications (USSR)	Domestic	6.2/0.714
99.0E	1976		Ekran-1 ⁱ	Ministry of Posts & Telecommunications (USSR)	Direct Broadcast	6.2/0.714
99.0E	1977		Ekran-2 ⁱ	Ministry of Posts & Telecommunications (USSR)	Direct Broadcast	6.2/0.714
102E	1980	2	ISCOM (Indian Satellite for Communications Technology) (APPLE) ⁿ	Indian Space Research Organization (India)	Experimental	0.148,6/0.136,4
108E	1982	7	Palapa-B	Perumtel (Indonesia)	Regional ^o	6/4
110E	1978	3	Yuri (BS-1) (Broadcast Satellite)	NASDA (Japan)	Direct Broadcast	14/12
110E			BS-2	NASDA (Japan)	Direct Broadcast	14/12
113E	1983	3-5	CS-2a (Communications Satellite)	Nippon Telephone & Telegraph (Japan)	Domestic	6,30/4,20
113E	1983	7	Palapa-B	Perumtel (Indonesia)	Regional ^o	6/4
118E	1984	7	Palapa-B	Perumtel (Indonesia)	Regional ^o	6/4

TABLE 1. GEOSYNCHRONOUS SATELLITE DATA (continued)

Longitude	Launch Date	Life (yr)	Satellite Name	Sponsor	Function	Up/Down-Link Frequency (GHz)
120E to 140EP	1983	3-5	CS-2b (Communications Satellite)	Nippon Telephone & Telegraph (Japan)	Domestic	6,30/4,20
125EC	1982		STW 1	Radio Management Bureau (Peoples Republic of China)	Experimental	6/4
128EM				Ministry of Posts & Telecommunications (Australia)	Domestic Direct Broadcast	14/12 ?
130E	1977	1	Kiku 2 (ETS II)	NASDA (Japan)	Experimental	0.148,2.1/ 0.136,1.7, 11.5,34.5
135E	1977	3	Sakura (Cherry Blossom) (CS-1)	NASDA (Japan)	Domestic	6,30/4,20
135E	1980	3-5	ECS-2 (ECS-B) (Experimental Communications Satellite)	NASDA (Japan)	Domestic	6,35/4,32
140E	1977	3	Himiwari (Sunflower) (GMS-1)	NASDA (Japan)	Meteorological	0.149,0.401, 2.0/0.137, 0.469,1.7
140E	1981	3	GMS-2 (Geostationary Meteorological Satellite)	NASDA (Japan)	Meteorological	0.149,0.402, 2.0/0.137, 0.469,1.7
140E	1980		Volna-6	Ministry of Posts & Telecommunications (USSR)	Maritime Aeronautical	1.6/1.5 1.6/1.5

142 COMSAT TECHNICAL REVIEW VOLUME 10 NUMBER 1, SPRING 1980

140E	1979-80		Stasionar-7 Network	Ministry of Posts & Telecommunications (USSR)	Domestic	6/4
140.0E	1981		Loutch-4h	Ministry of Posts & Telecommunications (USSR)	Domestic	14/11
172EC	1980	5	Fltsatcom-4	DOD (USA)	Government	0.29-0.32,1.8, 8/0.24-0.27, 2.2,7
174.0E		7	INTELSAT Pacific Ocean (primary)	INTELSAT	International	6,14/4,11
174.0E	1974	7	INTELSAT IV F-8	INTELSAT	International	6/4
175EC			West Pacific DSCS Network	DOD (USA)	Government	2,8/2,7
175EC	1977	5	DSCS-2 F8 (Defense Satellite Communications System II)	DOD (USA)	Government	2,8/2,7
175EC	1978	5	DSCS-2 F10 (Defense Satellite Communications System II)	DOD (USA)	Government	2,8/2,7
175EC	1978	5	DSCS-2 F12 (Defense Satellite Communications System II)	DOD (USA)	Government	2,8/2,7
175EC	1979	5	DSCS-2 F13 (Defense Satellite Communications System II)	DOD (USA)	Government	2,8/2,7
175EC	1982	10	DSCS-III (Defense Satellite Communications System III)	DOD (USA)	Government	2,8/2,7

CTR NOTE: 1980 GEOSYNCHRONOUS SATELLITE LOG 243

TABLE 1. GEOSYNCHRONOUS SATELLITE DATA (continued)

Longitude	Launch Date	Life (yr)	Satellite Name	Sponsor	Function	Up/Down-Link Frequency (GHz)
176.5E	1976	5	Marisat Pacific	COMSAT General Corporation (USA)	Government Maritime	0.3-0.312/ 0.248-0.26 1.6,6/1.5,4
176.5E ^C		10	Leasat (Pacific)	DOD (USA)	Government	0.24-0.40,8/7
179.0E			INTELSAT Pacific Network (spare)	INTELSAT	International	6,14/4,11
179.0E	1972	7	INTELSAT IV F-4	INTELSAT (spare)	International	6/4
189E ^C (171W)			TDRS-West (Tracking & Data Relay Satellite)	Western Union Space Communications Corporation (USA)	Government	2.0,15/2,2,13
190.0E (170W)	1980		Volna-7	Ministry of Posts & Telecommunications (USSR)	Land Maritime	0.335-0.399/ 0.24-0.328 1.6/1.5
190E (170W)	1980		Statsionar-10 Network	Ministry of Posts & Telecommunications (USSR)	Domestic	6/4
190.0E (170W)	1979		Gals-4	Ministry of Posts & Telecommunications (USSR)	Government	8/7
190E (170W)	1978-81		Loutch-P4 ^h	Ministry of Posts & Telecommunications (USSR)	Domestic	14/11
211E ^C (149W)	1966		ATS-1	NASA (USA)	Experimental	0.149,6/ 0.136,0.137,5

218E (142W)	1976	2	Hermes or CTS (Communications Technology Satellite)	Department of Communications (Canada) and NASA (USA)	Experimental	Inactive
220E (140W)			CBSS (Canadian Broadcasting Satellite System)	Department of Communications (Canada)	Direct Broadcast	14/12
220E (140W)	1982	8	Satcom F5 (Alaska)	RCA Americom (USA)	Domestic	6/4
225E ^C (135W)			East Pacific DSCS Network	DOD (USA)	Government	2,8/2,7
225E (135W)	1978	5	DSCS-2 F11 (Defense Satellite Communications System II)	DOD (USA)	Government	2,8/2,7
225E (135W)	1979	5	DSCS-2 F14 (Defense Satellite Communications System III)	DOD (USA)	Government	2,8/2,7
225E (135W)	1983	10	DSCS-III (Defense Satellite Communications System III)	DOD (USA)	Government	2,8/2,7
225E ^C (135W)	1977	5	NATO-3B (F-2)	NATO	Government	2,8/2,7
225E (135W)	1975	8	Satcom I	RCA Americom (USA)	Domestic	6/4
225E (135W)			Western US Meteorological Network	NOAA (USA)	Meteorological	0.402,2.0/ 0.136,0.468,1.7
225E (135W)	1978		GOES-3 (Geostationary Operational Environmental Satellite)	NOAA (USA)	Meteorological	0.402,2.0/ 0.136,0.468,1.7

TABLE I. GEOSYNCHRONOUS SATELLITE DATA (continued)

Longitude	Launch Date	Life (yr)	Satellite Name	Sponsor	Function	Up/Down-Link Frequency (GHz)
228E (132W)	1981	8	Satcom III's Replacement	RCA Americom (USA)	Domestic	6/4
230E (130W)	1978	5	DSCS-2 F9 (Defense Satellite Communications System II)	DOD (USA)	Government	2,8/2,7
232E (128W)	1976	7	Comstar D-1 (201)q	COMSAT General Corporation (USA)	Domestic	6/4
235E (125W)		10	SBS-C (spare)	Satellite Business Systems (USA)	Domestic	14/12
236.5E (123.5W)	1974	7	Westar II	Western Union Telegraph Company (USA)	Domestic	6/4
238E (122W)	1980	10	SBS-A	Satellite Business Systems (USA)	Domestic	14/12
241E (119W)	1981	10	SBS-B	Satellite Business Systems (USA)	Domestic	14/12
241E (119W)	1976	8	Satcom II	RCA Americom (USA)	Domestic	6/4
244E (116W)	1981	8	Anik-C2	Telesat Canada (Canada)	Domestic	14/12
246E (114W)	1975	7	Anik-A3	Telesat Canada (Canada)	Domestic	6/4
246E (114W)	1982	10	Anik-D	Telesat Canada (Canada)	Domestic	6/4
247E (113W)	1974		SMS 1 (Synchronous Meteorological Satellite) (spare)	NASA (USA)	Meteorological	0.402,2/0.136, 0.468,1.7
247.5E (112.5W)	1981	10	Anik-C1	Telesat Canada (Canada)	Domestic	14/12
250E (110W)	1976	5	LES-8 (Lincoln Experimental Satellite)	DOD & M.I.T. (USA)	Government	UHF,8,36/ UHF,7,32
251E (109W)	1978	7	Anik-B1	Telesat Canada (Canada)	Domestic	6,14/4,12
251E (109W)	1982	10	Anik-D	Telesat Canada (Canada)	Domestic	6/4
251E (109W)	1982	8	Anik-C3	Telesat Canada (Canada)	Domestic	14/12
253.5 (106.5W)	1973	7	Anik-A2	Telesat Canada (Canada)	Domestic	6/4
254.8E (105.2W)	1967		ATS-3c	NASA (USA)	Experimental	0.149,6/0.136, 0.137,4
255E (105W)	1977		GOES 2 (Geostationary Operational Environmental Satellite)	NOAA (USA)	Meteorological	0.402,2/0.136, 0.468,1.7
256E (104W)	1972	7	Anik-A1	Telesat Canada (Canada)	Domestic	6/4
256E (104W)	1982	10	Anik-D	Telesat Canada (Canada)	Domestic	6/4
257E (103W)	1983	10	Advanced Westar	Western Union Space Communications Corporation (USA)	Domestic	6,14/4,12

TABLE 1. GEOSYNCHRONOUS SATELLITE DATA (continued)

Longitude	Launch Date	Life (yr)	Satellite Name	Sponsor	Function	Up/Down-Link Frequency (GHz)
260E (100W)	1976	5	LES-9 (Lincoln Experimental Satellite)	DOD & M.I.T. (USA)	Government	UHF,8,36/ UHF,7,32
260E (100W)	1978	5	Fltsatcom-1 East Pacific	DOD (USA)	Government	0.29-0.32,1.8, 8/0.24-0.27, 2.2,7
260E (100W)	1984	10	Leasat	DOD (USA)	Government	UHF,8/UHF,7
261E (99W)	1974	7	Westar I	Western Union Telegraph Company (USA)	Domestic	6/4
261E (99W)	1982	10	Advanced Westar/TDRS (joint spare)	Western Union Space Communications Corporation (USA)	Government Domestic	2,15/2.2,13 6,14/4,12
265E (95W)	1976 1995	7	Comstar D-2 (202)	COMSAT General Corporation (USA)	Domestic	6/4
268E (92W)			CBSS (Canadian Broadcasting Satellite System)	Department of Communications (Canada)	Direct Broadcast	14/12
269E (91W)	1979	7	Westar III	Western Union Telegraph Company (USA)	Domestic	6/4
270W (90W)	1975		GOES 1 (Geostationary Operational Environmental Satellite)	NOAA (USA)	Meteorological	0.402,2/0.136, 0.468,1.7
270E (90W)	1988	5	Severe Storms Research Satellite	NASA (USA)	Meteorological	0.402,2,104/ 0.136,0.468, 1.7
273E (87W)	1978	7	Comstar D-3 (203)	COMSAT General Corporation (USA)	Domestic	6/4,18,28
275E (85W)	1968	2	LES-6 (Lincoln Experimental Satellite)	DOD & M.I.T.	Research	Inactive
277E (83W)	1980	10	Satcom-IV	RCA Americom (USA)	Domestic	6/4
281E (79W)	1982	7	Hughes 2	Hughes Communications, Inc. (USA)	Domestic	6/4
284.6E (75.4W)			Satcol-2 (spare)	Columbia	Domestic	6/4
285E (75W)			Satcol-1	Columbia	Domestic	6/4
285E (75W)			Brasilsat (SBTS)	Communications Ministry (Brazil)	Domestic	6/4
285E (75W)			Eastern US Meteorological Network	NOAA (USA)	Meteorological	0.402,2./ 0.136,0.468, 1.7
285E (75W)	1975		SMS 2 (Synchro-nous Meteorological Satellite)	NASA (USA)	Meteorological	0.402,2./ 0.136,0.468, 1.7
285E (75W)	1981	7	Hughes 1	Hughes Communications, Inc. (USA)	Domestic	6/4
287.5E (72.5W)			Satcol	Columbia	Domestic	6/4
289° (71W)	1978		IUE (International Ultraviolet Explorer)	NASA (USA)	Astronomy	0.149/0.137,2.2

TABLE 1. GEOSYNCHRONOUS SATELLITE DATA (continued)

Longitude	Launch Date	Life (yr)	Satellite Name	Sponsor	Function	Up/Down-Link Frequency (GHz)
290E ^c (70W)	1969		ATS-5 (Applications Technology Satellite 5)	NASA (USA)	Experimental	0.148/0.137
290E (70W)			Brasilsat (SBTS)	Communications Ministry (Brazil)	Domestic	6/4
292.5E (67.5W)			Brasilsat (SBTS)	Communications Ministry (Brazil)	Domestic	6/4
300E (60W)			Brasilsat (SBTS)	Communications Ministry (Brazil)	Domestic	6/4
303E ^c (57W)			General Purpose Communications Satellite	DOD (USA)	Government	UHF,8/UHF,7
310E ^c (50W)	1978	5	NATO-3C	NATO	Government	2,8/2,7
319E ^c (41W)	1981	3	TDRS (Tracking & Data Relay Satellite) East	Western Union Space Communications Corporation (USA)	Government	2.0,15/2.2,13
325.5E (34.5W)			INTELSAT Atlantic 5 Network (major path 1)	INTELSAT	International	6,14/4,11
325.5E (34.5W)	1977	7	INTELSAT IV-A F-4	INTELSAT	International	6/4
329E (31W)			INTELSAT Atlantic 2 Network (spare)	INTELSAT	International	6,14/4,11
330.5E (29.5)			INTELSAT Atlantic (spare)	INTELSAT	International	6,14/4,11
332.5E (25.5W)			INTELSAT Atlantic (spare)	INTELSAT	International Maritime ^f	6,14/4,11 1.6/1.5
332.5E (25.5W)	1976	7	INTELSAT IV-A F-2	INTELSAT	International	6/4
335E (25W)	1980		Volna-1	Ministry of Posts & Telecommunications (USSR)	Land Aeronautical Maritime	0.335-0.399/ 0.240-0.328 1.5/1.5 1.5/1.6
335.0E (25W)	1980		Statsionar-8 Network	Ministry of Posts & Telecommunications (USSR)	Domestic	6/4
335.0E (25W)			Gals-1	Ministry of Posts & Telecommunications (USSR)	Government	8/7
335.0E (25.0W)	1979-81		Loutch-P1 ^h	Ministry of Posts & Telecommunications (USSR)	Domestic	14/11
335E ^s (25W)	1981	2	Sirio 2	European Space Agency	Experimental Meteorological	0.148/0.137,1.7 2.1/1.7
335.5E (24.5W)			INTELSAT Atlantic 1 Network (primary path)	INTELSAT	International	6,14/4,11
335.5E (24.5W)	1975	7	INTELSAT IV-A F-1	INTELSAT	International	6/4
337E ^c (23W)	1980	5	Fltsatcom-3 Atlantic	DOD (USA)	Government	0.29-0.32,1.7, 8/0.25,2.2,7
337E ^c (23W)	1983	10	Leasat Atlantic	DOD (USA)	Government	UHF,8/UHF,7
338.5E (21.5W)			INTELSAT Atlantic 3 Network (spare)	INTELSAT	International	6,14/4,11

TABLE I. GEOSYNCHRONOUS SATELLITE DATA (continued)

Longi- tude	Launch Date	Life (yr)	Satellite Name	Sponsor	Function	Up/Down-Link Frequency (GHz)
338.5E (21.5W)	1971	7	INTELSAT IV F-3	INTELSAT	International	6/4
341.0E (19W)	1983	5	TV-SAT-A3	BMFT/DFLVR (Fed- eral Republic of Germany)	Direct Broadcast	2.1,19/2.3,12
341.0E (19W)	1983	5	TV-SAT-A3 (spare)	BMFT/DFLVR (Fed- eral Republic of Germany)	Direct Broadcast	2.1,19/2.3,12
341.0E (19W)			TV-SAT-A5	BMFT/DFLVR (Fed- eral Republic of Germany)	Direct Broadcast	2.1,19/2.3,12
341.0E (19W)	1983	5	TDF-1A	Telediffusion Francaise	Direct Broadcast	2.1,19/2.3,12
341.0E (19W)	1984	5	TDF-1B (spare)	Telediffusion Francaise	Direct Broadcast	2.1,19/2.3,12
341.0E (19W)				Tele-Luxembourg (Luxembourg)	Direct Broadcast	19/12
341E (19W)	1984		L-Sat (Large Satellite)	European Space Agency	Experimental Direct Broadcast	14,30/12,20 19/UHF,12
341.5E (18.5W)			INTELSAT Atlantic Network (major path 2)	INTELSAT	International Maritime ^f	6,14/4,11 1.6/1.5
341.5E (18.5W)	1975	7	INTELSAT IV F-1	INTELSAT	International	6/4

342E ^c (18W)	1976	5	NATO-3A (F-1)	NATO	Government	2,8/2,7
342E ^c (18W)			NATO-4	NATO	Government	8/7
345B (15W)	1976	5	Marisat 101 Atlantic	COMSAT General Corporation (USA)	Government Maritime	0.3-0.312/ 0.248-0.26 1.5,6/1.6,4 1.5,4
345E (15W)	1977	2	Sirio 1	CNR (Italy)	Experimental	0.148,18/0.137, 12
346.0E (14W)	1981		Loutch-1 ^h	Ministry of Posts & Telecommunications (USSR)	Domestic	14/11
346.5E (13.5W)			Stationsar-4 Network (includes Gorizont)	Ministry of Posts & Telecommunications (USSR)	Domestic	6/4
346.5E ^t (13.5W)	1978		Gorizont-1 ^j	USSR	Domestic Government	6/4 8/7
346.5E ^u (13.5W)	1979		Gorizont-2 ^j	USSR	Domestic Government	6/4 8/7
346.5E (13.5W)	1980		Volna-2	Ministry of Posts & Telecommunications (USSR)	Maritime Aeronautical	1.6/1.5 1.6/1.5
347E ^c (13W)			Atlantic DSCS Network	DOD (USA)	Government	2,8/2,7
347E (13W)	1977	5	DSCS-2 F7 (Defense Satellite Communi- cations System II)	DOD (USA)	Government	2,8/2,7
347E ^c (13W)	1981	10	DSCS-III (Defense Satellite Commu- nications Sys- tem III)	DOD (USA)	Government	2,8/2,7

TABLE 1. GEOSYNCHRONOUS SATELLITE DATA (continued)

Longitude	Launch Date	Life (yr)	Satellite Name	Sponsor	Function	Up/Down-Link Frequency (GHz)
347.5E (12.5W)	1981	5	Marecs-B	European Space Agency	Maritime	1.6,6/1.5,4
347.5E (12.5W)	1982	5	2nd Marecs (spare) ⁹	European Space Agency	Maritime	1.6,6/1.5,4
348.5E (11.5W)	1975	5	Symphonie-2	France & Federal Republic of Germany	Experimental	6/4
350E (10W)	1982		Telecom-1A	PTT (France)	Domestic	6,14/4,12
350E (10W)	1983		Telecom-1B (spare)	PTT (France)	Domestic	6,14/4,12
350E (10W)	1985		Italsat	CNR (Italy)	Domestic	30/20
356E (4W)			INTELSAT Residuals	INTELSAT	Miscellaneous	6,14/4,11
356E (4W)	1971	7	INTELSAT IV F-2	INTELSAT	International	6/4
359E (1W)			INTELSAT Atlantic Leases	INTELSAT	International	6,14/4,11
359E (1W)	1973	7	INTELSAT IV F-7	INTELSAT	Domestic	6/4

Footnotes for Table 1

- ^aDenmark, Iceland, Finland, Norway, and Sweden.
^bThe international registry is for 0 to 29 East.
^cThese satellites have inclination angles greater than 2°: ECS (Europe), up to 3°; Marecs, up to 3°; DSCS-2's, -3's, NATO-3's, Fltsatcoms, and Leasats, approximately 2°; ATS-1, 9.5°; ATS-3, 8°; LES-8 and -9, 25.3°; TDRS (at 189 and 319 East) under 7°. The IFRB filings for STW-1 and -2 do not state the intended inclination control. The inclinations of "inactive" satellites may be high.
^dThe Arab Satellite Communications Organization consists of the PTTs of the following nations: Algeria, Arab Yemen Republic, Bahrain, Democratic Yemen Republic, Dubai, Egypt, Iraq, Jordan, Kuwait, Lebanon, Libya, Morocco, Oman, Qatar, Saudi Arabia, Somalia, Sudan, Syria, and Tunisia.
^eSometimes referred to as Radouga or Raduca (rainbow).
^fThe maritime portion of this satellite may be utilized by the INMARSAT organization.
^gThe original launch date (1979) has passed without the launch having taken place.
^hSometimes referred to as Louch or Luch (ray or beam).
ⁱSometimes referred to as Ecran or Ecran (screen).
^jSometimes referred to as Horizont or Gordizont (horizon). International registry information is not available for this satellite series.
^kThe Loutch-2 equipment will be carried on the same spacecraft as Statsionar-5.
^lThe frequencies for GOMS are probably similar to the other geosynchronous meteorological satellites (see GOES/SMS, Himiwari, and Meteosat).
^mThe longitude shown is derived from the "Final Acts of the World Administrative Radio Conference" of 1977.
ⁿAPPLE stands for Ariane Passenger Payload Experiment.
^oThe region is the Association of Southeast Asian Nations (ASEAN).
^pThis satellite is to be located between 120 and 140 East. It is also known as the Domestic Satellite Communications System.
^qThe full capacity of these satellites is leased to the American Telephone & Telegraph Co. and the GTE Telephone System.
^rThis satellite was deliberately placed into an orbit with the following parameters: apogee, 45,799 km; perigee, 25,753 km; inclination, 28.3°, and the period of a geosynchronous satellite.
^sSirio 2 will be initially located at 335E (25W) but may later be moved to 20E.
^tThe orbital elements of Gorizont-1 are apogee, 49,023 km; perigee, 22,553 km; inclination 11.3°; and the period of a geosynchronous satellite. The location shown is an estimate based on the location of Gorizont-2.
^uThe orbital elements of Gorizont-2 are a height of 36,550 km (circular), inclination 0.8°, and a geosynchronous/geostationary period.

TABLE 2. FUTURE SATELLITE PROGRAMS

Launch Date	Life (yr)	Satellite Name	Sponsor	Function	Up/Down-Link Frequency (GHz)
	7	Comstar D-4 ^{a,b}	COMSAT General Corporation (USA)	Domestic	6/4
		Condor	Peru	Domestic	6/4
1985	2	System 85 (geostationary version)	NASA (USA)	Meteorological	
		Disaster Warning Satellite System	Department of Commerce (USA)	Direct Broadcast	
1980		GOES-D (Geostationary Operational Environmental Satellite) ^a	NOAA (USA)	Meteorological	0.402,2.0/ 0.136,0.468, 1.7
1981		GOES-E (Geostationary Operational Environmental Satellite) ^a	NOAA (USA)	Meteorological	0.402,2.0/ 0.136,0.468, 1.7
1983		GOES-F (Geostationary Operational Environmental Satellite) ^a	NOAA (USA)	Meteorological	0.402, 2.0/ 0.136,0.468, 1.7
1981	10	F1tsatcom (on-orbit spare) ^c	DOD (USA)	Government	UHF,8/UHF,7
1983-84	10	Satcom Series (2nd generation)	RCA Americom (USA)	Domestic	6/4
1984		AT&T-1	American Telephone & Telegraph (USA)	Domestic	6,14/4,12 ^d
1984		AT&T-2	American Telephone & Telegraph (USA)	Domestic	6,14/4,12 ^d

1985		AT&T-3	American Telephone & Telegraph (USA)	Domestic	6,14/4,12 ^d
1982		WU Gapfiller ^a	Western Union Corporation (USA)	Domestic	6/4
		Survsat (Survivable Satellite) ^c	DOD (USA)	Government	UHF,8/UHF,7
1985		Geostationary Metsat	Peoples Republic of China	Meteorological	
1980-85		INTELSAT V F-1 to F-8 ^f	INTELSAT	International Maritime ^e	6,14/4,11 1.6/1.5

^aThis satellite is intended to replace an already in-orbit satellite (ground spare) and may be located at an existing location after launch. The date of launch (if launched) will depend upon need.

^bThis satellite will be launched if needed.

^cThe inclination of these satellites will be greater than 2°.

^dFrequencies shown are the author's estimate.

^eThe maritime portion of those INTELSAT V's with 1.6/1.5-GHz equipment may be utilized by the INMARSAT organization.

^fThese satellites will be used in the INTELSAT network at locations shown in Table 1.

TABLE 3. SATELLITES AND OBJECTS THAT TRAVERSE THE GEOSTATIONARY ORBIT^a

Launch Date	Satellite Name	Sponsor	Function	Up/Down-Link Frequency (GHz)
1965	INTELSAT I (Early Bird)	INTELSAT	International	Inactive
1967	INTELSAT II F-2	INTELSAT	International	Inactive
1967	INTELSAT II F-3	INTELSAT	International	Inactive

TABLE 3. SATELLITES AND OBJECTS THAT TRAVERSE THE GEOSTATIONARY ORBIT^a

Launch Date	Satellite Name	Sponsor	Function	Up/Down-Link Frequency (GHz)
1967	INTELSAT II F-4	INTELSAT	International	Inactive
1968	INTELSAT III F-2	INTELSAT	International	Inactive
1970	INTELSAT III F-7	INTELSAT	International	Inactive
1970	INTELSAT III F-8 (pieces)	INTELSAT	International	AKM Failure
1974	Cosmos-637	USSR	Experimental	?
1963	Syncom-1 (pieces)	NASA (USA)	Experimental	AKM Failure
1963	Syncom-2	NASA (USA)	Experimental	Inactive
1964	Syncom-3	NASA (USA)	Experimental	Inactive
1976	Hermes (CTS) Hatch-covers (2)	Canada/USA	Experimental	Passive
1979	Satcom III	RCA Americom (USA)	Domestic	Inactive
1969	Skynet-1A	Department of Defence (UK)	Government	Inactive
1970	Skynet-1B	Department of Defence (UK)	Government	AKM Failure
1974	Skynet-2B	Department of Defence (UK)	Government	Inactive
1970	NATO-1	NATO	Government	Inactive
1971	NATO-2A	NATO	Government	Inactive
1971	NATO-2B	NATO	Government	Inactive
1969	Tacsat (Tactical Communications Satellite)	DOD (USA)	Government	Inactive
1974	Molniya-1S	USSR	Experimental	Inactive
1977	Himiwari Apogee Kick Motor	NASDA (Japan)	Meteorological	Passive ^b
1977	Meteosat-1 Apogee Kick Motor	European Space Agency	Meteorological	Passive ^b
1971	DSCS-2 F1 (Defense Satellite Communications System II)	DOD (USA)	Government	Inactive
1971	DSCS-2 F2 (Defense Satellite Communications System II)	DOD (USA)	Government	Inactive
1971	DSCS-2 Transtage	DOD (USA)	Government	Passive
1973	DSCS-2 F3 (Defense Satellite Communications System II)	DOD (USA)	Government	Inactive
1973	DSCS-2 Transtage	DOD (USA)	Government	Passive
1975	DSCS-2 Transtage	DOD (USA)	Government	Passive
1977	DSCS-2 Transtage	DOD (USA)	Government	Passive
1978	DSCS-2 Transtage	DOD (USA)	Government	Passive
1978	DSCS-2 Transtage	DOD (USA)	Government	Passive
1979	DSCS-2 Transtage	DOD (USA)	Government	Passive

TABLE 3. SATELLITES AND OBJECTS THAT TRAVERSE THE GEOSTATIONARY ORBIT^a
(continued)

Launch Date	Satellite Name	Sponsor	Function	Up/Down-Link Frequency (GHz)
1968	OV2 (Orbital Vehicle)	DOD (USA)	Experimental	Inactive
1968	OV5 (Orbital Vehicle)	DOD (USA)	Experimental	Inactive
1968	OV Transtage	DOD (USA)	Government	Passive
1970	ATS-6 Transtage	NASA (USA)	Experimental	Passive
1966	ATS-1 Apogee Kick Motor	NASA (USA)	Experimental	Passive
1967	ATS-3 Apogee Kick Motor	NASA (USA)	Experimental	Passive
1969	ATS-5 Apogee Kick Motor	NASA (USA)	Experimental	Passive
1974	SMS 1 Apogee Kick Motor	NASA (USA)	Meteorological	Passive
1974	SMS 1 Cooler Cover	NASA (USA)	Meteorological	Passive
1975	SMS 2 Apogee Kick Motor	NASA (USA)	Meteorological	Passive
1975	SMS 2 Cooler Cover	NASA (USA)	Meteorological	Passive
1975	GOES 1 Apogee Kick Motor	NOAA (USA)	Meteorological	Passive
1975	GOES 1 Cooler Cover	NOAA (USA)	Meteorological	Passive
1977	GOES 2 Apogee Kick Motor	NOAA (USA)	Meteorological	Passive
1977	GOES 2 Cooler Cover	NOAA (USA)	Meteorological	Passive
1978	GOES 3 Apogee Kick Motor	NOAA (USA)	Meteorological	Passive
1978	GOES 3 Cooler Cover	NOAA (USA)	Meteorological	Passive
1968	1968-063	DOD (USA)	Government	
1969	1969-036	DOD (USA)	Government	?
1970	1970-069	DOD (USA)	Government	?
1971	1971-039	DOD (USA)	Government	?
1972	1972-010	DOD (USA)	Government	?
1972	1972-101	DOD (USA)	Government	?
1973	1973-013	DOD (USA)	Government	?
1973	1973-040	DOD (USA)	Government	?
1975	1975-055	DOD (USA)	Government	?
1976	1976-050	DOD (USA)	Government	?
1977	1977-034	DOD (USA)	Government	?
1979	1979-053	DOD (USA)	Government	?
1978	Scatha (Spacecraft Charging at High Altitudes Experiment) ^c	DOD (USA)	Experimental	?
1979	Ayame (Experimental Communications Satellite 1 or ECS-1)	NASDA (Japan)	Experimental	Inactive
1976	LES-8 & -9 Transtage	DOD (USA)	Experimental	Passive

^aThe inclination of these satellites may be high. Data on the locations were not available (see text).

^bIf jettisoned.

^cThe orbit elements of Scatha are apogee, 43,549 km; perigee, 27,246 km; inclination, 7.6°; and period, 1,416.2 minutes.

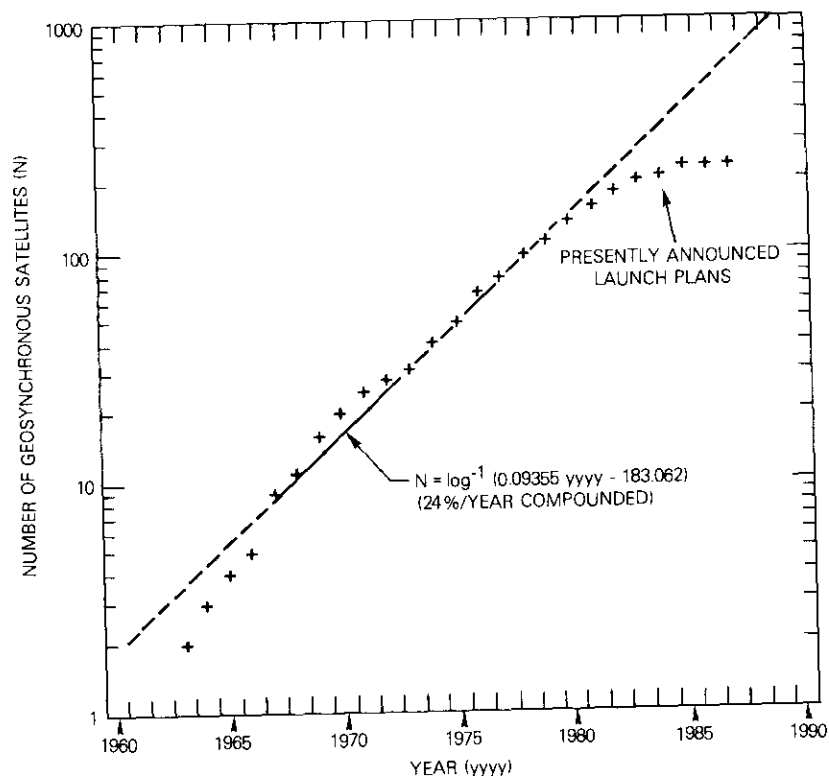


Figure 1. Number of Geosynchronous Satellites

Translations of Abstracts in this issue

La Conférence administrative mondiale des radio-communications de 1979, du point de vue des services de satellites de télécommunication

C. DORIAN, J.B. POTTS, E. REINHART ET H. WEISS

Sommaire

La Conférence administrative mondiale des radio-communications de 1979 (CAMR-79) étant désormais achevée, l'article passe en revue les résultats les plus importants de la conférence du point de vue de leur incidence sur les divers services spatiaux, afin que la communauté spatiale en soit saisie en temps utile. Il présente les aspects les plus importants des assignations de fréquence, les résultats des réunions des commissions techniques et quelques-uns des résultats plus généraux de la conférence. D'une façon globale, il estime que les résultats semblent généralement favoriser la croissance continue des services de télécommunications spatiales.

Expérience internationale en matière de réseau d'ordinateurs à grande vitesse par satellite

W. COOK, A. KAUL, G. HODGE, ET J. MARCHESE

Sommaire

On a établi un réseau expérimental à quatre noeuds d'ordinateurs pour étudier la conception des systèmes de télécommunication entre ordinateurs par satellite, et pour démontrer certaines applications de traitement de données à grande vitesse entre ordinateurs très éloignés les uns des autres. Le réseau était composé de quatre ordinateurs à unité centrale situés à différents endroits aux Etats-Unis et en Europe, communiquant entre eux en mode d'accès multiple par répartition dans le temps (AMRT). Le système AMRT à affectation fixe était formé de deux sous-réseaux à 1,544 Mbit/s fonctionnant avec deux répéteurs distincts du satellite Symphonie. Afin d'assurer des possibilités d'interconnexion complètes, chaque site pouvait avoir accès à l'un ou l'autre répéteur.

Les résultats de l'expérience ont démontré l'influence des divers paramètres de système de transmission et de système de traitement de données sur les

Sistema de comunicaciones de un observatorio sísmico automático

K. GREENE, W. SONES, M. GROSSMAN, M. JONES Y N. JACOBUS

Abstracto

El Sistema de Observatorio Sísmico Automático es una red de plataformas automáticas situadas en lugares remotos, con las cuales se recogen los datos generados por detectores de actividad sísmica. Cada plataforma transmite los datos por una portadora monocanal (SCPC) modulada mediante manipulación por desfasaje binaria (BPSK) a través de un enlace vía satélite hacia una terminal receptora central.

Para controlar las transmisiones se emite una señal modulada mediante manipulación por desplazamiento de frecuencia (FSK), desde la terminal central hacia todas las plataformas, con direccionamiento discreto de telemandos a estaciones específicas. Para reducir al mínimo el error de frecuencia en el enlace de telemandos, se utiliza un enlace piloto desde la terminal central y de retorno a ella, para detectar y compensar los desplazamientos de frecuencia causados por el convertidor-elevador del satélite y la estación terrena.

En este informe se examina el diseño del sistema, el cálculo del enlace, la implantación y perturbaciones de la radiofrecuencia, así como el fundamento para la selección de los métodos de modulación adoptados en el enlace piloto y en el de datos. Se presentan los resultados obtenidos con un sistema prototipo.

Author Index, CTR 1979

Code numbers listed below are to be used for ordering reprints from Lab Records, COMSAT Laboratories, P.O. Box 115, Clarksburg, Maryland.

- ACKERMANN, E., See Kaiser, J. [CTR79/179].
 BARGELLINI, P. L., "Foreword," Fall, pp. v-vi [CTR79/172].
 BARNES, A. J., see Cotner, C. B. [CTR79/185].
 BROWN, M. P., see Gray, L. F. [CTR79/164].
 CAMPANELLA, S. J., Colby, R. J., Pontano, B. A., Suyderhoud, H. & Onufry, M., "The INTELSAT TDMA Field Trial," Fall, pp. 293-340 [CTR79/173].
 CAMPANELLA, S. J. & Hodson, K., "Open-Loop TDMA Frame Acquisition and Synchronization," Fall, pp. 341-385 [CTR79/174].
 CHAKRABORTY, D., see Wolejsza, C. J. [CTR79/176].
 CHOU, S., "12-GHz 10-W Amplifier Using GaAs IMPATT Diodes," Fall, pp. 617-628 [CTR79/181].
 COLBY, R. J., see Campanella, S. J. [CTR79/173].
 COTNER, C. B. & Barnes, A. J., "Intelligible Crosstalk Between Large FDM-FM Carriers Amplified by Klystrons," Fall, pp. 705-716 [CTR79/185].
 FANG, R. J. & Lu, S., "Authentication Over Low Data Rate Channels with Feedback," Spring, pp. 1-14 [CTR79/159].
 FANG, R. J., see Lu, S. [CTR79/163].
 GRAY, L. F. & Brown, M. P., "Transmission Planning for the First U.S. Standard C (14/11 GHz) INTELSAT Earth Station," Spring, pp. 61-90 [CTR79/164].
 GREENE, K. H. & Hefele, R. F., "FSK Burst Receiver for Data Collection Systems," Fall, pp. 517-547 [CTR79/178].
 HEFELE, R. F., see Greene, K. H. [CTR79/178].
 HODSON, K., see Campanella, S. J. [CTR79/174].
 HYDE, G., see Rogers, D. [CTR79/170].
 JONES, M. E. & Wachs, M. R., "Optimum Filtering for QPSK in Bandwidth-Limited Nonlinear Satellite Channels," Fall, pp. 465-507 [CTR79/177].
 KAISER, J., Veenstra, I., Ackermann, E. & Seidel, F., "Small Earth Terminals at 12/14 GHz," Fall, pp. 549-601 [CTR79/179].
 KARMEL, P., "Statistical Properties of Antenna Sidelobes," Spring, pp. 91-120 [CTR79/165].
 KAUL, A. K., "A Model for Packet Switching Nodes Including Packet Retransmission Effects," Fall, pp. 669-688 [CTR79/183].
 KAUL, A. K., "Performance of Data Link Control Protocols over Synchronous Time-Division Multiplexed Communications Channels," Spring, pp. 203-231 [CTR79/168].
 KAUL, A. K., "The Effect of Buffer Access Time on HDLC Performance," Fall, pp. 689-703 [CTR79/184].
 KENNEDY, D. J., "Rain Depolarization Measurements at 4 GHz," Fall, pp. 629-668 [CTR79/182].

- LEE, L. N., "Note on Cryptosystems," Fall, pp. 717-721 [CTR79/186].
- LEE, L. N., see Lu, S. [CTR79/160], [CTR79/162], [CTR79/163].
- LEE, L. N. & Lu, S., "A Multiple Destination Cryptosystem for Broadcast Networks," Spring, pp. 25-36 [CTR79/161].
- LEE, Y. S. & Trushel, R. C., "Periodic Bandpass Characteristic of Microstrip Meander Line," Fall, pp. 604-615 [CTR79/180].
- LU, S. & Lee, L. N., "A Simple and Effective Public-Key Cryptosystem," Spring, pp. 15-24 [CTR79/160].
- LU, S. & Lee, L. N., "Message Redundancy Reduction by Multiple Substitution: A Preprocessing Scheme for Secure Communications," Spring, pp. 37-48 [CTR79/162].
- LU, S., Lee, L. N. & Fang, R. J., "An Integrated System for Secure and Reliable Communications Over Noisy Channels," Spring, pp. 49-60 [CTR79/163].
- LU, S., see Lee, L. N. [CTR79/161].
- ONUFY, M., see Campanella, S. J. [CTR79/173].
- PONTANO, B. A., see Campanella, S. J. [CTR79/173].
- RAMOS, A., "Air Bearing Testing of a Skewed Reaction Wheel System for Attitude Control," Spring, pp. 157-200 [CTR79/167].
- REVESZ, A. G., "Integrated Circuits in Communications Satellites," Spring, pp. 233-242 [CTR79/169].
- ROGERS, D. & Hyde, G., "Diversity Measurements of 11.6 GHz Rain Attenuation at Etam and Lenox, West Virginia," Spring, pp. 243-254 [CTR79/170].
- SCHAEFER, D. J., "Techniques for TDMA System Monitoring," Fall, pp. 387-412 [CTR79/175].
- SEIDEL, F., see Kaiser, J. [CTR79/179].
- STEGENS, R. E., "Design and Performance of Low-Cost Integrated MIC Up- and Down-Converters for Earth Station Applications," Spring, pp. 121-155 [CTR79/166].
- STEGENS, R. E., "Coplanar Waveguide FET Amplifiers for Communications Satellite Systems," Spring, pp. 255-266 [CTR79/171].
- SUYDERHOUD, H., see Campanella, S. J. [CTR79/173].
- TRUSHEL, R. C., see Lee, Y. S. [CTR79/180].
- VEENSTRA, I., see Kaiser, J. [CTR79/179].
- WACHS, M. R., see Jones, M. E. [CTR79/177].
- WELTI, G. R., "Frequency Reuse Limits for the Geostationary Orbit," Fall, pp. 723-730 [CTR79/187].
- WOLEJSZA, C. J. & Chakraborty, D., "TDMA Modem Design Criteria," Fall, pp. 413-464 [CTR79/176].

Comsat Authors Presentation and Publication Index—1979

The following is a cross-referenced index of technical publications and presentations by COMSAT authors outside of *COMSAT TECHNICAL REVIEW*. The number at the end of each entry is the reprint code by which copies may be ordered from Lab Records at COMSAT Laboratories, P.O. Box 115, Clarksburg, MD 20734.

- AGRAWAL, B. N. & Evan-Iwanowski, R. M.,* "Nonstationary and Nonlinear Vibration Analysis," *Shock and Vibration Digest*, Aug. 79, pp. 19-22 [79CLR57].
- AKAGAWA, M. & DiFonzo, D. F., "Beam Scanning Characteristics of Offset Gregorian Antennas," IEEE 1979 Int. Symposium on Antennas & Propagation, *DIGEST*, Vol. 1, pp. 262-265 [79CLR33].
- ALPER, J. R., see Ghais, A. F. [79CLR32].
- ASSAL, F. & Betaharon, K., "Computational Method for the Performance Evaluation of 4-Phase PSK Transmission Through Linear and Nonlinear Channels," *Satellite Communications*, NY: IEEE Press, 1979, pp. 248-255 [79CLR63].
- ASSAL, F. & Rozec, X.,* "Fast, Fully-Redundant, 4 GHz, 8×8 Microwave Switch Matrix for Communications Satellites," 9th European Microwave Conf., Sept. 79, *CONF. PROC.*, pp. 218-222 [79CLR65].
- ASSAL, F., see Shimamura, J. [79CLR66].
- ATIA, A. E., "A 14-GHz High-Power Filter," IEEE 1979 MTT-S Int. Microwave Symposium, *DIGEST*, pp. 261-263 [79CLR11].
- ATIA, A. E., see DiFonzo, D. F. [79CLR34].
- BARGELLINI, P. L., "A Synopsis of Commercial Satellite Communications Systems," *Satellite Communications*, NY: IEEE Press, 1979, pp. 29-43 [79CLR58].
- BARGELLINI, P. L., "Commercial U.S. Satellites," *IEEE Spectrum*, Oct. 79, pp. 30-37 [79CLR55].
- BARGELLINI, P. L., "Fifteen Years of Commercial Satellite Communications," Pacific Telecom. Conf., *PROC., IEEE*, 1979, pp. 2E-1-2E-13 [79CLR09].
- BARGELLINI, P. L., "Notes on Satellite Communications and Perspectives in Communications," Pres. at Arab Summer School on Science & Technology, Bloudan, Syria, June-July 79 [UPO78CL].
- BARGELLINI, P. L., "Technology and Economics of Space and Surface Telecommunications Systems," 26th Int. Congress on Electronics/19th Meeting on Space, *PROC.*, pp. 46-55 [79CLR25].
- BETAHARON, K., see Assal, F. [79CLR63].
- BILLERBECK, W. J., "Long-Term Prediction of Power System Performance for Geosynchronous Spacecraft," 14th IECEC, Aug. 79, *PROC.*, Vol. 2, pp. 1244-1249 [79CLR54].

*Non-COMSAT author.

- BILLERBECK, W. J., see Slifer, L. W.* [79CLR53].
- CALVIT, T. O., "A MARISAT 56 KBPS Ship-to-Shore Data Service," 1979 San Francisco RTCM Assembly Meeting, *RTCM Symposium Papers*, Vol. 2, pp. L1-L12 [79CLR67].
- CAMPANELLA, S. J. & Hodson, K.,† "Open-Loop TDMA Acquisition and Synchronization Experiment," *IEEE EASCON '79 RECORD*, pp. 408-412 [79CLR30].
- CARLSON, H. E., see Fleming, P. L. [79CLR12], [79CLR23], [79CLR24], [79CLR50], [79CLR62].
- CHAKRABORTY, D., see Uzunoglu, V. [79CLR37].
- CHANG, P. Y. & Shimbo, O.,† "Input Power Assignment of Multicarrier Systems from Given Output Power Levels," *IEEE COM-27*, Oct. 79, pp. 1577-1584 [79CLR46].
- CHARYK, J. V., "Space 2000—Impact on Intergovernmental Treaties and Agreements," 3d World Telecommunications Forum, ITU, Geneva, Sept. '79, Pt. I, pp. VII 5.1-VII 5.4 [79CLR68].
- CHILDS, W. H., see Lee, Y. S. [79CLR13].
- CHU, W. W.,* Gerla, M.,* Naylor, W. E.,* Treadwell, S.,* Mills, D., Spilling, P.* & Aagesen, F. A.,* "Experimental Results on the Packet Satellite Network," National Telecom. Conf., Nov. 79, *CONF. PROC.*, Vol. 3, pp. 45.3.1-45.3.4 [79CLR39].
- COLBY, R. J. & Pontano, B. A.,† "Operational Experience Gained from the INTELSAT TDMA Field Trial," *IEEE EASCON '79 RECORD*, pp. 413-418 [79CLR28].
- COOK, W., see Hodge, G.* [79CLR43].
- COX, W. A., see Fleming, P. L. [79CLR12], [79CLR24], [79CLR62].
- DIFONZO, D. F., Karmel, P. R. & Atia, A. E., "A Multiple Shaped Beam Reconfigurable Satellite Antenna," *IEEE AP-S Int. Symposium*, June 79, *DIGEST*, Vol. 2, pp. 457-460 [79CLR34].
- DIFONZO, D. F., see Akagawa, M. [79CLR33].
- EARLY, L. B., "Trends in Satellite Communications," *Technology Tomorrow*, Apr. 79, pp. 1, 10-12 [79CLR59].
- EDELSON, B. I., "Satellite Communications—Technology, Systems, and Business," Pres. before the Subcommittee on Space Sciences & Applications Committee on Science & Technology, U.S. House of Representatives, Sept. 79 [UPO72CL].
- EDELSON, B. I., "Satellite Communications for the 1980's," *The Future United States Space Program (Advances in Astronautical Sciences*, Vol. 38), San Diego: American Astronautical Soc., 1979, pp. 667-669 [79CLR15].
- EDELSON, B. I., "Technology for Future Satellite Communications," Pres. to the Institution of Electrical & Electronics Engineers, Ottawa, Feb. 79 [UPO70CL].
- EDELSON, B. I., see Morgan, W. L. [79CLR20].

*Non-COMSAT author.

†INTELSAT assignee.

- EDELSON, B. I., Fang, R. J. & Morgan, W. L., "Future Satellite Communications," Int. Conf. on Space Telecommunications and Radio Broadcasting Objectives for the 80's, Mar. 79, *PROC.*, pp. 391-401 [79CLR22].
- EDELSON, B. I., Fang, R. J. & Morgan, W. L., "Satellite Communications—Technology and Trends," Pres. at 34th All-Union Scientific Session of the A. S. Popov Society, Moscow, May 79 [UPO71CL].
- ESCH, F. H. & Morgan, W. L., "Orbital Antenna Farm Power Systems Challenges," 14th IECEC, Aug. 79, *PROC.*, Vol. 2, pp. 1207-1212 [79CLR48].
- FANG, D. J. & Harris, J. M., "Precipitation Attenuation Studies Based on Measurements of ATS-6 20/30 GHz Beacon Signals at Clarksburg, Md.," *IEEE AP-27*, Jan. 79, pp. 1-11 [79CLRO2].
- FANG, R. J., "A Simple Demand-Assigned Satellite Communications System," Pres. at National Telecom. Conf., Washington, D.C., Nov. 79 [UPO73CL].
- FANG, R. J., "Modulation Transfer from TDMA On-Off Bursting to FM Carriers in Memoryless Nonlinear Devices: Pt. 1—Power Spectra," *IEEE COM-27*, Jan. 79, pp. 94-100 [79CLRO5].
- FANG, R. J., see Edelson, B. I. [UPO71CL], [79CLR22].
- FLEMING, A. W.* & Ramos, A., "Precision Three-Axis Attitude Control via Skewed Reaction Wheel Momentum Management," AIAA Guidance & Control Conf., Aug. 79, *A Collection of Tech. Papers*, pp. 177-190, AIAA Paper 79-1719 [79CLR35].
- FLEMING, P. L. & Carlson, H. E., "Reflection-Mode Amplifier Utilizing GaAs Active-Medium-Propagation Devices," *Elect. Letters*, Nov. 79, pp. 787-788 [79CLR50].
- FLEMING, P. L. & Carlson, H. E., "Two-State Amplifier Utilizing GaAs Active-Medium-Propagation Devices," *Elect. Letters*, June 79, pp. 406-407 [79CLR23].
- FLEMING, P. L., Smith, T., Carlson, H. E. & Cox, W. A., "Continuous-Wave Operation of Active Medium Propagation Devices," *IEEE ED-26*, Sept. 79, pp. 1267-1272 [79CLR24].
- FLEMING, P. L., Smith, T., Carlson, H. E. & Cox, W. A., "GaAs SAMP Device for Ku-Band Switching," 1979 IEEE MTT-S Int. Microwave Symposium, *DIGEST*, pp. 253-255 [79CLR12].
- FLEMING, P. L., Smith, T., Carlson, H. E. & Cox, W. A., "GaAs SAMP Device for Ku-Band Switching," *IEEE MTT-27*, Dec. 79, pp. 1032-1035 [79CLR62].
- FREE, B. A., see Meadows, G. A. [79CLR60].
- GETSINGER, W. J., "Microstrip Characteristic Impedance," *IEEE MTT-27*, Apr. 79, p. 293 [79CLR21].
- GETSINGER, W. J., see Lee, Y. S. [79CLR18].
- GHAIS, A. F., Alper, J. R. & Oslund, J., "Transoceanic Telecommunications via Satellite," *Telecommunications*, May 79, pp. 59-62 [79CLR32].

*Non-COMSAT author.

†INTELSAT assignee.

- GOLDSTEIN, I., "Communications Satellites: A Revolution in International Broadcasting," *Broadcast Engineering*, May 79, pp. 66-69 [79CLR47].
- GOLDSTEIN, I., "Perspectives on Pacific Telecommunications Developments and Policies," Pacific Telecom. Conf., Jan. 79, *PROC., IEEE, 1979*, pp. 2D-8-2D-13 [79CLR08].
- GOLDSTEIN, I., "Satellites and Third World Communication Systems, Opportunities and Pitfalls," Pres. at US-Japan Symposium on Int. Comm., Boston, Oct. 79, [UP076CL].
- GORDON, G. D., "APL Is More Powerful Than SPEAKEASY," Pres. at 7th Annual SPEAKEASY Conf., Chicago, Aug. 79 [79CLR29].
- GREENE, K. H., & Hefele, R. F., "Random Multiple Access Receiver," Pres. at IEEE EASCON Conv., Arlington, Oct. 79 [UP081CL].
- HARRINGTON, J. V., see Morgan, W. L. [79CLR49].
- HARRIS, J. M., see Fang, D. J. [79CLR02].
- HEFELE, R. F., see Greene, K. H. [UP081CL].
- HELDER, G. K.* & Onufry, M., "Echo Cancellor Standardization in the C.C.I.T.T.," National Telecom. Conf., Nov. 79, *CONF. PROC.*, Vol. 3, pp. 48.5.1-48.5.5 [79CLR44].
- HELM, N. R., "Disaster via Satellite Communications, Parts 1 and 2," *Satellite Communications*, Mar. 79, pp. 16-19 & Apr. 79, pp. 20-21 [79CLR10].
- HINDIN, H. J., "Tunnel Diodes Flying High (Probing the News Article at COMSAT Labs)," *Electronics*, Apr. 79, pp. 81-82 [OUT011CL].
- HODGE, G.* Marchese, J.* Cook, W., Kaul, A., Popot, M.* & Lang, H.* "An International High-Speed Computer-Satellite Communications Network Experiment," Pres. at 30th Int. Astronautical Federation, Int. Astronautical Congress, Munich, Sept. 79, IAF Paper 79-282 [79CLR43].
- HORNA, O. A., "A Comparison of Identification Algorithms Employed in Echo Cancellor Implementation," National Telecom. Conf., Nov. 79, *CONF. PROC.*, Vol. 3, pp. 48.1.1-48.1.7 [79CLR41].
- JOHNSON, J. A., "Remote Sensing: An Opportunity for Private Enterprise in the United States," Pres. at EUROSPACE Int. Colloquium 'Librespace' on Free Enterprise in Space, Oct. 79 [UPO69CL].
- JOHNSON, J. A., "Satellite Telecommunications Markets in the Eighties—A U.S. View," Pres. at EUROSPACE 7th US-European Conf., Naples, Sept. 78 [UPO66CL].
- JOHNSON, J. A., "The Role of U.S. Private Enterprise in Satellite Telecommunications," Pres. at EUROSPACE Int. Colloquium 'Librespace' on Free Enterprise in Space, Oct. 79 [UPO68CL].
- KARMEL, P. R. "TEO11 Mode Sectorial Circular Cylindrical Cavity Filters," IEEE 79 MTT-S Int. Microwave Symposium, *DIGEST*, pp. 269-271 [79CLR14].
- KARMEL, P. R., see DiFonzo, D. F. [79CLR34].

*Non-COMSAT author.

- KASSER, J., "TDMA Satellite Onboard Switching Center Electronics," Int. Telemetry Conf., Nov. 79, *ITC/USA/79 PROC.*, Vol. 15, pp. 13-17 [79CLR51].
- KAUL, A., see Hodge, G.* [79CLR43].
- KIRSTEIN, P. T.* Bradbury, C.* Cringle, R. C.* Gamble, H. R.* Briner, R.* McNeill, D.* Cole, J.* Bressler, R.* & Mills, D., "SATNET Applications Activities," National Telecom. Conf., Nov. 79, *CONF. RECORD*, Vol. 3, pp. 45.5.1-45.5.7 [79CLR40].
- KWAN, R., "Advances in Electronic Message Systems," Pres. at Communicasia Conf., Singapore, Dec. 79 [UPO84CL].
- LEE, L-N., see Weng, M-I. [UPO74CL].
- LEE, Y. S. & Childs, W. H., "Temperature-Compensated BaTi409 Microstrip Delay Line," IEEE 79 MTT-S Int. Microwave Symposium, *DIGEST*, pp. 419-421 [79CLR13].
- LEE, Y. S., Getsinger, W. J. & Sparrow, L. R., "Barium Tetratitanate MIC Technology," *IEEE MTT-27*, July 79, pp. 655-660 [79CLR18].
- LIU, R., "Bibliography of Basic Books in Satellite Communications Engineering," Based on the collection at COMSAT Labs Technical Library, 1979 [UPO67CL].
- MCGARTY, T. P., "Unattended Earth Stations for Global Data Collection," Int. Conf. on Comm., *ICC '79 CONF. RECORD*, Vol. 1, pp. 6.1.1-6.1.5 [79CLR16].
- MCNEILL, D. A.* Cole, J.* Malman, J. H.* Milliken, W. C.* Rothschild, S., Redman, W. A., Hoversten, E. V.* & Blake, S.* "SATNET Monitoring and Control," National Telecom. Conf., Nov. 79, *CONF. RECORD*, Vol. 3, pp. 45.3.1-45.3.4 [79CLR38].
- MASS, J., "Diversity and Baseline Orientation," *IEEE AP-27*, Jan. 79, pp. 27-30 [79CLRO3].
- MEADOWS, G. A. & Free, B. A., "Ion Etching to Expose Crystal Structure," Pres. at Princeton/AIAA/DGLR 14th Int. Electric Propulsion Conf., Princeton, Oct.-Nov. 79, AIAA Paper 79-2117 [79CLR60].
- METZGER, S. "Computer Communications Via Satellite," Pres. at IBM Symposium, Haifa, Oct. 79 [UPO82CL].
- MILLS, D., see Chu, W. W.* et al. [79CLR39] & Kirsten, P. T.* et al. [79CLR40].
- MORGAN, W. L., "Ever Smaller Earth Stations, Crowded Satellites Imply Changes," *Microwave System News*, Apr. 79, pp. 81-90 [79CLR19].
- MORGAN, W. L., "Geosynchronous Satellite Log," *J. of the British Interplanetary Soc.*, Oct. 79 pp. 390-395 [79CLR61].
- MORGAN, W. L. "Integrating Large Space Stations Into Telecommunications Networks," *IEEE EASCON '79 RECORD*, Vol. 1, pp. 64-68 [79CLR31].
- MORGAN, W. L., "Large Geostationary Communications Platform," Pres. at Int. Astronautical Federation, 30th Congress, Munich, Sept. 79, Paper IAF-79-F-210 [79CLR26].

*Non-COMSAT author.

- MORGAN, W. L., see Edelson, B. I. [UPO71CL], [79CLR22] & Esch, F. H. [79CLR48].
- MORGAN, W. L. & Edelson, B. I., "The Orbital Antenna Farm Concept," *J. of the British Interplanetary Soc.*, 1979, pp. 243-254 [79CLR20].
- MORGAN, W. L. & Harrington, J. V., "Applications of Communications Satellites to Broadcasting," *Information for Your Future*, Fall 79, pp. 4-10 [79CLR49].
- NISHI, H., see Revesz, A. G. [79CLR64].
- NOGUCHI, T., †see Uzunoglu, V. [79CLR37].
- ONUFY, M., see Helder, G. K. [79CLR44] & Virupaksha, K. [79CLR42].
- OSLUND, J., see Ghais, A. F. [79CLR32].
- POLLACK, L., "Switching in Space," *IEEE Spectrum*, Oct. 79, pp. 32-33 [79CLR56].
- POLLACK, L., "Technologies for Future INTELSAT Satellites," Pres. at 17th Aerospace Sci. Meeting, New Orleans, Jan. 79, AIAA Paper 79-0244 [79CLR01].
- RAAG, H., "Design of the INTELPOST System," Pres. at CCITT Symposium on Telecom. Service, Geneva, May 79 [UPO83CL].
- RAMOS, A., see Fleming, A. W.* [79CLR35].
- REDMAN, W. A., see McNeill, D. A. [79CLR38].
- REVEZ, A. G., "On the Initial Oxidation Rate of Silicon," *J. of the Electrochem. Soc.*, Mar. 79, pp. 502-503 [79CLR07].
- REVEZ, A. G., "The Role of Hydrogen in SiO₂ Films on Silicon," *J. of the Electrochem. Soc.*, Jan. 79, pp. 122-130 [79CLR04].
- REVEZ, A. G. & Nishi, H., "GaAs/Ta₂O₅ and GaAs/Al₂O₃ Interface Structures," 6th Annual Conf. on Physics of Compound Semiconductor Interfaces, Jan. 79, *J. of Vacuum Sci. & Tech.*, Sept./Oct. 79, pp. 1487-1491 [79CLR64].
- ROTHSCHILD, S., see McNeill, D. A.,* [79CLR38].
- SHIMAMURA, J.,* Eguchi, I.* & Assal, F., "Satellites," 9th European Microwave Conf., Sept. 79, *CONF. PROC.*, pp. 213-217 [79CLR66].
- SINHA, A. K., "Burst Distribution and Switching Algorithms in an SS/TDMA System," Pres. at Pacific Telecom. Conf., Jan. 79 [UPO77CL].
- SLIFER, L. W.* & Billerbeck, W. J., "Synchronous Orbit Power Technology Needs," AIAA/NASA Conf. on Advanced Technology for Future Space Systems, May 79, *A Collection of Tech. Papers*, pp. 315-323, AIAA Paper 79-0916 [79CLR53].
- SMITH, T., see Fleming, P. L. [79CLR12], [79CLR24], [79CLR62].
- SNYDER, J., "Digital Phase-Locked Loop Finds Clock Signal in Bit Stream," *Electronics*, Aug. 79, pp. 126-130 [79CLR27].
- SPARROW, L. R., see Lee, Y. S. [79CLR18].
- SRINIVAS, D. N., "Intersatellite Link Tracking Antenna Pointing Requirements," Int. Telemetry Conf., *ITC/USA/79 PROC.*, Vol. 15, pp. 31-38 [79CLR52].

*Non-COMSAT author.
†INTELSAT assignee.

- STEGENS, R. E., "Microwave Integrated Subsystems for Satellite Earth Terminals," National Telecom. Conf., Nov. 79, *CONF. PROC.*, Vol. 1, pp. 2.3.1-2.3.5 [79CLR36].
- UZUNOGLU, V., "Phenomenon of Synchronization," Pres. at INFO II, Patras, Greece, July 79 [UPO75CL].
- UZUNOGLU, V., Noguchi, T., † Chakraborty, D. & Wolejsza, C. J., "Study of Adaptive Equalization in Digital Satellite Communications," National Telecom. Conf., Nov. 79, *CONF. PROC.*, Vol. 2, pp. 21.2.1-21.2.5 [79CLR37].
- VIRUPAKSHA, K. & Onufry, M., "Echo Path Considerations for the Echo Cancellation Process," National Telecom. Conf., Nov. 79, *CONF. PROC.*, Vol. 3, pp. 48.2.1-48.2.8 [79CLR42].
- WARNER, B. H., "Fast LSI Memories Cram More Information into Satellite-Communications Bands," *Electronic Design*, Apr. 79, pp. 118-121 [79CLR17].
- WELTI, G. R., "Bandwidth-Efficient Modulation for Multi-channel Telephone Carriers," National Telecom. Conf., Nov. 79, *CONF. PROC.*, Vol. 3, pp. 55.4.1-55.4.7 [79CLR45].
- WENG, M-I. & Lee, L-N., "Weighted Erasure Decoding for Binary Block Codes with Two-Bit Soft-Decision Demodulation," Pres. at National Telecom. Conf., Washington, D.C., Nov. 79 [UPO74CL].
- WILLIAMS, A. E., "Satellite Communications in the Shuttle Era," Pres. at Australian Astronautics Conv., Perth, Aug. 79 [UPO79CL].
- WOLEJSZA, C. J., see Uzunoglu, V. [79CLR37].
- ZAGHLOUL, A. I. & MacPhie, R. H.,* "Analysis of Finite Phased Arrays of Narrow Slots Using Correlation Matrix Method," *IEEE AP-27*, Mar. 79, pp. 261-266 [79CLR06].

*Non-COMSAT author.
†INTELSAT assignee.